Optimal Synthesis and Design of Advanced Chromatographic Process Concepts

Habilitationsschrift

von Dr.-Ing. Malte Kaspereit
geboren am 31. Juli 1973 in Merseburg

zur Verleihung des akademischen Grades

**Doktor-Ingenieur habilitatus
(Dr.-Ing. habil.)**

genehmigt von der Fakultät für Verfahrens- und Systemtechnik
der Otto-von-Guericke Universität Magdeburg am 5. Juli 2011.

Gutachter:

Prof. Dr.-Ing. Achim Kienle
Institut für Automatisierungstechnik, Otto-von-Guericke Universität Magdeburg

Prof. Dr.-Ing. Andreas Seidel-Morgenstern
Institut für Verfahrenstechnik, Otto-von-Guericke Universität Magdeburg

Prof. Dr. Marco Mazzotti
Institut für Verfahrenstechnik, Eidgenössische Technische Hochschule Zürich

Acknowledgment

Contents

Part I – Summary of Main Results

Part II – Enclosed Manuscripts

Part I

Summary of Main Results

Chapter 1

Introduction

Separation problems occur in basically any (bio)chemical production process that converts some kind of educt or reactant into a product. The isolation of the desired species from the mixtures of components delivered by such processes is one of the fundamental tasks in chemical engineering.

The difficulty of a separation depends on the properties of the involved substances. The problem is the more difficult, the closer the physico-chemical properties of desired and undesired species are to each other. Modern productions of fine chemicals, pharmaceuticals and biotechnological products entail more and more frequently the task of isolating a complex and sometimes "fragile" compound at high purity and yield from a mixture that contains very similar substances. Probably the most extreme example in this context is the separation of the enantiomers of a chiral compound, which is of critical relevance in pharmaceutical applications. These steroisomers differ solely in the spatial orientation of functional groups, rendering their material properties basically identical.

Preparative or process-scale chromatography is one of the methods of choice when tackling problems like enantioseparations or the biotechnological production of proteins, because here classical separation technologies like distillation or extraction usually fail. Further reasons for the increasing application of preparative chromatography are its capability of achieving very high purity as well as its flexibility. As formulated by Guiochon *et al.* [1, p. 2]: *"No industrial separation technique is more versatile than chromatography, nor better suited for the rapid production of milligram to ton quantities of highly pure products. None has a comparable separation power."*

Despite the undoubted capabilities and relevance of chromatographic processes, it is a common mindset among chemists and engineers to conceive the technology as "expensive" and "last resort". This is in part due to the periodic and nonlinear na-

ture of chromatographic processes, which makes their basic design more difficult than that of, for example, a distillation process.

On the other hand, operating and investment costs can be significant in chromatography, considering the required high-purity solvents, sophisticated stationary phases, as well as hardware for chromatographic columns and modern concepts like the simulated moving bed process.

This work is intended as a contribution towards improving the performance and applicability of chromatography as an industrial separation technique by devising advanced process concepts that fully exploit the potential of the technology. Strong focus is furthermore on the development of simple design methods for such concepts in order to foster their practical implementation.

A systematic approach is attempted by pursuing the different general options that exist from a process engineer's perspective for creating advanced processes. The developments are based on suitable mathematical process models which are applied in classical and modern frameworks for process synthesis and design.

The scope of most investigated concepts is on binary separations with a certain emphasis on the production of enantiomers. However, all results are readily applicable to other binary problems and some can be extended also to multi-component separations.

From an engineer's perspective, chromatographic processes have a high degree of freedom. This means that there exist many possible options for enhancing the performance of separations by chromatography. While this makes their optimal design difficult, it supports the expectation that purposeful interventions should lead to significant improvements of process performance.

The many interference options arise from the specific nature of chromatography. The technique exploits differences in the distribution equilibria of solutes between two phases. Consequently its separating capacity can be influenced directly by the choice of these phases and the operating conditions. Chromatography is a spatially distributed process. This suggests introducing also spatially distributed manipulations. Almost all chromatographic processes are operated periodically – incidentally also the "continuous" simulated moving bed technology. In conjunction with the typically nonlinear distribution equilibria, this causes a particular dynamic process behavior which is reflected in the more or less complex spatio-temporal patterns of the internal concentration profiles.

The internal concentration profiles of chromatographic processes can be effectively influenced by the chosen boundary conditions as well as their periodic modu-

lation. This can be exploited to enhance the performance in some of the concepts discussed in this work.

In addition to influencing the chromatographic process itself, also its embedment into the production scheme is of interest. While many works focus only on the local design of a chromatographic separation, a significant optimization potential arises when considering the interaction of chromatography with other processes in a specific production environment. The possibilities range from the simultaneous optimization of chromatography together with all units located upstream or downstream, over introducing recycle streams, up to the purposeful combination with additional separation technologies and/or chemical reactions treated here.

Finally, it is well known that process integration is an attractive approach for improving chemical processes [2]. Correspondingly, also the development of reactive chromatographic processes is in the scope of this work.

In batch chromatography it has been recognized early that not only the choice of stationary and mobile phase and the operating conditions – flow rate, temperature, amount and concentration of feed – can be used to control the separation efficiency. Already more than 60 years ago it was suggested to influence directly the adsorption strength of the components by additional eluent components. The first suggestion in this context was the use of strong adsorbing displacers [3], soon followed by the idea of gradient elution [4]. In particular gradient chromatography has since then become a standard tool in analytical and preparative applications. Various types have been proposed, for example, gradients of solvent strength, pH value, salts, or temperature. A related and increasingly relevant variant is supercritical fluid chromatography (SFC) [5]. An interesting extension of the gradient concept are also the gradients of the stationary phase proposed recently [6]. The vast variety of practical and theoretical works in gradient chromatography cannot be described here. Overviews can be found in, for example, [7, 8].

Due to its rather simple process setup, only few structural modifications of batch chromatography were investigated. Most important to mention is the implementation of recycle streams. There exists a number of concepts that recycle a partially resolved elution profile over a column to enhance the quality of separation, namely closed-loop recycling (CLR) [9–11], CLR with peak shaving [10] and steady-state recycling (SSR) in mixed-recylce [12] or closed-loop [13] mode, respectively. More details on SSR chromatography will be given in Section 3.2. Another option for a structural modification that inherits potential for performance improvement is to distribute the stationary phase within an optimized arrangement of a number of (identical) columns [14], [PII-6]. Finally, also many reactive chromatographic separations were investigated for single-column processes, see *e.g.* [15–23].

The use of gradients has naturally also been suggested for SMB processes. Besides temperature gradients [24–27], which are difficult to implement in practice, in particular solvent gradients were implemented successfully [28–32]. Gradients of the pH value [33] and salt concentration [34–37] play an increasing role in bioseparations. Also supercritical fluids were applied [38–43].

The more complex setup of SMB processes offers more options for structural modifications than in batch chromatography. An interesting idea that purposefully exploits the nonlinear adsorption behavior is the enrichment and partial recycling of the extract stream [44, 45] ("enriched extract", EE-SMB). Many investigations aim at extending applicability of the SMB technology to the separation of more then two components. Corresponding concepts for multi-component separations have been proposed. A natural choice is to apply cascades of SMB units [46, 47]. In other approaches side streams and more zones are used to separate three or more fractions [48–51], [52, 53] ("three-fraction", 3F-SMB).

The periodic nature of the SMB process has inspired various improved operating modes that are based on a dynamic variation of operating parameters. In a conventional SMB unit all operating parameters are held constant throughout operation. A "super-periodic" manipulation of one or more of them can enhance performance. The first reported example is to vary flow rates during the switching interval [54–56] (denoted as "PowerFeed"). Later, an asymmetric switching was proposed that results in a variable column configuration [57, 58] ("VariCol"). Also the feed concentration can be modulated [59–61] ("ModiCon"). Some of these concepts were compared in optimization studies [62, 63]. In another class of operating modes certain internal or external streams are turned on and off in sub-intervals between two switching events, for example, the feed stream [64, 65] ("Partial feed"). More generally, the performance can be enhanced by alternating internal recycling and product withdrawal intervals [66–68] ("Intermittent" operation, I-SMB). A related suggestion is to discharge some product [69] ("Partial discard"). The resulting decreasing yield can be circumvented by fractionating the product and installing a non-permanent recycle [70–72] ("Fractionation & feedback", FF-SMB). Concepts that realize a variable configuration by turning on and off streams were also developed for multi-fraction separations [73, 74].

The idea of performing chemical reactions in SMB units has attracted considerable interest. While Hashimoto's concept with side reactors [75] is conceived in the context of this work as a *partially* integrated process, many studies are devoted to analysis and application of *fully* integrated countercurrent and simulated moving bed systems that utilize chromatographic reactors, see *e.g.* [76–86].

The different advanced operating modes for SMB processes have been summarized in several reviews [87–90]. One is included in Part II of this work [PII-1].

Performance Improvement		

Operating modes
 • Gradients:
   additives, modifiers, ...
 • Recycling techniques
 • Super-periodic operation
	Process combinations
	 (Flowsheet level)
	 • Combined separations
	 • Combined separation
	   and reaction
		Integrated processes
		 (Apparatus level)
		 • Reactive separations
		 • Hybrid separations

Figure 1.1 – General approaches for the development of improved processes in preparative chromatography.

It appears useful to classify the various options for developing improved chromatographic processes that were discussed above. From a process engineering perspective the classification shown in Figure 1.1 is suggested. The concepts investigated in this work can be grouped into the three categories shown.

These three classes were also applied to structure this work. After a review of the theoretical fundamentals in Chapter 2, different *Operating modes* are investigated in Chapter 3, *Process combinations* are discussed in Chapter 4, and *Integrated processes* are developed in Chapter 5.

Chapter 2

Fundamentals

2.1   Basic Operating Modes in Chromatography

All processes and concepts to be discussed in this work are based on two fundamental chromatographic operating modes. These are the conventional single-column or batch chromatography, and the (semi-)continuous simulated moving bed process. Below the basic operating principles of both modes will be recapitulated briefly. More detailed explanations can be found in the standard literature, for example, in [1, 91].
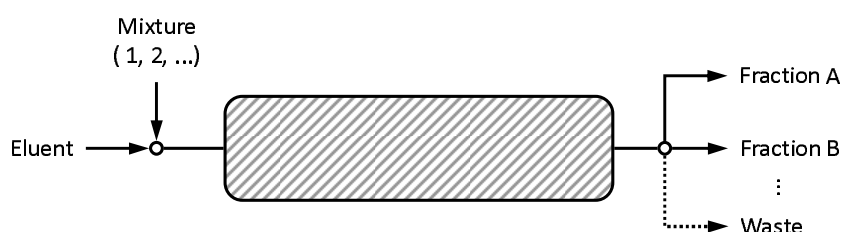
Figure 2.1 – Basic scheme of batch chromatography.

Single column or batch chromatography as illustrated in Fig. 2.1 is the most widely applied chromatographic operating mode. In the elution mode that is considered in this work, a finite volume of a mixture containing components 1, 2, etc. is injected into a continuous stream of eluent. Due to differences in their thermodynamic distribution equilibria, the solutes migrate at different velocities through the bed. The resulting elution bands are collected at the column's outlet in the product fractions A, B, etc.
Specific advantages of batch chromatography are its capability of separating multi-component mixtures with very similar properties, a rather fast method development, and its high versatility [1]. On the other hand, drawbacks are its discontinuous feed supply and its limited performance in terms of solvent consumption

and productivity, in particular when considering binary separations.
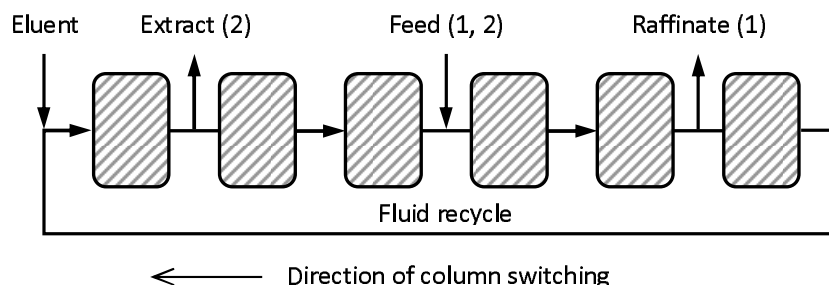
Figure 2.2 – Basic scheme of simulated moving bed (SMB) chromatography.

A sophisticated alternative to batch chromatography is the simulated moving bed (SMB) technology [92]. As illustrated in Fig. 2.2, this concept creates a counter-current between the fluid and solid phases by periodically switching the columns against the direction of the fluid flow. A conventional SMB process separates a continuous feed stream into two fractions. The weaker retained species is obtained in the raffinate port, while the stronger retained elutes with the extract stream. More details on the principles of SMB chromatography and improved operating concepts can be found in several reviews [88, 89, 93], [PII-1].

Obviously the classical SMB concept in Fig. 2.2 is particularly suited for binary problems. In fact, it became a standard technique for enantioseparations. Due to its countercurrent nature, it achieves a high driving force for the separation. Thereby a significantly lower solvent consumption is achieved in comparison to batch chromatography and, depending on the process configuration, often also a higher productivity.

2.2   Modeling of Chromatographic Processes

Designing a preparative chromatographic process typically requires an appropriate mathematical process model that can predict the elution profiles of the components with sufficient accuracy. In general the modeling task is not trivial due to the periodic nature and nonlinear dynamics of chromatography, but also due to the different dispersive effects that are responsible for band broadening. A considerable number of different models and modeling approaches exists. Below only a brief summary on the topic can be given. Extensive discussions on the derivation of the different models, proper initial and boundary conditions for the different process concepts, their (numerical) solution as well as comparisons and possible classifications can be found in, for example, in [1, 91, 94–97].

The core of any chromatographic process model is constituted by the mass balances for the individual components within a single column. In this context, the minimum requirement is to account for the convective transport of the solutes and to apply an expression for their distribution equilibria. Energy balances are less frequently used because preparative application is mainly restricted to liquid chromatography, where the heat effects due to the typically weak interactions can be neglected. The momentum balance is mostly replaced by some simple correlation for the pressure drop.

The following simplifying assumptions are commonly made in the derivation of the mass balance equations [91]:

- Homogeneously bed packed with uniform spherical particles,
- Constant density and viscosity of the mobile phase,
- Isothermal operation,
- Negligible radial distributions.

Apart from these simplifications, a number of dispersive effects can occur in a chromatographic column:

- Axial dispersion due to molecular and eddy diffusion between the particles,
- External mass transfer from the bulk to the particle boundary layer,
- Diffusion in the pores of the particles,
- Diffusion on the surface of the particles,
- Kinetics of adsorption and desorption onto the surface.

Various models have been proposed that differ with respect to the consideration and possible simplification of these dispersive effects. Table 2.1 gives an overview of those that are applied most frequently. Note that the table represents rather an ordered list than a strict classification. The models are arranged in the order of decreasing complexity and a subdivision is made according to the number of effects used to describe band broadening.

The choice of an appropriate model for a particular application depends on the dominating dispersive effect(s) and the required level of accuracy. Detailed models like the general rate model require significant experimental efforts for their parameterization and suffer from slow numerical solutions. Their use can be required in "difficult" applications where large molecules like proteins are separated on macroporous resins. In most practical cases it is sufficient to consider besides axial dispersion a kinetic effect that accounts in a "lumped" manner for all remaining contributions, like in the transport-dispersive and the reaction-dispersive

Table 2.1 – Overview on common chromatographic models. The asterisk (*) marks models that assume established adsorption equilibrium.

Band broadening due to ...	Dispersive effect(s)	Model name
... three and more contributions	Axial dispersion External mass transfer Intraparticle diffusion (Adsorption kinetics)	General rate model
	Axial dispersion External mass transfer Internal mass transfer (Adsorption kinetics)	Lumped pore diffusion model
... two contributions	Axial dispersion Overall mass transfer	Transport-dispersive model
	Axial dispersion Adsorption kinetics	Reaction-dispersive model
...single contribution	Adsorption kinetics	Reaction or Thomas model
	Overall mass transfer	Transport model
	Apparent dispersion	Equilibrium-dispersive model *
	Number of CSTRs	Equilibrium-stage model *
	Number of cells	Craig model *
No band broadening	–	Ideal or equilibrium model *

model, respectively. In many cases, in particular for "small molecules" and columns with high efficiency, even a single parameter is sufficient to describe band broadening. Particularly interesting in this context is the equilibrium dispersive model, for which the so-called Rouchon algorithm [98] yields very fast numerical solutions [1, 96].

A separate class in Table 2.1 are the two stage models below the dashed line. These are not based on continuous mass balances. The well-known equilibrium stage model by Martin and Synge [99] assumes a cascade of equilibrium stages which are continuously passed by the mobile phase. It is – at least for linear systems and sufficient column efficiency – analogous to the equilibrium-dispersive model. An exceptional approach is represented by the Craig model [100], which is based on a discrete number of equilibration steps.

The last entry in Table 2.1 is the ideal or equilibrium model of chromatography. It considers only convection and thermodynamics by assuming established adsorption equilibrium. Any dispersive effects are neglected. This limits its applicability for the detailed design in practical applications. However, its simplicity facilitates analytical solutions for many practically relevant applications. Therefore, the model is of great importance for the fundamental analysis of chromatographic processes and the derivation of simple design methods. Due to its relevance for this work, the ideal model will be discussed in more detail in Section 2.3.

2.3 Equilibrium Theory of Chromatography

A systematic development of new process concepts requires suitable tools for process analysis and design. The detailed models in Section 2.2 take into account not only the typically nonlinear adsorption of the components, but also dispersive effects due to mass transfer resistances, axial dispersion, etc. Unfortunately, under typical practical conditions their model equations have to be solved numerically. This makes them less useful when aiming at general insight into process behavior, performing basic process design or developing new concepts.

Equilibrium theory provides a more fundamental approach for the analysis and basic design of chromatographic processes. This powerful framework is equally applicable to conventional fixed-bed processes, countercurrent schemes as well as reactive chromatography. It is based on the strong simplifying assumptions of locally established thermodynamic equilibrium and negligible dispersive effects. These lead to simpler formulations of the governing mass balances for which ana-

lytical solutions can be derived.

The theory has been developed within more than 60 years. Wilson [101] realized in 1940 the existence of self-sharpening fronts in chromatograms, Weiss [102] noted the dispersive waves. DeVault [103] explained the shock physically and described the effects of competition and displacement considering convex upward and downward isotherms. Glückauf [104–106] solved the ideal model for sigmoidal and, importantly, for competitive Langmuir isotherms. The mathematical treatment was pushed forward by the concepts of weak solutions proposed by Lax [107] and that of coherence by Helfferich [108]. The theory arrived at a rather mature state with the comprehensive works by Helfferich [109] and Rhee and Amundson [110]. A more detailed historical overview is given in [111].
A summary of the mathematical fundamentals is found in the books by Rhee, Aris, and Amundson [84, 112]. Less mathematically oriented readers interested in constructing chromatograms might prefer the well-known book by Guiochon *et al.* [1]. Of particular relevance for this work are also the design methods for SMB processes developed by Mazzotti *et al.* [113–117] and the extension to reactive chromatography published by Kienle *et al.* [85, 86].

Below the main principles of equilibrium theory are summarized as far as they are required to understand the analysis and design methods for the different processes discussed in later chapters.

Single Column Chromatography

Under the assumption of established thermodynamic equilibrium and neglecting any dispersive effects, the mass balance equations for a single chromatographic column as in Fig. 2.1 can be written as

$$\frac{\partial c_i}{\partial t} + \frac{1-\varepsilon}{\varepsilon}\frac{\partial q_i}{\partial t} + u\frac{\partial c_i}{\partial x} = 0, \quad i = (1, N). \tag{2.1}$$

Equations (2.1) constitute the ideal or equilibrium model of chromatography. The independent time and space variables are t and x, while the dependent variables c_i and q_i are the fluid phase concentrations of component $i = 1 \ldots N$, and the corresponding solid phase loadings, respectively. $u = Q/(\varepsilon A)$ is the interstitial fluid velocity with ε as the bed porosity[1]

---

[1]For the sake of simplicity, this derivation assumes a non-porous stationary phase. Equations (2.1) hold for porous particles when replacing ε with the total porosity $\varepsilon_t = \varepsilon_b + (1-\varepsilon_b)\varepsilon_p$, where ε_b and ε_p are the bed and the intra-particle porosity, respectively, and by setting $u = Q/(\varepsilon_t A)$.

In many cases it is useful to re-formulate the model using the dimensionless time and space variables $\tau = tu/L$ and $z = x/L$, where L is the column length. With the phase ratio $F = (1-\varepsilon)/\varepsilon$, one obtains

$$\frac{\partial}{\partial \tau}(c_i + Fq_i) + \frac{\partial c_i}{\partial z} = 0, \quad i = (1,N). \tag{2.2}$$

The loadings q_i in Eq. (2.2) are related to the fluid phase concentrations by a thermodynamic equilibrium expression. For isothermal adsorption-based processes, this is called adsorption isotherm (for the sake of brevity here usually denoted as "isotherm"),

$$q_i = q_i(c_1, c_2, ..., c_N), \quad i = (1,N). \tag{2.3}$$

In general adsorption isotherms have to be determined experimentally. A number of specialized techniques exists for this task reviewed recently by Seidel-Morgenstern [118]. An accurate measurement – in particular of competitive equilibria – can be tedious, but the examples and methods to be discussed in this work will underline that significant efforts are justified for this.

Two main types of nonlinear and competitive isotherms will be considered below. The first is the famous model by Langmuir [119] which describes interactions with homogeneous surfaces. For competitive multi-component systems it is written as

$$q_i = q_{S,i} \frac{b_i c_i}{1 + \sum_j b_j c_j}, \quad i,j = (1,N), \tag{2.4}$$

with $q_{S,i}$ as the saturation capacities of the components and b_i as interaction parameters. Equations (2.4) constitute the equilibrium function most frequently applied in preparative chromatography.

The second isotherm to be used is the bi-Langmuir model [120]. This accounts for adsorption onto heterogeneous surfaces by assuming two different types *I* and *II* of Langmuir adsorption sites. It is particularly suitable for enantiomeric systems, since it allows describing separately a selective chiral and a non-selective achiral interaction [121]. In competitive multi-component form it is given by

$$q_i = q_{S,i}^I \frac{b_i^I c_i}{1 + \sum_j b_j^I c_j} + q_{S,i}^{II} \frac{b_i^{II} c_i}{1 + \sum_j b_k^{II} c_k}, \quad i,j,k = (1,N). \tag{2.5}$$

Note that thermodynamic consistency of Eqs. (2.4) and (2.5) is guaranteed only if the saturation capacities q_S are equal for all components. However, meeting this criterion is not required for the binary separations considered in this work.

Equations (2.2) form a reducible set of homogeneous quasilinear partial differential equations (PDEs) of first order. The equations are nonlinearly coupled if

Eqs. (2.3) are competitive equilibria. It is important to realize that the type of the PDE system and the nature of the solutions depend on this equilibrium function. The PDE system (2.2) is called *strictly hyperbolic*, if the Jacobian matrix J, that consists of the partial derivatives of the equilibrium function, has N real and distinct eigenvalues and N linearly independent eigenvectors. It is denoted just as *hyperbolic* or *weakly hyperbolic* if J has multiple real eigenvalues, as *parabolic degenerate* for multiple real eigenvalues and less than N independent eigenvectors and, finally, as *elliptic* for complex eigenvalues Equations (2.2) [122].

The theory applied here is most developed for strictly hyperbolic systems. It can be shown that strict hyperbolicity is always guaranteed for the Langmuir model in Eq. (2.4) [123]. This holds also under thermodynamically inconsistent conditions with different saturation capacities. Exceptions exist only in so-called watershed points located on the boundary of the concentration space. More recently in [124] strict hyperbolicity was also proven for the modified Langmuir model, which extends Eq. (2.4) by linear terms. For bi-Langmuir isotherms, Eq. (2.5), it was found in [124] that generally hyperbolicity depends on both, isotherm parameters *and* concentrations, and may fail. However, systems with N components are hyperbolic if the saturation capacities on each adsorption site $j = (I,II)$ are equal and positive. Moreover, for two-component systems, $N = 2$, strict hyperbolicity is given for positive $q_{S,i}^j$ and b_i^j. Like for Langmuir isotherms, multiple eigenvalues can occur only on the concentration axes. The binary separation problems with bi-Langmuir isotherms discussed in this work fall into this category.

A particular property of the model Eqs. (2.2) is that they describe wave phenomena. If the equilibrium Eq. (2.3) for a single solute is a nonlinear function $q = q(c)$, the migration velocity of each concentration value depends on the concentration itself. Moreover, if the equilibria in a multi-component system are competitive, $q_i = q_i(c_1, c_2, ...)$, as is the case in Eqs. (2.4) and (2.5), the migration velocities of all concentrations depend on the concentrations of all present adsorbing species. This gives rise to the emergence of the peculiar phenomena like dispersed waves and shock fronts that are characteristic for nonlinear chromatography.

In order to simulate a chromatographic process, the model equations have to be solved for a correspondingly defined initial value problem or a succession thereof. For example, a typical elution process in batch chromatography can be defined as two consecutive problems with constant initial conditions and a step-change in the boundary conditions. The first of these so-called Riemann problems corresponds to a step of the inlet concentrations from the pure eluent to the feed while the column is completely regenerated. The second problem is the regeneration of the now pre-loaded column by feeding again pure eluent. More complex scenarios can also be studied.

The solution of Riemann problems for such systems can be accomplished by the method of characteristics. For details the reader is referred to, for example, [84, 112]. To understand the procedures applied in this work it is sufficient to know that any discontinuity in the boundary or initial conditions will be resolved in at most N (as the number of components) simple waves, shocks, or contact discontinuities. For the isotherm models considered below, their propagation velocities, and thus the complete solution, can be calculated from the eigenvalues and eigenvectors of the Jacobian matrix J.

Let us consider a two-component system described by the Langmuir model (2.4) to elucidate the solution procedure. In this case the Jacobian J is given by

$$J = \begin{bmatrix} q_{11} & q_{12} \\ q_{21} & q_{22} \end{bmatrix} = \begin{bmatrix} \dfrac{a_1(1+b_2 c_2)}{N^2} & -\dfrac{a_1 b_2 c_1}{N^2} \\ -\dfrac{a_2 b_1 c_2}{N^2} & \dfrac{a_2(1+b_1 c_1)}{N^2} \end{bmatrix}, \quad (i = 1,2) \qquad (2.6)$$

$$\text{with } q_{ij} = \frac{\partial q_i}{\partial c_j}, \ N = 1 + b_1 c_1 + b_2 c_2, \ a_i = q_{S,i} b_i.$$

In the following $i = 1$ and $i = 2$ will denote the weaker and the stronger adsorbing component, respectively.

The eigenvalues λ of J are calculated from the following equation,

$$\lambda^2 - (q_{11} + q_{22})\lambda + q_{11}q_{22} - q_{12}q_{21} = 0, \qquad (2.7)$$

where the two solutions are ordered as $\lambda_1 < \lambda_2$. These eigenvalues define the slopes of characteristics C in the physical plane (z, τ), and are inversely proportional to the characteristic propagation velocity v_c of a given composition in a *simple wave*,

$$v_{c_j} = \frac{1}{1 + F\lambda_j}, \quad (j = 1,2). \qquad (2.8)$$

Note that the propagation velocities in the dimensionful (t,x) plane are obtained by multiplying v_{c_j} with the interstitial velocity $u = Q/(\varepsilon A)$.

Which of the two velocities v_{c_1} and v_{c_2} in Eq. (2.8) actually represents the valid solution depends on the initial and boundary conditions. In this context the eigenvectors of the matrix $M = I + FJ$, where I is the identity matrix, provide a useful tool. The eigenvectors define characteristics Γ in the concentration space. For the binary system considered here they can be calculated from the eigenvalues of J as

$$\Gamma_\pm : \quad \frac{dc_1}{dc_2} = \frac{\lambda_{1/2} - q_{22}}{q_{21}} = \xi_\pm. \qquad (2.9)$$

From Eq. (2.7) one finds

$$\xi_\pm = \frac{q_{11} - q_{22}}{2\,q_{21}} \pm \sqrt{\left(\frac{q_{11} - q_{22}}{2\,q_{21}}\right)^2 + \frac{q_{12}}{q_{21}}}\,.$$

The characteristics span a network in the concentration domain, the so-called hodograph space. They pre-define the paths that can be taken by simple wave solutions. It is worth emphasizing that the path grid itself depends on the isotherm parameters only and is, thus, independent of the process conditions. The latter, represented by the initial and boundary conditions, determine *which* of the two paths that exist in each composition (c_1, c_2) is taken by the solution (see below).

The expressions above hold *for simple waves only*. It is well known that for hyperbolic systems as given here by using the Langmuir isotherm also *shocks* can develop. These represent discontinuous, so-called weak solutions of the PDE system. Their velocity is found by replacing the eigenvalue in Eq. (2.8) by the finite differences

$$\tilde{\lambda} = \frac{[q_1]}{[c_1]} = \frac{[q_2]}{[c_2]}, \tag{2.10}$$

where the brackets $[\cdot]$ denote the differences of concentration and loadings left and right of the shock. This equation is known as jump or Rankine-Hugoniot condition from fluid mechanics [125].

The consequence of this is that in a given composition P there exist two shock paths, denoted here as Σ_+ or Σ_-, that connect P to two loci to be determined from Eq. (2.10). The two shock paths are tangent to the Γ characteristics in P. Note that the Σ are generally different from the Γ characteristics. In the case of Langmuir isotherms, however, both the Σ and Γ are straight lines and, thus, fall together. From Eq. (2.10) follows for the velocities of the shocks,

$$v_{s_j} = \frac{1}{1 + F \frac{[q_j]}{[c_j]}}, \quad (j = 1, 2). \tag{2.11}$$

Again, dimensionful velocities are obtained by multiplying v_{s_j} with the interstitial velocity u.

An illustration of the solution procedure for a full chromatographic cycle is given in Fig. 2.3. First the feed mixture (F) is injected into the initially empty column (state I). Later the column is regenerated by interchanging F and I.
The solution is now found by taking from the initial condition I first the "fast path" (corresponding to the smaller eigenvalue λ_1 and thus to the higher velocity) until the slower path (λ_2, lower velocity) is reached in P_1 that gives a connection
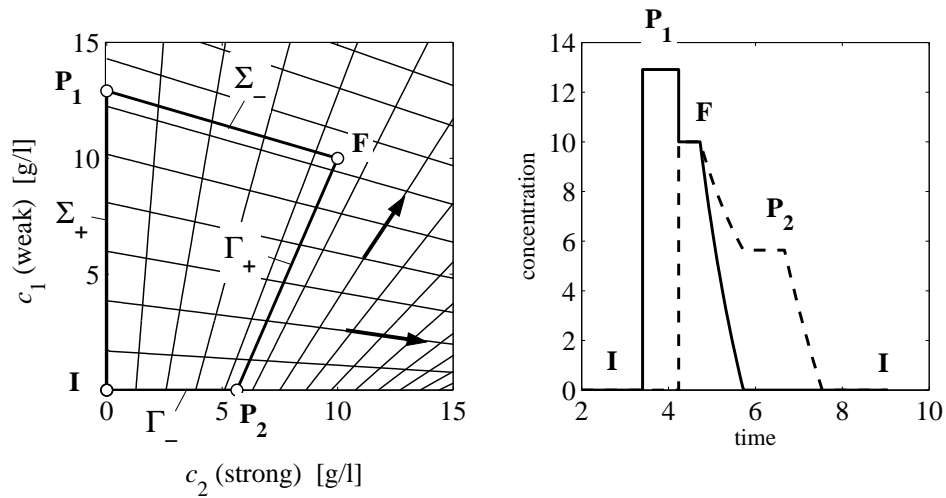
Figure 2.3 – Example for a complete chromatographic cycle for a large injection of a mixture (F) onto an empty column (I) for Langmuir isotherms. Left – hodograph plane. The Γ_+ ("fast paths") are the characteristics progressing towards the upper right, the Γ_- ("slow paths") towards the lower right of the diagram, respectively. The arrows mark the directions along the characteristics in which the eigenvalues λ_j decrease. Right – corresponding chromatogram.
Parameters: $a_1 = 2.0$, $a_2 = 3.0$, $b_1 = b_2 = 0.02\,\text{L/g}$, $c_{F,i} = 10$ g/L, $c_{I,i} = 0$.

to the boundary condition F. If along a path the eigenvalue decreases (i.e., in the direction of the arrows in the figure), the velocity increases and the corresponding transition is a shock. This is the case here for both paths during the loading, which are correspondingly a Σ_+ and a Σ_-.

In the elution step from F to I, the initial conditions are now given by F. Since first the fast path has to be followed, one has to move from F downwards along this to find a connection to I. Along the route, λ_2 increases (the velocity decreases), which corresponds to having a simple wave on a Γ_+. The same holds along the slow Γ_- from P_2 to the state I.

At the intersections of the characteristics the plateaus P_1 and P_2 develop provided the injection is sufficiently large. The corresponding chromatogram in the right of the figure follows now from the expressions for the velocities of the simple waves and shocks above, with the concentration values now known from the hodograph plot. It should be noted that for smaller injections the waves will interact with each other, causing an erosion of these plateaus. The solution is still possible (see *e.g.* [PII-2]) but is somewhat more involved.

Before considering also countercurrent chromatography, an alternative approach should be mentioned. The ω-transform [84] orthogonalizes the characteristics in the hodograph plane. This is particularly interesting when analyzing systems with

a larger number of components, because the construction rules for the solutions
can be conveniently implemented in the orthogonalized variables.

The following definition creates for Langmuir isotherms a one-to-one mapping
between the concentrations in the hodograph plane and the ω-values in the corre-
sponding domain,

$$\sum_{i=1}^{N} \frac{q_i b_i}{a_i - \omega} = 1\,, \quad (i = 1 \ldots N) \tag{2.12}$$

The solution can be fully constructed in the ω-space since also the velocities can
be expressed in terms of the ω_j values. The latter are related to the eigenvalues λ_j
by

$$\omega_j = \lambda_j \left(1 + \sum_j b_j c_j \right)\,, \quad (j = 1 \ldots N)\,. \tag{2.13}$$

An example for the application of the ω-transform is given in Section 3.1.

Simulated Moving Bed Chromatography

Applying equilibrium theory to SMB chromatography facilitated the development
of the "triangle theory" as the most important tool for the basic design such this
process for various types of adsoprtion equilibria and operating concepts, see *e.g.*
[113–117, 126, 127]. It is particularly popular for the relevant case of Langmuir
isotherms, since there it yields simple explicit equations for the optimal operating
conditions [128]. Furthermore, the determined separation regions allow for a ge-
neric view on the operating regime.

To allow for an easier understanding of the methods derived later, below a brief
outline is given on the underlying principles of applying equilibrium theory to this
type of problem.

In the context of equilibrium theory, it is common to consider the fully continuous
true moving bed (TMB) concept illustrated in Fig. 2.4 as an approximation of the
more complex periodically operated SMB process. The mass balances for a TMB
process read, written in the direction of the fluid phase flow,

$$\frac{\partial}{\partial \tau} \left(c_i + F q_i \right) + \frac{\partial}{\partial z} \left(m^j c_i - q_i \right) = 0 \tag{2.14}$$
$$\text{with} \quad (i = 1, 2)\,, \ (j = I ... IV)\,,$$

with $\tau = t F u_S / L$ and $z = x/L$ as dimensionless time and space variables, u_S the
interstitial solid phase velocity[2], and L as the section length. The m^j-values in

---

[2]Note that u_S is defined as $u_S = Q_S / [(1 - \varepsilon) A]$.

Eq. (2.14) represent the most important design parameters in countercurrent chromatography. They are defined as the dimensionless ratio of the liquid flow rate Q^j and the solid flow rate Q_S in the jth section of a TMB process and relate to the flow rates in the corresponding SMB process by, see *e.g.* [128],

$$m^j = \frac{Q^j}{Q_S} = \frac{u^j}{F u_S} = \frac{Q^{j,\,\text{SMB}} t_S - \varepsilon V}{V(1-\varepsilon)} \quad, \quad j = (I...IV) \tag{2.15}$$

where t_S is the switching time of the SMB unit and V the column volume.

Equations (2.14) are largely analogous to those for the batch column in Eqs. (2.2). In fact the single column is a special case of the TMB concept with a solid flow rate of zero. Therefore, many of the solution principles for single columns can be applied directly to TMB processes.

In analogy to the single column where the velocities for simple waves and shocks are given by Eqs. (2.8) and (2.11), holds for the characteristic velocity in a TMB section in case of a *simple wave*,

$$v_{c,j} = \frac{1 - \frac{1}{m}\lambda_j}{1 + F\lambda_j}, \quad (j=1,2), \tag{2.16}$$

and for a *shock*,

$$v_{s,j} = \frac{1 - \frac{1}{m}\frac{[q_j]}{[c_j]}}{1 + F\frac{[q_j]}{[c_j]}}, \quad (j=1,2). \tag{2.17}$$

Physical migration velocities are again obtained by multiplying the v with u. Note that, when introducing $m = u/(F u_S)$ into Eqs. (2.16) and (2.17), it immediately becomes apparent that the velocities for batch chromatography given in Eqs. (2.8)
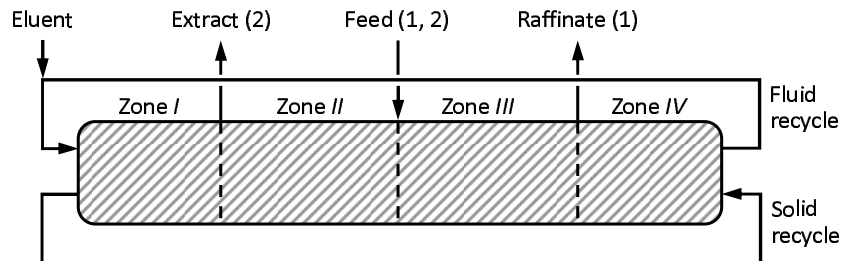
Figure 2.4 – Schematic representation of a true moving bed (TMB) process. The continuous concept is a simplified approximation of the periodically operated SMB process in Fig. 2.2.
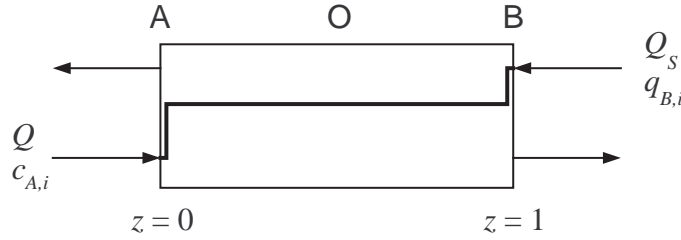
Figure 2.5 – Riemann problem for a single TMB section. The incoming streams and their compositions – the state A of the liquid phase entering from the left and the state B of the solid phase from the right – determine the values of the internal state O and at the outlets. The illustrated profile corresponds to a simple wave in steady state with two boundary discontinuities.

and (2.11) represent special cases where $u_S = 0$.

Also in the TMB process the simple waves map onto the Γ characteristics and the shocks onto the Σ paths, respectively. It is important to realize that the pathgrid spanned by the Γ characteristics in the hodograph plane is the same for TMB and batch processes, since it depends on the isotherm parameters only.

The actual course of the solution is found again by considering a Riemann problem, now for a single section as illustrated in Fig. 2.5. The incoming streams $c_{A,i}$ and $q_{B,i}$ are the boundary conditions that have to be connected by two characteristics or shocks, respectively, in the hodograh plane. The correct "pair" is found by comparing the eigenvalues or, alternatively, the ω-values for the boundary conditions, see [84].

In steady state only the state O can prevail in the interior of the section for which the velocity is zero. The position of O along the admissible path is determined by the m-value. Setting $v_{c,j} = 0$, one immediately finds from Eq. (2.16) for O on a $\Gamma+$ characteristic,

$$m = \lambda_1 ,\tag{2.18}$$

and for O an a Γ_- characteristic,

$$m = \lambda_2 .\tag{2.19}$$

For the shocks one obtains from Eq. (2.17),

$$m = \frac{[q_j]}{[c_j]} .\tag{2.20}$$

Different ranges hold for the m-value in which O lies either on the Γ_+ (Σ_+), Γ_- (Σ_-), at their intersection, or in either one of the boundary conditions, respectively.

The states leaving the zone do not have to be in equilibrium with the incoming streams ("boundary discontinuities"). They are obtained from balances around the top or bottom of the zone.

Detailed rules for constructing the complete solutions for transient and steady-state problems are given in [84]. To design the process in Fig. 2.4 the steady-state solutions for the four zones are combined with the material balances between and at the boundaries of the zones. However, additional assumptions are required to solve the equations. For the example of the complete separation of two components with Langmuir isotherms, the linear characteristics in conjunction with requiring complete regeneration in zones I and IV facilitated deriving the well-known explicit separation region in the m^{II}-m^{III} domain, see *e.g.* [128]. More recently explicit separation regions were also obtained for the concept of generalized Langmuir isotherms [126, 127].

Reactive Chromatography

For reactive chromatographic processes the mass balances are sets of heterogeneous partial differential equations, which complicates the situation significantly. However, by simplifying assumptions it is possible to transform the heterogeneous PDE system into a homogeneous one. Based on this the theoretical treatment above was extended to some special cases in [84].

A useful method evolves if the limiting case of simultaneously established adsorption and reaction equilibrium can be assumed. By introducing transformed variables based on the stoichiometry, as suggested by Doherty *et al.* for reactive distillation [129], various scenarios can be studied also in chromatographic reactors [85, 86]. Suitably defined variables eliminate the unknown reaction rates from the balance equations and thereby render the PDE system homogeneous, whereby the dimension of the problem reduces by the number of reactions [85]. The same solution procedures as in the non-reactive cases are applicable.

This approach is pursued in Chapter 5 for an isomerization reaction performed in an integrated SMB process.

Another aspect are heat effects that arise when in adiabatic operation of chromatographic columns. Heat effects have been studied exhaustively for non-reactive systems by Rhee *et al.* [84, 130], who introduced energy contents as transformed variables that render the system analogous to one with an additional species. The application of similar variables to reactive systems is discussed in Chapter 5.

Chapter 3

Advanced Operating Modes

3.1 Batch Chromatography with Adsorbing Additives

Additives or modifiers are frequently applied in preparative chromatography, for example, to improve the separability of the compounds or to stabilize the pH value. If such additive is *adsorbing competitively*, the presence of this additional component can give rise to significant nonlinear effects. Depending on its adsorptivity, resulting peak shapes can be difficult to interpret. Examples are peaks that imply a change from Langmuirian to anti-Langmuirian adsorption behavior although all compounds have Langmuir isotherms [131–133], or peak splitting caused by a modifier [134, 135]

In the enclosed manuscript [PII-4] three enantiomeric systems are investigated in detail wherein the additive (a buffer compound) has either weakest, intermediate or strongest adsorptivity in a set of competitive bi-Langmuir isotherms. The paper aims in particular at identifying possible benefits of adsorbing additives in batch chromatography, and gives suggestions regarding the optimal operation. A particular finding is that it is mandatory to take into account carefully the elution profile of the additive – which is often not visible in detector signals – when designing repetitive process cycles.

Apart from the results of this study it is useful to elucidate such situation in the frame of equilibrium theory. As an introductory example, let us consider the hodograph for a binary system with Langmuir isotherms in Fig. 2.3. It is clear that saturating an initially empty column with a binary mixture will cause two shock transitions. However, when injecting F: $(c_{F,1} = 10, c_{F,2} = 0)$g/L onto a column initially saturated with I: $(10, 10)$g/L, the solution will first follow the Γ_+ characteristic from I in the direction of decreasing velocity (*i.e.* downwards), before it

Table 3.1 – List of transitions in the ω space for the complete chromatographic cycle of a ternary separation. Transitions (arrows) from states (1) through (4) correspond to loading the feed F onto the column with initial conditions I. Transitions (4) through (7) mark the elution back to state I.

I = (1)		(2)		(3)		(4) = F		(5)		(6)		(7) = I
$\omega_{I,1}$	$\rightarrow$	$\omega_{F,1}$		$\omega_{F,1}$		$\omega_{F,1}$	$\rightarrow$	$\omega_{I,1}$		$\omega_{I,1}$		$\omega_{I,1}$
$\omega_{I,2}$		$\omega_{I,2}$	$\rightarrow$	$\omega_{F,2}$		$\omega_{F,2}$		$\omega_{F,2}$	$\rightarrow$	$\omega_{I,2}$		$\omega_{I,2}$
$\omega_{I,3}$		$\omega_{I,3}$		$\omega_{I,3}$	$\rightarrow$	$\omega_{F,3}$		$\omega_{F,3}$		$\omega_{F,3}$	$\rightarrow$	$\omega_{I,3}$

moves along a Γ_- into F. The resulting transitions are both simple waves, creating a "scent" of anti-Langmuirian behavior. This underlines that the solution depends not only on the adsorption isotherms, but just as well on the initial and boundary conditions. Along similar arguments also various other "bizarre" situations can be fully explained.

It should be clear from the simple binary example above that an interesting elution behavior is to be expected for ternary systems in which one component, the additive, is present in the initial conditions of the column. For the sake of simplicity the following example will rely on Langmuir isotherms, Eq. (2.4), which were fitted to the bi-Langmuir isotherms, Eq. (2.5), reported in [133]. It was found useful to determine the solution paths for this ternary problem using the ω transform. As explained in Section 2.3 this orthogonalizes the composition paths of the chromatographic cycle.

The ω transform results in simple construction rules for chromatograms that can be summarized in four steps: *i*) *Transformation* of initial and boundary conditions I and F into their ω coordinates by determining the $N = 3$ roots of Eq. (2.12) and sorting the elements of ω_I and ω_F in increasing order. *ii*) The *order of transitions* corresponds to the order of the elements of the ω values, as is illustrated in Table 3.1. *iii*) The *type of transition* is found by comparing the corresponding ω values. For example, if for the step from (1) to (2) in Table 3.1 $\omega_{I,1} < \omega_{F,1}$ this corresponds to a simple wave, while for $\omega_{I,1} > \omega_{F,1}$ a shock occurs. *iv*) The velocities are calculated from Eqs. (2.8) through (2.12) and the chromatogram is constructed. Note that for this illustrative example the case of wave interactions not considered.

The example shown in Fig. 3.1 corresponds to a large injection of the enantiomers of Alprenolol onto an analytical Chirobiotic T column [133]. The column is initially equilibrated with the eluent wherein the strongest adsorbing additive triethyl ammonium acetate is present as the only adsorbing component. The elution profiles calculated by the method above match closely those obtained numerically from an equilibrium-dispersive model for the Langmuir isotherms. For comparison the
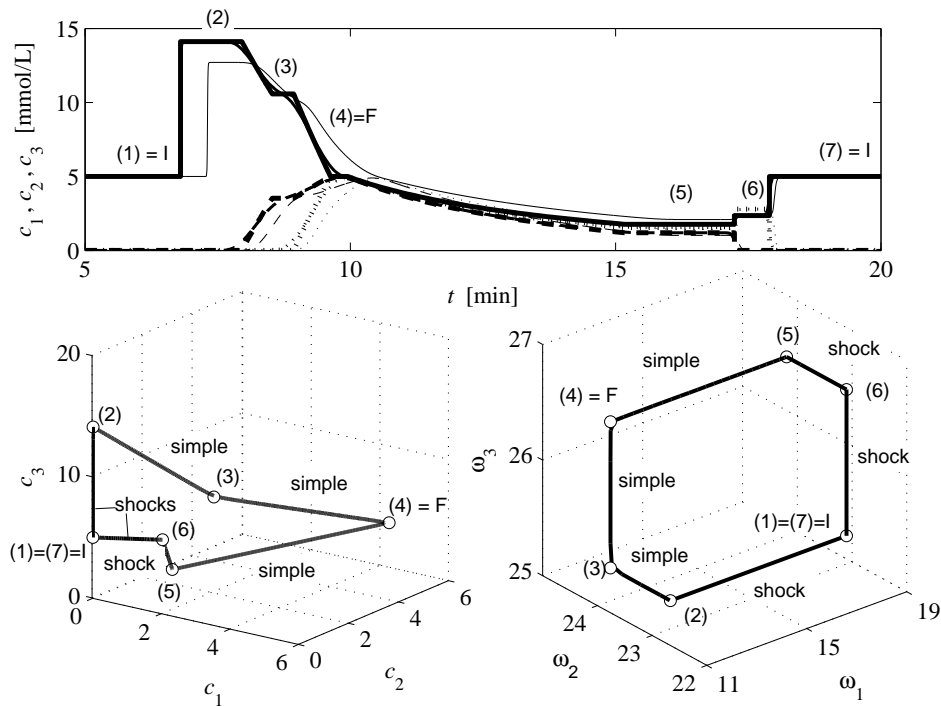
Figure 3.1 – Separation of two enantiomers by batch chromatography in the presence of an adsorbing additive. Chromatograms at the column outlet (top), in the hodograph plot and in the ω domain (bottom). The additive (solid lines) adsorbs strongest, the enantiomers intermediately (dotted) and weakest (dashed), respectively. Thick lines – solution by equilibrium theory, re-fitted Langmuir isotherms; medium – equilibrium-dispersive model corresponding to 11000 stages, Langmuir; thin – same model, bi-Langmuir.

Parameters: $V_F = 7\,\text{mL}$, $c_F = (5,5,5)\,\text{mmol/L}$, $c_I = (0,0,5)\,\text{mmol/L}$. Re-fitted Langmuir isotherms: $a_i = (22.75, 25.35, 27.86)$, $b_i = (0.07335, 0.07367, 0.1055)$. bi-Langmuir isotherms from [133]; for other parameters see [PII-4].

figure shows also the profiles for the original bi-Langmuir parameters given in [133]. The results closely reflect the numerical and experimental results reported for this system in Fig. 5a [133] and Fig. 3a [PII-4].

The transitions for the complete cycle in this "strongly distorted" chromatogram are: shock – simple wave – simple wave for loading, and simple wave – shock – shock for regeneration, respectively. This is accompanied by a pronounced tag-along in the simple wave from state (4) to (5). Another interesting aspect is that the chromatogram starts with a pronounced pure component "ghost peak" of the *strongest* adsorbing additive. This can be explained by the fact that the initial concentration $c_{I,3}$ lies above the two watershed points on this axis at $(0,0,0.939)$ and $(0,0,2.129)$ mmol/L. This part of the c_3 axis is a Γ_+ (or Σ_+ path) characteristic which is taken first in direction of increasing c_3 into point (2), before a Γ_- is taken

from (2) into (3).

The lower part of Fig. 3.1 reveals the usefulness of the ω transform for ternary systems. While it is difficult to interpret the hodograph representation (bottom, left), the paths in the ω plane (bottom, right) are easy to evaluate.

For more general design purposes a formulation appears desirable that accounts also for wave interaction. On the other hand, it might be of limited use due to the fact that most of the observed shocks are not very pronounced. Very high stage numbers are required to take advantage of, for example, the two separate final shocks between states (5) and (7) in Fig. 3.1. It is questionable if a column with such high efficiency will exhibit a pressure drop suitable for an industrial application.

As for the bi-Langmuir isotherms originally underlying the parameters used here, the ω transform is not applicable. In such case the solution procedures described in Section 2.3 have to be applied. Furthermore, it should be verified that the system is strictly hyperbolic in the concentration domain of interest, which is not always the case for ternary bi-Langmuir systems [124].

3.2   Steady-State Recycling Chromatography

When performing difficult chromatographic separations of valuable components it is a serious challenge to maximize the recovery yield. One of the options for this is closed-loop recycling (CLR) [9–11] where a partially separated elution profile is recycled over the column several times until sufficient separation is achieved. This can be accelerated to a certain extent by "peak shaving" [10] and "alternate pumping" [136]. Yet, CLR processes achieve only low productivities.

A more promising approach, in particular for binary separations, is steady-state recycling (SSR) chromatography [12]. In SSR processes a certain amount of fresh feed is added to each recycle fraction after collecting the purified leading and trailing edges of the elution profile (peak shaving). The process is operated such that it attains a periodic steady state after a number of cycles.

The main challenge in SSR chromatography is to design the process. There are two major process concepts. The closed-loop mode (CL-SSR) [13] attempts to preserve the partially separated elution profile. This is difficult to design because of the resulting dynamic injection profile. Here the classical mixed-recycle mode (MR-SSR) [12] is studied. In MR-SSR the recycle fraction is *mixed* with the fresh feed before the injection, which simplifies the design.

In the two enclosed manuscripts [PII- 2] and [PII- 3] new shortcut methods are proposed that allow for a rapid design and evaluation of MR-SSR processes for arbitrary purity requirements.

3.2.1 Design and Performance Under Ideal Conditions

The design task addressed here is to predict *a priori* the four cut times that lead to two product fractions that fulfill the purity requirements in steady state. This situation is illustrated in Fig. 1 [PII-2].
The operation principle of MR-SSR as shown in the figure corresponds to a scenario with piecewise constant initial and boundary conditions, for which equilibrium theory provides a powerful methodology. In the case of Langmuir adsorption isotherms a complete chromatogram can be constructed rather easily for a given column setup if the required operating parameters – flow rate, injection volume, and injection composition – are known, see Section 2.3. The disturbing aspect here is that the chromatogram at steady state is of interest, for which the injection composition is not known.

This problem can be solved without performing dynamic simulation. In [PII- 2] a method is proposed that predicts directly the steady state and the relevant cut times for arbitrary purity requirements for the case of Langmuir isotherms.
An analysis based on equilibrium theory revealed that the composition of the recycle always remains on the Γ_+ characteristic through the fresh feed, see Fig. 2 [PII-2], and that the amounts in the second product fraction are invariant from cycle to cycle. Furthermore, in a binary separation without waste fractions specifying the two purity requirements unambiguously fixes the relative mass fluxes in the two outlets relative to the feed amounts [137]. Combining these information with the "construction rules" of equilibrium theory yields largely explicit equations for the four cut times and the composition of the injection at steady state.

The approach makes analysing the performance of MR-SSR straightforward, because the injection volume remains as the only free operating parameter. In this context it was proven that under equilibrium conditions, *i.e.* negligible dispersion, MR-SSR guarantees a lower solvent consumption and higher product concentrations, but not the productivity of batch chromatography. These results are shown graphically in Fig. 4 [PII-2]. It will be demonstrated later that under dispersive conditions even the productivity of MR-SSR can exceed considerably that of a batch system.

Finally, an interesting aspect is that the knowledge of the injection composition at steady state permits eliminating the startup period of the process. This is done

by simply performing the very first injection(s) with a prepared mixture of that composition.

3.2.2 Design and Performance Under Nonideal Conditions

Under industrial conditions the assumptions made in the previous section will usually not hold any more. Dispersion can be significant and adsorption isotherms do not necessarily follow the Langmuir model. Solutions from equilibrium theory are useful here for basic design. The detailed design of recycling processes requires more efforts and is typically accomplished on the basis of the more detailed dynamic models described in Section 2.2 [10, 11, 138–141]. It should be realized that the cyclic and accumulative nature of SSR processes requires laborious experimental determination of very accurate model parameters.

Against this background an extension of the shortcut design method above to nonideal systems was proposed in [PII-3]. The method exploits the fact that for favourable isotherms the rear part of an overloaded chromatogram is largely independent of the injection volume. This holds even in the presence of strong dispersive effects, provided the isotherms are sufficiently nonlinear.
This common practical observation is exploited in [PII-3] insofar as that the numerical integration along the Γ_+ characteristic in the equilibrium design method above is replaced by simply integrating the rear part of a chromatogram. The result is a shortcut design method for MR-SSR chromatography under dispersive conditions that is not restricted to Langmuir isotherms, but applies to systems with favourable isotherms in general. The method holds again for arbitrary purity requirements and requires as input only a single experimental or simulated chromatogram. Isotherm parameters have not to be measured, and a dynamic simulation is not necessarily required.

The approach was validated for the separation of two cycloketones on a polymeric stationary phase. This system exhibits strongly nonlinear bi-Langmuir isotherms and a low column efficiency with 30 theoretical stages only.
A parametric study using a transport-dispersive model demonstrated that the calculated cut times are very close to the required values. The purity of the second fraction is always met with high accuracy, and only minor refinements of the cut times suffice to correct purity deviations of the first fraction, see Tab. 1 [PII-3].
These finding were supported in experimental investigations using the setup in Fig. 3.2. The purities in Tab. 3 [PII-3] are in all investigated scenarios close to the design specifications. It was also shown that the duration of the startup phase depends strongly on the desired product purity. High purity requirements, Fig. 5 [PII-3], cause a much longer startup phase than lower values, Fig. 6 [PII-3]. Although the
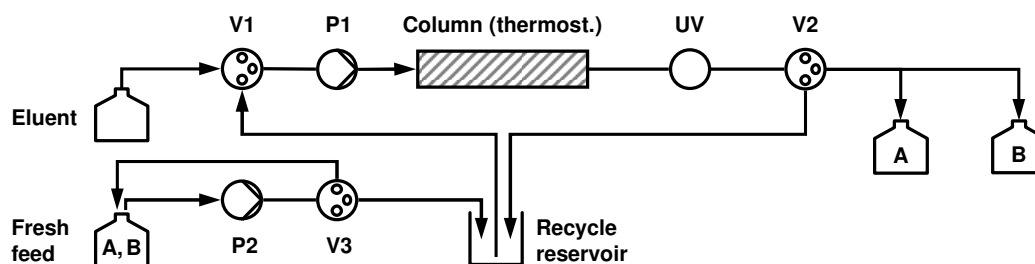
Figure 3.2 – Experimental setup for MR-SSR chromatography. Valve $V1$ controls injection and eluent flow, $V2$ performs product collection and recycling, $V3$ controls addition of fresh feed. The latter is pumped in a circle to eliminate possible failure of pump $P2$ due to frequent activation. Simpler setups are possible and have been tested.

design method does not give information on the steady state injection composition, this can be determined experimentally and then again be used to eliminate the startup, as shown in Fig. 7 [PII-3].

The role of column efficiency for process performance was elucidated using the design method together with the model. The results in Fig. 8 [PII-3] demonstrate a superior performance of MR-SSR in comparison to batch chromatography.

The design method was also used successfully for designing a pharmaceutical enantioseparation, where one component exhibited a sigmoidal isotherm. The MR-SSR process was combined with a subsequent crystallization. The results are illustrated in Chapter 4.

3.3   Simulated Moving Bed Chromatography

3.3.1   Design for bi-Langmuir Isotherms

As already mentioned earlier, the separation of enantiomers has become a key application of SMB chromatography. An accurate modeling of the adsorption behavior of enantiomers frequently requires using the bi-Langmuir model, Eq. (2.5), since this allows a differentiation between chiral and non-chiral interactions of the solutes with the chiral stationary phase.
For the basic design of SMB processes for bi-Langmuir systems, a solution for the m^j values has been provided by Mazzotti and co-workers in the frame of the "triangle theory" [117]. In spite of the relevance of the application area, the application of this rigorous method is rarely reported in the literature. This might be attributed to the fact that some practitioners face difficulties in its implementation, since one of its steps requires a non-trivial numerical scheme (see below).

In [117] this was obviously anticipated and a simple explicit shortcut method was suggested. However, the accuracy of the latter appears rather limited. Below an alternative shortcut design method is proposed, which is also explicit but approximates the rigorous solution with higher accuracy.

For bi-Langmuir isotherms the design problem can be solved only numerically because here in principle the characteristics in the hodograph plane are curved. On the other hand, a strong curvature of the characteristics is hardly observed for most parameter sets of bi-Langmuir isotherms reported in the literature. The idea of the new shortcut method is, thus, to approximate a specific Γ_+ characteristic by a straight line. This allows for a completely explicit solution. It is worth mentioning that the design method obtained such is *approximate* for bi-Langmuir, but *accurate* for Langmuir and modified Langmuir isotherms, respectively, where the characteristics are straight lines, *cf.* Fig. 2.3.

The shortcut approach follows, except for the simplification mentioned above, the rigorous solution in [117]. Below it will be summarized and illustrated. Figure 3.3 shows the solution in the hodograph plot (left) and the region of complete separation in the $m^{II} - m^{III}$ plane (right) for the parameters reported in [117]. In [117] it was proven that for $m^{III} = m^{III}_{\max}$, which holds in the part *wr* of the boundary of the separation region, the states of the Riemann problem for zone *II*, $D - M_2 - \beta$, and those for zone *III*, $D - M_3 - \gamma$, intersect in point $\beta = \gamma$. Furthermore, the material balance around the feed F is a straight line $\alpha - \beta - F$. Since the characteristic are nonlinear curves, the states β and M_2 have to be determined one from another through integration along the Γ_+ that connects both states. Simultaneously a small system of nonlinear equations has to be solved that results from the separation conditions and the shock velocities in zone *III*.

It is readily observed in Fig. 3.3 (left) that for the considered parameters the Γ characteristics are indeed almost linear. Therefore, the Γ_+ through the feed F basically coincides with the Γ_+ that connects β and M_2. Since in M_2 holds $c_1 = 0$ [117], assuming that this Γ_+ is a straight line gives for the approximated point M'_2 in the hodograph plane

$$c_1^{M'_2} = 0 \,, \tag{3.1a}$$

$$c_2^{M'_2} = c_2^F - \frac{c_1^F}{\xi_+^F} \,. \tag{3.1b}$$

where ξ_+^F is the local slope of the Γ_+ in the feed point $\left(c_1^F, c_2^F\right)$ according to Eq. (2.10). The partial derivatives q_{ij} in Eq. (2.10) can be calculated explicitly.
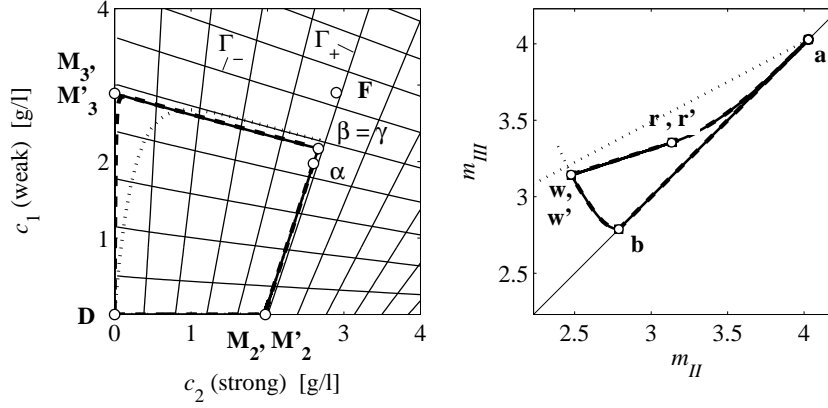
Figure 3.3 – Application of rigorous and shortcut design methods to the bi-Langmuir isotherms used in [117]. Left – hodograph representation, right – region of complete separation in the m^{II}-m^{III} plane. Solid thick lines – rigorous solution [117], dotted – shortcut method in [117], dashed – proposed new shortcut method. Concentration profiles (left) obtained from a TMB model with 1000 stages/zone for the optimal operating point w predicted by each method.
Parameters: $a_1^I = 2.688$, $a_2^I = 3.728$, $a_1^{II} = 0.1$, $a_2^{II} = 0.3$, $b_1^I = 0.0336\,\text{L/g}$, $b_2^I = 0.0466\,\text{L/g}$, $b_1^{II} = 1.0\,\text{L/g}$, $b_2^{II} = 3.0\,\text{L/g}$, $c_1^F = c_2^F = 2.9\,\text{g/L}$, $m^I = 1.1\left(a_2^I + a_2^{II}\right)$, $m^{IV} = 0.01$.

The Jacobian J for bi-Langmuir isotherms reads

$$J = \begin{bmatrix} q_{11} & q_{12} \\ q_{21} & q_{22} \end{bmatrix} = \begin{bmatrix} \dfrac{a_1^I}{N^I} + \dfrac{a_1^{II}}{N^{II}} - \dfrac{a_1^I b_1^I c_1}{N^{I^2}} - \dfrac{a_1^{II} b_1^{II} c_1}{N^{II^2}} & -\dfrac{a_1^I b_2^I c_1}{N^{I^2}} - \dfrac{a_1^{II} b_2^{II} c_1}{N^{II^2}} \\[3mm] -\dfrac{a_2^I b_1^I c_2}{N^{I^2}} - \dfrac{a_2^{II} b_1^{II} c_2}{N^{II^2}} & \dfrac{a_2^I}{N^I} + \dfrac{a_2^{II}}{N^{II}} - \dfrac{a_2^I b_2^I c_2}{N^{I^2}} - \dfrac{a_2^{II} b_2^{II} c_2}{N^{II^2}} \end{bmatrix},$$

(3.2)

where $N^I = 1 + b_1^I c_1 + b_2^I c_2$ and $N^{II} = 1 + b_1^{II} c_1 + b_2^{II} c_2$ and $a_i^j = q_{S,i}^j b_i^j$, $i = (1,2)$, $j = (I, II)$ in Eq. (2.5). Note that for calculating $c_2^{M_2'}$ one has to use $c_i = c_i^F$ when calculating the partial derivatives given in Eq. (3.2).

Once $c_2^{M_2'}$ has been determined, the region of complete separation in Fig. 3.3 follows from the simple expressions given below. For the points a, b, r, and w one finds along the procedure in [117]:

$$m_a^{II} = a_2^I + a_2^{II} \tag{3.3a}$$

$$m_a^{III} = m_a^{II} \tag{3.3b}$$

$$m_b^{II} = a_1^I + a_1^{II} \tag{3.3c}$$

$$m_b^{III} = m_b^{II} \tag{3.3d}$$

$$m_r^{II} = q_{22}\left(0, c_2^{M_2'}\right) \tag{3.3e}$$

$$m_r^{III} = m_r^{II} + \frac{q_2\left(0, c_2^{M_2'}\right) - m_r^{II} c_2^{M_2'}}{c_2^F} \tag{3.3f}$$

$$m_w^{II} = q_{11}\left(0, c_2^{M_2'}\right) \tag{3.3g}$$

$$m_w^{III} = m_w^{II} + \frac{q_2\left(0, c_2^{M_2'}\right) - m_w^{II} c_2^{M_2'}}{c_2^F} . \tag{3.3h}$$

For the curved boundaries of the separation regions the following expressions are obtained. Curve *ra* is calculated using $c_2 = 0 \ldots c_2^{M_2'}$ as running parameter and $m^{II} = m_{\max}^{II}$:

$$m^{II} = q_{22}\left(0, c_2\right), \tag{3.4a}$$

$$m^{III} = m^{II} + \frac{q_2\left(0, c_2\right) - m^{II} c_2}{c_2^F} . \tag{3.4b}$$

Curve *wb* is obtained for $c_2 = 0 \ldots c_2^{M_2'}$ in the same way, but here $m^{II} = m_{\min}^{II}$:

$$m^{II} = q_{11}\left(0, c_2\right), \tag{3.5a}$$

$$m^{III} = m^{II} + \frac{q_2\left(0, c_2\right) - m^{II} c_2}{c_2^F} . \tag{3.5b}$$

Finally, curve *wr*, which requires the numerical solution in the rigorous method, is taken as a straight line connecting points *w* and *r*.

It can be seen in the right panel of Fig. 3.3 that for the used parameters the regions of complete separation obtained by the rigorous method (solid lines) and the new shortcut method (dashed) almost coincide. This is due to the basically linear Γ characteristics. The shortcut method from [117] is less accurate (dotted). The latter is based on the simplifying assumption that β lies on a straight line connecting the origin and the feed *F* in the hodograph plane.
Furthermore, Fig. 3.3 (left) shows also concentration profiles obtained by an equilibrium stage model with 1000 stages per zone for the optimal operating points *w* predicted by the three design methods. The shortcut method from [117] (dotted lines) yields purities of 91.787% (raffinate) and 99.901% (extract). The purities obtained such by the shortcut method proposed here (raffinate: 99.579 %, extract: 99.992 %) are only slightly lower than found from the rigorous design (100.0 %, 99.993 %).

In order to critically evaluate the suggested method it is applied to a set of adsorption isotherms that were measured for the enantiomers of mandelic acid on
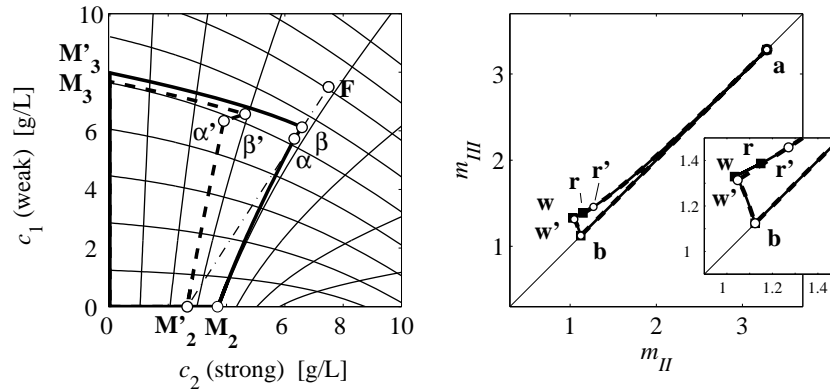
Figure 3.4 – Application of rigorous and shortcut design method to a set of bi-Langmuir isotherms measured for mandelic acid [137]. Points marked by (') denote the shortcut method. For symbols see Fig. 3.3.

Parameters: $a_1^I = a_2^I = 1.0366$, $b_1^I = b_2^I = 0.0073\,\text{L/g}$, $a_1^{II} = 0.0871$, $a_2^{II} = 2.2461$, $b_1^{II} = 0.0273\,\text{L/g}$, $b_2^{II} = 0.7041\,\text{L/g}$, $c_1^F = c_2^F = 7.5\,\text{g/L}$, $m^I = 1.1\,(a_2^I + a_2^{II})$, $m^{IV} = 0.01$.

a Chirobiotic T column [137]. As feed concentrations the reported upper validity limits of the isotherms has been applied.

Figure 3.4 (right) shows the determined separation regions. The regions are very narrow, which indicates that the high feed concentration renders the system rather nonlinear. Like in the previous example the differences between both predictions are very small. Since w and w' almost coincide, this is also reflected in the purities obtained from the stage model (raffinate: 99.987% from shortcut vs. 99.990%, extract in both cases 100%).

The hodograph representation in Fig. 3.4 (left) reveals curved characteristics for this example. A consequence of this is that the Γ and Σ do not coincide. This is clearly observed for the shocks in zone *III* that connect the states β to M_3 and β' to M_3', respectively. The shocks follow Σ_- paths that are tangent in β and β', respectively.

Although the obtained separation regions are very similar, the concentration profiles for points w and w' determined from the stage model differ significantly. As can be seen in the hodograph plane in Fig. 3.4 (left), the state M_2' predicted from Eq. (3.1b) (dash-dotted line $M_2' - F$) is clearly off the Γ_+ characteristic that holds for the rigorous design. However, the effect of this on the m-values in Eqs. (3.3a) through (3.5b) is small, which is why the separation regions are very similar. In view of practical application, the deviations are related to the nonlinearity of the isotherms rather than to the inaccuracy of the method.

As a final example a case is constructed where the Γ_+ characteristics are facing upwards. The corresponding results and parameters are given in Fig. 3.5. In this

Figure 3.5 – Application of rigorous and shortcut design methods to an arbitrary set of bi-Langmuir isotherms with convex upwards Γ_+ characteristics. For symbols see Fig. 3.3.
Parameters: $a_1^I = 0.1$, $a_2^I = a_1^{II} = 1.9$, $a_2^{II} = 0.3$, $b_1^I = 0.5\,\text{L/g}$, $b_2^I = 0.2\,\text{L/g}$, $b_1^{II} = 4.0\,\text{L/g}$, $b_2^{II} = 0.1\,\text{L/g}$, $c_1^F = c_2^F = 0.25\,\text{g/L}$, $m^I = 1.1\left(a_2^I + a_2^{II}\right)$, $m^{IV} = 0.01$.
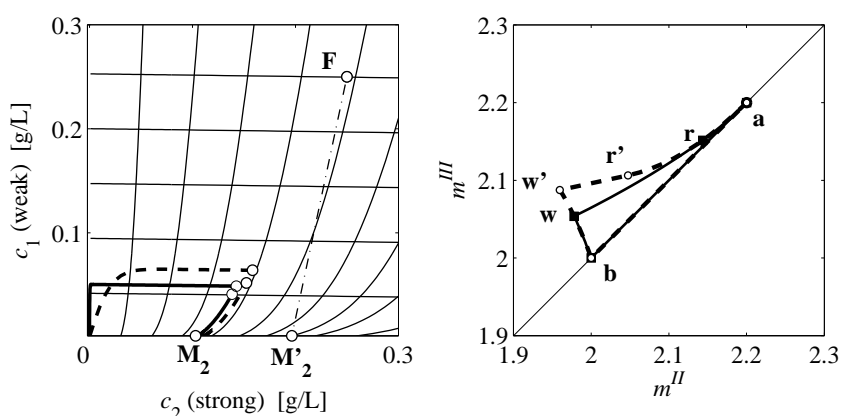
case, the shortcut method yields a too high concentration c_2 for point M_2'. The separation region found is larger than the correct one. Consequently, Eqs. (3.3g) and (3.3h) yield for point w' a too low m^{II} and a too high m^{III} value, respectively. The purity of the raffinate thus decreases (75.521 vs. 99.351%). The extract remains pure (99.939 vs. 99.993%).

Although the last example uses somewhat extreme parameters which seem not to reflect common practical situations, such scenario seems unfavourable with respect to the shortcut method. However, on the basis of Eq. (2.10) it can easily be verified if such case is at hand, or not.

3.3.2   Design for Limited Purity Requirements

Not all applications of SMB chromatography require that the feed mixture is separated completely into the pure components. It is then economically not useful to attain a significantly higher purity than required, because separation costs usually increase exponentially when approaching 100% purity. Also combining an SMB unit with a complementary separation process like crystallization can allow reducing the purity requirements to achieve, in turn, improved overall performance. Such processes are discussed in Section 4.2.

It is generally not trivial to design an SMB process for specific purity requirements lower than 100%. Usually this is done by computationally expensive parametric studies or optimization applied to a mathematical process model. In practi-

cal applications also control schemes can be used. Concerning basic design, only Storti *et al.* [142] reported regions of operating parameters for different outlet purities obtained using equilibrium theory, but under the requirement of complete regeneration of liquid and adsorbent phase in zones *I* and *IV* (for the zone configurations see Figs. 2.2 and 2.4). Under the same requirement Rajendran [143] presented a solution for linear isotherms.

The enclosed manuscript [PII-5] demonstrates for Langmuir isotherms that requiring complete regeneration leads to suboptimal performance and that the optimal operating point can be designed using equilibrium theory.
Parametric studies with an equilibrium stage TMB model revealed that the optimal strategy for Langmuir systems is to control the raffinate purity by allowing a partial breakthrough of the simple wave of the strong adsorbing component from zone *I* to zone *IV*. As shown in Fig. 4 [PII-5] the locus of the optimal operating point in (m^{II}, m^{III}) remains largely unaffected when gradually decreasing m^I, even if a significant portion of the simple wave migrates into zone *IV*. The attractive aspect is that lowering m^I or increasing m^{IV} corresponds to decreasing the desorbent stream. However, increasing m^{IV} leads to a rapid shrinking of the separation region, see Fig. 5 [PII-5]. A breakthrough of the shock of the weaker adsorbing component from zone *IV* into zone *I* should not be allowed since it causes a drastic decrease of the extract purity. Instead the latter should be controlled by permitting mixed simple waves within both zones *I* and *II*.

These observations were supported by an optimization study performed with the stage model. All four *m* values were optimized simultaneously. The results in Fig. 6 [PII-5] underline that this facilitates significantly improved process performance in comparison to requiring complete regeneration.
The concentration profiles for a one of the optimization are shown as an example in Fig. 3.6 (more examples can be found in Fig. 9 [PII-5]). An analysis in the frame of equilibrium theory reveals that this scenario differs from the case of complete separation and regeneration discussed in Sections 2.3 and 3.3.1. The hodograph representation in Fig. 3.6 exhibits several particular features:

- The raffinate R is located on the intersection of a Σ_+, the Σ_- through *III*, and the line defining its purity.
- The state in zone *II* is on the Γ_+ characteristic through the feed F[1].

---

[1] In [PII-5] it was stated that the states α and *III* left and right of the feed are "identical". This is not correct, as can be observed in Fig. 3.6. The states α, *III* and F lie on the straight line in the hodograph defined by the material balance around the feed, just as discussed for α, β (which is here denoted as *III*) and F in Section 3.3.1. However, it can be seen from the equations in [PII-5] that this erroneous assumption is *not* used in the design method.
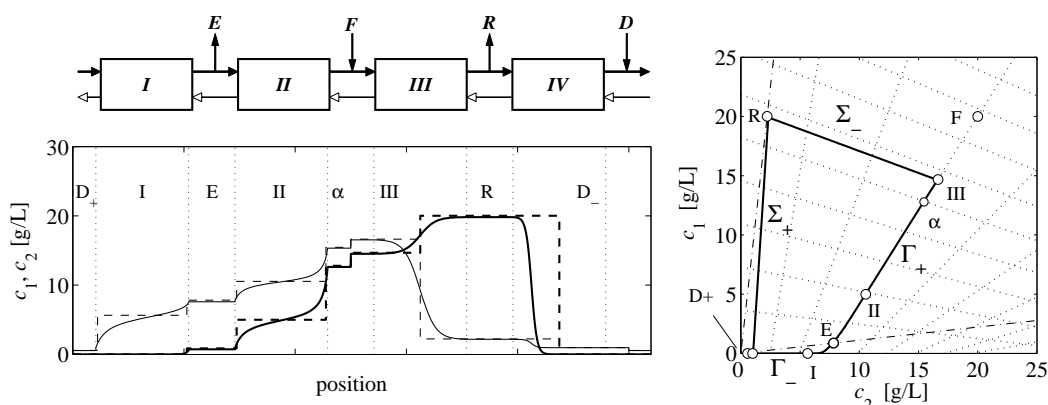
Figure 3.6 – Concentration profiles obtained from the shortcut design method in comparison to an optimization of all four m values in a TMB stage model. Raffinate and extract purity equal to 90%. Left – internal concentration profiles, right – hodograph representation. Solid lines – TMB model with 100 stages/zone, dashed – equilibrium theory, thick – weak adsorbing component 1, thick – strong adsorbing component2, symbols (right) – equilibrium theory, dash-dotted – purity requirements. For parameters see [PII-5].

- The extract E lies on a boundary discontinuity.
- The state in zone I is on a Γ_- characteristic with $c_1 = 0$ and $c_2 \neq 0$.

These findings were incorporated into the formulation of the material balances and wave velocities for the process in the frame of equilibrium theory. The resulting set of nonlinear equations can be solved to give the four optimal m values for a given set of purity requirements. The results shown in Fig. 6 [PII-5] and Fig. 7 [PII-5] match very closely those of the numerical optimization. A simple formulation with only three implicit equations is given in Appendix B of [PII-5].

Finally, it should be mentioned that the proposed method has limitations with respect to the minimal purities that can be applied. The corresponding minimum values are found when the state in zone I reaches the Γ_+ characteristic through F and/or the state in zone II reaches the feed composition.

A possible future extension of the approach would be to combine it with the shortcut design method for bi-Langmuir isotherms proposed in Section 3.3.1.

3.3.3 Gradients of Adsorbing Additives

Applying adsorbing additives as discussed in Section 3.1 for batch chromatography could also be an interesting strategy in SMB processes. A similar ternary problem was already analyzed in the frame of equilibrium theory in [116]. While
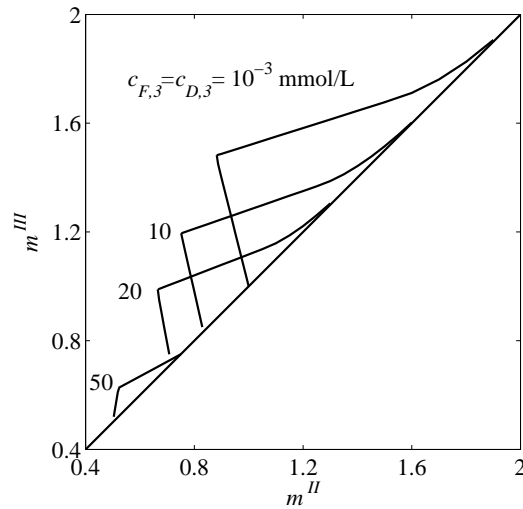
Figure 3.7 – Regions of complete separation for components 1 and 2 as function of concentration of the additive (component 3) in desorbent and feed. Additive strongest adsorbing. $c_{F,1} = c_{F,1} = 10$ mmol/L. For isotherm parameters see Fig. 3.1.

there focus was on the conditions for separation in zones *II* and *III*, here the influence of the additive on all zones is discussed.

For illustration the case of the additive being the strongest adsorbing component is considered for a system with Langmuir isotherms. The parameters applied are the same as given in Fig. 3.1, corresponding to the enantiomers of Alprenolol in [PII-4].

For the investigation, the Riemann problem illustrated in Fig. 2.5 in Section 2.3 was solved for all zones of a TMB process together with the mass balances between the zones. Complete regeneration of zones *I* and *IV* from the weakest and intermediate adsorbing components was required.
The resulting set of nonlinear equations was solved in Matlab. Like in Section 3.1 the ω-transform [84] is applied because it simplifies the implementation to some extent and facilitates a visual inspection of the solution paths, at least for the ternary problem at hand.

Based on the implementation the regions of complete regeneration can be determined numerically. Figure 3.7 shows selected regions for different additive concentrations adjusted to the same values in the feed and the desorbent streams, $c_{F,3} = c_{D,3}$. Similar to the binary case – the region for 10^{-3} mmol/L is basically identical to that found for a binary system from the expressions in [128] – one observes that the separation region shrinks with increasing additive levels, but the
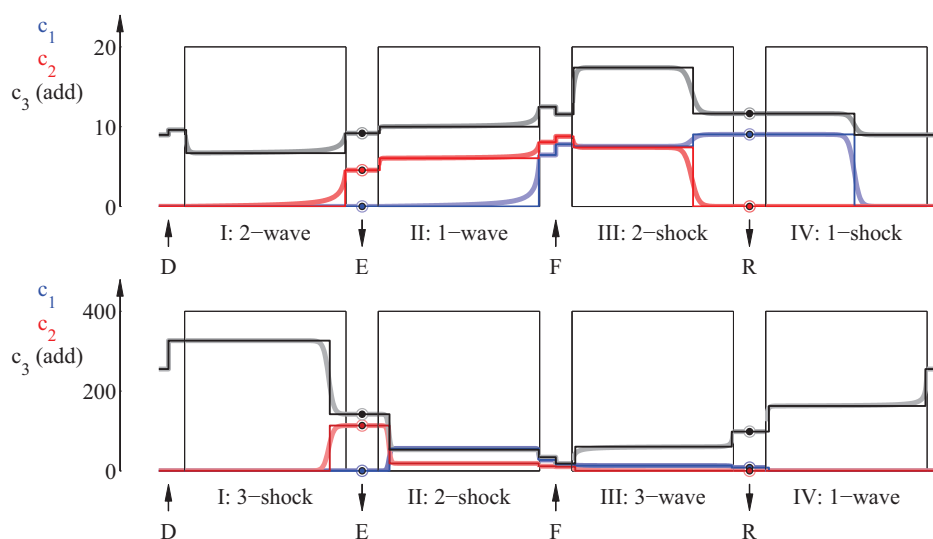
Figure 3.8 – Change of the type of transition in the zones by changing the additive level in the desorbent. Additive strongest adsorbing. Top – additive concentration $c_{D,3} = 10$ mmol/L, bottom – $c_{D,3} = 400$ mmol/L. Feed concentrations $c_{F,1...3} = 10$ mmol/L. Shaded lines – simulation using a TMB stage model with 10.000 stages. For isotherm parameters see Fig. 3.1. Notation of transitions according to [84].

regions are shifted towards lower m-values.

At the same time, for increasing $c_{F,3} = c_{D,3}$ process performance deteriorates in the optimal operating points. In contrast, performance improves with $c_{F,3} = c_{D,3}$ for the other two enantiomeric systems in [PII-4], where the additive is weakest (Atenolol) or indermediate (Propranolol) adsorbing, respectively.

Using the approach also the possible consequence of an additive gradient can be illustrated. A comparison between the optimal operating points for an isocratic and a gradient case is given in Fig. 3.8. In the former case, where the concentrations are comparable to the experimental conditions used earlier for the Alprenolol system [133], the types of the transitions in the zones – simple waves in zones *I* and *II* and shocks in *III* and *IV* – are the same as familiar from binary separations. On the other hand, the concentration profiles indicate that already this case will pose challenges in practical implementation where exact competitive isotherm parameters are usually not known for such system.

The situation gets more involved when increasing the additive level in the desorbent as in the lower part of Fig. 3.8. Here the types of transitions change for all zones from simple waves to shocks and *vice versa*.

Independent of the last extreme example, gradients of adsorbing additives can result for all cases in an improved performance, independently of the adsorptivity the additive. For a weaker or intermediate adsorbing additive an increased additive level in the desorbent is beneficial. For a strong adsorbing additive a positive effect is obtained only for a very high values of $c_{D,3}$ that correspond to the situation in the lower panel in Fig. 3.8.

On the other hand, as mentioned for batch chromatography, very high stage numbers are required to take advantage of such gradients. Furthermore, applying high additive concentrations will create additional downstream costs. A detailed study of the possible performance for such systems should thus be performed for industrially relevant conditions.

Apart from that, the observations above underline that in the design of SMB processes that employ an adsorbing additive all four zones should be considered in the design.

3.4   Optimal Column Arrangements

At the close of this chapter the optimal arrangement of a set of identical chromatographic columns is addressed. This approach might also be classified into the process combinations treated in the next chapter. However, it is categorized here under "advanced operating modes" because only units of the same type (chromatography) are combine with each other, while the next chapter is reserved to schemes that combine chromatography with unit operations of a different type.

Batch chromatography is still the method of choice for multi-component separations, although also ternary SMB variants were suggested, see *e.g.* [PII-1]. A common situation in industrial practice is that several identical columns are available – for example those in an SMB plant.

An obvious question in such case is how these columns should be arranged in an optimal (batch) process. The enclosed manuscript [PII-6] covers the scenario for using eight identical columns for a ternary separation with an intermediately adsorbing target component. The work extends the binary separation problem with five columns discussed in [14].

A set of eight columns facilitates a significant number of arrangements. A few examples are depicted in Fig. 1 [PII-6]. Besides 22 possible setups of batch columns in series or parallel, also 6 SMB-batch combinations and 2 SMB/SMB configurations are considered. The different options were evaluated based on the equilibrium-dispersive model by optimizing the operating conditions. These are

injection volume, cycle time and flow rate in batch systems, and (additionally) the m values for SMB units. The combinatorial complexity could be reduced to a certain extent by a formal evaluation approach for the batch setups. This allows evaluating all 22 options based on the results of only eight optimization runs.

Based on this approach it can be studied how different relevant aspects like feed concentration, particle size or purity requirements affect the optimal arrangement. The main findings are along engineering intuition. The particle size is of particular importance in such problem. Larger particles lead to "longer" arrangements with more columns in series. In turn, there exists an optimal particle size for a given column setup. SMB processes tolerate larger particles. Longer column trains are also required when increasing the purity and/or yield requirements.

For the used parameter set it was found that the batch arrangements outperformed the systems that inherited SMB processes. Simple cascades of standard SMB units were found inappropriate.

Although the results in [PII-6] cannot be generalized, it can be concluded that a flexible multi-column batch system is an interesting option for industrial applications.

Chapter 4

Process Combinations

4.1 SSR Chromatography with Solvent Removal

Chromatography utilizes a solvent as auxiliary phase. This usually entails an undesired dilution of the products. There are only few exceptions like in displacement chromatography or when collecting a concentrated intermediate plateau caused by competitive adsorption. The dilution is of major economical importance and plays a role for downstream operations. Combinations with, for example, crystallization or with a chemical reaction in a recycle setup (see next sections) usually require an intermediate concentration step.

Applying a partial solvent removal in SMB chromatography has been already proposed in the EE-SMB concept [44, 45]. As concerns SSR chromatography, it can be shown that the dilution of the recycle fraction (*cf.* Fig. 2 [PII-3]) worsens the higher the required purity. It is plausible that SSR processes would benefit from reducing this effect by a partial solvent removal.

There exist several options for incorporating such enrichment step in SSR processes. Paper [PII-7] analyses them in the frame of equilibrium theory and proposes a shortcut method for *a priori* design similar to that for ideal systems in Section 3.2.

Figure 4.1 shows the three possible options. Depending on whether the solvent removal is performed for the fresh feed itself (option I), within the recycle stream (II), or directly before the column (III), its operating line in the hodograph representation of the SSR process changes, as demonstrated in Fig. 3 [PII-7].

By extending the design approach for conventional SSR processes under ideal conditions one finds an explicit relation between the amount of fresh feed processable per cycle and the volume of solvent removed, see Eq. (22) in [PII-7]. As a result, in addition to the injection width – which is the only free operating para-
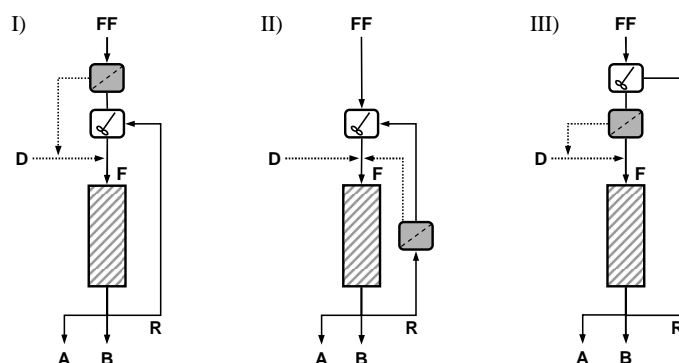
Figure 4.1 – The different options for performing a solvent removal in SSR chromatography [PII-7]. Setup I – enrichment of the fresh feed, II – enrichment of the recycle fraction, III – enrichment before injection.

meter in conventional SSR processes – also the amount of fresh feed introduced per cycle can be considered a design variable.

The three process options perform identically when operated with the same values for fresh feed volume and total injection width. However, they differ with respect to the feasible regions for adjusting these two parameters as shown in Fig. 5 [PII-7]. The scheme I has a rather restricted operational area. Options II and III can process larger fresh feed amounts. The variant III is the most flexible.

As concerns process performance, an SSR process with solvent removal can outperform batch chromatography in terms of eluent consumption, product concentration as well as productivity. Note that the latter does not hold for conventional SSR processes, see Section 3.2.1. While minimum solvent consumption is achieved in the region above the boundary G in Fig. 6 [PII-7], the highest productivity is found along the lines B and F. These findings are also underlined by the results of a parametric study summarized in Fig. 7 [PII-7].

A future extension of this approach should consider limited solubilities of feed components. These will impose additional boundaries on the operation regions.

4.2   Chromatography with Crystallization

A process concept that recently found significant interest is the combination of SMB chromatography and (enantio)selective crystallization [137, 144–148], where an SMB process delivers an only partially separated mixture and the pure product is obtained from a "cheaper" enantioselective crystallization. The approach exploits the fact that the performance of chromatography often improves significantly when lowering the purity requirements. Its overall benefit rises with increa-
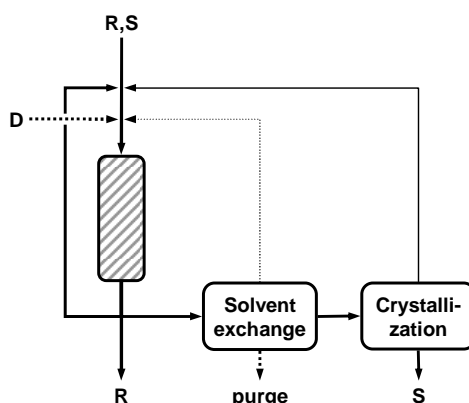
Figure 4.2 – Combination of chromatography and crystallization for the production of a pure target enantiomer *S* from a racemic mixture. Thin lines denote possible recycles of solvent and mother liquor that were not performed in the experiments.

sing purity demands [137, 146]. Figure 4.2 shows a scheme of the process, which is explained in more detail in Section 7.1 of [PII-1]. Note that usually a solvent removal is required as was discussed in the previous section.

Most of the mentioned investigations of this process combination focus on its laborious optimal design using more or less detailed models. In this context the simple shortcut design methods for SMB and SSR chromatography for limited purity requirements in Sections 3.2 and 3.3.2 are of obvious interest.
Up to now only few experimental studies were published. Below a challenging enantioseparation of an undisclosed pharmaceutical compound is investigated. The scope of the combination is extended to the application of SSR chromatography. Focus of the discussion is on chromatographic aspects.

Producing the desired weaker adsorbing enantiomer of the compound by batch chromatography was not economical, in spite of a separation factor of 1.42 under linear conditions. The reason is a peculiar adsorption behavior. Experiments with pure enantiomers and mixtures indicated a partially collaborative adsorption. Competitive isotherm parameters were determined by applying the inverse method ("peak fitting") simultaneously to a number of different experimental chromatograms. For a sufficiently accurate modelling the following complex and somewhat empirical isotherm model had to be developed:

$$q_i = \gamma c_i + q_S^I \frac{b_i^I c_i}{1 + \sum_j c_j b_j^I} + q_S^{II} \frac{b_i^{II} c_i + 2b_{q,i} c_i^2 + b_m c_1 c_2}{1 + \sum_k c_k b_k^{II} + \sum_n b_{q,n} c_n^2 + b_m c_1 c_2} \quad (4.1)$$

with $i = (1,2)$ and $j,k,n = 1 \ldots 2$. The model assumes linear (γ), Langmuir-type
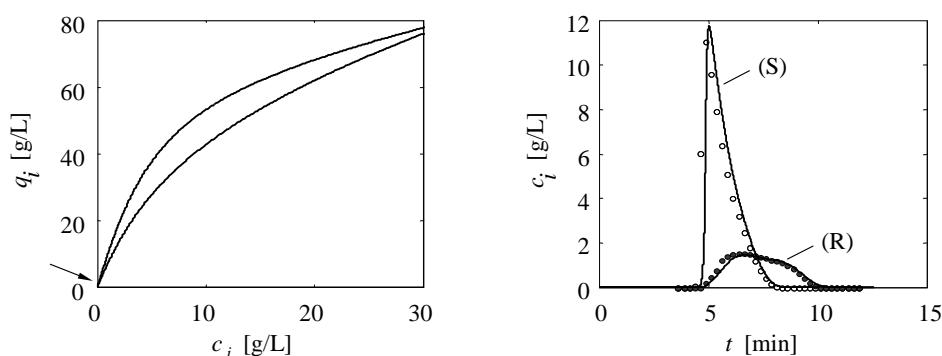
Figure 4.3 – Left – Competitive adsorption isotherms for the pharmaceutical component for $c_R = c_S$. The arrow indicates the concentration range where an inflection point occurs in the isotherm of the stronger retained species. Right – Model validation. Experiment (symbols) and simulated (lines) results for the injection of an asymmetric mixture.

Parameters. Isotherms, Eq. (4.1): $\gamma = 0.6331$, $q_S^I = 64.7$ g/L, $b_1^I = 0.0316$ L/g, $b_2^I = 0$, $q_S^{II} = 46.8$ g/L, $b_1^{II} = 0.1035$ L/g, $b_2^{II} = 0.2056$ L/g, $b_{q,1} = 0.0056$ L^2/g^2, $b_{q,2} = 0.0258$ L^2/g^2, $b_m = 0.0188$ L^2/g^2. Experiment: $c_{inj} = 20$ g/L (total, S:R = 3:1), $V_{inj} = 2$ mL, 2 mL/min.

(*I*) and competitive-collaborative adsorption on another adsorption site (*II*). Regarding the latter, interactions between the same species ($b_{q,i}$) and among the two enantiomers (b_m) are considered. Figure 4.3 shows the isotherms and one of the experiments performed to validate the used transport-dispersive model.

Despite the existence of an inflection "point" in the isotherm of the stronger adsorbing *R* at, for example, $c_R = 0.53$ g/L for $c_S = 0$ and at $c_S = c_R = 0.22$ g/L, the tail of the second component remains sufficiently constant over a wide range of injection parameters. Therefore the shortcut design method for SSR chromatography under nonideal conditions described in Section 3.2.2 could be applied to investigate the possible performance of an SSR process.

Figure 4.4 shows the obtained results for the a "symmetrical" purity requirement of 95% for both fractions, which was identified as suitable operating point. Note that in this case the optimal performance is not achieved by maximizing the feed concentration, but for an intermediate value of about $c_S = c_R = 12.5$ g/L. The figure reveals that the SSR process achieves a significantly better performance than a batch separation. Productivity is about 120% higher and solvent consumption 57% lower, respectively. The product concentrations (not shown) increase by 222% and 93%, respectively.

The mentioned operating point was then applied in an SSR experiment using an analytical column and the experimental setup in Fig. 3.2. The process was successfully started into immediate steady state by the procedure described in
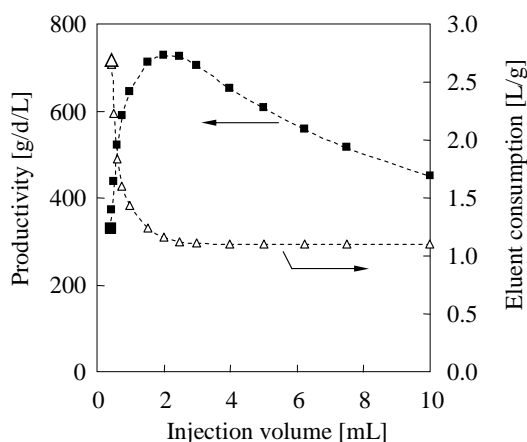
Figure 4.4 – Predicted performance of SSR chromatography as function of the injection volume for the pharmaceutical compound. Calculated using the shortcut method for nonideal systems in Section 3.2.2 for a purity of 95% for both fractions and an injection concentration of 25 g/L (rac.). Enlarged symbols mark the optimal operating point of batch chromatography when requiring the same yield and purity.

Section 3.2.2. After a total of 126 cycles (16 hours), 775 mL of the first product fraction were obtained with a purity of 93.4% (design value: 95%). This corresponds to a productivity of about 270 g/d/L. This is lower than the possible 730 g/d/L indicated in Fig. 4.4 because strict safety margins were applied between the cycles.

From the collected solution a total of 470 mg solid (S)-enantiomer was crystallized in enantiomerically pure form, which corresponds to a yield of 54%. Note that a rather conservative procedure was applied at this initial stage in order to keep a sufficient distance to the eutectic composition at 67%.[1]

The promising results of these initial experiments motivated the investigation of the more advanced process concept covered in the next section, where not only the recycle of the mother liquor (thin lines in Fig. 4.2) was practically implemented, but additionally a racemization of the (R)-enantiomer was performed to improve the overall yield.

4.3   Chromatography with Isomerization Reactions

The separation processes considered so far split a feed mixture into two fractions that fulfill given purity requirements. However, often only one of the components

---

is desired as product while the others are of no particular interest. This is particularly true in enantioseparations, since typically only one of the enantiomers has the desired physiological effect.

The production and subsequent separation of a 50/50 mixture of two enantiomers, which is a common industrial practice, therefore inherently limits the possible overall yield to 50% only. For a number of compounds this can be overcome by devising a combining of the (chromatographic) separation with an isomerization of the undesired enantiomer. The latter is denoted as racemization, and occurs in some cases spontaneously. It can also be triggered (bio)catalytically, under basic or, less frequently, acidic conditions.

The conventional approach for a corresponding process is to perform a racemization at the outlet of the undesired species and to recycle the racemized solution back to the inlet of the separation process. Such processes are discussed in [149–152] and [PII-9], [PII-10].

Besides the few mentioned theoretical works there is a lack of experimental results that would demonstrate a coupling of these unit operations with an actually closed recycle. An attempt in this direction was made by the author for the spontaneously racemizing enantiomers of Chlorthalidone by combining an SSR process with a homogeneous racemization in a heated vessel [152]. However, a reasonable steady state was not reached due to a strongly diluted recycle. A partial solvent removal would be required there.

Here the case study for the pharmaceutical compound from the previous section is continued for a combination of batch chromatography and a homogeneous catalytic racemization of the (R)-enantiomer. The concept is further extended by also including the enantioselective crystallization step discussed in the previous section. Again, focus will be on chromatographic aspects.

Figure 4.5 shows the complete flowsheet for this process. The racemization is performed here using a homogeneous catalyst. It can be seen that besides the three main units chromatography, crystallization and racemization also several solvent-related operations are performed. These are performed mainly to withdraw eluent components that are not compatible with the conditions required for crystallization or racemization. An interesting aspect is that the racemization is actually concluded by another crystallization step (not shown) in order to separate the racemate from the homogeneous catalyst.

The concept was validated experimentally at preparative scale by an industrial partner. For an optimal design the following main parameters have to be specified: flow rate, injection volume, and injection concentration in chromatography;
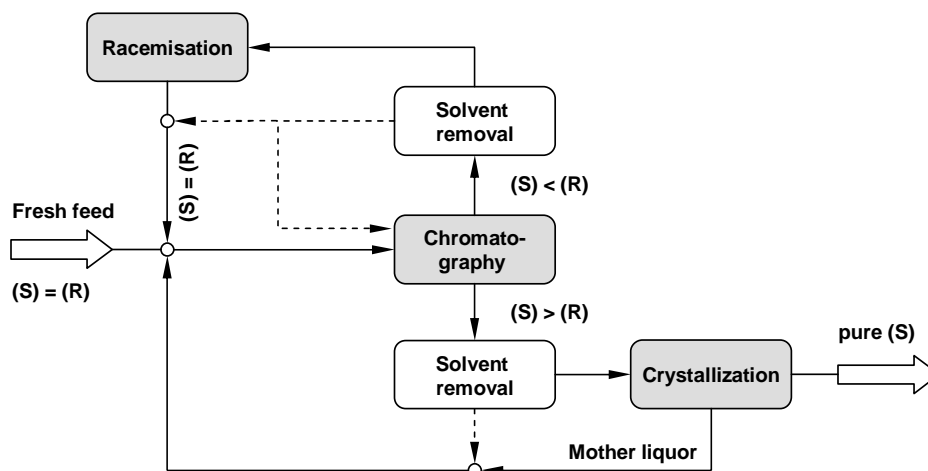
Figure 4.5 – Process combination of chromatography, enantioselective crystallization and racemization for the production of a single pure enantiomer at a yield of 100%.

coupling purity between chromatography and crystallization, coupling purity between chromatography and racemization, and final purity of the mother liquor in crystallization.

The flow rate was determined as 236 mL/min in a conventional scale up from the analytical 25×0.46 cm column used in Section 4.2 to a given 25×5 cm column by keeping constant the interstitial velocity. The purity of the mother liquor was specified to 75% to guarantee a safety margin to the eutectic of 67%.

An initial optimization for the remaining parameters using a conventional simplex algorithm [153] in MATLAB minimizing the ratio of productivity and eluent consumption showed poor convergence. This appears related to the simultaneous optimization of injection volume and feed concentration. Since it is known that concentration overloading is usually superior to volume overloading [154], it could be better to replace the two variables by the injected amount.

Since here it was also of interest to confirm the intermediate feed concentration found optimal for the SSR experiments in Section 4.2. Thus, a dense "scanning" of the operating parameters was performed. The optimal values found are an injection volume of 180 mL, racemic injection concentration of 24 g/L (similar to Section 4.2), a coupling purity to crystallization of 89 %, and a coupling purity to racemization of 76 %.

These operating parameters lead to an adequate overall process performance with a productivity of 469 g/d/L and a solvent consumption of 1.56 L/g. Most importantly, the process achieves an overall yield of 99.8% [2].

---

[2]The missing 0.2% are due to the fractionation strategy in chromatography that is based on

Based on this design the process was implemented and tested by an industrial partner [155–157]. Several cycles were performed where each processing step was performed batch-wise and the process was found sufficiently stable. This is considered as a successful validation of the concept.

Before concluding, it is interesting to note that in the optimal operating point both streams from chromatography have limited purity. This underlines again the usefulness of the corresponding design methods for SMB and SSR chromatography in Chapter 3. The methods can be extended for the process combination above by determining the feed composition for chromatography through corresponding mass balances.

Finally, the task of maximizing the yield by including an isomerization can also be accomplished by the reactive SMB processes expounded in Chapter 5.

4.4 Optimal Synthesis of Process Combinations

The case study in the previous sections illustrates that a number of competing process alternatives exist for producing a single enantiomer. Already when considering the possible combinations of an SMB unit with selective crystallization immediately four possible schemes are recognized: stand-alone chromatography, a single crystallizer at either one of the two outlets, or two at both outlets [146]. Taking into account also racemization, solvent removal, re-crystallization, purge streams, etc. it becomes evident that identifying all options is already tedious, let alone deciding on the optimal one.

In conventional process synthesis all useful process candidates are identified at first, then designed on the basis of suitable models, and finally evaluated against each other. Often this must be repeated if a different substance should be produced, because the economically optimal setup depends on process requirements, properties of the substance, operational constraints and cost factors.

An interesting alternative is to formulate this task as a mixed-integer nonlinear programming (MINLP) problem. This allows finding the optimal process by simultaneously optimizing the structure and the operating parameters. The approach is based on defining a suitable superstructure that inherits all useful process alternatives. Integer numbers with a value of either zero or unity serve as structural decision variables specifying the existence of a unit or stream. Operating parame-

---

threshold concentrations.

ters are continuous variables. This approach is well-known in particular for the synthesis of distillation sequences and heat exchanger networks [158–160].
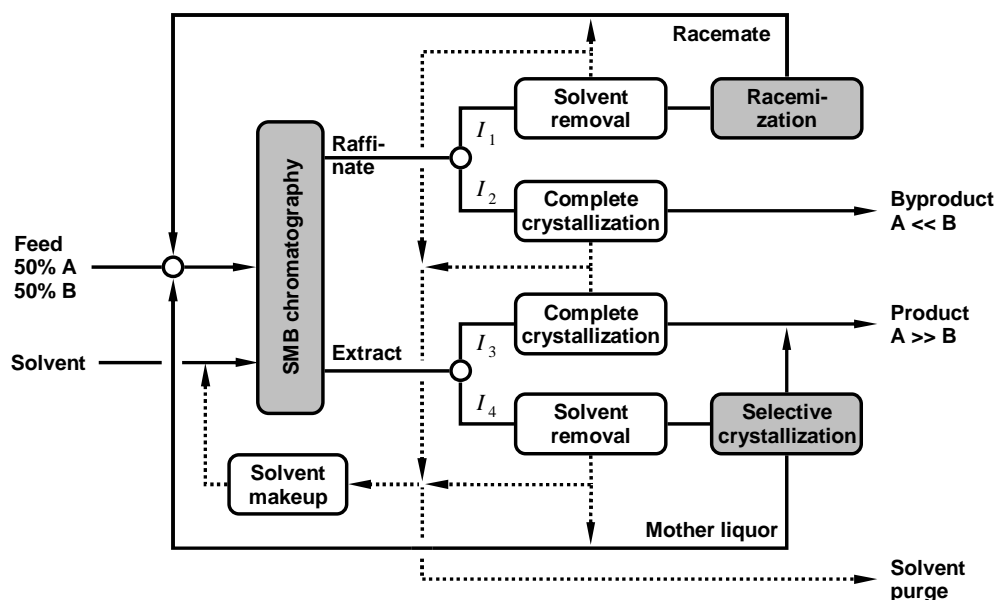
Figure 4.6 – Superstructure for the determination of an optimal process for the production of a stronger adsorbed enantiomer *A* from a racemic mixture.

Here this approach was extended to design process combinations for enantioseparations that inherit SMB chromatography. The problem was formulated in the modeling environment GAMS using a similar as in [161]. Figure 4.6 shows an example of an according superstructure. The SMB process is approximated by a steady-state equilibrium stage TMB model. Other units are modeled as simple splitters or mixers.

The integer variables $I_j \in \{0,1\}$, $j = 1\ldots 4$ are multiplied with the flow rates at the indicated positions. As constraints it is required that $I_1 + I_2 = 1$ and $I_3 + I_4 = 1$. This renders possible four different "trains" at the two SMB outlets. They can represent product ports ($I_1 = 0, I_2 = 1$) and ($I_3 = 1, I_4 = 0$), connected to the crystallizer ($I_3 = 0, I_4 = 1$), or sent to racemization ($I_1 = 1, I_2 = 0$), respectively.

The MINLP problem is solved in GAMS using SBB, a standard branch and bound method, in connection with the multi-method NLP solver CONOPT.

Different scenarios were investigated [157] minimizing cost functions of different degree of detail. Each of the inherited sub-structures can be identified as optimum, depending on the definition of the various possible cost factors and constraints on purity, yield, eutectic composition, etc.

Before concluding this section a few remarks seem useful. In principle the two trains defined by I_3 and I_4 in Fig. 4.6 could be replaced by a single crystallizer with a recycle ratio as NLP variable. However, a complete crystallization with total solvent removal has a different scope and cost function than a selective crystallization.

A limitation of this approach is related to the selective crystallization. To fully exploit the potential of such process combination, an optimum balance between column efficiency and pressure drop has to be found for the SMB process [137, 147]. A scale-up procedure based on a pressure drop relation and the van-Deemter equation as in [137, 146] was implemented. Yet, a reliable method for matching the dispersion between TMB and SMB models is lacking, which limits the accuracy of the predictions. A detailed design requires optimization using an SMB model as applied in [147]. A viable option seems also extending the MINLP approach in [63, 162, 163] into this direction.

Apart from such approaches for detailed design, the method illustrated above can serve as a valuable tool for a basic initial design of corresponding flowsheets.

Chapter 5

Integrated Reactive Processes

Reactive chromatographic processes combine a chemical reaction and the chromatographic separation of the products into a single apparatus, usually with the goal of improving the conversion for equilibrium-limited reactions.
Reactive chromatography has been studied intensively for batch and SMB chromatography in particular for reversible reactions with stoichiometries of $A \rightleftharpoons B + C$ and $A + B \rightleftharpoons C + D$, see *e.g.* [15, 17–23, 82, 83, 85, 164]. The majority of publications investigates esterifications, ester hydrolyses and transesterifications due to the favourable adsorptivity of the components and the catalytic activity of the used stationary phases.

In the following the focus is on aspects and concepts less frequently considered in reactive chromatography. Section 5.1 studies the role of temperature effects in reactive liquid chromatography. In Section 5.2 investigates the possible integration of SMB chromatography and isomerization reactions. The according stoichiometry $A \rightleftharpoons B$ has rarely been considered for difficult applications like the production of a pure enantiomers from racemates discussed in Chapter 4.

5.1 Thermal Effects in Reactive Chromatography

Thermal effects are usually neglected in non-reactive liquid chromatography by assuming that heats of adsorption are negligible in comparison to the heat transport by the eluent. It will be elucidated below that in non-isothermal reactive liquid chromatography heat effects due to adsorption and reaction should be taken into account.

These aspects are investigated experimentally and theoretically in the enclosed manuscript [PII-8]. The studied model reaction is the esterification of methanol

51

with acetic acid performed at ambient temperature in a thermally insulated semi-preparative column of 47.5 x 2.6 cm, equipped with six thermocouples along the bed. The reaction is catalyzed by the stationary phase, an acidic cation exchanger in H^+ form. The heat of this weakly exothermic reaction is $\Delta_r H = -4.6$ kJ/mol, which is in the order of typical heats of adsorption, at least for reversed-phase chromatography [165].

Fig. 2 [PII-8] shows for a frontal analysis experiment that a moving, self-amplifying thermal wave develops in the column under adiabatic conditions. The overall temperature change is about $+5\,K$, but a maximum temperature increase of 20 K is observed. This is significant and needs to be accounted for when aiming at detailed process modeling.

When performing non-reactive frontal analysis by replacing water from the column with 94% ethanol as shown in Fig. 3 [PII-8], significant effects can also be observed. The endothermic desorption of water causes a sharp negative temperature change, which is almost completely cancelled out by the exothermic mixing of ethanol and water. Finally, when switching to pure ethanol after 50 min, a broad negative temperature response appears. This is caused by the displacement of the strongest adsorbed water molecules.

It is obvious that such temperature waves must affect process performance. Although not applied here, it is worthwhile considering the propagation velocities of concentration wave, u_c, and that of a thermal wave, u_T, as given by equilibrium theory for non-reactive chromatography [84]:

$$u_c = \frac{u}{1 + F\,\frac{\partial q}{\partial c}}, \tag{5.1}$$

$$u_T = \frac{u}{1 + F\,\frac{\rho_s c_{p,s}}{\partial \rho_l c_{p,l}}}. \tag{5.2}$$

The analogy is obvious. The velocity of the temperature wave is controlled by the ration of the heat capacities in Eq. (5.2). Furthermore, it is known that these velocities are coupled through the enthalpies of adsorption. This facilitates an analysis based on reduced variables that represent energy contents [84]. In [PII-8] an analogous approach was used to define the equations of a more detailed model of the reactive problem without having to consider an energy balance.

A numerical study using this model demonstrates that the development of the thermal waves can have beneficial effects. As shown in the elution and temperature profiles in Fig. 4 [PII-8], self-sharpening fronts can develop even for linear

isotherms. On the other hand, also severe tailing is observed towards the end of the elution.

Despite the latter, the thermal waves can improve productivity and conversion in such systems, as shown in Fig. 6 [PII-8]. The main parameter that controls the performance is the mentioned heat capacity ratio in Eq. (5.2).

These results underline that a non-isothermal operation, although it increases the complexity in modeling and design, represents an interesting concept for reactive chromatography.

5.2 Integrated SMB Processes for Equilibrium-limited Isomerization Reactions

Process concepts applying reactive SMB chromatography to equilibrium-limited isomerization reactions could be interesting alternatives to the conventional reactor-separator processes discussed in Section 4.3. However, they have been studied mainly in the context of obtaining products with limited purity as, for example, in the interconversion of sucrose and fructose. Only few works investigate the production of compounds with high purity as required when producing enantiomers. More details on the existing literature can be found in the introductions of [PII-9] and [PII-10].

The reason for the lack of processes for this type of problem is the stoichiometry $A \rightleftharpoons B$ of reversible isomerizations. A simultaneous occurrence of reaction and separation prohibits here obtaining a pure compound at sufficient productivity. As a consequence the functionalities "reaction" and "separation" should be distributed spatially along the chromatographic process. This can be achieved by using side reactors as proposed by Hashimoto [75]. However, as will be shown, side reactors are of limited use when aiming at high product purity.

Below the results of a systematic development of corresponding integrated SMB processes are summarized. Although focus is on producing single enantiomers, it is emphasized that most results are generally valid and can be applied directly to other isomerization problems.

5.2.1 Conceptional Process Development

In a first step, simple TMB models are applied to gain insight into the general behavior and specific requirements on reactive SMB processes with an integrated

racemization.
For this purpose, the three general concepts for process integration shown in Fig. 1 [PII-9] are considered. These are conventional reactor-separator-recycle processes, processes with side reactors, and reactive chromatographic processes (in the following also denoted as "fully integrated"). Based on these concepts, the five processes shown in Fig. 2 [PII-9] can be defined, the first of which reflecting the idea pursued in Section 4.3. The author published first results in this direction for the enantiomers of Chlorthalidone [152].

The performance in terms of the specific eluent consumption is maximized for each scheme using the parameters from [152]. Optimized variables are the m-values in the individual zones as well as the Damköhler numbers in the zones of the integrated processes 4 and 5 in Fig. 2 [PII-9]. This allows creating an optimal spatial distribution of the reaction functionality within these units.

The results in Tables 2 and 3 in [PII-9] can be summarized as follows. The best performance will be achieved by a fully integrated process that utilizes chromatographic reactors with a reaction rate "adjustable" to different values in the individual zones. The reaction should preferably be restricted to the regeneration zone. Furthermore, the achievable benefit increases for the integrated systems with increasing purity requirements, increasing separation factor, and for more favourable reaction equilibria.

The superior performance of these (hypothetical) processes is due to an effect denoted as reaction-assisted regeneration. This means that performing the reaction in the regeneration zone actually facilitates there an easier regeneration of the solid or the fluid phase. This is seen when inspecting the determined m-values. If the weaker adsorbing enantiomer is produced (Tab. 2 [PII-9]), in the reactive zone I of processes 4 and 5 significantly lower m-values suffice for regeneration than required in the non-reactive SMB unit of process 1. Similarly, m^{III} and m^{IV} are higher when the stronger adsorbing species is obtained (Tab. 3 [PII-9]). The data reveal also that this effect is less pronounced for the Hashimoto process.
The m-values actually required for completely regenerating a reactive zone can be determined from equilibrium theory by introducing transformed concentration variables. The necessary values for the case of Langmuir isotherms are tabulated in the manuscript for homogeneous and heterogeneous reactions. Fig. 2 [PII-9] shows them for the mentioned zone I.

A more detailed elucidation of this effect for bi-Langmuir isotherms will be given in Section 5.2.3 together with a design method derived from equilibrium theory for the 3-zone processes.

5.2.2   Optimization-based Synthesis of SMB Processes

In view of the limitations of TMB models and practical implementation, the analysis above is extended in [PII-10] to more realistic SMB processes. In SMB units the existence of several columns in each zone corresponds to having more structural options. A generation of the possible process variants is, thus, more difficult than for the TMB processes considered so far. Therefore here an MINLP approach is applied to simultaneously optimize process setup and conditions. However, due to the periodic nature of SMB processes this is more difficult than for the flowsheets optimization discussed in Section 4.4.

In order to cope with this the five different superstructures shown in Fig. 1 [PII-10] and Fig. 2 [PII-10] were defined that reflect the different concepts for process integration already illustrated in Fig. 1 [PII-9]. The structures inherit a total of 130 possible setups. The models were formulated in the simulation environment DIVA, and the MINLP problem was solved using an evolutionary algorithm.

The trends observed earlier for TMB processes were confirmed in a first step by assuming idealized conditions with established reaction equilibrium and negligible size of side reactors. The fully integrated processes with four and three zones, numbered as 3 and 5 in [PII-10], achieve a better performance than the conventional reactor-separator scheme (1) and the Hashimoto concepts (2 and 4), see Tables 1 and 2 in [PII-10].

These differences increase under more realistic conditions with a limited reaction rate and finite holdup of side reactors. The Hashimoto concept is clearly outperformed by the fully integrated processes, in particular when producing the weaker adsorbing component, see Tab. 4 [PII-10]. A large number of columns and side reactors would be required, see Fig. 4 [PII-10], which in turn limits throughput. Furthermore, the holdup of these reactors necessitates higher flow rates for column regeneration as illustrated in Fig. 5 [PII-10].

The developed three-zone process (5) in Figs. 1 and 2 in [PII-10] appears particularly interesting not only due to its good overall performance, but also for its simple structure without a unit for solvent removal. As discussed earlier, such solvent removal is indeed beneficial, but difficult to implement in practice.

A detailed study of this process demonstrates that it should be capable of producing a pure enantiomer from a racemic mixture. As shown in Fig. 7 [PII-10], the most influential parameter for this process is the adjustable ratio of the reaction rates in the zones responsible for chemical conversion and that in the separation zones, respectively.

As concerns a practical implementation, it is expected that a corresponding ratio can be adjusted in an SMB process by applying a suitable gradient that affects the

reaction kinetics. Envisaged options are gradients of the temperature, pH value, homogeneous catalysts, enzymes, inhibitors, and solvents.

A systematic scanning of the parameter space for the 3-zone process proposed in Section 5.2.2 reveals that there exist, in analogy to the "triangle theory" for non-reactive SMB processes, regions of feasible operating parameters for the m-values. These are shown as functions of the purity requirements and the mentioned reaction rate ratio in Fig. 6 [PII-10] and Fig. 8 [PII-10].

In summary the studies above revealed several interesting ideas for integrated SMB processes that can be applied to isomerization problems. A developed simple three zone process is of particular interest. The following two sections are devoted to the simplified design of this concept and its experimental validation, respectively.

5.2.3   Design Method for a Developed 3-zone Process

The results obtained above for the integrated SMB process with three zones motivate a more detailed investigation. Here in particular the question is addressed whether the separation region shown in Fig. 8 [PII-10] can be determined.

As discussed above the improved performance of the integrated processes stems from the easier regeneration facilitated by the reaction. An analysis in the frame of equilibrium theory for the case of Langmuir isotherms is given in [PII-9].

This analysis is extended here to the bi-Langmuir model. The results are used to derive a design method for the 3-zone processes above that hold in all cases of interest, that is, independently of the desired product, type of reaction (homogeneous or heterogeneous), and for both Langmuir and bi-Langmuir isotherms.

For the sake of brevity mathematical details will be published elsewhere [166].

Required m-values for complete regeneration

The problem to be solved is to calculate the optimal m-values that completely regenerate a zone in which the isomerization reaction occurs. That is, for process 5 in Fig. 1 [PII-10] the minimum value of m^I is desired that displaces the simple wave from this zone (denotes as m_w below). Analogously, for process 5 in Fig. 2 [PII-10] the maximum value of m^{III} is sought for that guarantees that the shock remains stationary in this zone (denoted as m_s).

This problem is studied first numerically for single zones for both scenarios. Figure 5.1 shows the corresponding Riemann problems together with the m-values
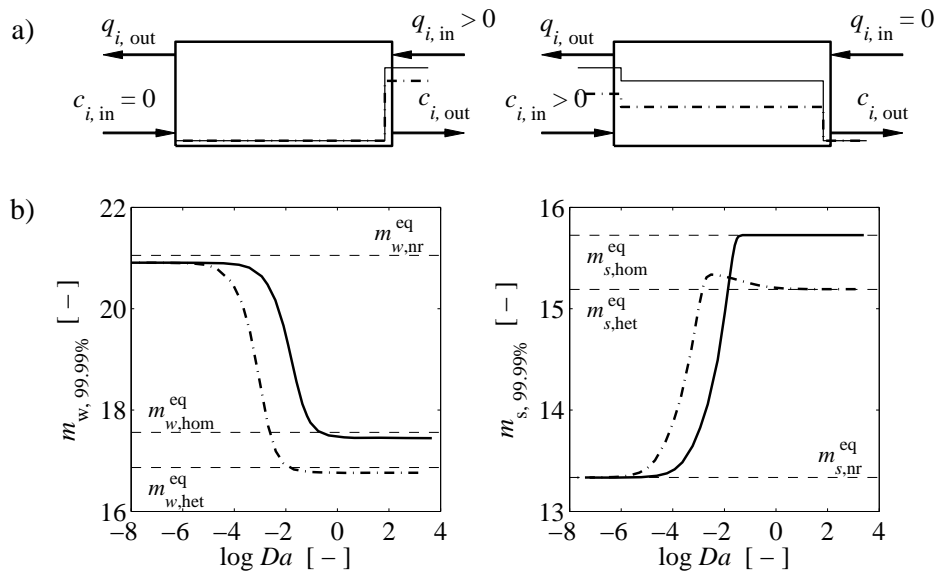
Figure 5.1 – Regeneration of single TMB zones for bi-Langmuir isotherms in the presence of an isomerization reaction. Left – regeneration of solid for a simple wave, achieved if $q_{i,\text{out}} = 0$. Right – regeneration of fluid for a shock, achieved if $c_{i,\text{out}} = 0$. a) Riemann problems considered. b) m-values required for 99.99% regeneration obtained numerically for above scenarios as function of Da for homogeneous (solid lines) and heterogeneous (dashed) reaction. Dashed lines mark the solutions from equilibrium theory (superscript eq) given in Table 5.1 below. Subscripts $\text{eq}, \text{nr}, \text{hom}, \text{het}$ denote equilibrium theory, non-reactive case, homogeneous and heterogeneous reaction, respectively.

Parameters: 500 equilibrium stages, reaction rate constant $k = 10^5 \ \text{min}^{-1}$, other in [PII-10].

Table 5.1 – Optimal m-values for complete regeneration of reactive zones for simultaneously established reaction and adsorption equilibria. The case of Langmuir isotherms is included for $H_{i,2} = 0$.

	Regeneration of fluid for simple wave, m_w	Regeneration of solid for shock, m_s
Non-reactive case	$\sum\limits_{i=1}^{2} H_{A,i}$	$\sum\limits_{i=1}^{2} \dfrac{H_{B,i}}{1 + b_{B,i}c_B}$, $(c_A = 0)$
Homogeneous reaction	$\sum\limits_{i=1}^{2} \dfrac{H_{A,i} + H_{B,i}K_{eq}}{1 + K_{eq}}$	$\sum\limits_{i=1}^{2} \dfrac{H_{A,i} + H_{B,i}K_{eq}}{1 + K_{eq} + (b_{A,i} + b_{B,i}K_{eq})C}$
Heterogeneous reaction	$\dfrac{(1 + K'_{eq})(H_{A,1} + H_{A,2})(H_{B,1} + H_{B,2})}{K'_{eq}(H_{A,1} + H_{A,2}) + (H_{B,1} + H_{B,2})}$	$\dfrac{1 + K'_{eq}}{2K'_{eq}}\left[K'_{eq}q_A/C + q_B/C\right]$

.

that achieve complete regeneration as function of the Damköhler number, Da, for both types of reactions. The effect of the reaction-assisted regeneration discussed earlier is clearly observed. Furthermore, the results are very close to the values predicted by equilibrium theory to be discussed next.

An analysis of the scenarios in Fig. 5.1 a) is possible by introducing transformed concentration variables that take into account the simultaneous reaction and adsorption equilibrium. These transform the mass balances of the reactive case, which is a set of heterogeneous PDEs, into a homogeneous PDE system [85, 167]. This can be solved by the conventional solution strategies of equilibrium theory, as demonstrated in [PII-9] for the case of Langmuir isotherms. This treatment is extended here to the bi-Langmuir model[1].

For the reversible isomerization reaction $A \rightleftharpoons B$ one can define for the fluid and

---

[1]The author is grateful to J. G. Palacios and D. Flockerzi who performed the derivation of the m-values for complete regeneration reported here.

the solid phase,[2]

$$C = c_A + c_B, \qquad (5.3)$$

$$Q = q_A + q_B. \qquad (5.4)$$

For the two desired m-values then holds in analogy to a non-reactive separation,

$$m_w = \left.\frac{dQ(C)}{dC}\right|_{C=0}, \qquad (5.5)$$

$$m_s = \frac{Q(C)}{C}. \qquad (5.6)$$

To calculate the m-values from these equations, explicit expressions of the transformed equilibrium function $Q(C)$ will be useful. These can be found by deriving corresponding relations for $c_i(C)$, as shown below.

For a *homogeneous* reaction,

$$K_{eq} = \frac{c_B}{c_A}, \qquad (5.7)$$

one finds from Eq. (5.3)

$$c_A = \frac{1}{1 + K_{eq}} C, \qquad (5.8a)$$

$$c_B = \frac{K_{eq}}{1 + K_{eq}} C. \qquad (5.8b)$$

For a *heterogeneous* reaction with an reaction equilibrium given by

$$K'_{eq} = \frac{q_B}{q_A}, \qquad (5.9)$$

one finds by a more involved derivation from Eq. (5.9) and Eq. (5.9) a quadratic relation between c_A and C:

$$A_2 c_A^2 - 2A_1(C)c_A + A_0(C) \overset{!}{=} 0, \qquad (5.10)$$

with $\qquad\qquad\qquad\qquad\qquad\qquad\qquad\qquad\qquad\qquad$ (5.11)

$$A_2 = K'_{eq}(a_{12} - a_{11}) + (a_{22} + a_{21}),$$

$$A_1 = \frac{1}{2}\left[(K'_{eq}\gamma_1 + \gamma_2) + (K'_{eq}a_{12} - a_{21} + 2a_{22})C\right],$$

$$A_0 = C(\gamma_2 + a_{22}C),$$

$$\gamma_1 = H_{A,1} + H_{A,2}, \gamma_2 = H_{B,1} + H_{B,2},$$

---

[2]For the sake of simplicity the notation in [PII-10] is applied. Species A is stronger adsorbing than B, $i = 1,2$ correspond to the two terms I and II of the bi-Langmuir model, Eq. (2.5).

$$a_{11} = H_{A,1}b_{A,2} + H_{A,2}b_{A,1} \, , a_{12} = H_{A,1}b_{B,2} + H_{A,2}b_{B,1} \, ,$$
$$a_{21} = H_{B,1}b_{B,2} + H_{B,2}b_{B,1} \, , a_{22} = H_{B,1}b_{A,2} + H_{B,2}b_{A,1} \, .$$

For the isotherm parameters from [152] studied here, A_2 turns out to be non-negative, which leads to

$$c_A = \frac{A_0(C)}{A_1(C) + \sqrt{\left[A_1^2(C) - A_2 A_0(C)\right]}} \, . \tag{5.12}$$

Equations (5.8) and (5.12) can now be substituted into the bi-Langmuir isotherms, Eq. (2.5). From the calculated loadings q_i, $Q(C)$ is calculated from Eq. (5.4) and, finally, the desired m-values from Eqs. (5.5) and (5.6).
Table 5.1 summarizes the resulting expressions for the minimum m_w and maximum m_s for homogeneous and heterogeneous reactions.

Design method

The expressions in Table 5.1 are valuable for deriving a design method for the reactive 3-zone processes, since they readily specify the optimal m-values in the regeneration zones under the requirement case of complete separation. On this basis it is possible to establish regions of complete separation for the remaining two zones of each process configuration.

However, the reactive zones under investigation here require a special consideration. In an SMB system the concentration profiles are moving periodically into and out of a reactive zone, which facilitates a complete conversion of the undesired species and simultaneously a complete regeneration of this zone. However, this is a contradiction in the context of TMB processes, since there a completely regenerated zone would have no capacity for the reaction to take place.

This conflict is resolved by introducing the concept of a *reactive boundary*. This means that the components transported towards a reactive zone are immediately converted once they reach the boundary of the zone. Thus, the liquid (solid) leaving this boundary is in reaction equilibrium with the entering solid (liquid).
The reaction takes place in the zone either right or left of the feed node. Thus, introducing the concept of the reactive boundary allows determining the states left and right of the feed node for each process configuration. The region of complete separation is then found along the lines of the shortcut design method for non-reactive SMB processes explained in Section 3.3.1. The problem is formulated implicitly with the concentrations of the two components either left or right of the feed state as unknowns.
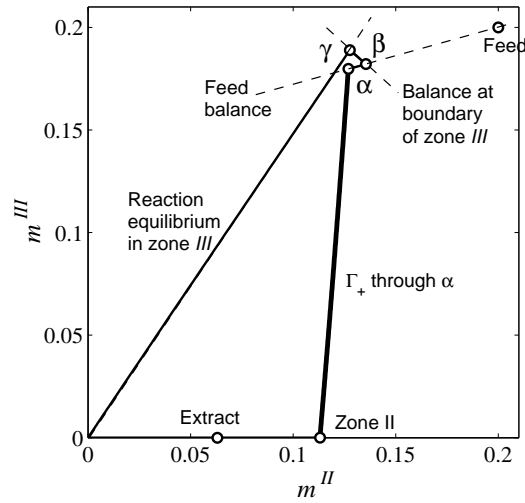
Figure 5.2 – Illustration for the example of producing the stronger adsorbing enantiomer by process 5 in Fig. 2 [PII-10] with a heterogeneous reaction in zone *III*. Symbols – prediction from equilibrium theory, dashed – balances mentioned in the text, solid – TMB model. Parameters: 400 stages per zone, $k_{het} = 10^6$. $m_{I...III} = (25.0, 13.6, 15.395)$, bi-Langmuir isotherms from [PII-10].

This is illustrated for the production of a stronger adsorbing enantiomer by process 5 in Fig. 2 [PII-10] with a heterogeneous reaction taking place in zone *III*. The states α and β are those left and right of the feed *F*. For stream β, which "hits" the reactive boundary, holds $C = c_{A,\beta} + c_{B,\beta}$. This is subjected to reaction equilibrium according to

$$c_A^* = C \frac{K_{eq}'}{1 + K_{eq}'}, \tag{5.13a}$$

$$c_B^* = C \frac{1}{1 + K_{eq}'}. \tag{5.13b}$$

State γ is the composition of the solid leaving the reactive boundary and entering zone *II*, which is in adsorption equilibrium with the c_i^* above. The composition in zone *II* is found from the slope of the Γ_+ characteristic through α as explained in the shortcut method in Section 3.3.1 and shown in the figure. The composition of the extract *E* follows from a simple mass balance around the process.

In a similar manner the design problem can be solved for the remaining three configurations. This is shown in Fig. 5.3. The good agreement with numerically determined separation regions confirms that the developed shortcut design method is suitable for the integrated 3-zone processes.
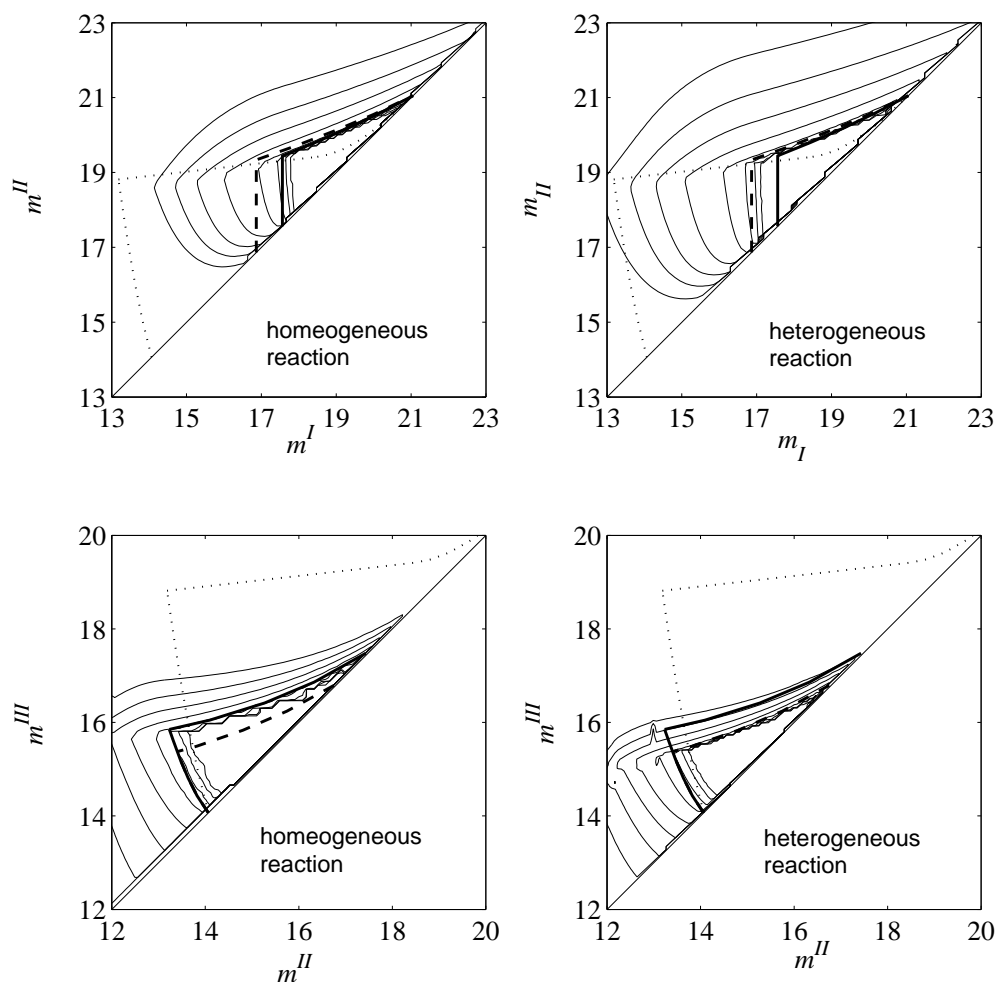
Figure 5.3 – Regions of complete separation predicted for the four possible process configurations of the 3-zone process. Top – production of the weaker adsorbed component *B*, *cf.* Fig. 1 [PII-10]. Bottom – stronger adsorbing component *A*, *cf.* Fig. 2 [PII-10]. Homogeneous reaction (solid, thick lines) vs. heterogeneous reaction (dashed, thick). Numerically determined regions (solid, thin) shown for comparison for purities of 80, 90, 95, 99, 99.9, 99.99, 99.999 and 100 %, respectively. Also for comparison is shown the separation region four a non-reactive four-zone process (dotted) as determined by the method in Section 3.3.1.

Parameters: TMB model with 400 stages per zone, feed $c_{F,i} = 0.2$ g/L, $K_{eq} = K'_{eq} = 1$, reaction rate constants 10^5 min^{-1}. bi-Langmuir isotherms in [PII-10].

5.2.4   Experimental Validation of a Developed 3-zone Process

In the previous sections an integrated 3-zone SMB process was developed that was projected to be capable of producing a single pure enantiomer from a racemic mixture, thereby increasing the yield of such production from 50 to 100%. Below a summary of its experimental validation is given as published in [PII-11].

The enantiomers of Chlorthalidone (CTD) served again as model system. CTD is known to racemize spontaneously at ambient conditions, with a reaction rate depending significantly on temperature and pH value [168, 169]. This lets one expect that a sufficient ratio of the reaction rate, see Section 5.2.2, can be adjusted within the process by either a temperature or pH gradient, respectively. As demonstrated in [PII-9] the pH allows for the stronger manipulation.

In a first step, the initial data on the racemization kinetics as function of temperature in [152] are extended by determining them also as function of the pH value in the range pH=5.3...9.0. Compared to the acidic conditions (pH = 1.0...6.5) applied by Lamparter [169] the reaction rate increases drastically towards pH = 9.0, see Fig. 4 [PII-11].
Regarding the desired strong change of the reactivity within the SMB process, a step gradient from pH=5.3 to 9.0 corresponds to a ratio of the rate constants of 5600, which is much higher than attainable by a temperature shift (*cf.* [152]).
Accordingly, the adsorption isotherms of the CTD enantiomers were determined in this pH range by the inverse method. A bi-Langmuir model with the saturation capacity of the achiral site expressed as a sigmoidal function of the pH value gives a sufficient model accuracy, see Fig. 6 [PII-11].

The determined parameters are used in an SMB model to design the process. Goal is to produce the weaker adsorbing enantiomer at a purity of 100%. It is worth mentioning that this can hardly be accomplished by a Hashimoto setup [170].
Scanning the corresponding region of m-values yields the operating region shown in Fig. 7 [PII-11]. This suggests that a sufficiently large parameter range exists where a pure enantiomer can be produced.

The concept is then investigated experimentally at bench scale for several operating points. The 2-zone open-loop system in Fig. 2 [PII-11] was equipped with two 6.5 x 1.6cm columns per zone. The chosen setup facilitates monitoring the functioning of the reaction assisted regeneration in zone *I* in an additional zone shown on the right in Fig. 2 [PII-11]. The additional zone in the middle was used only to have a symmetrical setup within the used 16-port carousel SMB system.

The purities achieved in the experiments correspond to the design predictions as summarized in Tab. 3 [PII-11]. Values up to the detection limit of 98% were achieved and the occurrence of a reaction-assisted regeneration was affirmed. Small amounts of side products could be reduced by adjusting the feed strategy.

The obtained results confirm that this integrated process is capable of producing a pure single enantiomer at a yield of 100%. The concept can be extended to other types of "reactive" gradients, for example, gradients of temperature, modifiers or additives, homogeneous catalysts, enzymes, or inhibitors of heterogeneous catalysts. It should be readily applicable to further enantiomeric systems and other isomerization problems, provided the compound of interest allows for a sufficient tuning of the reaction rate by a suitable gradient.

Concluding Remarks

The processes and design methods discussed in this work were devised with the goal of further improving the performance and applicability of chromatography for challenging industrial separation problems.

The concepts elucidated in the frame of advanced operating modes demonstrate that a significant potential exists for enhancing the performance of chromatographic separations. The theoretical and experimental results obtained for SSR chromatography underline that such achievements can be made even on the basis of simple process setups. The shortcut design methods for SSR and SMB processes that were developed on the basis of equilibrium theory could help lowering the hurdles for practitioners who are interested in applying these technologies.

Combining chromatography with other separation processes or (bio)chemical reactions exhibits several options to enhance performance. The developed design methods for SMB and SSR chromatography for limited purity requirements are particularly useful for this type of processes. Promising results were obtained in first steps towards industrial implementation of a sophisticated combined process. The optimization-based synthesis of flowsheets was found a viable strategy to cope with the multidude of process alternatives.

Although the considered concepts are based on rather simple ideas, they pose challenges that deserve further practical and theoretical studies related to, for example, their implementation as fully continuous schemes and the dynamic behavior and control of such combined processes.

Finally, also reactive chromatography offers interesting prospects. A new process concept was developed that is suitable for the challenging problem of producing of a pure enantiomer from a racemate at complete yield. Using a generic approach, first the optimal properties of the process were identified and analyzed, before it was translated into a process setup and finally also validated successfully. It is expected that the concept can be extended in different directions and utilized in further application areas.

References

[1] G. Guiochon, D. G. Shirazi, A. Felinger, and A. M. Katti. Fundamentals of Preparative and Nonlinear Chromatography. 2nd Edition, Academic Press, Boston, USA, 2006.

[2] K. Sundmacher, A. Kienle, and A. Seidel-Morgenstern (Eds.). Integrated Chemical Processes. Wiley-VCH, 2005.

[3] A. Tiselius. Displacement development in adsorption analysis. *Arkiv Kemi Min Geol A* 16A (1943) 1–11.

[4] R. S. Alm, R. J. P. Williams, and A. Tiselius. Gradient Elution Analysis – I. A General Treatment. *Act Chem Scand* 6 (1952) 826–836.

[5] K. Anton and C. Berger (Eds.). Supercritical Fluid Chromatography with Packed Columns: Techniques and applications. Marcel Dekker, 1998.

[6] B. Sreedhar and A. Seidel-Morgenstern. Preparative separation of multi-component mixtures using stationary phase gradients. *J Chromatogr A* 1215 (2008) 133 – 144.

[7] P. Jandera and J. Churáček. Gradient Elution in Column Liquid Chromatography: Theory and Practice. Elsevier Science, Amsterdam, 1985.

[8] L. R. Snyder and J. W. Dolan. High-Performance Gradient Elution: The Practical Application of the Linear-Solvent-Strength Model. John Wiley & Sons, Hoboken, New Jersey, 2007.

[9] K. Bombaugh, W. Dark, and R. Levangie. High resolution steric chromatography. *J Chromatogr Sci* 7 (1969) 42.

[10] A. Seidel-Morgenstern and G. Guiochon. Theoretical Study of Recycling in Preparative Chromatography. *AIChE J* 39 (1993) 809–819.

[11] C. Heuer, A. Seidel-Morgenstern, and P. Hugo. Experimental investigation and modelling of closed-loop recycling in preparative chromatography. *Chem Eng Sci* 50 (1995) 1115–1127.

[12] M. Bailly and D. Tondeur. Recycle optimization in non-linear productive chromatography – I Mixing recycle with fresh feed. *Chem Eng Sci* 37 (1982) 1199–1212.

[13] C. M. Grill. Closed-loop recycling with periodic intra-profile injection: a new binary preparative chromatographic technique. *J Chromatogr A* 796 (1998) 101–113.

[14] G. Ziomek, D. Antos, L. Tobiska, and A. Seidel-Morgenstern. Comparison of possible arrangements of five identical columns in preparative chromatography. *J Chromatogr A* 1116 (2006) 179–188.

[15] M. Sardin and J. Villermaux. Synthese de l'Acetate de Menthyle par Chromatographie Reactive. *Chem Eng J* 30 (1985) 91–101.

[16] M. Sardin, D. Schweich, and J. Villermaux. In: G. Ganetsos and P. Barker (Eds.): Preparative and Production Scale Chromatography., vol. 61. Chapter: Preparative fixed-bed chromatographic reactor. Marcel Dekker, 1993 477–521.

[17] M. Mazzotti, D. Gelosa, B. Neri, and M. Morbidelli. Dynamics of a chromatographic reactor: esterification catalysed by acidic resins. *Ind Eng Chem Res* 36 (1997) 3163–3172.

[18] D. Gelosa, M. Ramaioli, G. Valente, and M. Morbidelli. Chromatographic Reactors: Esterification of Glycerol with Acetic Acid Using Acidic Polymeric Resins. *Ind Eng Chem Res* 42 (2003) 6536–6544.

[19] D. Gelosa, A. Sliepcevich, and M. Morbidelli. Chromatographic Reactors with Reactive Desorbents. *Ind Eng Chem Res* 45 (2006) 3922–3925.

[20] T. Falk and A. Seidel-Morgenstern. Comparison between a fixed-bed reactor and a chromatographic reactor. *Chem Eng Sci* 54 (1999) 1479–1485.

[21] P. T. Mai, T. D. Vu, K. X. Mai, and A. Seidel-Morgenstern. Analysis of Heterogeneously Catalyzed Ester Hydrolysis Performed in a Chromatographic Reactor and in a Reaction Calorimeter. *Ind Eng Chem Res* 43 (2004) 4691–4702.

[22] T. D. Vu, A. Seidel-Morgenstern, S. Grüner, and A. Kienle. Analysis of Ester Hydrolysis Reactions in a Chromatographic Reactor using Equilibrium Theory and a Rate Model. *Ind Eng Chem Res* 44 (2005) 9565–9574.

[23] G. Ströhlein, Y. Assuncao, N. Dube, A. Bardow, M. Mazzotti, and M. Morbidelli. Esterification of acrylic acid with methanol by reactive chromatography: Experiments and simulations. *Chem Eng Sci* 61 (2006) 5296–5306.

[24] C. B. Ching and D. M. Ruthven. Experimental-study of a simulated countercurrent adsorption system – IV. Non-isothermal operation. *Chem Eng Sci* 41 (1986) 3063–3071.

[25] C. Migliorini, M. Wendlinger, M. Mazzotti, and M. Morbidelli. Temperature gradient operation of a simulated moving bed unit. *Ind Eng Chem Res* 40 (2001) 2606–2617.

[26] J. Kim, N. Abunasser, P. Wankat, A. Stawarz, and Y.-M. Koo. Thermally Assisted Simulated Moving Bed Systems. *Adsorption* 11 (2005) 579–584.

[27] W. Jin and P. C. Wankat. Thermal operation of four-zone simulated moving beds. *Ind Eng Chem Res* 46 (2007) 7208–7220.

[28] T. B. Jensen, T. G. Reijns, H. A. Billiet, and L. A. van der Wielen. Novel simulated moving-bed method for reduced solvent consumption. *J Chromatogr A* 873 (2000) 149–162.

[29] D. Antos and A. Seidel-Morgenstern. Application of gradients in simulated moving

bed processes. *Chem Eng Sci* 56 (2001) 6667–6682.

[30] S. Abel, M. Mazzotti, and M. Morbidelli. Solvent gradient operation of simulated moving beds. I. Linear isotherms. *J Chromatogr A* 944 (2002) 23–39.

[31] S. Abel, M. Mazzotti, and M. Morbidelli. Solvent gradient operation of simulated moving beds. II. Langmuir isotherms. *J Chromatogr A* 1026 (2004) 47–55.

[32] S. Abel. Design and Operation of Simulated Moving Bed Processes for Fine Chemical and Pharmaceutical Separations. Ph.D. thesis, Eidgenössische Technische Hochschule Zürich (2004).

[33] N. Gottschlich and V. Kasche. Purification of monoclonal antibodies by simulated moving-bed chromatography. *J Chromatogr A* 765 (1997) 201–206.

[34] J. Houwing, S. H. van Hateren, H. A. H. Billiet, and L. A. M. van der Wielen. Effect of salt gradients on the separation of dilute mixtures of proteins by ion-exchange in simulated moving beds. *J Chromatogr A* 952 (2002) 85–98.

[35] J. Houwing, T. B. Jensen, S. H. van Hateren, H. A. H. Billiet, and L. A. M. van der Wielen. Positioning of salt gradients in ion-exchange SMB. *AIChE J* 49 (2003) 665–674.

[36] L. Gueorguieva, L. F. Vallejo, U. Rinas, and A. Seidel-Morgenstern. Discontinuous and continuous separation of the monomeric and dimeric forms of human bone morphogenetic protein-2 from renaturation batches. *J Chromatogr A* 1135 (2006) 142–150.

[37] P. Li, G. H. Xiu, and A. E. Rodrigues. Proteins separation and purification by salt gradient ion-exchange SMB. *AIChE J* 53 (2007) 2419–2431.

[38] R.-M. Nicoud, M. Perrut, and G. Hotier. Method and apparatus for fractionation of a mixture on a simulated fluidized bed in the presence of a compressed gas, a supercritical fluid or a subcritical liquid. U.S. patent 5 422 007 (1995).

[39] J.-Y. Clavier, R. M. Nicoud, and M. Perrut. In: P. R. von Rohr and C. Trepp (Eds.): High-Pressure Chemical Engineering. Chapter: A new efficient fractionation process: The simulated moving bed with supercritical eluent. Elsevier Science, London, 1996.

[40] M. Mazzotti, G. Storti, and M. Morbidelli. Supercritical fluid simulated moving bed chromatography. *J Chromatogr A* 786 (1997) 309–320.

[41] O. D. Giovanni, M. Mazzotti, M. Morbidelli, F. Denet, W. Hauck, and R. M. Nicoud. Supercritical fluid simulated moving bed chromatography II. Langmuir isotherm. *J Chromatogr A* 919 (2001) 1–12.

[42] A. Depta, T. Giese, M. Johannsen, and G. Brunner. Separation of stereoisomers in a simulated moving bed-supercritical fluid chromatography plant. *J Chromatogr A* 865 (1999) 175–186.

[43] M. Johannsen, S. Peper, and A. Depta. Simulated moving bed chromatography

with supercritical fluids for the resolution of bi-naphthol enantiomers and phytol isomers. *J Biochem Bioph Meth* 54 (2002) 85–102.

[44] S. Abdelmoumen, L. Muhr, M. Bailly, and O. Ludemann-Hombourger. The M3C Process: A New Multicolumn Chromatographic Process Integrating a Concentration Step. I - The Equilibrium Model. *Sep Sci Technol* 41 (2006) 2639–2663.

[45] G. Paredes, H. K. Rhee, and M. Mazzotti. Design of simulated-moving-bed chromatography with enriched extract operation (EE-SMB): Langmuir isotherms. *Ind Eng Chem Res* 45 (2006) 6289–6301.

[46] J. S. Hur and P. C. Wankat. Hybrid simulated moving bed and chromatography systems for center-cut separation from quaternary mixtures: Linear isotherm systems. *Ind Eng Chem Res* 45 (2006) 8713–8722.

[47] L. C. Keßler and A. Seidel-Morgenstern. Theoretical study of multicomponent continuous countercurrent chromatography based on connected 4-zone units. *J Chromatogr A* 1126 (2006) 323–337.

[48] R. Wooley, Z. Ma, and N. H. L. Wang. A nine-zone simulating moving bed for the recovery of glucose and xylose from biomass hydrolyzate. *Ind Eng Chem Res* 37 (1998) 3699–3709.

[49] Y. A. Beste and W. Arlt. Side-Stream Simulated Moving-Bed Chromatography for Multicomponent Separation. *Chem Eng Technol* 25 (2002) 956–962.

[50] J. K. Kim, Y. F. Zang, and P. C. Wankat. Single-cascade simulated moving bed systems for the separation of ternary mixtures. *Ind Eng Chem Res* 42 (2003) 4849–4860.

[51] J. S. Hur and P. C. Wankat. New design of simulated moving bed (SMB) for ternary separations. *Ind Eng Chem Res* 44 (2005) 1906–1913.

[52] S. Abel, M. U. Bäbler, C. Arpagaus, M. Mazzotti, and J. Stadle. Two-fraction and three-fraction continuous simulated moving bed separation of nucleosides. *J Chromatogr A* 1043 (2004) 201–210.

[53] G. Paredes, S. Abel, M. Mazzotti, M. Morbidelli, and J. Stadler. Analysis of a Simulated Moving Bed Operation for Three-Fraction Separations (3F-SMB). *Ind Eng Chem Res* 43 (2004) 6157–6167.

[54] M. Kearney and K. Hieb. Time variable simulated moving bed process. US patent 5 102 553 (1992).

[55] E. Kloppenburg and E. D. Gilles. A new concept for operating simulated moving-bed processes. *Chem Eng Technol* 22 (1999) 813–817.

[56] Z. Zhang, M. Mazzotti, and M. Morbidelli. PowerFeed operation of simulated moving bed units: changing flow-rates during the switching interval. *J Chromatogr A* 1006 (2003) 87–99.

[57] O. Ludemann-Hombourger, R. Nicoud, and M. Bailly. The "VariCol" process: a

new multicolumn continuous chromatographic process. *Sep Sci Technol* 35 (2000) 1829–1862.

[58] Z. Zhang, K. Hidajat, A. K. Ray, and M. Morbidelli. Multiobjective Optimization of SMB and Varicol Process for Chiral Separation. *AIChE J* 48 (2002) 2800–2816.

[59] H. Schramm, M. Kaspereit, A. Kienle, and A. Seidel-Morgenstern. Improving Simulated Moving Bed Processes by Cyclic Modulation of the Feed Concentration. *Chem Eng Technol* 25 (2002) 1151–1155.

[60] H. Schramm, A. Kienle, M. Kaspereit, and A. Seidel-Morgenstern. Improved operation of simulated moving bed processes through cyclic modulation of feed flow and feed concentration. *Chem Eng Sci* 58 (2003) 5217–5227.

[61] H. Schramm, M. Kaspereit, A. Kienle, and A. Seidel-Morgenstern. Simulated moving bed process with cyclic modulation of the feed concentration. *J Chromatogr A* 1006 (2003) 77–86.

[62] Z. Zhang, M. Mazzotti, and M. Morbidelli. Continuous Chromatographic Processes with a Small Number of Columns: Comparison of Simulated Moving Bed with Varicol, PowerFeed, and ModiCon. *Korean J Chem Eng* 21 (2004) 454–464.

[63] Y. Kawajiri and L. T. Biegler. Large scale nonlinear optimization for asymmetric operation and design of Simulated Moving Beds. *J Chromatogr A* 1133 (2006) 226–240.

[64] Y. Zang and P. C. Wankat. SMB Operation Strategy – Partial Feed. *Ind Eng Chem Res* 41 (2002) 2504–2511.

[65] Y. Zang and P. C. Wankat. Three-Zone Simulated Moving Bed with Partial Feed and Selective Withdrawal. *Ind Eng Chem Res* 41 (2002) 5283–5289.

[66] D. Acetti, C. Langel, E. Brenna, C. Fuganti, and M. Mazzotti. Intermittent simulated moving bed chromatographic separation of (RS,RS)-2-(2,4-difluorophenyl)butane-1,2,3-triol. *J Chromatogr A* 1217 (2010) 2840 – 2846.

[67] S. Katsuo and M. Mazzotti. Intermittent simulated moving bed chromatography: 1. Design criteria and cyclic steady-state. *J Chromatogr A* 1217 (2010) 1354–1361.

[68] S. Katsuo and M. Mazzotti. Intermittent simulated moving bed chromatography: 2. Separation of Tröger's base enantiomers. *J Chromatogr A* 1217 (2010) 3067 – 3075.

[69] Y.-S. Bae and C.-H. Lee. Partial-discard strategy for obtaining high purity products using simulated moving bed chromatography. *J Chromatogr A* 1122 (2006) 161– 173.

[70] L. C. Keßler and A. Seidel-Morgenstern. Improving performance of simulated moving bed chromatography by fractionation and feed-back of outlet streams. *J Chromatogr A* 1207 (2008) 55 – 71.

[71] S. Li, Y. Kawajiri, J. Raisch, and A. Seidel-Morgenstern. Optimization of simulated

moving bed chromatography with fractionation and feedback: Part I. Fractionation of one outlet. *J Chromatogr A* 1217 (2010) 5337 – 5348.

[72] S. Li, Y. Kawajiri, J. Raisch, and A. Seidel-Morgenstern. Optimization of simulated moving bed chromatography with fractionation and feedback: Part II. Fractionation of both outlets. *J Chromatogr A* 1217 (2010) 5349 – 5357.

[73] G. Ströhlein, L. Aumann, M. Mazzotti, and M. Morbidelli. A continuous, countercurrent multi-column chromatographic process incorporating modifier gradients for ternary separations. *J Chromatogr A* 1126 (2006) 338–346.

[74] J. S. Hur and P. C. Wankat. Two-zone SMB/chromatography for center-cut separation from ternary mixtures: Linear isotherm systems. *Ind Eng Chem Res* 45 (2006) 1426–1433.

[75] K. Hashimoto, S. Adachi, H. Noujima, and Y. Ueda. A new process combining adsorption and enzyme reaction for producing higher-fructose syrup. *Biotechnol Bioeng* 25 (1983) 2371–2393.

[76] B. Cho, R. Aris, and R. Carr. The mathematical theory of a countercurrent catalytic reactor. *Proc R Soc Lond A* 383 (1982) 147–189.

[77] A. K. Ray, R. W. Carr, and R. Aris. The Simulated Countercurrent Moving Bed Chromatographic Reactor – A Novel Reactor-Separator. *Chem Eng Sci* 49 (1994) 469–480.

[78] A. Y. Tonkovich and R. W. Carr. Modeling of the Simulated Countercurrent Moving-Bed Chromatographic Reactor used for the Oxidative Coupling of Methane. *Chem Eng Sci* 49 (1994) 4657–4665.

[79] A. Y. Tonkovich and R. W. Carr. A Simulated Countercurrent Moving-Bed Chromatographic Reactor for the Oxidative Coupling of Methane: Experimental Results. *Chem Eng Sci* 49 (1994) 4647–4656.

[80] A. K. Ray and R. W. Carr. Experimental Study of a Laboratory-scale Simulated Countercurrent Moving Bed Chromatographic Reactor. *Chem Eng Sci* 50 (1995) 2195–2202.

[81] A. V. Kruglov, M. C. Bjorklund, and R. W. Carr. Optimization of the Simulated Countercurrent Moving-Bed Chromatographic Reactor for the oxidative Coupling of Methane. *Chem Eng Sci* 51 (1996) 2945–2950.

[82] M. Mazzotti, A. Kruglov, B. Neri, D. Gelosa, and M. Morbidelli. A Continuous Chromatographic Reactor: SMBR. *Chem Eng Sci* 51 (1996) 1827–1836.

[83] F. Lode, M. Houmard, C. Migliorini, M. Mazzotti, and M. Morbidelli. Continuous reactive chromatography. *Chem Eng Sci* 56 (2001) 269–291.

[84] H.-K. Rhee, R. Aris, and N. R. Amundson. First-order Partial Differential Equations. Vol. II - Theory and Applications of Hyperbolic Systems of Quasilinear Equations. Dover Publications, 2001.

[85] S. Grüner and A. Kienle. Equilibrium theory and nonlinear waves for reactive distillation columns and chromatographic reactors. *Chem Eng Sci* 59 (2004) 901–918.

[86] S. Grüner, M. Mangold, and A. Kienle. Dynamics of reaction separation processes in the limit of chemical equilibrium. *AIChE J* 52 (2006) 1010–1026.

[87] J. Blehaut and R.-M. Nicoud. Recent aspects in simulated moving bed. *Analusis Mag* 26 (1998) M60–M70.

[88] P. S. Gomes, M. Minceva, and A. E. Rodrigues. Simulated moving bed technology: old and new. *Adsorption* 12 (2006) 375–392.

[89] A. Seidel-Morgenstern, L. C. Keßler, and M. Kaspereit. New Developments in Simulated Moving Bed Chromatography. *Chem Eng Technol* 31 (2008) 826–837.

[90] A. Seidel-Morgenstern, L. C. Keßler, and M. Kaspereit. Neue Entwicklungen auf dem Gebiet der simulierten Gegenstromchromatographie. *Chem Ing Tech* 80 (2008) 725–740.

[91] H. Schmidt-Traub (Ed.). Preparative chromatography of fine chemical and pharmaceutical agents. Wiley-VCH, Weinheim, 2005.

[92] D. B. Broughton and C. G. Gerhold;. Continuous Sorption Process Employing Fixed Bed of Sorbent and Moving Inlets and Outlets. U.S. Patent 2 985 589 (1961).

[93] C. Y. Chin and N.-H. L. Wang. Simulated Moving Bed Equipment Designs. *Sep Purif Rev* 33 (2004) 77–155.

[94] M. Czok and G. Guiochon. The physical sense of simulation models of liquid chromatography: propagation through a grid or solution of the mass balance equation. *Anal Chem* 62 (1990) 189–200.

[95] G. Guiochon and B. Lin. Modeling for Preparative Chromatography. Academic Press, San Diego, USA, 2003.

[96] A. Seidel-Morgenstern. Mathematische Modellierung der präparativen Flüssigchromatographie. Deutscher Universitätsverlag, Wiesbaden, 1995.

[97] D. Antos. Gradient techniques in preparative chromatography – Modelling and experimental realization. Oficyna Wydawnicza Politechniki Rzszowskiej, Rzeszów, Poland, 2003.

[98] P. Rouchon, M. Schonauer, P. Valentin, and G. Guiochon. Numerical Solution of Band Propagation in Nonlinear Chromatography. *Sep Sci Technol* 22 (1987) 1793–1833.

[99] A. J. P. Martin and R. L. M. Synge. A new form of chromatogram employing two liquid phases. *Biochem J* 35 (1941) 1358–1368.

[100] L. C. Craig. Identification of Small Amounts of Organic Compounds by Distribution Studies. II. Separation By Counter-current Distribution. *J Biol Chem* 155 (1944) 519–534.

[101] J. Wilson. A theory of chromatography. *J Am Chem Soc* 62 (1940) 1583–1591.

[102] J. Weiss. 81. On the theory of chromatography. *J Chem Soc* (1943) 297–303.

[103] D. DeVault. The Theory of Chromatography. *J Am Chem Soc* 65 (1943) 532–540.

[104] E. Glückauf. Contributions to the theory of chromatography. *P Roy Soc Lond A Mat* 186 (1946) 35–57.

[105] E. Glückauf. Theory of chromatography. Part II. Chromatograms of a single solute. *J Chem Soc* (1947) 1302–1308.

[106] E. Glückauf. Theory of chromatography. VII. The general theory of two solutes following non-linear isotherms. *Discuss Faraday Soc* 7 (1949) 12–25.

[107] P. D. Lax. Hyperbolic systems of conservation laws II. *Comm Pure Appl Math* 10 (1957) 537–566.

[108] F. G. Helfferich. Multicomponent Ion Exchange in Fixed Beds. Generalized Equilibrium Theory for Systems with Constant Separation Factors. *Ind Eng Chem Fund* 6 (1967) 362–364.

[109] F. Helfferich and G. Klein. Multicomponent chromatography. Marcel Dekker, New York, 1970.

[110] H.-K. Rhee, R. Aris, and N. R. Amundson. On the Theory of Multicomponent Chromatography. *Philos T Roy Soc A* 267 (1970) 419–455.

[111] G. Guiochon and S. Golshan-Shirazi. A retrospective on the solution of the ideal model of chromatography. *J Chromatogr A* 658 (1994) 173 – 177.

[112] H.-K. Rhee, R. Aris, and N. R. Amundson. First-order Partial Differential Equations. Vol. I – Theory and Applications of Single Equations. Dover Publications, 2001.

[113] G. Storti, M. Mazzotti, M. Morbidelli, and S. Carrà. Robust design of binary countercurrent adsorption separation processes. *AIChE J* 39 (1993) 471–492.

[114] M. Mazzotti, G. Storti, and M. Morbidelli. Robust design of countercurrent adsorption separation processes: 2. Multicomponent systems. *AIChE J* 40 (1994) 1825–1842.

[115] M. Mazzotti, G. Storti, and M. Morbidelli. Robust design of countercurrent adsorption separation: 3. Nonstoichiometric systems. *AIChE J* 42 (1996) 2784–2796.

[116] M. Mazzotti, G. Storti, and M. Morbidelli. Robust design of countercurrent adsorption separation processes: 4. Desorbent in the feed. *AIChE J* 43 (1997) 64–72.

[117] C. Migliorini, M. Mazzotti, and M. Morbidelli. Robust design of countercurrent adsorption separation processes: 5. Nonconstant selectivity. *AIChE J* 46 (2000) 1384–1399.

[118] A. Seidel-Morgenstern. Experimental determination of single solute and competitive adsorption isotherms. *J Chromatogr A* 1037 (2004) 255–272.

[119] I. Langmuir. The Constitution And Fundamental Properties Of Solids And Liquids. Part I. Solids. *J Am Chem Soc* 38 (1916) 2221–2295.

[120] D. Graham. The Characterization of Physical Adsorption Systems. I. The Equilibrium Function and Standard Free Energy of Adsorption. *J Phys Chem* 57 (1953) 665–669.

[121] S. Jacobson, S. Golshan-Shirazi, and G. Guiochon. Isotherm selection for band profile simulations in preparative chromatography. *AIChE J* 37 (1991) 836–844.

[122] A. Kienle. Nichtlineare Wellenphänomene und Stabilität stationärer Zustände in Destillationskolonnen. Fortschrittsberichte Reihe 3 Nr. 506, VDI Verlag, Düsseldorf, 1997.

[123] E. Kvaalen, L. Neel, and D. Tondeur. Directions of quasi-static mass and energy transfer between phases in multicomponent open systems: Implications in separation science. *Chem Eng Sci* 40 (1985) 1191 – 1204.

[124] D. Flockerzi, M. Kaspereit, and A. Kienle. Spectral properties of modified Langmuir and Bi-Langmuir isotherms. *Chem Eng Sci* (subm.).

[125] F. G. Helfferich and P. W. Carr. Non-linear waves in chromatography : I. Waves, shocks, and shapes. *J Chromatogr A* 629 (1993) 97–122.

[126] M. Mazzotti. Equilibrium theory based design of simulated moving bed processes for a generalized Langmuir isotherm. *J Chromatogr A* 1126 (2006) 311–322.

[127] M. Mazzotti. Design of Simulated Moving Bed Separations: Generalized Langmuir Isotherm. *Ind Eng Chem Res* 45 (2006) 6311–6324.

[128] M. Mazzotti, G. Storti, and M. Morbidelli. Optimal operation of simulated moving bed units for nonlinear chromatographic separations. *J Chromatogr A* 769 (1997) 3–24.

[129] M. F. Doherty and G. Buzad. Reactive distillation by design. *T I Chem Eng-Lond* 70 (1992) 448–458.

[130] H.-K. Rhee and N. R. Amundson. An Analysis of an Adiabatic Adsorption Column: Part I. Theoretical Development. *Chem Eng J* 1 (1970) 241–254.

[131] T. Fornstedt and G. Guiochon. Theoretical Study of High-Concentration Elution Profiles and Large System Peaks in Nonlinear Chromatography. *Anal Chem* 66 (1994) 2116–2128.

[132] T. Fornstedt and G. A. Guiochon. Comparison between Experimental and Theoretical Profiles of High Concentration Elution Bands and Large System Peaks in Nonlinear Chromatography. *Anal Chem* 66 (1994) 2686–2693.

[133] R. Arnell, P. Forssen, and T. Fornstedt. Tuneable peak deformations in chiral liquid chromatography. *Anal Chem* 79 (2007) 5838–5847.

[134] G. Ströhlein, M. Mazzotti, and M. Morbidelli. Analysis of sample-solvent induced modifier-solute peak interactions in biochromatography using equilibrium theory

and detailed simulations. *J Chromatogr A* 1091 (2005) 60–71.

[135] G. Ströhlein, L. Aumann, L. Melter, K. Buscher, B. Schenkel, M. Mazzotti, and M. Morbidelli. Experimental verification of sample-solvent induced modifier-solute peak interactions in biochromatography. *J Chromatogr A* 1117 (2006) 146–153.

[136] I. Duvdevani, J. A. Biesenberger, and M. Tan. Recycle gel permeation chromatography. III. Design modifications and some results with polycarbonate. *J Polym Sci B* 9 (1971) 429–434.

[137] M. Kaspereit, K. Gedicke, A. W. Zahn, V. Mahoney, and A. Seidel-Morgenstern. Shortcut method for evaluation and design of a hybrid process for enantioseparations. *J Chromatogr A* 1092 (2005) 43–54.

[138] D. Schlinge, P. Scherpian, and G. Schembecker. Comparison of process concepts for preparative chromatography. *Chem Eng Sci* 65 (2010) 5373–5381.

[139] P. Scherpian and G. Schembecker. Scaling-up recycling chromatography. *Chem Eng Sci* 64 (2009) 4068 – 4080.

[140] F. Charton, M. Bailly, and G. Guiochon. Recycling in preparative liquid chromatography. *J Chromatogr A* 687 (1994) 13–31.

[141] I. Quiñones, C. Grill, L. Miller, and G. Guiochon. Modeling of separations by closed-loop steady-state recycling chromatography of a racemic pharmaceutical intermediate. *J Chromatogr A* 867 (2000) 1–21.

[142] G. Storti, R. Baciocchi, M. Mazzotti, and M. Morbidelli. Design of Optimal Operating Conditions of Simulated Moving Bed Adsorptive Separation Units. *Ind Eng Chem Res* 34 (1995) 288–301.

[143] A. Rajendran. Equilibrium theory-based design of simulated moving bed processes under reduced purity requirements: Linear isotherms. *J Chromatogr A* 1185 (2008) 216 – 222.

[144] B.-G. Lim, C.-B. Ching, R. B. H. Tan, and S.-C. Ng. Recovery of (−)-praziquantel from racemic mixtures by continuous chromatography and crystallisation. *Chem Eng Sci* 50 (1995) 2289–2298.

[145] H. Lorenz, P. Sheehan, and A. Seidel-Morgenstern. Coupling of simulated moving bed chromatography and fractional crystallisation for efficient enantioseparation. *J Chromatogr A* 908 (2001) 201–14.

[146] M. Kaspereit. Separation of Enantiomers by a Process Combination of Chromatography and Crystallisation. Shaker Verlag, Aachen, Germany, 2006.

[147] M. Amanullah and M. Mazzotti. Optimization of a hybrid chromatography-crystallization process for the separation of Tröger's base enantiomers. *J Chromatogr A* 1107 (2006) 36–45.

[148] K. Gedicke, M. Kaspereit, W. Beckmann, U. Budde, H. Lorenz, and A. Seidel-

Morgenstern. Conceptual Design & Fesibility Study of Combining Continuous Chromatography and Crystallisation for Stereoisomer Separations. *Chem Eng Res Des* 85 (2007) 928–936.

[149] T. Borren and H. Schmidt-Traub. Vergleich chromatographischer Reaktorkonzepte. *Chem Ing Tech* 76 (2004) 805–814.

[150] M. Bechtold, S. Makart, M. Heinemann, and S. Panke. Integrated operation of continuous chromatography and biotransformations for the generic high yield production of fine chemicals. *J Biotechnol* 124 (2006) 146 – 162.

[151] T. Borren. Untersuchungen zu chromatographischen Reaktoren mit verteilten Funktionalitäten. Fortschritt-Berichte VDI : Reihe 3, Verfahrenstechnik 876, 2007.

[152] M. Kaspereit, J. García Palacios, T. Meixús Fernández, and A. Kienle. In: B. Braunschweig and X. Joulia (Eds.): *Computer-Aided Chemical Engineering*, vol. 25 – 18th Europ. Symp. Comp. Aid. Proc. Engng. (ESCAPE-18). Chapter: Systematic Design of Production Processes for Enantiomers with Integration of Chromatography and Racemisation Reactions. 2008, p. 97–102.

[153] J. C. Lagarias, J. A. Reeds, M. H. Wright, and P. E. Wright. Convergence Properties of the Nelder-Mead Simplex Method in Low Dimensions. *SIAM J Optimiz* 9 (1998) 112–147.

[154] S. Golshan-Shirazi and G. Guiochon. Modeling of preparative liquid chromatography. *J Chromatogr A* 658 (1994) 149 – 171.

[155] J. v. Langermann, Max Planck Institute, Magdeburg, Germany and M. Hedberg, AstraZeneca, Södertälje, Sweden. Personal communication (2011).

[156] J.-E. Bäckvall, M. Hedberg, M. Kaspereit, A. Kienle, H. Lorenz, A. Seidel-Morgenstern, M. Shakeri, and J. von Langermann. Design of an Integrated Process for the Resolution of a Pharmaceutical Compound (working title). *Org Process Rev Dev* (in prep.).

[157] M. Kaspereit, S. Swernath, J. G. Palacios, and A. Kienle. Evaluation of competing process concepts for the production of pure enantiomers. *Org Process Rev Dev* (in prep.).

[158] C. A. Floudas. Nonlinear and Mixed-Integer Optimization: Fundamentals and Applications. Oxford University Press, New York, Oxford, 1995.

[159] L. T. Biegler, I. E. Grossmann, and A. W. Westerberg. Systematic Methods of Chemical Process Design. Prentice Hall, 1997.

[160] H. Yeomans and I. E. Grossmann. A systematic modeling framework of superstructure optimization in process synthesis. *Comp Chem Engng* 23 (1999) 709–731.

[161] J. Gangadwala and A. Kienle. MINLP optimization of butyl acetate synthesis. *Chem Engng Proc* 46 (2007) 107–118.

[162] Y. Kawajiri and L. T. Biegler. Nonlinear programming superstructure for optimal

dynamic operations of simulated moving bed processes. *Ind Eng Chem Res* 45 (2006) 8503–8513.

[163] Y. Kawajiri and L. T. Biegler. Optimization strategies for simulated moving bed and PowerFeed processes. *AIChE J* 52 (2006) 1343–1350.

[164] T. Falk and A. Seidel-Morgenstern. Analysis of a discontinuously operated chromatographic reactor. *Chem Eng Sci* 57 (2002) 1599–1606.

[165] T. Yun, G. Zhong, and G. Guiochon. Simulated moving bed under linear conditions: Experimental vs. calculated results. *AIChE J* 43 (1997) 935–945.

[166] M. Kaspereit, J. G. Palacios, and D. F. und A. Kienle. Design of reactive and non-reactive simulated moving bed processes for Langmuir and bi-Langmuir isotherms using equilibrium theory (working title) (in prep.).

[167] D. Flockerzi, A. Bohmann, and A. Kienle. On the existence and computation of reaction invariants. *Chem Eng Sci* 62 (2007) 4811 – 4816.

[168] G. Severin. Spontaneous Racemization of Chlorthalidone: Kinetics and Activation Parameters. *Chirality* 4 (1992) 222–226.

[169] E. Lamparter, G. Blaschke, and J. Schlüter. Racemization of Chlorthalidone in the Presence of Liposomes. *Chirality* 5 (1993) 370–374.

[170] T. Borren and J. Fricke. In: H. Schmidt-Traub (Ed.): Preparative chromatography of fine chemical and pharmaceutical agents. Chapter: Chromatographic Reactors. Wiley-VCH, Weinheim, 2005.

Part II

Enclosed Manuscripts

List of Enclosed Manuscripts

PII – 1   M. Kaspereit. In: E. Grushka and N. Grinberg (Eds.): Advances in Chromatography. Chapter: Advanced operating concepts for Simulated Moving Bed Processes. CRC Press, Taylor & Francis, Boca Raton/Fla, USA, 2009, 165–192.

PII – 2   T. Sainio and M. Kaspereit. Analysis of steady state recycling chromatography using equilibrium theory. *Sep Purif Technol* 66 (2009) 9–18.

PII – 3   M. Kaspereit and T. Sainio. Simplified Design of Steady-State Recycling Chromatography Under Ideal and Nonideal Conditions. *Chem Engng Sci* (2011, submitted).

PII – 4   P. Forssén, R. Arnell, M. Kaspereit, A. Seidel-Morgenstern, and T. Fornstedt. Effects of a Strongly Adsorbed Additive on Process Performance in Chiral Preparative Chromatography. *J Chromatogr A* 1212 (2008) 89–97.

PII – 5   M. Kaspereit, A. Seidel-Morgenstern, and A. Kienle. Design of Simulated Moving Bed Chromatography Under Reduced Purity Requirements. *J Chromatogr A* 1162 (2007) 2–13.

PII – 6   J. García Palacios, M. Kaspereit, G. Ziomek, D. Antos, and A. Seidel-Morgenstern. Optimization and Analysis of Possible Column Arrangements for Multicomponent Separations by Preparative Chromatography. *Ind Eng Chem Res* 48 (2009) 11.148–11.157.

PII – 7   J. Siitonen, T. Sainio, and M. Kaspereit. Theoretical analysis of steady state recycling chromatography with solvent removal. *Sep Purif Technol* 78 (2011) 21–32.

PII – 8   T. Sainio, M. Kaspereit, A. Kienle, and A. Seidel-Morgenstern. Thermal effects in reactive liquid chromatography. *Chem Engng Sci* 62 (2007) 5674–5681.

PII – 9   J. García Palacios, M. Kaspereit, and A. Kienle. Conceptual Design of Integrated Chromatographic Processes for the Production of Single (Stereo-)Isomers. *Chem Eng Technol* 32 (2009) 1392–1402.

PII – 10   J. García Palacios, M. Kaspereit, and A. Kienle. Integrated Simulated Moving Bed Processes for the Production of Single Enantiomers. *Chem Eng Technol* 34 (2011) 688–698.

PII – 11   J. García Palacios, B. Kramer, A. Kienle, and M. Kaspereit. Experimental Validation of a new Integrated Simulated Moving Bed Process for the Production of Single Enantiomers. *J Chromatogr A* 1218 (2011) 2232–2239.

Advanced operating concepts
for Simulated Moving Bed processes

Malte Kaspereit

Max Planck Institute for Dynamics of Complex Technical Systems,
D-39106 Magdeburg, Germany

Table of contents

1 INTRODUCTION

About ten years ago, Zhong and Guiochon stated in an earlier volume of this series with respect to Simulated Moving Bed (SMB) chromatography that „*many expect it to modify considerably the landscape of industrial separations/purifications in the near future*" [1]. This contribution will not give a detailed judgment on the current state of the industrial landscape. Nonetheless, it should be emphasized that in the meantime SMB technology matured from an interesting academic engineering problem to a process that found its entry into the standard portfolio of most companies within the pharmaceutical and fine chemicals industry, as well as into the syllabus of university programs for chemical and process engineering, biotechnology, etc.

The main reason for the success of SMB chromatography lies in it's numerously quoted benefits with respect to process performance. In comparison to batch chromatography, the process usually facilitates drastically lower eluent consumption, higher product concentrations at high yield and acceptable productivity.

Another important aspect that supports the more frequent utilization of SMB technology is related to the availability of useful tools for analysis and design of the process. Significant advances with respect to a detailed understanding of this process have been achieved, in particular, within the last 15 years. To some extent this is due to the fact that the SMB process is intriguing to many chemical engineers because of its similarities (as well as due to its differences) to conventional continuous separation processes like rectification. Not surprising, the first simple design method for (linear) SMB processes was based on a concept similar to the famous McCabe-Thiele diagram [2]. By now, several useful design tools have been derived on the basis of simple models. An important driver for the more recent advances is also the rapid development of computer capacities. This allowed performing optimizations on the basis of more realistic and, consequently, computationally more expensive models of SMB processes. The range of applications of SMB chromatography has widened within the last years. Currently these range from rather classical hydrocarbon and sugar separations, over (still) challenging enantioseparations, to ambitious biotechnological problems like purifications of proteins or plasmid DNA.

The significant research efforts that were devoted to investigations and design of this process or to its application to challenging separation problems are also reflected in the number of publications related to SMB technology. This number has been rising more or less continuously since the invention of the process (see Figure 1).

Another indicator substantiating that SMB is a maturing technology are the numerous innovative operating concepts and structural modifications that have been suggested in order to further enhance the performance of SMB processes, or to extend its range of applications to new fields like multi-component separations or integrated reactive separations.

This contribution will review the most relevant of these advanced operating concepts. The main principles behind the different approaches as well as possible resulting benefits will be explained. However, also specific limitations and disadvantages shall be discussed.

2 CONVENTIONAL SMB PROCESSES

In this section the fundamentals of classical SMB processes will be explained in order to provide for an easy understanding of the more advanced operating concepts to be discussed in later sections.

2.1 Principle

SMB chromatography was developed against the background of classical continuous separation processes in the area of chemical engineering. A self-evident concept to perform such continuous separation is to apply a countercurrent between the phases involved. For example, in rectification (i.e., continuous distillation), such countercurrent is adjusted between the liquid and the gaseous phase, respectively. Only this makes possible the continuous introduction of feed and withdrawal of products.

As concerns chromatography, it turned out that a countercurrent between solid and fluid phase is too difficult to establish due to severe problems related to the transport of the solid (e.g., particle abrasion and mixing of the solid phase). It should be noted, however, that such "True Moving Bed" (TMB) chromatography remains as an important theoretical concept used for process design and optimization.

The SMB concept was developed as a workaround for the mentioned solid-related problems occurring in TMB units. The classical scheme of SMB chromatography as shown in Figure 2 is was patented by Universal Oil Products in 1961 [3] and still represents the most commonly used setup.

desorbent   extract (B)   feed (A+B)   raffinate (A)

zone I   zone II   zone III   zone IV

direction of port switching and liquid flow

resulting simulated solid movement
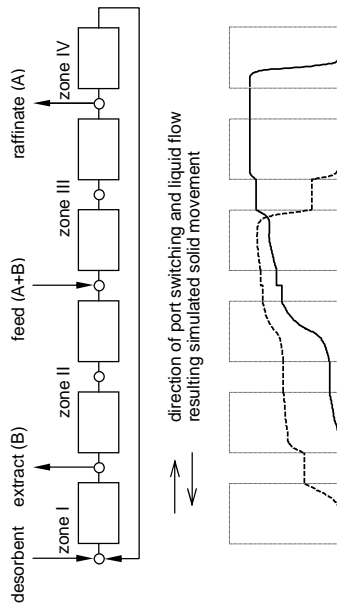
Figure 2: Classical four-zone SMB process. Top – example scheme with a 1/2/2/1 column configuration. Bottom – typical internal concentration profiles at the middle of a switching interval (non-linear adsorption isotherms). Solid line – weakly adsorbing component A, dashed line – stronger adsorbing component B.

The unit basically consists of a series connection of regular chromatographic columns. In contrast to the TMB concept, the desired countercurrent between the solid and the liquid phase is here "simulated" (hence the name) by periodically switching all columns in the direction opposite to the liquid flow. Alternatively, all product ports can be switched periodically in the direction of the liquid flow. The scheme contains four in- and outlet ports – two inlets for feed and desorbent, and two outlets denoted as raffinate and extract, respectively. These four ports divide the unit into four zones (I...IV) that have different liquid flow rates and perform different specific tasks.

The task of the left-most zone I is the regeneration of the solid phase. Using a rather large flow rate in this zone assures that any remaining traces of the adsorbed components are eluted and transported towards the extract port. The flow rate within zone II is adjusted such, that the stronger adsorbing component B is allowed to establish a concentration wave here, while the flow is chosen high enough to ensure complete elution of the weaker adsorbing component A. Similarly, in zone III the flow is low enough to allow migration of the faster component A towards the raffinate port, while component B migrates too slow to pass this zone. Finally, in zone IV a very low flow rate is adjusted. Therefore, the liquid phase leaving the columns in this zone should not contain any adsorbed components. With respect to these tasks just described, zones II and III are often denoted as "separation zones", while zones I and IV are frequently referred to as "regeneration zones".

Due to the periodical shifting and continuous supply or withdrawal of feed, desorbent and products, the process reaches a periodically repetitive state after a certain number of switching intervals. This is often denoted as "periodic" or "cyclic" steady state. This situation is characterized by the fact that at the end of a switching interval the same concentration profiles are obtained throughout the unit as were at the end of the preceding interval (and will be in all successive periods). The number of switches necessary to reach this situation is difficult to

predict and depends on several parameters [4]. As a rough rule of thumb, for a well-designed SMB system approximately 20 x (no. of columns) switching events are often sufficient. An important characteristic of the process is also that due to its periodic nature the concentrations at the two outlet ports vary during each interval (i.e., one observes "saw tooth profiles" for the product concentrations).

2.2 Some remarks on advantages and disadvantages

In comparison to batch chromatography, the SMB process has several advantages with respect to process performance. These have been quoted numerous times. However, there are also some misconceptions and disadvantages which deserve a short discussion.

The main performance parameters for preparative chromatographic processes are the purity of the products, specific productivity (defined as mass flux of desired product per unit volume), and specific eluent consumption (amount of solvent required per mass of product obtained).

It is well known that SMB processes are superior to batch chromatography concerning their significantly lower specific eluent consumption. Consequently, they also deliver products of higher concentration. Furthermore, reasonably high productivities can be achieved without sacrificing the recovery yield. The latter might be attributed to the fact that SMB units as such do not comprise waste streams. In addition to the above, the periodic nature of the SMB process can be regarded as an advantage (even though it makes the process more complex). In fact, this periodicity is the basis for several innovative operating concepts that enhance process performance. Examples are the asynchronous shifting of ports and the dynamic modulation of concentrations or flow rates. Such advanced operating modes will later be discussed in detail.

However, there are two more aspects often claimed to be specific advantages of SMB over batch chromatography. One is the presumably continuous nature of SMB. This is a misconception since, when considering an SMB and a reasonably designed preparative batch scheme (for example, a „touching band separation"), one finds that both are periodic or pseudo-continuous processes. As such, both deliver products with periodically changing compositions. Furthermore, they are not very different or complex with respect to automization. Therefore, a periodically operated batch process does not differ significantly with respect to its "discontinuous" nature.
A second argument that was propagated for many years is that SMB processes allow for higher productivity than batch chromatography. This claim does not hold, since batch schemes frequently can be optimized such that they operate at significantly higher specific productivity (i.e., the ratio of product flux and volume of stationary phase) than the corresponding separation by SMB chromatography. To a large extent this is due to less severe pressure drop constraints in batch systems. However, as already indicated, beyond a certain limit this is at the expense of a strongly decreasing yield.

Besides the undisputed benefits of (classical) SMB processes, there are also several disadvantages in comparison to batch chromatography. Most noteworthy is the capability of batch systems to perform multi-component separations – often with 100% purity for each

component. Obviously, since a conventional SMB unit has only two outlets, it can deliver only two pure products at the same time. Even this is possible only if the feed is a binary mixture. If the feed mixture contains more than two solutes, the classical SMB scheme can provide only the least or the strongest adsorbing component in pure form. Furthermore, the SMB process as such is more complex than batch elution. For a detailed design, so-called hybrid models (i.e., mathematical models that contain besides continuous variables also discontinuous ones; here this is due to the switching events) have to be implemented. Generally, these have to be treated using numerical methods and the solution is (still) numerically rather expensive. Other unfavorable aspects are the somewhat higher investment and maintenance costs for SMB units. Moreover, batch chromatography is generally easier to monitor than an SMB process. The latter requires more than one detecting device at different positions in the unit. These detectors are often even difficult to connect (e.g., when considering a "carousel" unit with rotating columns). Finally, it is difficult to apply concepts from batch chromatography that allow for improved process performance (e.g., the use of gradients) also to SMB processes.

However, the disadvantages mentioned above are also a driver for the innovative operating concepts for SMB processes that are in the focus of this contribution.

2.3 Basic design for complete separation

A detailed design of an SMB process requires the optimization of a rather large number of operating parameters; for example, flow rates, feed concentration, column length and diameter, column configuration, particle size, etc. These parameters are by no means independent. Consequently, such detailed design is a challenging task. Publications covering this are rare; a practicable procedure can be found in [5]. Due to the complexity, established design procedures focus on the most important parameters, which are the four internal flow rates of the unit. Most SMB applications aim at the maximization of the product purity. For such cases that typically demand the complete separation of the components, useful design tools are available which allow for a direct prediction of necessary operating conditions. Methods that deserve to be mentioned are the well-known "triangle theory" (see, e.g., [6, 7]) and the "standing wave analysis" [8, 9]. The former considers the adsorption isotherms as the main factor influencing the behavior of an SMB unit. The latter additionally takes into account dispersive effects, but it requires a certain reconciliation using numerical models or experiments.
Below the "triangle theory" will be explained briefly, since it represents the most commonly used design method. The approach is based on local equilibrium theory for a TMB process and has been elaborated for most of the relevant types of adsorption isotherms [10-13]. More recently, it was further extended to the (somewhat academic) case of a generalized Langmuir adsorption isotherm [14, 15].

The design of any SMB process requires the specification of the adsorption isotherms. For the sake of brevity here only competitive mixture adsorption isotherms of the Langmuir-type will

be considered. These relate the concentrations of the species on the solid surface (q_i) and in the liquid phase (c_i), respectively, in thermodynamic equilibrium by

$$q_i(\bar{c}) = \frac{a_i c_i}{1 + b_A c_A + b_B c_B} \qquad i = (A,B) \qquad (1)$$

As already mentioned, the main design parameters for a unit as shown in Figure 2 are the dimensionless flow rate ratios m_j for each zone j; These are defined as quotient of the liquid zone flow rate and the solid flow rate, respectively. For TMB and SMB systems, these ratios are given by

$$m_j = \frac{Q_j^{TMB} - Q_S \varepsilon_p}{Q_S(1-\varepsilon_p)} = \frac{Q_j^{SMB} t_S - V_c(1-\varepsilon)}{V_c(1-\varepsilon)} \qquad j = (1...4) \qquad (2)$$

Using equilibrium theory, analytical expressions can be derived for m_j values necessary to achieve complete separation. The solutions are valid if dispersive effects, e.g. due to axial dispersion or finite mass transfer resistances, can be neglected. For a system described by the Langmuir adsorption isotherms (1), optimal values for all m_j that guarantee complete separation (i.e., 100% purity – superscript "100") can be calculated explicitly [7]:

$$m_I^{100} = a_B \qquad (3)$$

$$m_{II}^{100} = \frac{a_A \varpi_G}{a_B} \qquad (4)$$

$$m_{III}^{100} = \frac{\varpi_G\left[\varpi_F(a_B - a_A) + a_A(a_A - \varpi_F)\right]}{a_A(a_B - \varpi_F)} \qquad (5)$$

$$m_{IV}^{100} = \frac{1}{2}\left\{ a_A m_{III} + b_A c_{A,F}\Delta m - \sqrt{\left[a_A + m_{III} + a_A c_{A,F}\Delta m\right]^2 - 4 a_A m_{III}} \right\} \qquad (6)$$

In the equations above, $c_{i,F}$ denotes the feed concentrations and $\Delta m = m_{III} - m_{II}$. Furthermore, the $\varpi_{G/F}$ are the solutions of the quadratic equation

$$\left(1 + b_A c_{A,F} + b_B c_{B,F}\right)\varpi^2 - \left[a_A\left(1 + b_B c_{B,F}\right) + a_B\left(1 + b_A c_{A,F}\right)\right]\varpi + a_A a_B = 0 \qquad (7)$$

As for the dispersive effects inherent to any real chromatographic plant, most probably flow rates calculated from the m_j^{100} above will not deliver pure products. To account for this frequently safety factors, $\beta_j \geq 1$, are introduced that should counterbalance these deviations:

$$m_j = \begin{cases} \beta_j\, m_j^{100} : j = (I,II) \\ m_j^{100}/\beta_j : j = (III,IV) \end{cases} \qquad (8)$$

In addition to the explicit calculation of optimum m_j-values, the design approach also allows to define a region of operating parameters within the parameter space (m_{II}, m_{III}) that guarantees for complete separation of the components. This region resembles a triangle (giving the method its name). An example is shown in Figure 3. Noteworthy, the vertex of such region represents

the optimal operating point in terms of productivity and solvent consumption. For details on determination of the region the interested reader is referred to, for example, [7].

The separation triangle is a very popular tool for the basic design of SMB processes, since it gives explicit solutions and allows for a rather generic view on possible operating points. The results can also serve as good initial values in detailed design studies using more elaborated mathematical process models that account for dispersive effects (e.g., axial dispersion and mass transfer limitations).

It should be noted that equilibrium theory can also be applied to design processes with basically any desired product purity lower than 100% for extract and raffinate. A corresponding method was developed recently [16]. For a given set of desired outlet purity values the method allows to determine optimum flow rates and product concentrations by solving a simple set of algebraic equations.
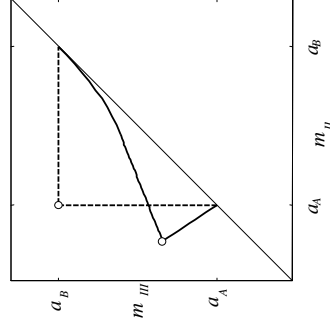
Figure 3: Regions of complete separation in the m_{II} / m_{III} - diagram. Dashed lines – linear adsorption isotherms; solid lines – Langmuir adsorption isotherms; points – optimum operating points. The a_i correspond to the slopes of the Langmuir isotherms (1) at infinite dilution (i.e., the Henry constants of the components).

3　CLASSIFICATION OF ADVANCED OPERATING MODES

The conventional SMB concept described in the previous section has retained basically unchanged for several decades. During the last years, however, a number of more sophisticated operating modes were proposed that should further improve the performance of the process, or that are intended to overcome some of its limitations. In this section, an attempt is made to classify these approaches. Figure 4 shows a corresponding scheme that suggests – from a process engineering perspective – four different categories.

The first category exploits the idea of *manipulating the strength of adsorption* in a *spatially distributed* manner. This basically subsumes all kinds of SMB processes incorporating

category are combined separations. An example is to purposefully couple SMB chromatography and selective crystallization in order to exploit synergisms. Integrated SMB processes and combined schemes will be discussed in section 7.

4 SMB PROCESSES WITH GRADIENTS

The application of gradients is one of the most promising approaches to improve the performance of SMB processes. Analogous to batch chromatography, gradients are applied in order to manipulate the strength of adsorption in a purposeful way. First corresponding suggestions were made with respect to gradients of temperature [2], solvent strength [20], and pressure-gradients when using super-critical fluids [21, 22]. Surprisingly, detailed investigations of the most straightforward technique, solvent gradients, were performed only recently and published independently by Jensen [18] and Antos [19].

The implementation of a gradient in an SMB unit is shown schematically in Figure 5 for the example of a gradient of solvent strength or salt concentration. In the figure, gray shadows mark the positions where modifications are established in comparison to the conventional SMB process (Figure 2). The rationale of the process is analogous to batch-gradient chromatography. Obviously, it is of interest to increase the solvent strength in places where fast desorption is favored. In particular this hold for the "regeneration zone" *I*. This is attained by adding a high fraction of of a "strong" solvent (the so-called modifier) to the desorbent stream. In contrast, in zones *III* and *IV*, adsorption should prevail and, consequently, the feed stream should less or none of the modifier. As a result of such gradients, significantly higher product concentrations, productivity, and lower overall eluent can be achieved. It should be noted that the same general principle as shown in the figure also holds for alternative kinds of modifiers.

D ... pure strong solvent (or high salt content)
F ... feed components in weak solvent (or low salt content)
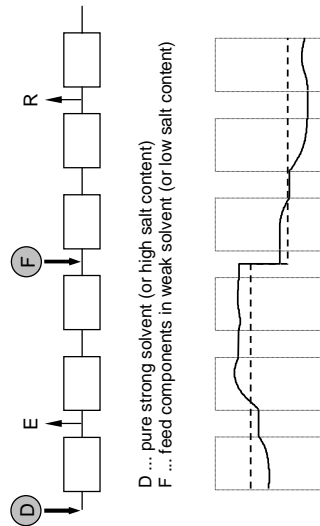
Figure 5 : Principle of solvent gradient SMB processes (recycle stream omitted). Top – SMB setup with a "strong" eluent in the desorbent and "weak" eluent in the feed stream, respectively. Bottom – resulting concentration profile of the modifier (i.e., desorption strenght throughout the unit). Dashed line – desired ideal profile; solid line – dynamic profile of a modifier with non-linear adsorption isotherms.

Solvent-gradient SMB (SG-SMB) systems were investigated most intensively. Therefore it will be discussed here in most detail. Suitably designed solvent-gradient SMB processes achieve

10

---

gradients. Gradients are popular in batch chromatography for already more than 50 years [17]. Corresponding SMB schemes have been developed more recently, e.g. [18, 19]. The suggested SMB processes use the same modifiers that are known from batch chromatography (organic modifiers, salts, etc.). Note that the figure also assigns the use of super critical fluids (SFC) to this category. This is due to the possibility to adjust different pressure levels in the zones, which lead to a distributed strength of adsorption. More details on gradient SMB processes will be given in the next section.

Advanced operating concepts for SMB processes

Spatial manipulation of adsorption	Super-periodic processes	Structural modifications	Process integration and combination
Gradient-SMBs: – solvent strength, – temperature, – salts, – SFC, ...	Dynamic parameter variations: – concentrations, – flow rates, – column config., – feed periods, ...	Multi-component separations (additional zones or coupled SMBs) Extract enrichment	SMB reactor Combination SMB / selective crystallization

Figure 4: A rough classification of advanced operating concepts for SMB processes.

The second category in Figure 4 is denoted as *super-periodic processes*. These have in common that – in addition to the periodic switching of columns in classical SMB processes – further variables are manipulated dynamically *during each switching interval*. This increases the degree of freedom (i.e., the number of design parameters) and therefore allows for a further optimization of the process. Examples are flow rates ("Powerfeed"-SMB) or feed concentrations ("Modicon" process) that are changed during the tact, or a variable column configuration (achieved by asynchronously switching the columns, "VariCol" process). Selected processes belonging to this class will be discussed in section 5.

The third group of processes is characterized by more or less fundamental *modifications of the structure* of the SMB process. Mainly, this subsumes schemes intended for multi-component separations in order to overcome the severe limitation of SMB processes to binary separations. Such processes contain additional zones and internal recycles. Noteworthy, in contrast to the second category, they usually entail a reduced degree of freedom (e.g., due to the couplings of zones or internal recycles). Section 6 gives an overview on corresponding attempts.

The last category refers to processes that *integrate new functionalities* into the SMB process or that *combine SMB units with complimentary processes*. Most prominent are here SMB reactors, where reaction and separation are performed simultaneously in the same apparatus. Analogously to the famous concept of reactive distillation, this aims in particular at enhancing the conversion in equilibrium-limited reactions. Ideally, the educts of a chemical reaction are fed into the unit and pure products are obtained at complete conversion. The main problem is here that the feasibility depends strongly on several parameters (i.e., the stoichiometry, the order of adsorptivities, the adsorption isotherms, and the reaction rate). Also placed within this

9

The figure emphasizes the strong dependency of adsorption isotherm parameters on modifier concentration. In particular, it should be noted that in the example the separation factor $\alpha = a_2/a_1$ rises significantly with increasing c_{mod}. This has an interesting consequence. It has been demonstrated in [25] that the performance of SMB processes improves drastically with increasing separation factors. Considering further, that by using a solvent gradient, also the concentrations in the SMB unit increase strongly (see above), situations can arise where these concentrations exceed the solubility limits. Since this should be regarded infeasible, in such case an isocratic SMB might be equivalent to its gradient analogue. In other words, the question arises if an optimized isocratic SMB unit that operates at the solubility limit can be outperformed by a solvent-gradient SMB process, or not. This aspect has not been investigated yet. However, it was touched by Abel et al. [26], who pointed out that the gradient process should at least allow for a larger separation triangle (cf. Figure 3) which will improve process robustness.

The design of gradient SMB chromatography is obviously more complex than an isocratic process. Different strategies were investigated. Abel et al. were able to derive design guidelines from equilibrium theory [23,26]. A different approach is to perform parametric studies. These aim at determining a separation triangle analogous to the one shown in Figure 3 by "scanning" of the m_{II} / m_{III} - parameter space. For this purpose, a fast algorithm was applied to systems with linear isotherms [39, 40]. For nonlinear processes, also more detailed models were applied (e.g., [19]). More recently, also advanced optimization methods have been applied in order to determine directly the optimum operating parameters. Examples are stochastic optimization [41], or a hybrid approach that combines simulated annealing and the simplex algorithm [42].

In addition to the solvent-gradient SMB processes discussed above, also the use of salt gradients has become popular [27,28,29,30,31]. These are of interest in bioseparations, where very often high salt concentrations are necessary in order to trigger desorption of strongly adsorbed proteins. Due to the relevance of this application problem the author expects that salt gradients will be the main driving force for future developments in field of gradient SMB processes. The principle of operation is basically the same as for solvent-gradient SMBs (i.e., a high salt could be applied in the desorbent, and a low salt concentration in the feed, respectively). However, an interesting aspect is that also less obvious shapes of the salt profile might be beneficial (e.g., "upward" vs. "downward" gradients), which depends to a certain extent on the objectives with respect to productivity and eluent consumption [29]. In general, however, the design procedures for salt gradient SMB processes are similar to those for solvent gradients.

Besides the use of solvent modifiers and salts, which certainly are the most important versions within this category, more gradient SMB concepts have been investigated. The use of higher temperatures in regeneration zones and lower temperatures in separation zones has been suggested already at an early stage [2]. In a theoretical study design criteria were derived from equilibrium theory and the process was found to be promising [32]. However, it can be expected that practical realizations could suffer severely from difficulties with respect to controlling a desired temperature profile. The temperature control must include connecting tubes and valves. Furthermore, very low switching times might be necessary to achieve

remarkable performance parameters. Most notably, the specific solvent consumption can be drastically decreased and, as a consequence, to the same extent the product concentrations increase. Both theoretical as well as experimental studies confirmed reductions of solvent consumption by 50% [18], 60% [19] or even 90% [23], respectively. These numbers remain impressive, even when considering that in none of these investigations a detailed optimization of the two process options was performed.

There are two important aspects related to the modifier in such processes. The first is that within the SMB unit, a distinct concentration profile will establish that has to be accounted for by a proper mass balance [19]. On one hand, the modifier can be a (linearly or non-linearly) adsorbing species, or it can be non-retained. On the other hand, as is indicated in Figure 5, its resulting composition profile is not equivalent to that within a TMB process, but is determined by the periodic switching of the columns [19,26]. This problem has not been accounted for in earlier works (see, e.g., [18]).

The second aspect becomes clear when considering that the adsorption isotherm parameters for the components to be separated depend strongly on the modifier content. Therefore, expressions are required that properly describe this dependency. Usually, empirical functions have to be applied. A viable procedure was applied in [19] and [31], which was based on an earlier work [24]. The modifier was assumed to adsorb according to a single-component Langmuir isotherm equation (1) (i.e., without any competitive effects caused by the other species). The dependency of the Langmuir-parameters for the components to be separated were described according to

$$a_i(c_{mod}) = (p_{a,i} c_{mod})^{-r_{a,i}} \qquad (9)$$

$$b_i(c_{mod}) = (p_{b,i} c_{mod})^{-r_{b,i}} \qquad (10)$$

where c_{mod} denotes the concentration of the modifier. The p- and r-values are constants to be determined experimentally. In total this results to eight parameters, which indicates the significant experimental effort when developing a separation by gradient SMB chromatography. Figure 6 exemplifies the typical relationship described by the two expressions above.
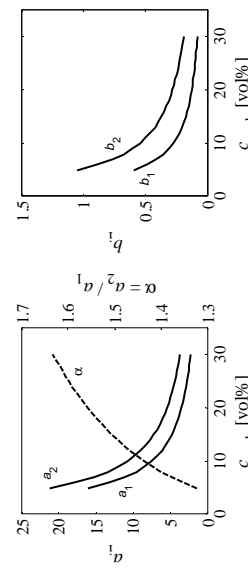

Figure 6: Dependency of Langmuir adsorption isotherm parameters on modifier concentration according to Eqs. (9) and (10). Left – Henry constants and separation factor $\alpha = a_2/a_1$; right – b_i-values. Parameters taken from [19].

uniform temperatures within the columns, which will entail low productivities. As another concept, also pH gradients were suggested in [33, 34, 35], although this was not discussed as a new general concept for SMB processes. So far, no general investigation of pH-gradient SMB chromatography has been reported. A somewhat more "exotic" idea is the application of voltage gradients in true moving bed electrophoresis [36, 37]. Although not being suitable for large-scale applications, it should be mentioned that the concept allows for a direct control of the concentration profiles within such unit. As a last concept, gradients of micelles should also be mentioned. These were used as surfactants in a study of a size-exclusion separation by SMB chromatography [38].

5   SMB PROCESSES WITH SUPER-PERIODIC MODULATIONS

The gradient-based approaches explained above reflect a somewhat "chemical view" on the SMB process. The operating modes covered in this section might be perceived as originating rather from a "process engineering perspective". While gradient systems attempt a direct manipulation of the adsorption, the approaches to be discussed here introduce an additional degree of freedom by periodically changing fifferent operating parameters during each switching interval.

5.1   Modulation of flow rates ("Powerfeed")

In a conventional SMB chromatography, all volumetric flows are held constant. The idea of varying these flow rates during each switching interval was originally introduced as a patent by Kearney and Hieb [43]. Later, Kloppenburg and Gilles [44] performed optimizations of this process. More recently, the idea was investigated in more detail by Mazzotti and co-workers (see, e.g., [45, 46]), who introduced the synonym "Powerfeed" for this operating concept. Schramm [47] applied control algorithms for the automatic optimization of the process. All authors found that when comparing Powerfeed to conventional SMB systems, significant improvements of solvent consumption and productivity can be achieved.

The principle of this process is explained in Figure 7. In contrast to gradient SMB systems, where modifications of the classical concept concern only feed and desorbent (cf. Figure 5), here such modifications are applied throughout the whole unit.
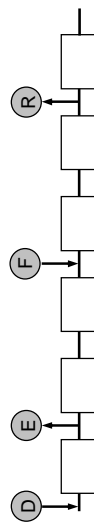

Figure 7: Principle of Powerfeed operation. In contrast to the conventional SMB process, all flow rates can be subject to modulations within each switching interval. (Recycle stream omitted.)
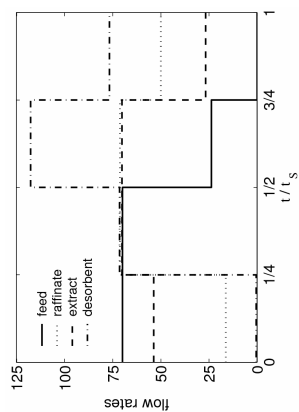
Figure 8: Example for flow rate modulations during each switching interval in a 'Powerfeed' process (data according to optimization results in [44]).

Figure 8 shows an example of such flow rate variation. The data in the figure were adopted from [44], wherein the authors divided each switching interval into four sub-intervals. Piecewise constant profiles were assumed for the flow rates, which were obtained from optimization procedures.

The figure indicates that optimal flow rate sequences cannot be designed on the basis of intuition (see, for example, the profile of the desorbent stream). As a consequence, design procedures either rely on some optimization algorithm or on process control concepts. Examples for successfully applied optimization methods are a simple double-layer optimization scheme [48], combinations of discretization approaches with NLP solvers [44, 49], and genetic algorithms [45].

The "Partial feed" operating mode proposed by Zang and Wankat [50] has already been recognized as being a special variant of the Powerfeed concept [48]. In this operating mode, only the feed flow rate is subject to variations. More specifically, the feed is turned on only during for a certain time in the middle of the switching interval. The original concept is explained in Figure 9. It is obviously less complex than the general Powerfeed modus described above, since time-dependent are only the flow rates of feed, zone III and raffinate, respectively. Nonetheless, in comparison to a standard SMB process, a significantly advantageous performance was obtained (reduction of solvent consumption by about 59%, productivity increase of 70%) [50].

As another specific subset of Powerfeed processes, the "Outlet Swing Strategy" might be mentioned [51]. There flow rates of raffinate and extract are varied in a two-step manner basically between zero (i.e., no flow) and a maximum value. This is achieved by manipulating streams in zones I and IV (i.e., between ports D and E, and ports R and D). In contrast to the Partial feed approach, this concept aims at "stretching" the concentration profiles for systems with nonlinear adsorption isotherms. However, due to the restriction to the mentioned flow rates, the achievable performance improvement appears not very pronounced.

Figure 9: Partial feed concept. Top – general scheme of a corresponding setup. Dotted lines: time-dependent streams. Recycle omitted. Bottom – example for typical time profile of feed flow rate.

The Powerfeed concept has been compared to classical SMB operation as well as to other advanced approaches like Modicon and Varicol. Although such comparisons hold only for the specific chromatographic system they were made for, the numbers given below should give a certain feeling on the process performance improvements achievable. For the separation of cycloketones by an SMB unit with 8 columns it was found that the Powerfeed mode allows for an increase of productivity and a decrease of solvent consumption by 20% and 18% [47], respectively. Under different chromatographic conditions for the same system, improvements were found to be 15% and 13%, respectively [52]. Zhang et al. [53] demonstrated that the benefits are increasing the fewer columns are applied. In an elaborated optimization study they calculated for an enantioseparation problem (racemate of 1,2,3,4-tetrahydro-1-naphthol, Chiralpak AD, see [54]) increases of productivity by about 25% for a 5-column unit, and 45% for a 4-column process, respectively (extract purity 95%; interpolated from Figs. 2 and 4 in [53]).

Despite these promising results (which have been verified also experimentally), some drawbacks of Powerfeed should be mentioned. Besides the efforts necessary to identify optimum flow rates, the changing flow rates can represent additional stress factors for the stationary phase and, depending on the practical implementation, also for the pumps of the unit [47].

5.2 Modulation of feed concentration ("Modicon")

An alternative concept relying on dynamic parameter variation is the "Modicon" process [47, 52, 55, 56, 57]. In this operating mode the feed concentration is varied during the switching interval. Such concentration alteration aims at a purposeful manipulation of the nonlinear concentration profiles within the unit; the concept is therefore only beneficial in the case of nonlinear adsorption isotherms.

The principle of Modicon is exemplified in Figure 10. As a simplification, each switching interval can again be divided into sub-intervals (analogous to the Powerfeed mode above) in which a different feed concentration is applied. An example of a beneficial shape of such feed concentration profile is given in the middle of the figure. In the case of Langmuir adsorption isotherms (1), the application of a very low concentration in the beginning of each interval (e.g., by injecting only eluent) was found most useful, while the concentration should as high as possible towards the end of the interval. The result of this modulation is shown in the lower part of the figure. In the example the same total amount of feed components is fed into the unit. In comparison to a conventional SMB process, in the Modicon process the concentration profile of the strong adsorbing component is shifted "backwards" (i.e., further away from the raffinate outlet; marked by the arrow). This indicates that in Modicon mode a higher feed flow rate can be used in order to re-position this front (i.e., to adjust again the same raffinate purity). Such increased flow rate entails a higher productivity of the two components and lower eluent consumption.

With respect to the design of this operating mode, it was found (as already indicated) that for adsorption isotherms of the Langmuir-type the feed mixture should be introduced as late as possible in the switching interval, with the highest possible concentration. However, in general such profile should be verified/optimized using a mathematical process model.
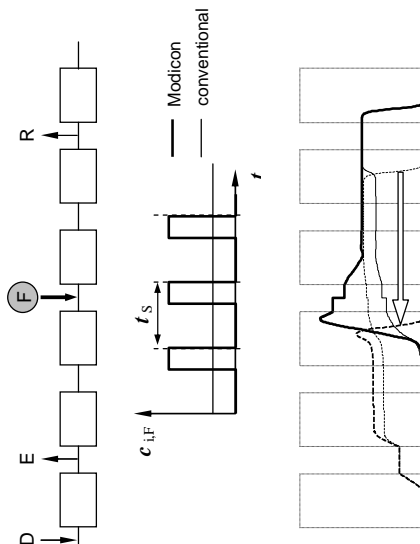
Figure 10: Principle of the Modicon process. Top – the schematic setup corresponds to a classical SMB, only the feed concentration is varied during each switching interval. Recycle stream omitted. Middle –feed concentration profile for a classical SMB processes (thin line) and Modicon (thick line). Bottom – comparison of typical internal concentration profiles for both process options.

The benefits resulting from applying the Modicon concept are similar to the results given earlier for the Powerfeed mode. In comparison to the classical SMB process, improvements with respect to productivity / solvent consumption / average product concentrations were reported as 33% / 22% / 32% [52], or even as high as 165% / 58% / 151% [47]. Zhang et al. presented somewhat less enthusiastic numbers, but found very similar productivity
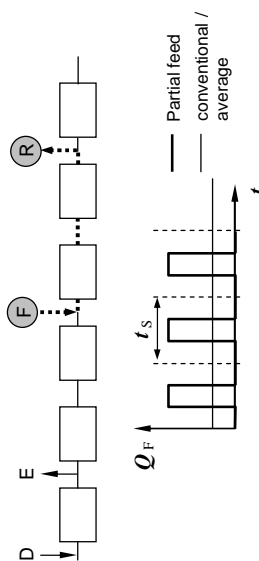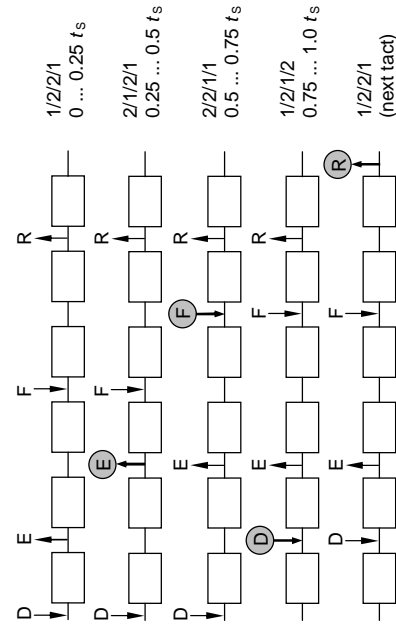
Figure 11: General principle of the Varicol process for a six-column setup. The main feature of the VariCol operating mode is the asynchronous shifting of the in- and outlet ports. In the example, the switching interval consists of four sub-intervals; in each of which only one of the ports is shifted. The resulting average column configuration is 1.5/1.5/1.75/1.25. (Recycle stream omitted.)

enhancements as for the Powerfeed mode: approximately 26% for a 5-column unit and 44% for a 4-column process, respectively (extract purity 95%; interpolated from Figs. 2 and 4 in [53]). An interesting result of the Modicon mode is also that it leads (at the same time-averaged feed concentration) to an enlargement of the separation regions (cf. Figure 3) which might be utilized for a more robust operation in the case of very nonlinear adsorption isotherms [57].

The very positive performance values listed above should be perceived in against the background of the limitations of the Modicon concept. As already mentioned, the concept exploits the nonlinearity of the adsorption isotherms. As a consequence, it does not produce any significant effect for systems with linear isotherms. Furthermore, the feed concentrations can be modulated only within the solubility limits of the components to be separated. Finally, an important technological aspect is that in a real SMB plant, ideal rectangular shapes of the feed concentration profile (as were shown in Figure 10, middle) cannot be achieved due to delay times, back-mixing, and non-perfect gradient devices. The deformation of the profiles decreases to a certain extent the possible benefits of the concept. However, the deformed profile needs to be "positioned" accurately. This can be achieved by corresponding measurements (e.g., experiments without column) and accounting for the real shape in model-based design. Schramm [47] demonstrated also experimentally that a Modicon process designed in such way allows for a significant performance improvement.

5.3 Modulation of column configuration ("Varicol")

A very popular variant of the SMB process, which is also successfully marketed, is the "Varicol" process [54, 58]. This concept is depicted in Figure 11.. As can be seen, in this process the inlet and outlet ports are not shifted simultaneously at the end of each switching interval, but asynchronously at specific times. The figure shows an example where the switching period is divided into four sub-intervals; at the end of each only one port is shifted (in a sequence extract-feed-desorbent-raffinate). This corresponds to a variation of the column configuration during each interval. As a consequence, one can specify time-averaged zone lengths or column configurations. For example, the switching mimic shown in the figure leads to a time-averaged column configuration of 1.5/1.5/1.75/1.25 columns per zone.
This modulation aims at the optimal exploitation of adsorbent in each zone. The most intriguing consequence of this is that Varicol allows reducing the number of necessary columns. In fact, the concept can be operated even with fewer columns than zones; for example, with only three columns that operate all four zones. As a consequence of fewer columns, the specific productivity of Varicol processes is also higher than that of conventional SMB systems.

It should be noted that during design not only the optimum column switching policy has to be found (which is not possible on the basis of intuition). In addition, also optimum flow rates in Varicol differ from those in a conventional SMB process [54]. This makes the design a complex optimization task.

Using a genetic algorithm for this design problem, in [59] it was found that the possible benefits resulting from asynchronous switching depend strongly on purity requirements. For example, it was reported that in comparison to the equivalent regular SMB process, the productivity of Varicol is higher by 10%, 25% and 127% for purity requirements of raffinate and extract of 90%, 95% and 99%, respectively.

As limitations of the Varicol concept should be mentioned the complexity of designing this process (see above) and its restriction to SMB systems that are based on the assembly of several multi-port valves. So-called carousel SMB units (which are based on a single rotary valve that holds and physically moves all columns) do not facilitate an asynchronous shifting. Although a corresponding extension of such systems should be possible by installing several external valves, to the author's best knowledge no such attempt has been published.

5.4 Further (hybrid) concepts

An obvious idea is to exploit modulations of more than one of the operational variables discussed above (i.e., flow rates, concentration, and column configuration). Zhang et al. [53] investigated different such "hybrid" concepts that combine two or all of the concepts Varicol, Powerfeed and Modicon, respectively, in one unit. They performed optimizations for the different options using a genetic algorithm and found (as can be expected) that these approaches further improve process performance. However, they also concluded that the additional gain that can be achieved is much smaller than when comparing conventional SMB chromatography to the individual advanced concepts.

A significant problem related to any kind of these approaches is to find optimum parameters, because the complexity of the design problem increases drastically by such combination; it is practically impossible to design them based on engineering experience or intuition. Furthermore, it is very time consuming to study in detail all possible process options using mathematical process models. In this context, a very promising approach has been suggested by Kawajiri and Biegler, who performed an optimization-based synthesis of the optimal process for the example of combining Powerfeed and Varicol. The main idea is to first create a so-called superstructure that inherits all possible options (even such options that might at first appear detrimental) [60]. This is followed by an optimization that identifies the optimal "sub-process" and the optimal parameters [49,61,62]. This approach should be extensible to include also further parameters (e.g., gradients, multi-component problems, chemical reactions, etc.).

As a last aspect of such hybrid schemes, it should be considered that – despite the advantages that are theoretically possible – they will most certainly suffer from a decreased robustness of operation (i.e., the sensitivity of the process against small disturbances will be high). This will be more severe the more parameters are varied. Usually, such issues are addressed only by researchers who study control schemes for SMB processes. However, with respect to the hybrid schemes above, this problem has not yet been investigated sufficiently.

6 SMB PROCESSES WITH STRUCTURAL MODIFICATIONS

This section will explain operating concepts that entail significant structural modifications of the classical four-zone SMB scheme.

6.1 Multi-component separations

The inherent restriction of conventional SMB systems to binary separation has been a motivation for development of sophisticated SMB-based processes. A large number of suggestions have been published, in particular for ternary separations. Here only the fundamental principles will be explained.

Figure 12 shows some example processes that clarify the possible approaches for ternary separations. The first and most obvious is to couple several SMB units (left; see e.g., 63). An alternative to this is also to combine SMB and batch chromatography [64]. The problem of such series connections (and the "explosion" of the number of possibilities with increasing number of components) is well-known from the design of distillation trains (where no such dilution problem persists). The other main idea with respect to SMB is the introduction of further zones (see e.g. [65] for system with nine zones). In the middle of the figure an eight-zone SMB system is shown that performs a complete separation (a "sharp split") between the least adsorbing compound A and the mixture B+C, which is then recycled to a lower part of the unit. The opposite scenario is shown in the right, where the split is performed between the two "heavy" components B and C. Besides the options shown in the figure there is also the possibility to use different adsorbents packed into alternating columns [66].

There are several significant problems related to multi-component SMB separations. An issue is certainly that usually the feed of the second unit (in SMB cascades) and the recycle in multi-zone systems is strongly diluted. This limits the overall performance. Furthermore, in multi-zone SMB systems the volume of diluted recycle will usually be too large to be re-introduced

completely. As indicated in the figure, purge streams are necessary to overcome this problem [67]. Another relevant problem related to both approaches is the reduced degree of freedom resulting from the coupling. In case of directly coupled processes (i.e., SMB cascades), one design parameter for the connected unit is lost. For multi-zone systems the switching time is equal throughout all zones, which represents a serious drawback.
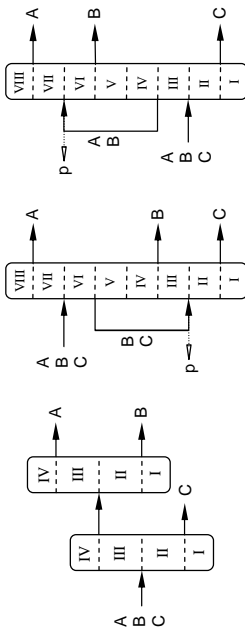
Figure 12: Examples for the general SMB-based approaches capable of performing ternary separations. Left – coupling of several SMB units. Middle – eight-zone SMB system performing the split A/BC. Right – eight-zone SMB process with a split AB/C. Necessary purge streams are marked by "p".

As can be seen from Figure 12, there is a vast range of possible processes, in particular if more than three components should be separated. A detailed discussion of all options is beyond the scope of this work; the interested reader is instead referred to several reviews. A comprehensive and detailed overview was given by Chin and Wang [68], who also addressed hardware issues (e.g., valve design and system setup). Further reviews were given, for example, by Kurup et al [69] and Kessler and Seidel-Morgenstern [67].

6.2 SMB process with extract enrichment

An interesting process first described in a patent [70], is an SMB system combined with a recycle of enriched extract. Following the vogue of appointing a name to new SMB concepts, in two current investigations the process was called "M3C-SMB" [71] and "EE-SMB" (for Enriched Extract SMB) [72], respectively.
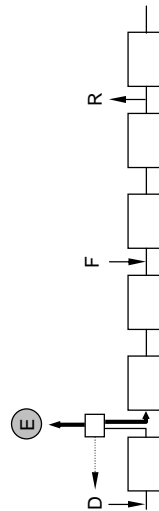
Figure 13: Scheme of an SMB process with an enriched extract stream. The output of zone I is withdrawn completely, enriched (e.g. by evaporation), and partially recycled into zone II.

Figure 13 explains the concept. The main idea is to withdraw completely the liquid output of zone *I* and to enhance its concentrations (for example, by an evaporation step). A part of this liquid is kept as product and the remainder is recycled into zone *II*. For systems with nonlinear and favorable adsorption isotherms (e.g., Langmuir isotherms (1)), the now high concentration of the stronger adsorbing component entering zone *II* causes a displacement of the less adsorbing component. The concentration front of this weak species is moved to the right (i.e., towards the feed port). Therefore, the extract purity increases or, alternatively, the throughput can be enhanced. Paredes et al. [72] predicted for a model system a possible productivity enhancement of 150%.

As has been demonstrated in [71] and [72], the process can be designed on using equilibrium theory. An important aspect of both design procedures is that the authors require that the concentration of the recycle should exceed a certain minimum limit. This limit is given by the so-called watershed point. The intention of this is convert the dispersive waves of the components in zone *II* (as shown in the bottom of Figure 2) into shock waves. However, as was also indicated in [72], a positive effect can already be obtained by concentration enrichments below the watershed point.

It should be noted that for the design of the concept several constraints have to be considered. The main question is whether the watershed point can be reached, or not. On one hand, usually rather high concentrations are necessary for this; on the other hand, these must lie within the solubility range. To conclude, for a given chromatographic system the following parameters must "fit together": i) the mass stream obtained from zone *I*, ii) the solubility of the compounds, and iii) the thermodynamics (i.e., adsorption isotherms).

The reader might have noticed that the process requires an additional unit operation (e.g., an evaporator). Therefore, it might well be classified as one of the process combination concepts that will be discussed in the section. However, the main aspect considered here is the recycle with its highly concentrated stream rather than the source of this solution.

7 INTEGRATED SMB PROCESSES AND PROCESS COMBINATIONS

The SMB process as such is nowadays quite well-understood. Therefore, it is not surprising that current work focuses also on its assembly within its typical plant environment. It is desired to identify and to exploit synergisms that may arise when combining SMB chromatography with other unit operations. This section will discuss the two main possibilities. The first is to couple SMB units to other processes (here: to crystallization). The second is to integrate a chemical reaction into the system (SMB reactors).

7.1 Combination of SMB and selective crystallization

A well-known fact in engineering is that costs of a separation decrease significantly if purity requirements can be lowered. A very cost-intensive application for SMB chromatography is the separation of enantiomers. This is the background for the suggested process combination in Figure 14.

In this scheme, the SMB is coupled to one or two crystallizers. These can deliver pure solid enantiomers if their feed streams exceed a certain minimum purity (the eutectic composition) with respect to the desired enantiomer. Therefore, the SMB unit is operated only at limited

purity, which allows for several possible benefits (i.e., significantly less or a cheaper chiral stationary phase, higher throughput, etc.).
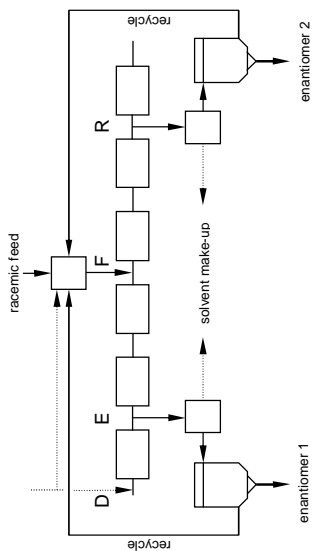

Figure 14: Schematic setup of a combined process of SMB chromatography and enantioselective crystallization. The SMB process delivers only partially separated products. Pure enantiomers are obtained from crystallization. Unresolved mother liquor is recycled.

The idea of such coupling was suggested by Lim et al. [73]; its full potential was recognized first by Blehaut and Nicoud [74]. A more detailed discussion was presented by Lorenz et al. [75].
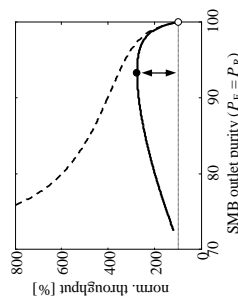

Figure 15 Performance of a stand-alone SMB process (dashed line) and the process combination with crystallization (solid line). Open symbol – throughput of the stand-alone SMB process; filled symbol – process combination (both options deliver pure enantiomers).

As indicated above, the potential of the combination stems from the improved performance of SMB chromatography when lowering the purity requirements. This relationship is exemplified in Figure 15, where a purity-performance characteristic of an SMB process is shown (dashed line). It can be seen that already a slight decrease of the purity below the (typically required) 100% allows for a strongly increased throughput. From such characteristic (which can be determined *a priori* from, for example, model-based calculations) the throughput of the combined scheme can be calculated from simple algebraic relations [76].

The concept was investigated in detail for different enantiomeric systems [76 - 79] and diastereomeric systems [79]. It was demonstrated that under favourable conditions the performance of the process combination can be significantly higher than that of a stand-alone separation by SMB chromatography. Under somewhat idealized conditions, possible increases of productivity by up to 200% and a decrease of solvent consumption up to 70% were projected [78]. The main factor is the eutectic composition; a high purity of the eutectic leads to high purity requirements on the SMB separation, low yields in the crystallization and, as a consequence, an increased recycle load for the SMB unit. Most advantageous are conglomerate forming systems which have a eutectic at 50%. The occurrence of impurities in the crystallization can be detrimental [79]. Besides this, it can be expected that the benefits are more pronounced for difficult chromatographic separations; and that (in the case of cooling crystallization) the solubility equilibria should have a sufficient temperature-dependency [78].

It is worth mentioning that recently a method was derived from equilibrium theory that allows to design SMB processes for limited purity requirements. For any pair of desired raffinate and extract purity, optimum flow rates, product concentrations and process performance (i.e., characteristics as the one shown in Figure 15) can be calculated easily by solving a simple system of nonlinear equations [16].

To conclude, for systems that fulfil certain conditions, the process combination of SMB chromatography and selective crystallization can be promising enough to consider the additional efforts necessary to establish the somewhat complex scheme shown above.

7.2 Integration or combination with chemical reactions

As a last important field of current research, the combination of SMB chromatography and chemical reactions will be considered. In particular, the idea to perform an equilibrium-limited chemical reaction within an SMB unit is intriguing for many engineers (which is certainly inspired by other successful examples like reactive distillation).

The investigations performed in this direction are manifold; again, only the main ideas can be summarized here. Figure 16 demonstrates the three different options that are used to deal with equilibrium-limited chemical reactions.

The classical concept (top) is the reactor-separator setup, where an SMB process is connected to some chemical reactor to separate its output; unconverted reactants are recycled. This was suggested, for example, for application with sucrose inversion (i.e., sucrose = fructose + glucose) and dextrane production [80] and was reviewed more recently in the context of also other biotransformation reactions [81]. Another option, which is an extension of this concept, is the Hashimoto process (middle) [82]. This was developed for isomerization problems. Here, the reaction is functionally distributed within the unit by including several reactors in certain zones. It should be mentioned that so far this concept was applied only for certain limiting cases. It was investigated for systems with anti-Langmurian adsorption behaviour and the stronger adsorbing component as target product; for example for fructose-glucose isomerization using enzymes as catalysts and ion exchange resins as adsorbent [82, 83].

The last concept in the figure is the SMB reactor (SMBR, bottom). In an SMBR, a reactive adsorbent is packed into columns usually arranged as a classical four-zone scheme (bottom). This process is useful for reactions with two products; that is, for reactions with a stoichiometry of the form $A \rightleftharpoons C+D$ or $A+B \rightleftharpoons C+D$, respectively. In the example shown, the reactants are introduced through the feed port (A) and as the desorbent (B), respectively. Ideally, the products C and D are obtained in pure for at the two outlets. The stoichiometry $A \rightleftharpoons C+D$ holds, for example, for the already mentioned sucrose inversion and was investigated, for example, in [84, 85, 86]. Esterification and transesterification reactions, for which SMB reactors have been studied most frequently, follow the scheme $A+B \rightleftharpoons C+D$; corresponding studies were reported in, for example, [87, 88, 89, 90, 91, 92, 93]. There are many more problems that have been investigated with respect to SMB reactors. The reader is kindly referred to several publications that give a corresponding overview [94, 95, 96].
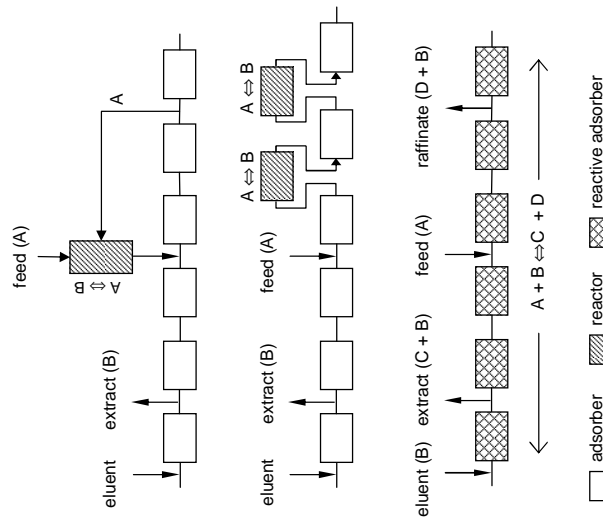
Figure 16: Examples for the general possibilities for combining SMB processes with chemical reactions. Top - classical reactor-separator system with recycle (e.g., for isomerization problems). Middle – the partially integrated Hashimoto process (isomerization). Bottom - fully integrated SMB reactor using a reactive adsorbent for a reaction of type $A + B \leftrightarrow C + D$.

The design of SMB reactors is a challenging task; the corresponding mathematical framework is rather involved [97, 98, 99]. Obviously, the stoichiometry of the reaction is of major importance and will influence the configuration of the setup. Apart from that, the reaction

kinetics and the order of adsorptivities decide about the feasibility of an integrated concept. An interesting theoretical work in this context was published by Grüner and Kienle [100], who were able to develop a concept based on equilibrium theory that allows evaluating the feasibility of such integrated process based on the stoichiometry and the adsorption isotherms of a given system. Mazzotti and co-workers established basic design criteria based on equilibrium theory [102]. Detailed design of an SMBR requires again optimizations of "numerical" models (see, e.g. [102]).

Despite the many investigations, the SMB reactor has not yet become a relevant commercial success. This is certainly due to the complexity of design, the efforts necessary to determine required physico-chemical parameters and the mentioned feasibility restrictions. Furthermore, it can be shown that also in liquid reactive chromatography thermal effects must not be underestimated [93]. However, the concept should not be considered as being only of academic interest, but also as promising with respect to possible industrial applications. Future work will certainly provide further qualitative and quantitative criteria that substantially aid the design of such processes.

8 CONCLUSIONS

SMB chromatography is a maturing technology. This becomes particularly clear when considering the numerous advanced operating concepts that are suggested to improve its performance.

The goal of this contribution was to explain the main principles that allow to realize performance improvements of SMB processes. The toe-holds for this are the direct manipulation of adsorption strength (i.e., gradients), the dynamic variation of operational variables, modifications of process structure, and the purposeful combination or integration of other functionalities.

Not all proposed approaches could be covered in detail and there are constantly evolving more and more process schemes with rising complexity. Several schemes combine characteristics of both SMB and batch chromatography (e.g., the so-called JO process 103). Some concepts even exploit almost all of the above main principles. For example, a partially counter-current concept was developed that employs multiple columns, asynchronous switching and gradients for multi-component separations of bio-molecules [104]. Also not considered here were chromatographic processes that try to mimic SMB behaviour (i.e., steady state recycling [105, 106] or so-called single-column SMB analogs [107, 108]). However, they represent interesting alternatives to SMB units, in particular when it comes to investment costs.

When considering the large number of innovative operating modes that are available for SMB chromatography, one must keep in mind that the design of any advanced scheme becomes more and more tedious with increasing the number of manipulated variables. Thus, a particular challenge for the future is to support practitioners with respect to two important problems: to choose the right process configuration for a given separation problem (that is still "reasonably simple" enough to be implemented in practice) and to find the optimal design parameters for this process. In light of this background it appears of high interest to develop corresponding criteria and guidelines that support the choice of the operating mode, as well as tools and methods for process design.

REFERENCES

1. G. Zhong, and G. Guiochon, in *Advances in Chromatography*, Vol. 39, P.R. Brown, and E. Grushka, Eds., Marcel Dekker Inc., New York, 1998, p. 352

2. D. M. Ruthven, and C. B. Ching, *Chem. Eng. Sci.*, 44:1011 (1989).

3. D. B. Broughton, and C. G. Gerhold, U.S. patent 2.985.589 (1961).

4. H. Kniep, PhD thesis, Otto-von-Guericke Universität Magdeburg, (1998).

5. F. Charton, and R.-M. Nicoud, *J. Chromatogr. A*, 702:97 (1995).

6. G. Storti, M. Mazzotti, M. Morbidelli, and S. Carra, *AIChE J.*, 39:471 (1993).

7. M. Mazzotti, G. Storti, and M. Morbidelli, *J. Chromatogr. A*, 769:3 (1997).

8. Z. Ma, and N.-H.L. Wang, *AIChE J.*, 43:2488 (1997).

9. T. Mallmann, B.D. Burris, Z. Ma, and N.-H.L. Wang, *AIChE J.*, 44:2628 (1998).

10. M. Mazzotti, G. Storti, and M. Morbidelli, *AIChE J.*, 40:1825 (1994).

11. M. Mazzotti, G. Storti, and M. Morbidelli, *AIChE J.*, 42:2784 (1996).

12. M. Mazzotti, G. Storti, and M. Morbidelli, *AIChE J.*, 43:64 (1997).

13. C. Migliorini, M. Mazzotti, and M. Morbidelli, *AIChE J.*, 46:1384 (2000).

14. M. Mazzotti, *Ind. Eng. Chem. Res.*, 45:6311 (2006).

15. M. Mazzotti, *J. Chromatogr. A*, 1126:311 (2006).

16. M. Kaspereit, A. Seidel-Morgenstern, and A. Kienle, *J. Chromatogr. A*, 1162:2 (2007).

17. R.S. Alm, R.J.P. Williams, and A. Tiselius, *Acta Chem. Scand.*, 6:826 (1952).

18. T.B. Jensen, T.G.P. Reijns, H.A.H. Billiet, L.A.M. van der Wielen, *J. Chromatogr. A*, 873:149 (2000).

19. D. Antos, and A. Seidel-Morgenstern, *Chem. Eng. Sci.*, 56:6667 (2001).

20. R.-M. Nicoud, M. Perrut, and G. Hotier, U.S. patent No. 5.422.007 (1995).

21. J.Y. Clavier, R.-M. Nicoud, and M. Perrut, in: P. R. von Rohr, C. Trepp (Eds.), High pressure Chemical Engineering, London, Elsevier Science. pp. 429-434 (1995).

22. M. Mazzotti, G. Storti, and M. Morbidelli, *J. Chromatogr. A*, 786:309 (1997).

23. S. Abel, M. Mazzotti, and M. Morbidelli, *J. Chromatogr. A*, 944:23 (2002).

24. E. Soczewinski, *Anal. Chem.*, 41:179 (1969).

25. M. Kaspereit, P. Jandera, M. Skavrada, and A. Seidel-Morgenstern, *J. Chromatogr. A*, 944:249 (2002).

26. S. Abel, M. Mazzotti, and M. Morbidelli, *J. Chromatogr. A*, 1026:47 (2004).

27. J. Houwing, H.A.H. Billiet, L.A.M. van der Wielen, *J. Chromatogr. A*, 944:189 (2002).

28. J. Houwing, S.H. van Hateren, H.A.H. Billiet, L.A.M. van der Wielen, *J. Chromatogr. A*, 952:85 (2002).

29. J. Houwing, T.B. Jensen, S.H. van Hateren, H.A.H. Billiet, and L.A.M. van der Wielen, *AIChE J.*, 49:665 (2003).

30. P. Li, G.H. Xiu, and A.E. Rodrigues, *AIChE J.*, 53:2419 (2007).
31. L. Gueorguieva, L.F. Vallejo, U. Rinas, and A. Seidel-Morgenstern, *J. Chromatogr. A*, 1135:142 (2006).
32. C. Migliorini, M. Wendlinger, M. Mazzotti, and M. Morbidelli, *Ind. Eng. Chem. Res.*, 40:2606 (2001).
33. N. Gottschlich, S. Weidgen, and V. Kasche, *J. Chromatogr. A*, 719:267 (1996).
34. N. Gottschlich, and V. Kasche, *J. Chromatogr. A* 765:201 (1997).
35. J. Thommes, J.P. Pieracci, M. Bisschops, A.M. Sonnenfeld, L. Conley, and M. Pennings, U.S. patent 7.220.356 (2007).
36. B.M. Thome, and C.F. Ivory, *Electrophoresis* 28:1477 (2007).
37. B.M. Thome, and C.F. Ivory, *J. Chromatogr. A* 1129:119 (2006).
38. D.A. Horneman, M. Ottens, J.T.F. Keurentjes, and L.A.M. van der Wielen, *J. Chromatogr. A* 1113:130 (2006).
39. D. Beltscheva, P. Hugo, and A. Seidel-Morgenstern, *J. Chromatogr. A* 989:31 (2003).
40. D. Antos, and A. Seidel-Morgenstern, *J. Chromatogr. A* 944:77 (2002).
41. G. Ziomek, M. Kaspereit, J. Jezowski, A. Seidel-Morgenstern, and D. Antos, *J. Chromatogr. A* 1070:111 (2005).
42. K. Kaczmarski, and D. Antos, *Acta Chromatogr.* 17:20 (2006).
43. M. Kearney, K. Hieb, U.S. patent 5.102.553 (1992).
44. E. Kloppenburg, and E. Gilles, *Chem. Eng. Technol.*, 22:813 (1999).
45. Z. Zhang, M. Mazzotti, and M. Morbidelli, *J. Chromatogr. A*, 1006:87 (2003).
46. Z. Zhang, M. Morbidelli, and M. Mazzotti, *AIChE J.*, 50:625 (2004).
47. H. Schramm, PhD thesis, Otto-von-Guericke Universität Magdeburg, Shaker, Aachen (Germany), 2005.
48. Y. Zang, and P.C. Wankat, *Ind. Eng. Chem. Res.* 42:4840 (2003).
49. Y. Kawajiri, and L.T. Biegler, *AIChE J.* 52:1343 (2006).
50. Y. Zang, and P.C. Wankat, *Ind. Eng. Chem. Res.* 41:2504 (2002).
51. P.S. Gomes, and A.E. Rodrigues, *Sep. Sci. Technol.* 42:223 (2007).
52. H. Schramm, A. Kienle, M. Kaspereit, and A. Seidel-Morgenstern, *Chem. Engng. Sci.* 58: 5217 (2003).
53. Z. Zhang, M. Mazzotti, and M. Morbidelli, *Korean J. Chem. Eng.* 21:454 (2004).
54. O. Ludemann-Hombourger, R.-M. Nicoud, M. Bailly, *Sep. Sci. Technol.* 35:1829 (2000).
55. H. Schramm, M. Kaspereit, A. Kienle, and A. Seidel-Morgenstern, *Chem. Eng. Technol.* 25:1151 (2002).
56. H. Schramm, S. Grüner, and A. Kienle, *J. Chromatogr. A* 1006:3 (2003).
57. H. Schramm, M. Kaspereit, A. Kienle, and A. Seidel-Morgenstern, *J. Chromatogr. A* 1006:77 (2003).
58. O. Ludemann-Hombourger, G. Pigorini, R.-M. Nicoud, D. Ross, and G. Terfloth, *J. Chromatogr. A* 947:59 (2002).
59. Z. Zhang, K. Hidajat, A. Ray, and M. Morbidelli, *AIChE J.* 48:2800 (2002).
60. Y. Kawajiri, and L.T. Biegler, *Ind. Eng. Chem. Res.* 45:8503 (2006).
61. Y. Kawajiri, and L.T. Biegler, *AIChE J.* 52:1343 (2006).

62. Y. Kawajiri, and L.T. Biegler, *J. Chromatogr. A* 1133:226 (2006).
63. P.C. Wankat, *Ind. Eng. Chem. Res.* 40:6185 (2001).
64. G. Ziomek, D. Antos, L. Tobiska, and A. Seidel-Morgenstern, *J. Chromatogr. A* 1116:179 (2006).
65. R. Wooley, Z. Ma, N.-H.L. Wang, *Ind. Eng. Chem. Res.* 37:3699 (1998).
66. K. Hashimoto, Y. Shirai, S. Adachi, *J. Chem. Eng. Jpn.* 26:52 (1993).
67. L.C. Keßler, and A. Seidel-Morgenstern, *J. Chromatogr. A* 1126:323 (2006).
68. C.Y. Chin, and N.-H.L. Wang, *Sep. Purif. Rev.* 33:77 (2004).
69. A.S. Kurup, K. Hidajat, and A.K. Ray, *Ind. Eng. Chem. Res.* 45:6251 (2006).
70. M. Bailly, R.-M. Nicoud, A. Philippe, and O. Ludemann- Hombourger, Patent appl. WO/2004/039468 (2004).
71. S. Abdelmoumen, L. Muhr, M. Bailly, and O. Ludemann- Hombourger, *Sep. Sci. Technol.* 41:2639 (2006).
72. G. Paredes, H.K. Rhee, and M. Mazzotti, *Ind. Eng. Chem. Res.* 45:6289 (2006).
73. B. Lim, C. Ching, R.B.H. Tan, and S. Ng, *Chem. Eng. Sci.* 50:2289 (1995).
74. J. Blehaut, and R.-M. Nicoud, *Analusis Mag.* 26:M60 (1998).
75. H. Lorenz, P. Sheehan, and A. Seidel-Morgenstern, *J. Chromatogr. A* 908:201 (2001).
76. M. Kaspereit, K. Gedicke, V. Zahn, A.W. Mahoney, and A. Seidel-Morgenstern, *J. Chromatogr. A* 1092:55 (2005).
77. M. Amanullah, and M. Mazzotti, *J. Chromatogr. A* 1107:36 (2006).
78. M. Kaspereit, PhD thesis, Otto-von-Guericke Universität Magdeburg, Shaker, Aachen (Germany), 2006.
79. K. Gedicke, M. Kaspereit, W. Beckmann, U. Budde, H. Lorenz, and A. Seidel-Morgenstern, *Chem. Eng. Res. Des.* 85:928 (2007).
80. P.E. Barker, G. Ganetsos, J. Ajongwei, and A. Akintoye, *Chem. Eng. J. Bioch. Eng.* 50:B23 (1992).
81. M. Bechtold, S. Makart, M. Heinemann, and S. Panke, *J. Biotechnol.* 124:146 (2006).
82. K. Hashimoto, S. Adachi, H. Noujima, and Y. Ueda, *Biotechnol. Bioeng.* 23:2371 (1983).
83. T. Borren, and H. Schmidt-Traub, *Chem-Ing-Tech* 76:805 (2004).
84. J. Fricke, M. Meurer, J. Dreisörner, and H. Schmidt-Traub, *Chem. Eng. Sci.* 54:1487 (2004).
85. M. Meurer, U. Altenhöner, J. Strube, and H. Schmidt-Traub, *J. Chromatogr. A* 769:71 (1997).
86. D. Azevedo, and A.E. Rodrigues, *Chem. Eng. J.* 82:95 (2001).
87. M. Kawase, T. Suzuki, K. Inoue, K. Yoshimoto, and K. Hashimoto, *Chem. Eng. Sci.* 51:2971 (1996).
88. G. Ströhlein, Y. Assuncao, N. Dube, A. Bardow, M. Mazzotti, and M. Morbidelli, *Chem. Eng. Sci.* 61:5296 (2006).
89. J.P. Meissner, and G. Carta, *Ind. Eng. Chem. Res.* 41:4722 (2002).
90. C. Migliorini, M. Fillinger, M. Mazzotti, and M. Morbidelli, *Chem. Eng. Sci.* 54:2475 (1999).

91. V.M.T.M. Silva, and A.E. Rodrigues, *AIChE. J.* 51:2752 (2005).

92. W.F. Yu, K. Hidajat, and A.K. Ray, *Chem. Eng. J.* 112:57 (2005).

93. T. Sainio, M. Kaspereit, A. Kienle, and A. Seidel-Morgenstern, *Chem. Eng. Sci.* 62:5674 (2007).

94. F. Lode, M. Houmard, C. Migliorini, M. Mazzotti, and M. Morbidelli, *Chem. Eng. Sci.* 56:269 (2001).

95. M. Mazzotti, A. Kruglov, B. Neri, D. Gelosa, and M. Morbidelli, *Chem. Eng. Sci.* 51:1827 (1996).

96. G. Ströhlein, F. Lode, M. Mazzotti, and M. Morbidelli, *Chem. Eng. Sci.* 59:4951 (2004).

97. B. Cho, R. Aris, R. Carr, *Proc. R. Soc. Lond. A* 383:147 (1982).

98. H.-K. Rhee, R. Aris, and N.R. Amundson, First-order Partial Differential Equations. Vol. I -- Theory and Applications of Single Equations, Dover Publications (2001).

99. H.-K. Rhee, R. Aris, and N.R. Amundson, First-order Partial Differential Equations. Vol. II - Theory and Applications of Hyperbolic Systems of Quasilinear Equations, Dover Publications (2001).

100. S. Grüner, and A. Kienle, *Chem. Eng. Sci.* 59:901 (2004).

101. G. Ströhlein, M. Mazzotti, and M. Morbidelli, *Chem. Eng. Sci.* 60:1525 (2005).

102. Z.Y. Zhang, K. Hidajat, and A.K. Ray, *Ind. Eng. Chem. Res.* 41:3213 (2002).

103. V. Mata, and A.E. Rodrigues, *J. Chromatogr. A* 939:23 (2001).

104. G. Ströhlein, L. Aumann, M. Mazzotti, and M. Morbidelli, *J. Chromatogr. A* 1126:338 (2006).

105. C.M. Grill, *J. Chromatogr. A* 796:101 (1998).

106. T.Q. Yan, and C. Orihuela, *J. of Chromatogr. A* 1156:220 (2007).

107. N. Abunasser, and P.C. Wankat, *Sep. Sci. Technol.* 40:3239 (2005).

108. R.C.R. Rodrigues, J.M.M. Araújo, and J.P.B. Mota, *J. Chromatogr. A* 1162:14 (2007).

Contents lists available at ScienceDirect

Separation and Purification Technology

journal homepage: www.elsevier.com/locate/seppur

Analysis of steady state recycling chromatography using equilibrium theory

Tuomo Sainio [a], Malte Kaspereit [b],*

[a] *Lappeenranta University of Technology, Skinnarilankatu 34, FIN-53850 Lappeenranta, Finland*
[b] *Max-Planck-Institut für Dynamik komplexer technischer Systeme, Sandtorstrasse 1,*
D-39106 Magdeburg, Germany

ABSTRACT

This paper presents a method for analysis and design of steady state recycling (SSR) chromatography under arbitrary purity or yield requirements. The approach applies to SSR processes in mixed-recycle operation and allows for the direct prediction of the steady state and the design parameters without performing dynamic simulations. Therefore, it simplifies optimal design of SSR processes and evaluation of process performance, while allowing minimizing the startup time of the process.

It was shown that, when the purity and/or yield of the product fractions is specified, the total injection width is the only free operating parameter in mixed-recycle SSR chromatography. Theoretical analysis of the process revealed that the productivity is necessarily lower than that of an optimized separation by batch chromatography. On the other hand, the SSR process always outperforms batch chromatography in terms of eluent consumption and product concentrations.

© 2008 Elsevier B.V. All rights reserved.

1. Introduction

Chromatography is one of the most important separation techniques in the pharmaceutical and fine chemical industries. Chromatography is successfully applied to numerous difficult preparative problems such as, for example, the separation of enantiomers [1].

When optimizing preparative chromatographic processes, one can observe a distinct trade-off between performance parameters. For example, an unconstrained maximization of throughput leads to very high injection volumes, which entail large portions of the chromatogram to be remained unresolved. Discarding the latter is barely acceptable in the case of expensive substances.

For binary separations, simulated moving bed (SMB) chromatography is an option to circumvent this problem, since this process has no waste stream. However, besides SMB systems, which suffer from rather high investment costs, several interesting single-column techniques have been suggested that enhance the yield by recycling the chromatogram partially or as a whole. In closed-loop recycling [2–4], the whole elution profile is recycled several times over the same column until complete separation is achieved. Back mixing that occurs in the recycle pump can be averted (at the expense of higher eluent consumption) by sophisticated column or pump arrangements (e.g., "alternate pumping" [5]). Further improvement is achieved by so-called peak shaving (see e.g., [3]),

wherein the pure leading and trailing sections of the chromatogram are collected ("shaved"), while only the unresolved remainder is recycled.

Steady state recycling (SSR) chromatography is a further development of the above concepts. In SSR processes, in addition to collecting the purified leading and trailing parts of the elution profile, a constant amount of fresh feed is added to each recycle fraction, which causes the process to attain a periodic steady state.

Different operating modes were proposed for SSR chromatography. In "mixed-recycle" mode [6], the whole recycle fraction is first collected and mixed with fresh feed before re-injection. Based on the equilibrium theory, an approach for analysis and design of this process was devised for the case of complete separation [6–9]. Using numerical simulations, it was shown that the mixed-recycle mode allows a reduction of eluent consumption also for systems with limited efficiency and, under certain conditions, enhancement of productivity [10].

Another SSR operating policy, the "closed-loop" mode [11], has gained considerable attraction. In order to preserve the already achieved partial separation of the recycle fraction, closed-loop recycling is combined with the injection of (unmixed) fresh feed. This concept appears particularly useful for very difficult separations and its feasibility has been demonstrated in several experimental studies [11–15]. Besides this, also other modes were proposed; for example, "segmented recycling" (i.e., injection of the mixed-recycle fraction before the fresh feed) and "combination of recyclings" (re-injection of the dispersed tail of the stronger adsorbing component, followed by the recycle fraction and, finally, fresh feed) [9,10].

Nomenclature

A	coefficient matrix in Eq. (7)
b	Langmuir parameter ($L\,mol^{-1}$, $L\,g^{-1}$)
c	concentration ($mol\,L^{-1}$, $g\,L^{-1}$)
$\bar{c}$	average concentration in a product fraction ($mol\,L^{-1}$, $g\,L^{-1}$)
EC	eluent consumption
m	mass (g)
P^j	purity of fraction j with respect to a target component
P_i	plateau in a chromatogram with constant concentration of i
PR	productivity
q	stationary phase concentration, $mol\,L^{-1}$, $g\,L^{-1}$
q_m	saturation capacity of the adsorbent, $mol\,L^{-1}$, $g\,L^{-1}$
R	recycle ratio
t	dimensionless time relative to beginning of cycle
u	interstitial velocity
V	injection volume (L)
x	dimensionless space coordinate
Y	yield with respect to a target component

Greek symbols

ε	bed porosity
ϕ	phase ratio
τ	dimensionless time relative to the end of injection
ξ	slope of characteristic in the hodograph plane
Γ	characteristic of a simple wave
$\sum$	shock wave

Subscripts

1, 2	components to be separated
A1	beginning of product fraction A
A2	end of product fraction A
B1	beginning of product fraction B
B2	end of product fraction B
col	column
cycle	cycle of an SSR process
inj	injection
P	injection plateau
rec	recycle fraction
+	faster wave or shock
−	slower wave or shock

Superscripts

A	product fraction A
B	product fraction B
F	steady state feed
F0	fresh feed
P1F	pure component 1 plateau
T	transmitted wave

Although closed-loop SSR chromatography is (apparently in contrast to the mixed-recycle option) successfully commercialized by the company Novasep (Pompey, France), so far only an empirical experimental design method exists for this process (see e.g., [11]). Unfortunately, the procedure neither allows the *a priori* estimation of the steady state, nor does it guarantee the fulfillment of purity requirements or optimum performance. The mentioned equilibrium analysis for SSR processes with mixed-recycle (e.g., [6,9]) meets these criteria, but suffers from a certain complexity. Finally, both design approaches hold only for two pure product fractions.

In view of the above aspects, the main goal of this work is to provide a theoretical framework that allows (i) for a straightforward analysis and optimal design of SSR chromatography, and (ii) to apply SSR processes to separation problems with arbitrary purity requirements. For this purpose, we will extend the application range of equilibrium theory to mixed-recycle SSR processes under arbitrary purity requirements.

This contribution is structured as follows. After a short summary of the main principles of SSR chromatography, the theoretical framework will be developed. It will be shown that the steady state of an SSR process can be predicted directly from the adsorption isotherms and the composition of the fresh feed, which largely simplifies process analysis and optimal design. Subsequently, the method will be used to assess the performance of SSR chromatography with mixed-recycle for a generic example with competitive Langmuir adsorption isotherms. As will be shown, the approach is a useful tool for evaluation and design of process performance, since it predicts the optimum performance of an SSR process and allows to minimize the startup time of the process. Finally, a short discussion will be given on practical aspects and the applicability of the method to design mixed-recycle SSR processes.

2. Principle of SSR chromatography

The principle of SSR chromatography and different technological options for its practical realization have been described in detail elsewhere (e.g., [10–12]). Here we will explain only the most fundamental aspects.

Fig. 1 (top) contains a scheme of an SSR process. Depending on the operating mode (i.e., mixed-recycle or closed-loop SSR), one or more pumps and several multi-port valves are required to realize the alternating streams of fresh feed mixture ($F0$), eluent (E), and recycle (R), and the collection of the product fractions A and B, respectively.

There are several options to initiate an SSR process. The commonly used approach results in concentration profiles as shown in Fig. 1 (bottom). The process is started by injecting a small amount of fresh feed mixture ($F0$) onto the initially unloaded column. The actual SSR cycle starts at time t_{A1}, when the column effluent is directed to fraction A to collect the less adsorbed component 1 (solid lines). Between t_{A2} and t_{B1} the recycle fraction elutes, which
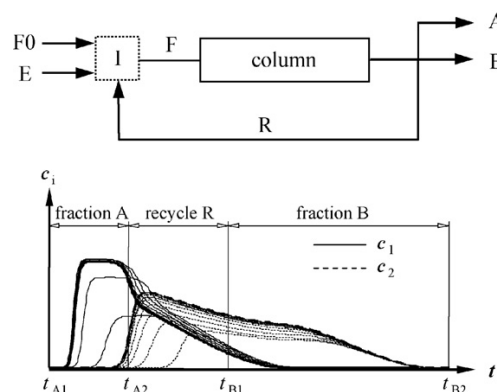
Fig. 1. (Top) Schematic representation of an SSR process. $F0$, fresh feed; F, column feed; E, eluent; A, product fraction (weaker adsorbing component 1); B, product fraction (strong adsorbing component 2); R, recycle fraction; I, injection port (injection loop in closed-loop mode, or mixer in mixed-recycle mode). (Bottom) Example for fraction collection and startup behavior in mixed-recycle mode. The diagram shows an overlay of the concentration profiles at column outlet for cycles 1, 3,. . .,25. Thick lines: concentration profiles at steady state (cycle 25). The cut times are relative to the start of the corresponding injection.

contains both species. In mixed-recycle mode, the whole recycle fraction is collected in a reservoir, mixed with fresh feed and then injected. In closed-loop recycling mode, the outlet is now connected to the column inlet; fresh feed is injected again at a certain position during this step by switching an injection loop into the recycle stream. In both modes, after time t_{B1}, fraction B (containing an excess of component 2, dashed lines) is collected until the chromatogram is eluted completely at t_{B2}.

By repeating the above procedure several times, the two components accumulate in the system until a periodic steady state is attained in which the chromatograms and the average product compositions do not vary from cycle to cycle. This is shown in the bottom of Fig. 1. Please note that in the example four cut times (t_{A1}, t_{A2}, t_{B1} and t_{B2}) were chosen such that two product fractions are obtained with purities below 100%. Such cases are in the scope of this work.

It should be emphasized that a systematic comparison of the performance of closed-loop and mixed-recycle SSR processes is beyond the scope of this work. However, the mixed-recycle mode has – besides the disadvantage of "destroying" the already partially resolved concentration profile of the recycle – also some distinct advantages and can outperform batch chromatography [10]. Therefore, a brief discussion of relevant aspects will be given in Section 5.

A significant problem related to SSR chromatography is that an optimal design is difficult due the dynamic character of the process. Obviously, given the purity requirements as constraints, the main design parameters are the injection volume and the cut times. However, the optimal values for these parameters depend on the steady state concentration profiles and *vice versa*. As already mentioned, the only existing design approach for the closed-loop operating mode is an empirical shortcut method based on an experimental procedure [11]. Although the method is thoughtful and simple to apply even with only little knowledge of system properties, its drawback is that it gives no prediction with respect to the steady state and process performance. These are accessible only by actually carrying out an SSR process until steady state is obtained. Furthermore, the approach does not guarantee the intended complete separation or optimal process performance. For the mixed-recycle mode, on the other hand, an equilibrium-design approach [6,9] is available for the limiting case of 100% purity and yield.

Another important aspect is the startup behavior (cf. Fig. 1, bottom). Process performance (i.e., product concentrations, productivity, and eluent consumption) is limited during this startup phase and – depending on the operating parameters – a rather large number of cycles can be required to attain steady state. Approximately 20 cycles seem to be necessary [11–13]. However, if the steady state (i.e., the recycle composition and volume) is known, the duration of the startup could be minimized to only a single cycle by initiating the process with a "full injection" (i.e., volume of recycle plus fresh feed) with steady state concentrations [6].

As will be shown in the next section, analyzing the mixed-recycle SSR operation in the frame of equilibrium theory allows for a direct prediction of the steady state for corresponding SSR processes with arbitrary purity requirements and, thus, to tackle some of the shortcomings of the existing design approaches.

3. Theory of SSR chromatography

As usual in designing separation processes, the goal is to find operating parameters that lead to optimal process performance. In the present case, these are the four cut times (t_{A1}, t_{A2}, t_{B1}, and t_{B2}) shown in Fig. 1 and the injection width (Δt_{inj}). Here we present a method for choosing the operating parameters such that, in the steady state, arbitrary purity and/or yield constraints can be satisfied. For this purpose we will adopt the so-called equilibrium theory

of chromatography for systems that follow the competitive Langmuir adsorption model. The approach is similar to that chosen by Bailly and Tondeur, and Charton [6,9], but will be extended here to the case of arbitrary purity and yield requirements.

As will be shown below, it is possible to determine three of the four cut times directly from the isotherm parameters, without carrying out a dynamic column simulation from the initial state of the system to the steady state. In fact, these three cut times (i.e., t_{A2}, t_{B1}, and t_{B2} in Fig. 1) are sufficient to fully determine the steady state feed concentrations. The fourth cut time (t_{A1}) is required only to assess process performance. Under certain conditions, also t_{A1} can be determined explicitly; otherwise a single integration of a steady state chromatogram is required.

3.1. Design specifications

In this work, it is assumed that the desired purities of the product fractions are known as design constraints. With respect to Fig. 1, these are given by

$$P^A = \frac{m_1^A}{m_1^A + m_2^A} = \int_{t_{A1}}^{t_{A2}} \frac{c_1}{c_1 + c_2} dt \tag{1}$$

$$P^B = \frac{m_2^B}{m_1^B + m_2^B} = \int_{t_{B1}}^{t_{B2}} \frac{c_2}{c_1 + c_2} dt \tag{2}$$

where m_i^j denotes the mass of component $i = (1, 2)$ in product fraction $j = (A, B)$. As an alternative to the specifications of desired purities, the yields of the components in the desired product fractions can be given. These are defined as follows

$$Y_1 = \frac{m_1^A}{m_1^{F0}} = \frac{\int_{t_{A1}}^{t_{A2}} c_1 \, dt}{c_1^{F0}[\Delta t_{inj} - (t_{B1} - t_{A2})]} \tag{3}$$

$$Y_2 = \frac{m_2^B}{m_2^{F0}} = \frac{\int_{t_{B1}}^{t_{B2}} c_2 \, dt}{c_2^{F0}[\Delta t_{inj} - (t_{B1} - t_{A2})]} \tag{4}$$

where the dimensionless injection width $\Delta t_{inj} = (V_{fresh} - V_{rec})/\varepsilon V_{col}$ refers to the width of the pulse that is fed into the column after mixing the recycle fraction and the fresh feed.

It should be noted that, since the SSR process represents a binary separation without a waste stream, the purity and yield constraints in Eqs. (1)–(4) are interchangeable [16,17]. From global mass balances around such a process the following relations between the purities and the yields can be derived

$$Y_1 = \frac{P^A}{P^{F0}} \frac{P^{F0} + P^B - 1}{P^A + P^B - 1} \tag{5}$$

$$Y_2 = \frac{P^B}{1 - P^{F0}} \frac{P^A - P^{F0}}{P^A + P^B - 1} \tag{6}$$

where P^{F0} is defined as $P^{F0} = c_1^{F0}/(c_1^{F0} + c_2^{F0})$. In other words, by specifying any two of the four quantities, the remaining two are also determined. In principle, any combination of constraints could be used to determine the cut times and the resulting steady state feed concentrations of the SSR process. However, the most convenient calculation method is obtained by choosing P^B and Y_2, which will be applied below.

3.2. Hodograph representation of mixed-recycle SSR processes

From a mathematical modeling point of view, operation of a chromatography column in SSR mode does not introduce new phenomena into the calculation domain since fractionation of the effluent stream and mixing of the recycle are performed outside the column. Therefore, in the limit of infinite column efficiency, the conventional ideal model of chromatography, given in Eqs. (7) and

(8), can be used to describe the propagation of the concentration states in the column:

$$\mathbf{A}\frac{\partial \mathbf{c}}{\partial t} + \frac{\partial \mathbf{c}}{\partial x} = 0 \tag{7}$$

where

$$\mathbf{A} = \begin{bmatrix} 1 + \phi\dfrac{\partial q_1}{\partial c_1} & \phi\dfrac{\partial q_1}{\partial c_2} \\ \phi\dfrac{\partial q_2}{\partial c_1} & 1 + \phi\dfrac{\partial q_2}{\partial c_2} \end{bmatrix}, \quad \mathbf{c} = \begin{bmatrix} c_1 \\ c_2 \end{bmatrix} \tag{8}$$

and q is stationary phase concentration, ϕ is phase ratio, x is a reduced space coordinate (at column outlet, $x = 1$), and t is a reduced time (elution time of a non-retained component is $t = 1$).

The following discussion is limited to binary systems with adsorption according to competitive Langmuir adsorption isotherms given by

$$q_i = \frac{q_{m,i} b_i c_i}{1 + b_1 c_1 + b_2 c_2}, \quad i = 1, 2 \tag{9}$$

For this isotherm model, Eq. (7) has no analytical solution when the space coordinate, x, and time, t, are the independent variables. However, if the concentrations c_1 and c_2 are used as the independent variables, the model forms a coupled system of two linear first-order partial differential equations, which can be solved analytically by the *method of characteristics*. This is the basis of the so-called equilibrium theory, which we now apply to SSR chromatography. Equilibrium theory is described extensively in the literature [18–20], and only the most relevant aspects can be covered here.

The solutions of Eq. (7) can be constructed in the so-called hodograph plane spanned by the concentrations c_1 and c_2. An example is given in Fig. 2c. Regions of the solution where the independent variables c_1 and c_2 are functionally related are called *simple waves*. For Langmuir isotherms, simple waves correspond to segments on straight lines, called *characteristics* (dashed lines in Fig. 2c). Characteristics running from the lower left to the upper right are referred to as Γ_+ characteristics, those directed from upper left to lower right as Γ_- characteristics, respectively. Their slopes dc_1/dc_2 can be calculated explicitly from the right eigen*vectors* of the coefficient matrix $\mathbf{A}$ in Eq. (8), and therefore depend on the isotherm parameters only. Two distinct propagation velocities are associated with each state (c_1 and c_2), because it can be a part of the solution on either a Γ_+ or a Γ_- characteristic. These velocities can be obtained from the eigenvalues of $\mathbf{A}$. Regions

of the solution where c_1 and c_2 are constant are represented by single points on the hodograph plane.

It is well known that the non-linear nature of Eq. (7) can give rise to discontinuities (such as shock waves) in the solution. In the case of Langmuir isotherms, the images of such discontinuities on the hodograph plane also fall onto the characteristics. Often, the corresponding shock paths are called Σ_+ and Σ_- shocks, respectively. The propagation velocities of shock waves are given by the mass balance across the discontinuity.

Let us recall that a pulse injection into a chromatographic column consists of two step-wise changes of the inlet concentrations. The first step changes the input concentration from the initial state (i.e., pure eluent) to the injection mixture. In the second step (at the end of the injection), the input composition is changed back to the initial state. The network of characteristics in the hodograph plane can be seen to determine the "legal solution path" for the response of the chromatographic column to such step-wise change, because the initial and final states must be connected by the characteristics. For example, let us assume that the chromatogram in Fig. 2a corresponds to a wide pulse of fresh feed with concentrations c_i^{F0}. The corresponding hodograph plot in Fig. 2c shows that the shocks in the front of the elution profile connect the initial state O and the injection plateau $F0$ by segments O–P_1^{F0} and P_1^{F0}–$F0$. The mixed simple wave eluted after the injection plateau maps on the line segment $F0$–P_2, whereas the pure component 2 wave maps onto the portion O–P_2 of the abscissa. Each of the plateaus in the elution profile represents a single point in the hodograph plane, marked with the corresponding letters. The actual *route* between initial state O and "final" state $F0$ is fixed unambiguously, since the initial state always lies on a Γ_+ characteristic and the final state on a Γ_- characteristic [18,19].

It is emphasized that for Langmuir isotherms, explicit equations exist for calculating the slopes of the characteristics, their intersection points, as well as the propagation velocities associated with each concentration state (see e.g., [18–21]). The only information needed is the isotherm parameters, phase ratio, and the initial and final concentrations.

With respect to SSR chromatography, the question now arises, where would the steady state feed concentration be located in the hodograph plane if the process is carried out by mixing the recycle fraction and fresh feed? Let us assume that the process is started with a wide pulse of fresh feed ($F0$), resulting in the chromatogram in Fig. 2a and the corresponding hodograph plot (O–P_1F0–$F0$–P_2–O) in Fig. 2c. The concentration state eluted at cut time t_{B1} during the first injection lies on the segment $F0$–P_2 for any feasible purity
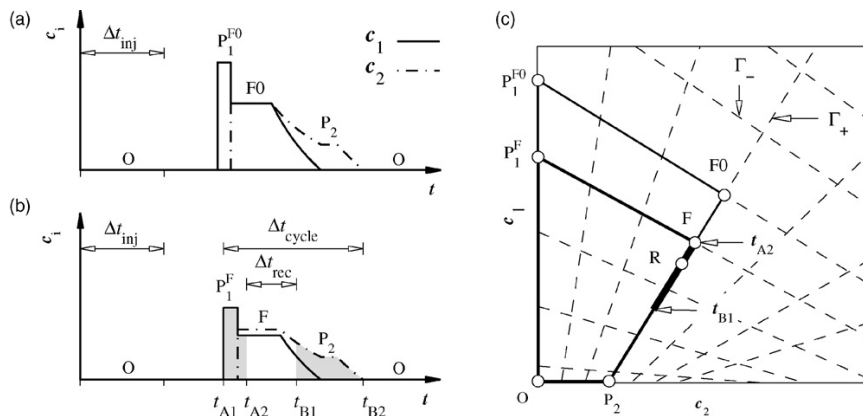

Fig. 2. Steady state recycling chromatography in mixed-recycle operation. (a) Chromatogram for first injection (injection of fresh feed, concentrations c_i^{F0}). (b) Chromatogram at steady state (injection concentrations c_i^{F}). (c) Corresponding hodograph representations.

constraint P^B. This is because the concentrations at the rear of the profile cannot exceed $F0$, and placing the cut position on line segment P_2–O would mean that some pure product is lost since only part of the pure component 2 profile is collected in product fraction B. Also the concentration state eluted at t_{A2} must lie on the line segment $F0$–P_2 because the cut position is located either on the mixed wave or, in the case of large injection width and high P^A, on the injection plateau. As a consequence, the entire recycle fraction (bold line in Fig. 2c) must map on a segment of the Γ_+ characteristic passing through the fresh feed composition $F0$. The volume-averaged composition of the recycle is, therefore, represented by a single point (R) within the same line segment. The important consequence of this is that, according to the lever rule, also the composition of the next injection (with results from mixing the fresh feed, $F0$, with the recycle R), must map to a point on the same Γ_+ characteristic.

In other words, the feed composition cannot move away from the Γ_+ characteristic that passes through (c_1^{F0}, c_2^{F0}) during the subsequent cycles. Eventually, a steady state is reached with feed composition F in the hodograph plot. The corresponding chromatogram is displayed in the bottom of Fig. 2b.

It is clear that, as long as the SSR process is operated such that the purity and yield constraints can be fulfilled, the image of the rear part of the elution profile in the hodograph plane, and thus also in the chromatogram, remains unaltered. This valuable information provides the basis for determining the cut times that fulfill arbitrary purity requirements in steady state. Bailly and Tondeur [6] applied the same principle to determine cut times in the limiting case of 100% purity of both product fractions. It should be noted, however, that the method presented below for choosing the cut times is not limited to pure products and complete yield.

3.3. Determination of cut times t_{A2}, t_{B1}, and t_{B2}

Since the rear of the profile remains unaltered, we start by determining cut times t_{B1} and t_{B2}. Evidently, the cut time t_{B2} should be chosen such that it matches the time of complete elution of the injection (cf. Fig. 2b). It is thus obtained by setting $c_1 = c_2 = 0$ and calculating the eigenvalue of $\mathbf{A}$ corresponding to the Γ_- simple wave on the abscissa. For Langmuir isotherms, the resulting well-known expression for t_{B2} is

$$t_{B2} = \Delta t_{inj} + 1 + \phi \frac{d\,q_2}{d\,c_2}\bigg|_{\substack{c_1 = 0 \\ c_2 = 0}} = \Delta t_{inj} + 1 + \phi q_{m,2} b_2 \qquad (10)$$

As a next step, cut time t_{B1} is chosen such that the purity constraint of product fraction B, Eq. (2), is fulfilled. Although an explicit expression for t_{B1} can be obtained, it is rather complex and it was found more convenient to use a fast numerical technique: while using a search algorithm to find the lower integration limit that satisfies Eq. (2), the integral terms in this equation are evaluated analytically. The required analytical expressions for $c_i(t)$ are given, for example, by Guiochon et al. [21]

As noted earlier, purity constraints can equivalently be given as yield constraints. Once t_{B2} is obtained, the yield constraint of component 2, displayed in Eq. (4), can be solved for t_{A2}:

$$t_{A2} = t_{B1} - \Delta t_{inj} + \frac{\int_{t_{B1}}^{t_{B2}} c_2 \, dt}{c_2^{F0} Y_2} \qquad (11)$$

As seen in the equation, the beginning and end of the recycle fraction can be determined without knowing the steady state feed concentration.

It is also interesting to note that the cut time t_{A2} is independent of the injection width. This is observed by rewriting Eq. (11) in terms

of the elution time relative to the end of the injection, $\tau = t - \Delta t_{inj}$, as follows:

$$t_{A2} = \tau_{B1} + \frac{\int_{\tau_{B1}}^{\tau_{B2}} c_2 \, d\tau}{c_2^{F0} Y_2} \qquad (12)$$

Since this transformation is merely a linear shift on the abscissa, the value of the integral term remains unaffected. Applying the same transformation to Eq. (2) shows that also τ_{B1} is independent of injection width.

3.4. Determination of steady state feed composition

The steady state feed concentration, c_1^F, corresponding to a given injection width can be calculated from the following mass balance of component 1 around the feed node

$$c_1^F \Delta t_{inj} = \int_{t_{A2}}^{t_{B1}} c_1 \, dt + c_1^{F0} [\Delta t_{inj} - (t_{B1} - t_{A2})] \qquad (13)$$

A functional relationship between c_1^F and c_2^F is given by the slope ξ_+^{F0} of the Γ_+ characteristic that passes through $F0$ (see Fig. 2c), which depends on the isotherm parameters and the fresh feed composition. Thus, for c_2^F holds

$$c_2^F = c_2^{F0} + \frac{1}{\xi_+^{F0}}(c_1^F - c_1^{F0}) \qquad (14)$$

It is interesting to note that the steady state feed composition becomes independent of Δt_{inj} when t_{A2} is located on the injection plateau (i.e., for large injection volumes). This is observed by rewriting Eq. (13) as

$$c_1^F \Delta t_{inj} = (\Delta t_{inj} + \tau_P - t_{A2})c_1^F + \int_{\tau_P}^{\tau_{B1}} c_1 \, d\tau + c_1^{F0}(\Delta t_{inj} $$
$$- (\Delta t_{inj} + \tau_{B1} - t_{A2})) \qquad (15)$$

which can be re-arranged to give

$$c_1^F = \frac{\int_{\tau_P}^{\tau_{B1}} c_1 \, d\tau + c_1^{F0}(t_{A2} - \tau_{B1})}{t_{A2} - \tau_P} \qquad (16)$$

Here τ_P denotes the elution time of the end of the injection plateau relative to the end of the injection and thus depends on c_1^F and the isotherm parameters only. Since t_{A2} and τ_{B1} are also independent of Δt_{inj}, so is the steady state feed concentration.

3.5. Determination of t_{A1}

So far, we have considered only the rear part of the elution profile, which proved to be sufficient to determine the steady state feed concentrations and three of the four cut times. The remaining cut time, t_{A1}, should obviously be chosen equal to the elution time of the pure component 1 shock (cf. Fig. 2b) to minimize the cycle time. The task is therefore to evaluate the elution time of the front shock that corresponds to the steady state feed concentration.

According to the equilibrium theory, the propagation velocity of a shock depends on its height. In the case of a *large injection* width, such as depicted in Fig. 2b, the plateau P_1^F in the front of the elution profile is not eroded during elution. The velocity of the shock is thus constant, and the cut time t_{A1} can be calculated analytically by

using the following equation:

$$t_{A1} = 1 + \phi \frac{q_1(c_1^{P1F}, 0)}{c_1^{P1F}} \tag{17}$$

where the height of the plateau $c_1^{P1F} = c_1^F - \xi_-^F c_2^F$, is obtained from the slope ξ_-^F of the Γ_- characteristic passing though the steady state feed on the hodograph plane (point F in Fig. 2c).

A typical chromatogram obtained for *small injection* widths is displayed in Fig. 3a. As seen in the figure, for sufficiently small injections, the pure component 1 plateau erodes completely, and the height of the shock decreases while it propagates through the column. In this case, the velocity of the shock is not constant, and a closed-form solution for t_{A1} cannot be found. Several approaches have been applied in the literature for solving this problem. Guiochon et al. [21] describe a calculation method that combines an analytical solution for the rear part of the chromatogram with a numerical scheme for calculating the front of the chromatogram. Rhee et al. [19] present a step-by-step procedure for solving Eq. (7) by tracking the trajectories of the shocks and simple waves in a distance–time plane. The method applied in this work is adapted from that of Rhee et al. For the sake of brevity, only the necessary steps to determine t_{A1}, instead of constructing the entire chromatogram, are described below.

The distance–time diagram representation of a chromatogram corresponding to small injection is displayed in Fig. 3b. The slopes of the shocks (thick solid lines) and simple wave boundaries (thin solid lines) are inversely proportional to their velocities in the column. In order to determine t_{A1}, the location of the point A_1, where the first shock (Σ_+) reaches the outlet of the column, has to be found.

The two shocks in the front of the elution profile propagate with constant velocities as long as the shock heights are constant. They are, thus, represented by straight lines from the origin until points I_1 and I_2 in the diagram, where interaction of waves starts. These two points are easily mapped on the x–τ plane because the slopes of the intersecting lines are explicitly given by the isotherm data and the steady state feed concentration. The propagation directions of the shocks are obtained from the so-called jump condition as shown in Eq. (18), and the slopes of the simple wave boundaries are obtained from the eigenvalues of the coefficient matrix A in Eq. (8):

$$\frac{d\tau}{dx}\bigg|_{\Sigma_+} = 1 + \phi \frac{q_1^{P1F}(c_1^{P1F}, 0)}{c_1^{P1F}}, \qquad \frac{d\tau}{dx}\bigg|_{\Sigma_-} = 1 + \phi \frac{q_2^F(c_1^F, c_2^F)}{c_2^F} \tag{18}$$

At I_1, the injection plateau vanishes because the mixture wave (Γ_+) reaches the mixture shock (Σ_-). The result of the subsequent wave interaction is a transmitted Γ_+ wave, which contains only component 1. This new wave is indicated with dashed lines in both the chromatogram and the distance–time diagram in Fig. 3 and denoted by Γ_+^T.

As seen in the diagram, the pure component 1 shock travels with a constant velocity until point I_2, where it begins to interact with the transmitted Γ_+^T wave. During the interaction, the height of the shock decreases, and its propagation velocity is thus reduced. This is observed as a curved trajectory I_2–A_1 of the shock in the figure. For simplicity, a numerical scheme was used to track this trajectory. It is known that everywhere between I_2 and A_1, the height of the Σ_+ shock matches the concentration c_1 on the Γ_+^T wave. Therefore, the Γ_+^T wave that results from interaction between the Σ_- shock and the Γ_+ wave was stored as a tabulated function. Starting from I_2, a small step in the direction determined by the velocity of the Σ_+ shock was taken. The height of the shock at this new point was obtained by numerically solving for the concentration c_1 that is found on the Γ_+^T wave at this point. The direction of the Σ_+ shock was updated, and the procedure was repeated until arriving at A_1 (i.e., until $x = 1$).

3.6. Possible extensions of the theory

The above discussion was limited to binary systems with competitive Langmuir adsorption isotherms. However, the method presented here can be applied equally well to multicomponent mixtures when cut times t_{A2} and t_{B1} are located on the first mixed simple wave (where none of the concentrations is zero). In other cases, the steady state feed concentration moves away from the Γ_+ characteristic passing through the fresh feed point in the multidimensional hodograph space, and the cut time t_{A2} cannot be determined by integration of the profiles from the rear.

Further, it is well known that ion exchange equilibria with constant selectivities can be treated analogously to Langmuirian systems [23]. A ternary system reduces to a binary system when the compositions are expressed in equivalent fractions. In fact, the original work on SSR chromatography by Bailly and Tondeur [6] considered ion exchange in the system H$^+$/Na$^+$/K$^+$.

4. Performance evaluation of mixed-recycle SSR chromatography

The most common performance parameters of chromatographic processes are the productivity, *PR*, and eluent consumption, *EC*. In addition, the average product concentrations, $\bar{c}_1^A$ and $\bar{c}_2^B$ are of interest. The yields, Y_1 and Y_2, could also be interpreted as performance parameters, but are treated here as constraints because they are interchangeable with P^A and P^B (see Eqs. (5) and (6)).

Eluent consumption and productivity are here defined for component 1 as follows (and analogously for component 2):

$$EC_1 = \frac{V_{col}\varepsilon(\Delta t_{cycle} - \Delta t_{inj})}{m_1^A} = \frac{\Delta t_{cycle} - \Delta t_{inj}}{Y_1 c_1^{F0}(\Delta t_{inj} - \Delta t_{rec})} \tag{19}$$

$$PR_1 = \frac{m_1^A}{\Delta t_{cycle}} = \frac{Y_1 c_1^{F0} V_{col}\varepsilon(\Delta t_{inj} - \Delta t_{rec})}{\Delta t_{cycle}} \tag{20}$$

The average concentrations in the product fractions A and B are obtained by integration of the elution profiles with the determined cut times as limits

$$\bar{c}_1^A = \frac{1}{t_{A2} - t_{A1}} \int_{t_{A1}}^{t_{A2}} c_1 \, dt, \qquad \bar{c}_2^B = \frac{1}{t_{B2} - t_{B1}} \int_{t_{B1}}^{t_{B2}} c_2 \, dt \tag{21}$$

It was shown above, that for given purity or yield constraints and a given fresh feed composition, the *injection width is the only freely adjustable operating parameter*. Therefore, we first introduce the explicit dependency of the operational parameters (i.e., the times required for recycling and complete cycle) on the injection width. This has not been attempted in previous works on SSR processes. This allows analyzing its influence on the performance parameters (productivity, eluent consumption, and product concentrations). It should be noted again that the term "injection width" refers to the volume of the pulse obtained by mixing together the recycle fraction and the fresh feed relative to the volume of the column.

To predict the optimum performance of the SSR process, we assume that "stacked injections" can be accomplished. This means that injection times are chosen such that no gap exists between fraction B of the *n*th cycle and fraction A of (*n* + 1)th cycle (which is possible in mixed-recycle mode). In this case the cycle time is

$$\Delta t_{cycle} = t_{B2} - t_{A1} = \Delta t_{inj} + \tau_{B2} - t_{A1} \tag{22}$$

In practice, a safety gap might be desired between the cycles. In such cases the cycle time can be increased accordingly. Overlaps between cycles are not considered here.

The width of the recycle fraction, $\Delta t_{rec} = t_{B1} - t_{A2}$, increases linearly with increasing Δt_{inj}, as is observed by rearranging Eq. (11)
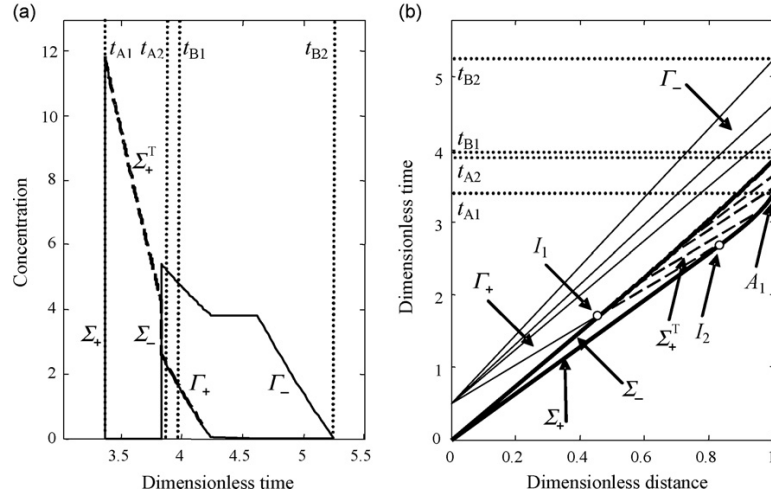
Fig. 3. Determination of t_{A1} by integration of Eq. (7) in the t–x plane. (a) Typical chromatogram for the case of small Δt_{inj} (wave interaction). (b) Trajectories of the shocks and simple waves in t–x plane. Thick lines: shock waves; thin lines: boundaries of simple waves; dashed line: transmitted Γ_+^T wave.

and differentiating with respect to the injection width

$$\frac{\partial \Delta t_{rec}}{\partial \Delta t_{inj}} = \frac{\partial (t_{B1} - t_{A2})}{\partial \Delta t_{inj}} = 1 \qquad (23)$$

Using this information, it is found that the amount of fresh feed introduced to the process during each cycle, and consequently the amount of products obtained in steady state, is independent of injection width

$$\frac{\partial m_1^{F0}}{\partial \Delta t_{inj}} = c_1^{F0} V_{col} \varepsilon \frac{\partial (\Delta t_{inj} - t_{rec})}{\partial \Delta t_{inj}} = 0 \qquad (24)$$

This result means that, in an SSR process, the specification of desired yields or purity requirements fixes the achievable throughput per cycle, which cannot be altered by changing the injection width.

As discussed earlier, the elution time of the pure component 1 shock, t_{A1}, depends on its height. As long as the plateau P_1^F (see Fig. 2b) has not completely eroded, the height of the shock depends on c_1^F only, which was above shown to be constant for large injections. In this case, one obtains from Eqs. (10) and (22) that the cycle time is directly proportional to the injection width (since τ_{B2} is independent of Δt_{inj}):

$$\frac{\partial t_{cycle}}{\partial \Delta t_{inj}} = \frac{\partial}{\partial \Delta t_{inj}} (\tau_{B2} + \Delta t_{inj} - t_{A1}) = 1 \, (\text{large } \Delta t_{inj}) \qquad (25)$$

In case of small injections, on the other hand, no closed form expression for t_{A1} can be given. A parametric analysis using the approach described in Section 3.5, and applying small and large separation factors, low and high purities, as well as weakly and strongly non-linear adsorption isotherms indicated that, in a mixed-recycle SSR process, t_{A1} always increases with Δt_{inj}. Moreover, the derivative $\partial t_{A1}/\partial \Delta t_{inj}$ was found to be positive but less than unity in all cases. Therefore, we propose the following empirical inequality for the present analysis

$$0 < \frac{\partial t_{cycle}}{\partial \Delta t_{inj}} = 1 - \frac{\partial t_{A1}}{\partial \Delta t_{inj}} \le 1 \qquad (26)$$

4.1. Effect of injection width on performance parameters

Using Eqs. (23)–(26) together with the definition of eluent consumption yields Eq. (27), which states that the eluent consumption

decreases monotonically or remains constant with increasing injection width.

$$\frac{\partial EC_1}{\partial \Delta t_{inj}} = \frac{1}{Y_1 c_1^{F0}} \left(\frac{\partial t_{cycle}}{\partial \Delta t_{inj}} - 1 \right) \le 0 \qquad (27)$$

The equality sign refers to large injections where the pure component 1 plateau has not eroded. In other words, increasing the injection width Δt_{inj} improves the performance in terms of eluent consumption. The same result is obtained if the analysis is carried out for component 2.

For productivity, PR_1, a similar treatment as above yields Eq. (28). Accepting the empirical inequality in Eq. (26) implies that the productivity of mixed-recycle SSR processes always decreases with increasing injection width, which is in accordance with our observations.

$$\frac{\partial PR_1}{\partial \Delta t_{inj}} = -\frac{Y_1 m_1^{F0}}{(\Delta t_{cycle})^2} \left(1 - \frac{\partial t_{A1}}{\partial \Delta t_{inj}} \right) < 0 \qquad (28)$$

For the average concentration of component 1 in product fraction A we derive Eq. (29). Again, for such large injection the plateau P1 prevails, $\partial t_{A1}/\partial \Delta t_{inj} = 0$ and the average concentration is constant. In the case of small injections, an increase in concentration is expected because $\partial t_{A1}/\partial \Delta t_{inj}$ was found to be a positive number in the parametric analysis.

$$\frac{\partial \bar{c}_1^A}{\partial \Delta t_{inj}} = \frac{\partial}{\partial \Delta t_{inj}} \left(\frac{Y_1 c_1^{F0} (\Delta t_{inj} - \Delta t_{rec})}{t_{A2} - t_{A1}} \right)$$
$$= \frac{Y_1 c_1^{F0} (\Delta t_{inj} - \Delta t_{rec})}{(t_{A2} - t_{A1})^2} \frac{\partial t_{A1}}{\partial \Delta t_{inj}} \qquad (29)$$

The average concentration of product fraction B, on the other hand, is always independent of injection width, as observed in the following equation:

$$\frac{\partial \bar{c}_2^B}{\partial \Delta t_{inj}} = \frac{\partial}{\partial \Delta t_{inj}} \left(\frac{Y_2 c_2^{F0} (\Delta t_{inj} - \Delta t_{rec})}{t_{B2} - t_{B1}} \right) = 0 \qquad (30)$$

Finally, it should be noted that there exists a minimum injection width below which the design constraints (P, Y) cannot be matched exactly, but will be exceeded. In other words, for a sufficiently small injection, separation of the components becomes so

good that, if the purity constraints are to be fulfilled for both product fractions simultaneously, there will be no recycle fraction. The minimum injection width is thus readily obtained from Eq. (4) by setting $t_{A2} = t_{B1}$, which yields

$$\Delta t_{\text{inj,min}} = \frac{\int_{\tau_{B1}}^{\tau_{B2}} c_2 \, dt}{c_2^{F0} Y_2} \tag{31}$$

The above findings can be summarized as follows:

- The throughput per cycle is independent of Δt_{inj}.
- The cycle and recycle times always increase with increasing Δt_{inj}.
- Correspondingly, the productivity *PR* always decreases with increasing Δt_{inj}.
- Eluent consumption *EC* decreases with increasing Δt_{inj} for small injections, but is independent of Δt_{inj} for large injections.
- Concentration of product fraction A increases with Δt_{inj} for small injections, but is independent of Δt_{inj} for large injections.
- Concentration of product fraction B is always independent of Δt_{inj}.
- Purity constraints can be matched exactly only above a certain minimum injection width relative to column size.

Finally, it should be emphasized that these results are obtained by using dimensionless times (relative to the elution time of a non-retained compound) instead of real times, and the performance parameters are thus independent of the physical dimensions of the column.

4.2. Performance of the SSR process for a generic example

The calculation method presented above was applied to study the performance of mixed-recycle SSR chromatography for varying purity requirements of the product fractions. In view of the above findings, the effect of the operating parameter, Δt_{inj}, on *PR*, *EC*, and product concentrations was of particular interest. A generic example system was considered with fresh feed concentrations of $c_1^{F0} = c_2^{F0} = 10 \, \text{g L}^{-1}$. The parameters of the Langmuir isotherms, Eq. (9), were $q_{m,1} = q_{m,2} = 100 \, \text{g L}^{-1}$, $b_1 = 0.02 \, \text{L g}^{-1}$, and $b_2 = 0.025 \, \text{L g}^{-1}$, respectively. The phase ratio, ϕ, was chosen equal to 1.5.

The dependence of the performance parameters on the injection width and purity constraints is displayed in Fig. 4. Eluent consumption and productivity are presented for component 1 only, since behavior for component 2 is similar. The dashed lines in the subfigures indicate the minimum injection width as determined from Eq. (31), below which the purity specifications cannot be matched exactly for both product fractions. In other words, the dashed lines represent the performance of batch chromatography operated in "stacked injections" mode with the same purity and yield constraints as the SSR process.

The eluent consumption (Fig. 4A) is found to be higher for higher purity requirements, and to decrease with increasing injection width until it levels off as the injection width becomes sufficiently large. The trend is therefore the same as predicted in Eq. (27). This result should be interpreted such an SSR process is always superior to batch chromatography in terms of eluent consumption.

Also the behavior of the productivity (Fig. 4B) is in accordance with the analysis presented above, see Eq. (28). The decrease in productivity with increasing Δt_{inj} can be explained also by
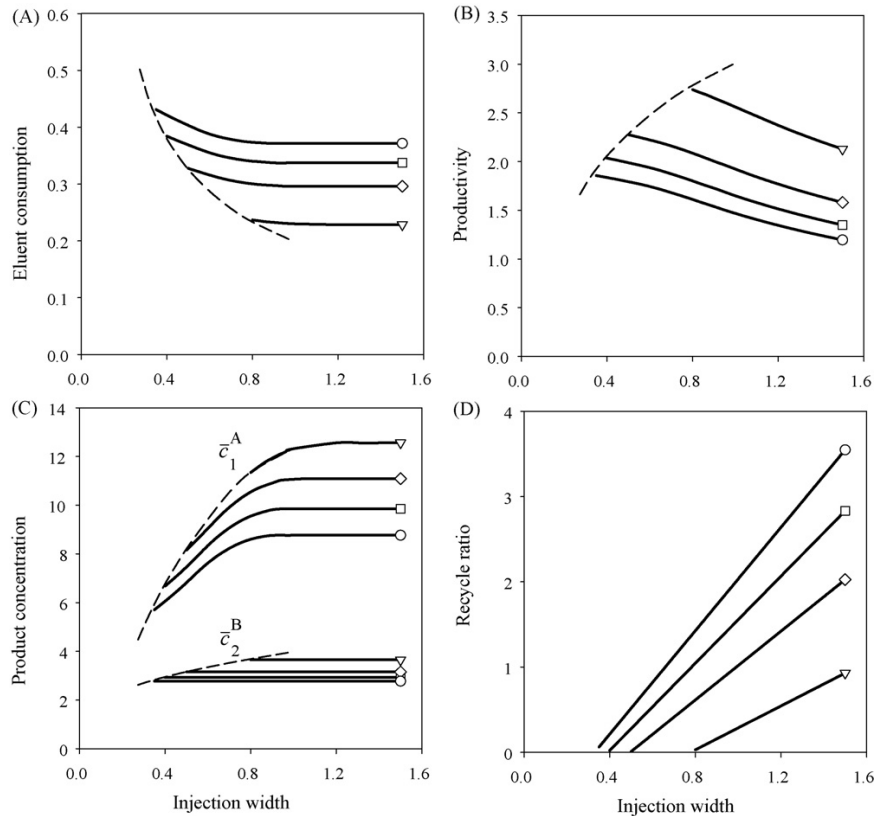

Fig. 4. Effect of injection width Δt_{inj} on the performance of mixed-recycle SSR chromatography. Purity constraints ($P^A = P^B$): $\triangledown = 80\%$, $\diamond = 90\%$, $\square = 95\%$, $\bigcirc = 98\%$. Isotherm parameters and feed concentrations are given in the text.

considering that the recycle ratio, defined as $R = \Delta t_{rec}/(\Delta t_{inj} - \Delta t_{rec})$, increases rapidly as a function of injection width and increasing purity requirements (see Fig. 4D). A high recycle ratio obviously means a less efficient operation in terms of adsorbent usage since less fresh feed is introduced compared to the size of the recycle fraction. Batch chromatography has a recycle ratio of zero, and its productivity is always higher than that of SSR chromatography.

It is seen in Fig. 4C that using larger injections results in higher concentration of component 1 in product fraction A. The concentration of component 2 in product fraction B; however remains constant. These results are in accordance with Eqs. (29) and (30). With respect to the concentration of product fraction A, the SSR process always outperforms batch chromatography.

It is further observed in Fig. 4C that, just as in batch chromatography, also in mixed-recycle SSR processes the first eluted component can be obtained in higher concentration than in the fresh feed. This is the case for low purities and large injection widths only, however.

As usual in chromatographic separation, the optimum operating point is characterized by a trade-off between productivity, eluent consumption, and concentrations of the product fractions. It is interesting to note that, although lowering the purity constraints results in enhanced performance in terms of the considered performance parameters, it also narrows the range of feasible injection widths.

5. Applicability of the design method and operational aspects

5.1. Accelerated startup and quality of prediction

An obvious question is how well applies the developed equilibrium-design approach to real chromatographic separations that always involve dispersive effects (due to mass-transfer resistances, axial dispersion, etc.). Furthermore, it should be clarified if the direct prediction of the steady state can be used to speed up the startup of the process. Below we will give an example that allows for a discussion of these two aspects.

Fig. 5 shows steady state concentration profiles obtained from the equilibrium method for an injection width of $\Delta t_{inj} = 1$ and a desired purity of 98% for both fractions (dashed lines). The corresponding predicted cut times are $t_{A1} = 3.549$, $t_{A2} = 3.918$, $t_{B1} = 4.588$, and $t_{B2} = 5.75$, respectively; the feed concentrations in steady state are $c_1^F = 5.470$ and $c_2^F = 7.200$. The cut times were applied in dynamic cycle-to-cycle simulations using the equilibrium dispersive model (see e.g., [21]), assuming a column with 1500 theoretical stages. Three different startup procedures were investigated. In the first option (Fig. 5, left) the process is started by the small injec-

tion fresh feed that is injected in each cycle (cf. Fig. 1, bottom). It can be observed that approximately 20 cycles are required to reach steady state during which performance improves slowly. The second option (middle of Fig. 5) applies initially a full injection of fresh feed (i.e., the injected volume corresponds to the sum of the volumes of recycle fraction and fresh feed). Steady state is obtained considerably faster (about five cycles). Although this option achieves better performance during startup, compared to the first option, during the first five cycles the purity of fraction A is off spec. In the third procedure (Fig. 5, right), the initial injection is performed using the predicted steady state feed concentrations (it is assumed that a corresponding mixture could be prepared for this first injection). Steady state is obtained basically with the third cycle and purity requirements are always fulfilled.

It is important to realize that all three scenarios lead to an identical steady state. Furthermore, a comparison with the concentration profiles predicted with the ideal model (dashed lines) shows a close agreement. However, in all cases, the limited column efficiency leads to lower product purities than the required 98% for both fractions (i.e., 97.0% is obtained for fraction A, and 94.5% for fraction B). Such deviations could be expected; they will be higher for systems where thermodynamic effects are less predominant (i.e., less efficient columns, smaller injection volumes and lower concentrations, respectively).

A viable option to rectify this mismatch could be to start the process according to (Fig. 5, right). Since steady state is obtained rapidly, product purities can be readily verified and cut times might be patiently adjusted. In this respect, the mixed-recycle SSR process is easier to operate that the closed-loop mode, which allows verifying the obtained purities only after attaining a steady state.

5.2. Operational aspects

A short comparison of operational aspects of the mixed-recycle and the closed-loop SSR modes appears useful here, since the mixed-recycle mode seems to be largely neglected among practitioners. The main reason for this is the obvious loss of already achieved partial separation in this mode. However, in closed-loop mode, the recycle pump also causes significant back-mixing. Another important aspect is that in closed-loop SSR operation, the injection time point is coupled to the elution of the recycle. In contrast to this, in mixed-recycle mode these time points can be freely chosen and optimized such that the process operates in "stacked injections" mode (i.e., no gap exists between fraction B of the nth cycle and fraction A of $(n+1)$th cycle). In fact, for long columns, even *several* elution profiles might pass simultaneously through the column. While a small safety gap is required in both modes to prevent
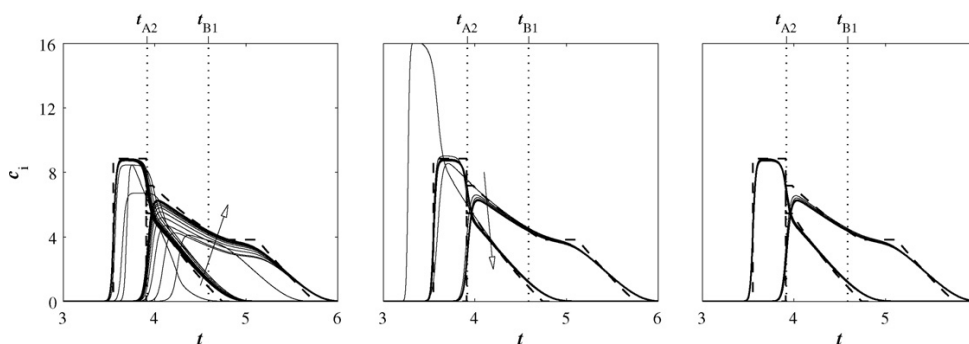
Fig. 5. Transient behavior of mixed-recycle SSR processes. Startup procedures (first cycle): small injection of fresh feed (left), full injection of fresh feed (middle), full injection of steady state concentrations predicted by design method (right). Solid line: calculated using an equilibrium dispersive model with 1500 theoretical stages. Dashed line: predicted steady state, calculated with the ideal model (Eq. (7)). In all three cases, identical design parameters were applied (see text). Thick line: cycle 25.

overlaps of product fractions due to dispersion, the closed-loop mode requires additional regeneration time for the injection loop.

Despite the mentioned drawbacks of the closed-loop operation, an intriguing aspect of this mode is that the injection of the highly concentrated fresh feed can actually result in a beneficial change of the migration behavior of the components (for non-linear isotherms). Model calculations indicate that, when using the cut times predicted with the above method in a closed-loop SSR process, higher purities of the first fraction can be obtained. This effect is related to non-linear interaction of the concentrations fronts. Similar effects are found in, for example, displacement chromatography (see [21]) or in advanced operating modes of SMB processes [22]. More elaborated recycle modes as proposed in Ref. [7] introduce a similar effect also in mixed-recycle mode. Further investigations of this aspect appear desirable.

Another aspect is related to a possible overlapping between consecutive cycles, which could be achieved in the mixed-recycle mode. For real systems, a small overlap might lead to shorter cycles. However, typically it is beneficial to only overlap low-concentrated parts of the bands that result from dispersion. This cannot be addressed using equilibrium theory. There, an overlapping shock front of the weak component would drastically decrease the purity of the "strong fraction". More restrictive cut times would result that, in turn, constrict throughput (by larger recycle fractions or smaller injections). An analysis of this interesting, but difficult interplay is beyond the scope of this work.

Due to the specific advantages of the two operating modes, no general conclusion is possible which of the two modes will actually achieve better process performance. For a given system, both modes will have to be evaluated based on optimizations using appropriate models.

6. Conclusions

Analysis and optimal design of SSR chromatography in mixed-recycle operation were investigated in the framework of the equilibrium theory. A method was developed for direct prediction of the steady state and the relevant cut times corresponding to arbitrary purity or yield requirements for systems with competitive Langmuir adsorption isotherms.

With this method, the steady state of the SSR process is obtained on the basis of adsorption isotherm parameters only, without requiring simulations using a dynamic column model. This greatly simplifies the design of SSR processes.

Theoretical analysis of SSR chromatography with mixed-recycle revealed that the total injection width is the only free operating parameter since purity or yield specifications determine the cut times.

An intriguing finding is also that the achievable throughput per cycle is independent of total injection width, while the time periods for the whole cycle and the recycle increase linearly with this parameter. As a consequence, the productivity of such an SSR process is necessarily lower than that of an optimized separation by batch chromatography. On the other hand, the SSR process always outperforms batch chromatography in terms of eluent consumption and product concentrations.

The developed method also enables quantitative evaluation of process performance. The above theoretical findings were fully supported by results of a case study for a generic example system.

A brief discussion was given on the applicability of the equilibrium design approach to finite efficiency systems. Besides the expected deviations with respect to the ideal model, it could be demonstrated that using this design procedure allows to significantly shorten the startup time of the process, and thus to improve performance.

Further work appears interesting with respect to a detailed comparison between different operating modes for SSR chromatography, in particular since some of them entail an interesting dynamic behavior.

Acknowledgements

References

[1] G. Subramanian (Ed.), Chiral Separation Techniques—A Practical Approach, Wiley-VCH, Weinheim, 2000.
[2] K.J. Bombaugh, W.A. Dark, R.F. Levangie, J. Chromatogr. Sci. 7 (1969) 42.
[3] A. Seidel-Morgenstern, G. Guiochon, AIChE J. 39 (1993) 809.
[4] C. Heuer, A. Seidel-Morgenstern, P. Hugo, Chem. Eng. Sci. 50 (1995) 1115.
[5] I. Duvdevani, J.A. Biesenberger, M. Tan, Polym. Lett. 9 (1971) 429.
[6] M. Bailly, D. Tondeur, Chem. Eng. Sci. 37 (1982) 1199.
[7] M. Bailly, D. Tondeur, Chem. Eng. Process 18 (1984) 293.
[8] D. Tondeur, M. Bailly, in: P. Barker, G. Ganetsos (Eds.), Preparative and Production-scale Chromatography, Chromatographic Science Series, vol. 61, Marcel-Dekker, New York, 1993, pp. 79–109.
[9] F. Charton, Optimisation des coupes et recyclages en chromatographie preparative industrielle, PhD thesis, Institut National Polytechnique de Lorraine, Nancy, 1995.
[10] F. Charton, M. Bailly, G. Guiochon, J. Chromatogr. A 687 (1994) 13.
[11] C.M. Grill, J. Chromatogr. A 796 (1998) 101.
[12] C.M. Grill, L. Miller, J. Chromatogr. A 827 (1998) 359.
[13] C.M. Grill, L. Miller, T.Q. Yan, J. Chromatogr. A 1026 (2004) 101.
[14] J. Kennedy, M. Belvo, V. Sharp, J. Williams, J. Chromatogr. A 1046 (2004) 55.
[15] T.Q. Yan, C. Orihuela, J. Chromatogr. A 1156 (2007) 220.
[16] M. Kaspereit, K. Gedicke, V. Zahn, A.W. Mahoney, A. Seidel-Morgenstern, J. Chromatogr. A 1092 (2005) 43.
[17] M. Kaspereit, Separation of Enantiomers by a Process Combination of Chromatograhy and Crystallisation, Shaker, Germany, 2006, p. 98.
[18] H.-K. Rhee, R. Aris, N.R. Amundson, First-order partial differential equations Theory and Applications of Single Equations, vol. I, Englewood Cliffs, Dover, 2001.
[19] H.-K. Rhee, R. Aris, N.R. Amundson, First-order partial differential equations Theory and Applications of Hyperbolic Systems of Quasilinear Equations, vol. II, Englewood Cliffs, Dover, 2001.
[20] F. Helfferich, G. Klein, Multicomponent Chromatography, Marcel-Dekker, New York, 1970.
[21] G. Guiochon, D.G. Shirazi, A. Felinger, A.M. Katti, Fundamentals of Preparative and Nonlinear Chromatography, Academic Press, Boston, 2006.
[22] H. Schramm, A. Kienle, M. Kaspereit, A. Seidel-Morgenstern, Chem. Eng. Sci. 58 (2003) 5217.
[23] P.C. Wankat, Rate-controlled Separations, Elsevier, New York, 1990.

Simplified Design of Steady-State Recycling Chromatography Under Ideal and Nonideal Conditions

M. Kaspereit[a,*], T. Sainio[b]

[a]*Max Planck Institute for Dynamics of Complex Technical Systems, Sandtorstr. 1, D-39106 Magdeburg, Germany*
[b]*Lappeenranta University of Technology, Skinnarilankatu 34, FIN-53850 Lappeenranta, Finland*

Abstract

In a recent contribution a design method for steady-state recycling chromatography in so-called mixed-recycle mode (MR-SSR) has been proposed (Sainio and Kaspereit, 2009). The method holds under ideal, dispersion-free conditions for chromatographic systems with competitive Langmuir adsorption isotherms. Here this approach is extended to practically relevant nonideal conditions with significant dispersive effects and convex-upward adsorption isotherms in general. The developed shortcut design method allows designing MR-SSR processes based on a simple procedure applied to a single conventional chromatogram. The method is validated experimentally for the separation of two cycloketones on a polymeric stationary phase. The performance of the MR-SSR process is compared to batch chromatography by means of a simulation study.

1. Introduction

Preparative liquid chromatography plays an important role in the production of fine chemicals, commodities, drugs, sugars, and biotechnological products (Schmidt-Traub, 2005). A significant contingent of the corresponding chromatographic processes perform binary separations. Examples are resolutions of mixtures of isomers, enantiomers, sugars, etc.. Also many chromatographic purifications in downstream processing and various isolations of intermediates in multi-step syntheses represent essentially binary separation problems.

Most chromatographic processes rely on conventional single-column batch chromatography. Besides its capability to accomplish difficult binary and multi-component separations, the major limitation of batch chromatography is the significant trade-off between achievable product purity on one hand and process performance on the other hand. As a general rule, high product purity can be achieved only at the expense of a loss in performance in terms of reduced recovery yield and/or decreased throughput and increased solvent consumption.

One option to overcome this limitation is Simulated Moving Bed (SMB) chromatography that utilizes multiple columns; see e.g. (Seidel-Morgenstern et al., 2008; Kaspereit, 2009). SMB processes frequently achieve a superior performance when comparing them to batch chromatography. Since conventional SMB setups do not have any waste outlet, they achieve maximum yield in binary separations.

Another option for maximizing yield is to apply recycling techniques in single-column setups. Here typically larger amounts than in batch chromatography are injected into the column, which results in elution profiles at the column's outlet that include an only partially resolved fraction. This part or even the complete chromatogram is then recycled back to the colum inlet. Such processes are attractive because the corresponding simpler installations require significantly lower investments than SMB processes.

The simplest recycling technique is closed-loop recycling (CLR) chromatography. Here the unresolved fraction or the whole elution profile is recycled several times directly to the column inlet, until the originally injected mixture is separated sufficiently. However, the CLR concept is of limited practical interest due to its low productivity.

A significantly better process performance is achieved by steady-state recycling (SSR) chromatography (Bailly and Tondeur, 1982). In SSR processes, a certain constant amount of fresh feed is added to each recycle fraction. The process attains a periodic steady state. There are two major operating modes. In closed-loop mode, CL-SSR, (Grill, 1998), the partially resolved fraction is recycled directly back to the column. The fresh feed is introduced at some point along this fraction. In mixed-recycle operation, MR-SSR, (Bailly and Tondeur, 1982), the recycle fraction is first collected completely, then mixed with the fresh feed, and subsequently re-injected. Alternatively, the fresh feed can also be injected before or after the recycle, which itself might be divided into several sub-segments (Charton et al., 1994). As will be discussed briefly also in Section 2, the MR-SSR mode is of interest because it offers a higher degree of flexibility and is easier to design.

SSR chromatography currently finds an increased interest. Grill and Miller (2005) reported the use of CL-SSR for three-

---
[*]Corresponding author
  Email address: `kaspereit@mpi-magdeburg.mpg.de` (M. Kaspereit)

fraction separations. Lee and Wankat (2009) performed a comprehensive study of three and four fraction separations by MR-SSR, where they considered different recycle policies. A comparison of the performance of CL-SSR to other chromatographic techniques was given in (Schlinge et al., 2010).

With the exception of (Bailly and Tondeur, 1982) the mentioned works do not discuss the fundamental design task of specifying the time points that define the different fractions. As concerns CL-SSR processes, this is complicated by the complex temporal pattern of the concentration profile of each injection. Correspondingly, CL-SSR schemes can be designed only empirically by skillful interpretation of experiments, or based upon detailed dynamic process models that require highly accurate parametrization. In contrast, the injection in MR-SSR processes represents a simple piece-wise constant boundary condition. This was exploited first by Bailly and Tondeur (1982), who applied equilibrium theory to calculate the cut times on the basis of the ideal model for 100% pure products. This approach was extended recently by Sainio and Kaspereit (2009) to arbitrary purity requirements. An intriguing feature of these methods is that they predict the appropriate cut times and the steady state itself *a priori*, without requiring dynamic simulations.

The mentioned design methods based on equilibrium theory are limited to adsorption equilibria of the Langmuir type and to idealized systems with negligible dispersive effects. Here we further extend the scope of this approach to more realistic systems with significant dispersive effects and so-called favorable adsorption isotherms in general. A corresponding simple shortcut-method is devised that predicts the cut times for any purity requirement using only a single chromatogram as input.

This paper is organized as follows. In the next section, the principle of MR-SSR chromatography and basic theoretical fundamentals are explained. Subsequently, the design method for ideal dispersion-free conditions is briefly reviewed. On this basis, the shortcut design method for nonideal dispersive conditions is derived. The new method is first evaluated based on a dynamic process simulation. Afterwards, it is validated experimentally for a model system. Finally, a model-based study is performed to compare the performance of MR-SSR processes and batch chromatography as a function of column efficiency.

2. Fundamentals

2.1. Principle and Operational Aspects

Figure 1 shows a schematic setup of steady-state-recycling chromatography in mixed-recycle mode (MR-SSR). At first the column is operated at a constant volumetric flow rate of the eluent D. At a given time point, an injection is performed from the injection tank onto the column by switching valve 1. After the desired total injection volume V_{inj} has been realized, valve 1 is switched back to the eluent. Subsequently, a given volume V_F of fresh feed F is introduced into the injection tank. At the outlet of the column, valve 2 is used to direct the column's effluent either to one of the two product fractions A and B, or to the
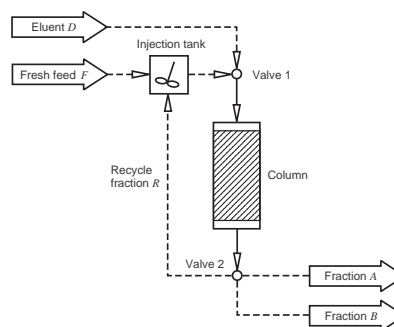

Figure 1: Schematic setup of steady-state recycling chromatography in mixed-recycle mode (MR-SSR). Solid lines – constantly active streams, dashed lines – periodically active streams.

recycle R, which is sent back to the injection tank. In product fraction A the weaker adsorbing component 1 is collected in excess, while in fraction B the stronger adsorbing component 2 is obtained. The recycle fraction R contains the insufficiently resolved mixture of both components that elutes between these two fractions. Repeating the whole procedure several times keeping the same time intervals between the different switching events forces the process into a periodic steady state.

Figure 2 shows as an example the startup behavior of an MR-SSR process initiated with a full injection of fresh feed. It can be seen that several cycles are required until a periodic steady-state is achieved. Note that the column's capacity is exploited fully by allowing always two successive injections to migrate through the column.

On the right of Fig. 2, the 20th cycle of the process is shown in more detail together with the different relevant time intervals indicated as boxes along the time axis. Specifically, we define the following time points and intervals:

- $t_{AS} \leq t < t_{AE}$: collection of fraction A,

- $t_{AE} \leq t \leq t_{BS}$: collection of recycle fraction R,

- $t_{BS} < t \leq t_{BE}$: collection of fraction B.

These four cut times t_{AS}, t_{AE}, t_{BS}, and t_{BE} are the main design variables of the SSR process. The design task addressed in this work is to determine these times for given values of column geometry, total injection volume and composition of the fresh feed, such that the purity requirements on the two products are met in steady state.

It can be expected that an MR-SSR process will be outperformed by a carefully optimized CL-SSR, since the latter preserves the partial separation of the recycle fraction. An exploitable degree of freedom of CL-SSR is also the time point for introducing the fresh feed into the recycle, which influences the nonlinear dynamics of the process. On the other hand, in this mode the start of the actual injection depends directly on the elution of the recycle fraction. This makes it difficult to attain an optimal "stacked injections" (Guiochon et al., 2006)
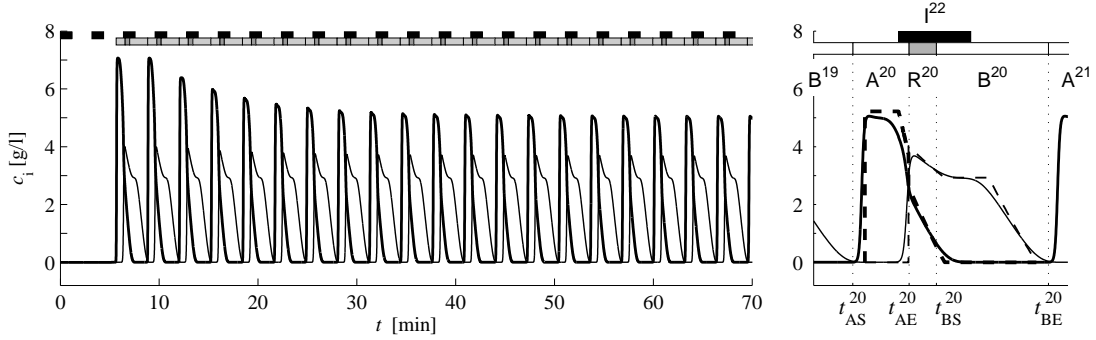
Figure 2: Simulation example for an MR-SSR process. Left – startup behavior during the first 20 consecutive cycles. Right – details for cycle no. 20 and superimposed solution of equilibrium theory (dashed lines) according to (Sainio and Kaspereit, 2009). Thick lines – weak adsorbing, thin lines – strong adsorbing component. Boxes indicate the time intervals for fractionation (product fractions A and B, recycle fraction R), and injection (I), respectively. The injection tank initially contains fresh feed. Equilibrium-dispersive model with NTP=2500, Q=2 mL/min, V_{inj}=2.36 mL, $c_{F,i}$=5 g/L, l=10 cm, d=1 cm, and F=1.5. Langmuir adsorption isotherms, Eq. (8), with q_S=100 g/L, b_1=0.02 L/g, b_2=0.025 L/g.

scenario, where the cycle time is minimized by preventing non-productive gaps between the elution profiles of consecutive cycles. This would require optimizing column length or introduction of an additional column-external residence time. The latter could be provided by an appropriately sized injection loop (Grill and Miller, 2005). Finally, the design of CL-SSR is difficult due to the complex temporal pattern of the injection. An example for the latter is given in Fig. 3b in (Schlinge et al., 2010).

The MR-SSR mode is more flexible in several aspects. Firstly, the events at the column's inlet and outlet are decoupled making the time point for re-injection a degree of freedom. The desired "stacked injection" scenario is achieved easily. An example is given in Fig. 2 (right), where the 22nd injection is performed already during the 20th cycle. This will minimize the time between the 21st fraction B and the 22nd fraction A. It can be seen in Fig. 2 that injection and recycling can occur at the same time. It should be noted that in the example shown a time-constant injection profile was enforced by storing the recycle fraction temporarily in an additional reservoir. This is not necessarily required in practice.

Another degree of freedom of MR-SSR are the initial conditions for the injection reservoir. The process can be started with a solution of fresh feed (cf. Fig. 2) or a diluted feed mixture. The latter can help keeping product specifications during startup. A useful alternative strategy suggested in (Sainio and Kaspereit, 2009) is to provide for the first injection(s) a solution whose composition corresponds to the steady-state injection. This will drive the process immediately into the periodic steady-state. In CL-SSR processes this is much more difficult, since the steady-state injection *profile* would have to be provided for the first injection(s).

Apart from that, the recycle reservoir of an MR-SSR process facilitates additional unit operations like a partial solvent removal (Siitonen et al., 2010) or isomerization reactions. Finally, the constant injection concentration profile of an MR-SSR process greatly simplifies its design.

2.2. Fundamental Relations

Once the four cut times have been specified, all relevant operating and performance parameters of the process can be calculated. The cut times are defined relative to the time point of the injection of each cycle and are kept constant throughout the process (i.e., they are not varied from cycle to cycle). Therefore, the cycle time,

$$\Delta t_{\text{cycle}} = t_{BE} - t_{AS} , \tag{1}$$

is also constant throughout operation. Note that Eq. (1) specifies also the interval between two subsequent injections that leads directly to the desired "stacked injections" scenario mentioned earlier. The volumes of total injection, V_{inj}, fresh feed, V_F, and recycle fraction, V_R, are also constant. They are related by

$$V_{inj} = V_F + V_R . \tag{2}$$

here V_R is given by

$$V_R = Q\left(t_{BS} - t_{AE}\right) . \tag{3}$$

The integral purities P_A and P_B of the two product fractions are defined with respect to their target components,

$$P_A = \frac{m_{1A}}{m_{1A} + m_{2A}} , \tag{4a}$$

$$P_B = \frac{m_{2B}}{m_{1B} + m_{2B}} . \tag{4b}$$

The amount m_{ij} of component i in fraction j is given by

$$m_{ij} = Q \int_{t_{jS}}^{t_{jE}} c_i(t)\, \mathrm{d}t \quad i = (1,2),\ j = (A,B). \tag{5}$$

Finally, process performance is assessed based on the specific productivity, PR, and eluent consumption, EC:

$$PR_i = \frac{m_{ij}}{\Delta t_{\text{cycle}} \epsilon V} , \tag{6a}$$

$$EC_i = \frac{Q \Delta t_{\text{cycle}} - V_R}{m_{ij}} \, , \qquad (6b)$$

In Eq. (6), $i = 1$ and $j = A$ when producing the weaker adsorbing component in the first fraction; $i = 2$ and $j = B$ if the stronger adsorbing solute is obtained from the second fraction.

2.3. Dynamic Modelling

It is emphasized that the dynamic process models described here were applied mainly for assessing the design methods and validation of the experiments. They are not required for application of the design methods.

Two different models are used in this work. For validation of the experiments and the theoretical study in Section 6 the transport-dispersive model is applied. The component mass balances for this are

$$\frac{\partial c_i}{\partial t} + F \frac{\partial q_i}{\partial t} + u \frac{\partial c_i}{\partial z} = D_{\text{ax}} \frac{\partial^2 c_i}{\partial z^2} \, , \qquad (7a)$$

$$\frac{\partial q_i}{\partial t} = k_{\text{fi}} \left[q_i^* \left(\overline{c} \right) - q_i \right] \quad i = (1, 2) \, , \qquad (7b)$$

where Eq. (7b) describes the mass transfer between mobile and stationary phase by a conventional solid film LDF approach. The model equations were implemented in Matlab and solved using an explicit backward-forward finite difference scheme, where the axial dispersion term is approximated numerically by the step size in the spatial discretisation. Details can be found in (Antos and Seidel-Morgenstern, 2001; Antos, 2003).

For the evaluation of the design method in Section 4 we apply the computationally more efficient equilibrium-dispersive model solved by the Rouchon algorithm (Guiochon et al., 2006). The model assumes local equilibrium, $q_i = q_i^*$ in Eq. (7a) and correspondingly omits Eq. (7b). For the dispersion coefficient in Eq. (7a) then holds $D_{\text{ax}} = u \, l / (2 \, NTP)$ with NTP as the number of theoretical stages.

To solve the model equations, the competitive adsorption equilibria $q_i^* \left(\overline{c} \right)$ have to be described. Here we use the frequently applied Langmuir and bi-Langmuir models. For the former holds

$$q_i^* = \frac{q_s \, b_i \, c_i}{1 + \sum_{j=1}^{2} b_j \, c_j} \quad i = (1, 2) \, . \qquad (8)$$

The latter assumes two different adsorption sites I and II of the Langmuir-type:

$$q_i^* = \frac{q_s^I \, b_i^I \, c_i}{1 + \sum_{j=1}^{2} b_j^I \, c_j} + \frac{q_s^{II} \, b_i^{II} \, c_i}{1 + \sum_{j=1}^{2} b_j^{II} \, c_j} \quad i = (1, 2) \, . \qquad (9)$$

3. Design of MR-SSR chromatography

As illustrated above, the main design variables of an MR-SSR process are the four cut times (fractionation times) t_{AS}, t_{AE}, t_{BS} and t_{BE}. The design task is to determine these cut times for given values of column geometry, total injection volume and composition of the fresh feed, such that the purity requirements

on the two product fractions are fulfilled in the periodic steady state.

Two shortcut design methods for MR-SSR processes are discussed here that predict these times *a priori* without dynamic simulations. The first holds for ideal conditions without dispersive effects. The second is an extension that applies to more realistic conditions with finite column efficiency.

3.1. Design Under Ideal Conditions

The method described in this section fully predicts the cut times and the periodic steady state of an MR-SSR process for any set of purity requirements under dispersion-free conditions. It applies to Langmuir adsorption isotherms, Eq. (8). The approach originally introduced in (Sainio and Kaspereit, 2009) is reviewed here since it represents the basis for the shortcut method to be derived for non-ideal conditions.

If dispersive effects are negligible, chromatographic processes are described by the ideal model. This corresponds to Eq. (7a) with $D_{\text{ax}} = 0$ under equilibrium conditions, $q_i = q_i^*$. For Langmuir isotherms, Eq. (8), the model can be solved by applying local equilibrium theory, for example using the method of characteristics (Rhee et al., 2001a), (Rhee et al., 2001b). This allows explicit construction of binary chromatograms. For detailed instructions, see e.g. (Guiochon et al., 2006).

An important feature of chromatograms obtained from the ideal model for sufficiently large injections in conjunction with convex-upward or 'favorable' isotherms like Eqs. (8) or (9) is that their rear parts are basically independent of the injection volume. They are only shifted in time by the duration of the injection. With respect to the MR-SSR process, it was proven in (Sainio and Kaspereit, 2009) that for Langmuir isotherms the rear parts of the elution profiles in steady state – and consequently also the composition of the product fraction B – is the same as for an injection of fresh feed. This facilitates determining the cut times and predicting the steady state based on the rear part of a chromatogram that would be obtained from an injection of fresh feed with volume V_{inj}. From this, the four cut times are then found as follows (Sainio and Kaspereit, 2009).

The end of fraction B, t_{BE}, is set equal to the very "rear end" of the chromatogram. For favorable isotherms, equilibrium theory yields for this

$$t_{BE} = t_0 \left(1 + F \frac{dq_2}{dc_2} \bigg|_{c_i = 0} \right) + \Delta t_{\text{inj}} \, , \qquad (10)$$

where $\Delta t_{\text{inj}} = V_{\text{inj}} / Q$ is the duration of the whole injection, and t_0 is the retention time of a non-adsorbing component, $t_0 = \epsilon V / Q$. As an example, for Langmuir isotherms, Eq. (8), one obtains from Eq. (10) the expression $t_{BE} = t_0 \left(1 + F \, q_s \, b_2 \right) + \Delta t_{\text{inj}}$.

To find the start time of fraction B, t_{BS}, the rear part of the chromatogram is integrated backwards. Starting at $t = t_{BE}$, the amounts $m_{iB} (t)$ are determined according to Eq. (5) until the purity from Eq. (4b) matches the required value $P_{B,\text{req}}$:

$$t_{BS} = \max \{ t < t_{BE} : P_B (t) = P_{B,\text{req}} \} \, . \qquad (11)$$
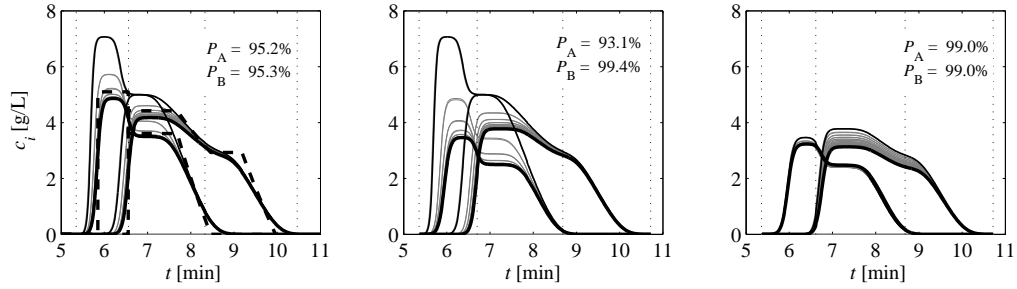
Figure 3: Overlay of concentration profiles of 40 cycles for MR-SSR processes operated with cut times predicted by different approaches for a purity requirement of 99% for both fractions and a stage number of 1000. Intermediate black lines – design chromatogram and first cycle, thick black lines – final 40th cycle, thin grey lines – transient cycles. Left – design method for ideal systems without dispersion applied to a fresh feed injection (dashed lines denote equilibrium solution). Center – shortcut design method for systems with dispersion applied to fresh feed. Right – refined cut times from shortcut method applied to the steady state injection mixture of the previous case. See text for other parameters.

Note that for Langmuir isotherms t_{BS} could be determined explicitly, but the corresponding expression is lengthy and does not provide further insight. A numerical integration of the profile is recommended here since it can be applied also directly to the non-Langmuirian systems to be studied later.

The end time of fraction A, t_{AE}, can be determined from a simple consideration on mass and volume balances. For a binary separation without waste stream in steady state, the yields of the two components are functions of the product purities only. In particular, it holds for component 2 (Kaspereit et al., 2005)

$$Y_2 = \frac{m_{2B}}{m_{2F}} = \frac{P_B}{1 - P_F} \cdot \frac{P_A - P_F}{P_A + P_B - 1}, \qquad (12)$$

where $P_F = m_{1F}/(m_{1F} + m_{2F})$ is the purity of the fresh feed. The product amount m_{2B} in Eq. (12) is already known from the backward integration. Therefore, the amount of component 2 introduced with the fresh feed in each cycle, m_{2F}, follows immediately from Eq. (12) as

$$m_{2F} = V_F\, c_{2F} = \frac{m_{2B}}{Y_2}, \qquad (13)$$

with c_{2F} as the fresh feed concentration of component 2. For the volume of fresh feed holds accoring to Eq. (2) $V_F = V_{inj} - V_R$. Substituting this and Eq. (3) into Eq. (13) yields

$$t_{AE} = t_{BS} - \Delta t_{inj} + \frac{m_{2B}}{Y_2\, Q\, c_{F2}}. \qquad (14)$$

Finally, the optimal start of fraction A, t_{AS}, corresponds to the retention time of the shockfront of pure component 1. If the injection is large enough to cause a plateau of pure first component with a concentration of c_1', it holds

$$t_{AS} = 1 + F \frac{q_1\left(c_1', 0\right)}{c_1'}. \qquad (15)$$

If the injection is smaller and the plateau is eroded completely, t_{AS} can be found by simple numerical iteration schemes as given in (Sainio and Kaspereit, 2009) or (Guiochon et al., 2006).

In addition to the four cut times, the design method also predicts explicitly the injection concentrations at steady state, which allows calculating the complete chromatogram in steady state. As shown in the example in Fig. 2 (right), a good agreement can be achieved between the 'dispersion-free' design prediction from equilibrium theory (dashed lines) and the full dynamic process model (solid lines). As mentioned earlier, the knowledge of the steady-state injection composition also permits eliminating the startup period of the process. A corresponding example will also be given in the experimental section of this paper.

3.2. Shortcut Design Under Nonideal Conditions

Here we introduce a shortcut design method that applies also to practical conditions with significant band-broadening effects. It is not restricted to Langmuir adsorption isotherms as the method above, but can be used for convex-upward isotherms in general; like, for example, the bi-Langmuir model, Eq. (9). It is emphasized that neither the isotherm parameters have to be known, nor dynamic simulations are required to predict the cut times.

It is a common observation that also under dispersive conditions caused by mass transfer resistances and axial dispersion the rear of chromatograms remains sufficiently independent of the injection conditions. With respect to MR-SSR processes, one can then expect that the steady-state compositon of fraction B will not vary significantly from a fresh feed injection of the same volume.

Based on this assumption we propose the following approach. First, a design chromatogram is obtained for an injection of fresh feed with volume V_{inj}. This can be an experimental chromatogram or, if a column model and parameters are available, a simulated one. From the design chromatogram, the cut times are now obtained as follows.

The end of fraction B, t_{BE} is selected as the end of the chromatogram, for example based on a specified low threshhold concentration. If the initial slope of the adsorption isotherm is known, also Eq. (10) can be applied, if necessary adding a small safety time.

The start of fraction B, t_{BS}, is found again by backwards-integration of the chromatogram as described above. If an experimental chromatogram is used, it needs to be decomposed first into the individual concentration profiles. This is possible using, for example, two different detector signals or wavelengths, or by fractionation and subsequent off-line analysis. For coarse fractionations it can be useful to perform a spline-interpolation of the data.

The end of fraction A, t_{AE} can again be calculated from the purity requirements and Eq. (14), because the same considerations on volume and mass conservation are valid as under ideal conditions.

The start of fraction A, t_{AS}, is the only time that cannot be predicted directly. A useful and safe first choice is to set t_{AS} based on a threshold close to the front of the design chromatogram. In SSR operation, the diluted recycle will decrease the height of this shock, which correspondingly will elute later. After a few cycles of the actual SSR run, t_{AS} can be further increased to minimize the cycle time. If a dynamic process model is available, this time can be chosen easily based on a threshold concentration.

It is worth mentioning that, in contrast to the method for ideal conditions, this shortcut approach does not provide information on the steady state itself. As a concequence, the startup period can be eliminated only if the composition of the recycle fraction has been determined either from an initial SSR experiment or based on process simulation.

4. Model-based Evaluation of the Shortcut Method

Shortcut design methods can never be exact since they rely on simplifying assumptions. The main simplification behind the design method for non-ideal systems above is that the composition of the second fraction is invariable from cycle to cycle.

Below we perform a simulation study in order to examine the accuracy of the shortcut method for nonideal conditions. For this purpose we apply the method for different purity requirements (80, 90, and 99%) and column efficiencies in terms of the number of theoretical stages (NTP=500, 1000, and 1500). The full dynamics of the process are simulated using the equilibrium-dispersive model. The results achieved at steady state are compared to the design specifications. The same Langmuir isotherms and operating parameters are applied that were used to create Fig. 2, with the exception of a total injection volume of $V_{inj} = 5$ mL. In order to prevent overlapping of consecutive elution profiles, which cannot be considered by the design approach, an additional safety time of 1min was considered between successive injections.

Figure 3 shows as examples the evolution of the outlet concentration profiles of an MR-SSR process designed by the different approaches for a required purity of 99% and a stage number of NTP=1000. In a first step, dispersion is neglected and the cut times are predicted by the method for ideal systems described in Section 3.1 (Fig. 3, left). As assumed, the concentration profiles in the second fraction are basically invariant during operation, which holds also in all further cases studied. Furthermore, the profiles are rather close to those calculated using the

ideal model, even though the column has a limited efficiency (dashed lines). However, the purity of both product fractions (P_A, P_B) is around 95%, which is lower than desired. This is due to the neglected dispersion that causes limited amounts of each component to occur as impurity in the other fraction.

The middle of Fig. 3 contains the results obtained by the shortcut method for nonideal systems (Section 3.2). Since the integration step in the shortcut method fully takes into account the effect of dispersion on the second fraction, the purity of this fraction (99.4%) is very close to specification. On the other hand, dispersion is neglected in the calculation of the cut time t_{AE} from Eq. (14). In steady state this time falls on the steep shock layer in front of the second component's profile. This leads to a purity of fraction A below 95%.

Due to the steepness of the mentioned front, already small adjustments of the cut times are sufficient to fully meet the purity requirements. A simple strategy was applied, which is applicable also experimentally. The final concentration profiles of the example in the middle of the figure were used as the design experiment for the shortcut method and, in addition, a simple grid search was performed around the values of t_{AE} and t_{BS} obtained. For the results shown in the right of Fig. 3, t_{AE} had to be decreased by only 0.088min (5s or 1.3%) in comparison to the case in the middle of the same figure. The correction for t_{BS} was virtually zero (-0.001min). Please note that the final injection concentrations of the example in the middle of the figure were also used as the starting values for the first injections. As already mentioned, this is a viable strategy for a startup of the process close to the steady state.

Analogous calculations were performed for lower purity requirements and different column efficiencies. The results are summarized in Table 1. As can be expected, the initial purity deviations obtained from the shortcut method for nonideal systems (index 0) decrease with increasing stage number. Furthermore, the deviations decrease with decreasing purity requirements. This is due to the cut time t_{AE} moving further away from the mentioned steep shock layer for lower purities. Finally, it is observed from the table that in all cases very small adjustments of the cut times are sufficient to establish the required purities. The largest necessary correction is 0.132min (8s) – for a cut time of approximatley 7 minutes.

In summary, it was found that the shortcut design method for nonideal conditions very closely predicts the required cut times for MR-SSR processes, which is the scope of this method. Furthermore, in all cases studied, the purity of the second fraction was met with high accuracy. For very high purity requirements for the first fraction, it's predicted end time can fall onto a shock layer. In such cases, a minor adjustment of the cut times suffices.

5. Experimental Validation for a Model System

In this section the shortcut design method is validated experimentally under different scenarios. The model system chosen for this comprises typical practical conditions that pose

Table 1: Application of the shortcut design method for different purity requirements and column efficiencies.

		$NTP = 500$ [a]			$NTP = 1000$ [b]			$NTP = 1500$ [c]		
$P_{A,req}$	[%]	80	90	99	80	90	99	80	90	99
$P_{B,req}$	[%]	80	90	99	80	90	99	80	90	99
$t_{AE,0}$	[min]	6.722	6.634	6.821	6.715	6.599	6.702	6.712	6.587	5.448
$t_{BS,0}$	[min]	7.773	8.240	8.946	7.706	8.119	8.683	7.688	8.084	6.669
$P_{A,0}$	[%]	78.79	86.32	87.65	79.49	88.60	93.11	79.37	88.71	94.40
$P_{B,0}$	[%]	81.87	91.86	99.50	81.10	91.21	99.38	81.06	91.24	99.37
Δt_{AE}	[min]	-0.041	-0.080	-0.132	-0.019	-0.034	-0.088	-0.021	-0.030	-0.071
Δt_{BS}	[min]	-0.083	-0.074	0.070	-0.048	-0.052	-0.001	-0.044	-0.051	-0.023
P_A	[%]	80.02	89.99	98.99	80.00	90.00	98.99	80.02	89.98	99.00
P_B	[%]	80.01	90.03	99.00	79.99	89.99	99.00	79.99	90.00	99.01

[a] $t_{AS} = 5.081$ min, $t_{BE} = 11.040$ min   [b] $t_{AS} = 5.358$ min, $t_{BE} = 10.716$ min   [c] $t_{AS} = 5.448$ min, $t_{BE} = 10.542$ min

challenges to process design: limited column efficiency in terms of the stage number and significantly nonlinear convex-upward ("favourable") adsorption isotherms that have to be described by the bi-Langmuir model instead of simpler Langmuir isotherms.

5.1. Experimental systems

Experiments were performed using the same chromatographic column in two different laboratories at the Max Planck Institute, in Magdeburg, Germany (system 1) and Lappeenranta University of Technology, Lappeenranta, Finland (system 2).

The compounds to be separated were cyclopentanone (puriss. grade, purity >99%) as weaker adsorbing component 1, and cyclehexanone (puriss. grade, purity > 99.5%) as the stronger adsorbing component 2 (both Merck, Darmstadt, Germany). All experiments were performed at $23°C$, using water / ethanol 80/20 (v/v) as eluent. Water was purified and de-ionized prior to use (Millipore units; Millipore, Billerica/MA, USA). The stationary phase was the apolar polyaromatic resin XAD-16 (Rohm & Haas, USA) with a mean pore size of 100Åand an original particle size between 0.5 and 1mm. The resin was ground with a Retsch ZM200 mill (Retsch, Haan, Germany) and sieved to obtain a final particle size in the range between 125 and 250μm.

The resin was packed into a jacketed glass column (max. pressure 25bar) with adjustable bed length and an inner diameter of 1.5cm (KronLab, Dinslaken, Germany). The height of the packed bed was 10.2cm. The column was placed into a thermostat (Ecoline RE306 in System 1, C6 CS in System 2; both Lauda, Lauda-Königshofen, Germany). Chromatograms of SSR experiments were recorded at 280 and 300nm with UV detectors Smartline 2500 (Knauer, Berlin, Germany) for system 1 and a Model 2487 (Waters, Milford/MA, USA) for system 2.

The SSR setup for system 1 was realized using K-6 and K-16 valves (Knauer) controlled via RS232 by a custom Labview (National Instruments, Austin/TX, USA) program. For system 2, MV-7, MV-8 and PSV-50 valves (Pharmacia, Uppsala, Sweden) were used that were controlled via a serial port hub and a second custom Labview program. For scenarios 1 and 2 (see SSR experiments below) two pumps were used in connection with selection valves (one for delivering the eluent and performing the injection, the other for adding fresh feed into the

injection tank). For scenario 3, three pumps were applied together with selection valves (one each for the eluent, the injection, and the fresh feed). The pumps used were Wellchrom K-1001 (Knauer) for system 1, and model 515 (Waters) for system 2, respectively.

Samples collected during the experiments were analyzed by HPLC on an Ultimate 3000 (Dionex, Sunnyvale/CA, USA; system 1) and an Model 1100 (Agilent, Santa Clara/CA, USA; system 2). A reversed phase column was applied (Zorbax Eclipse XDB-18; Agilent). The analysis was performed at $35°C$ using as eluent 70/30 water / methanol at a flow rate of 1.2 mL/min.

5.2. Parameter determination
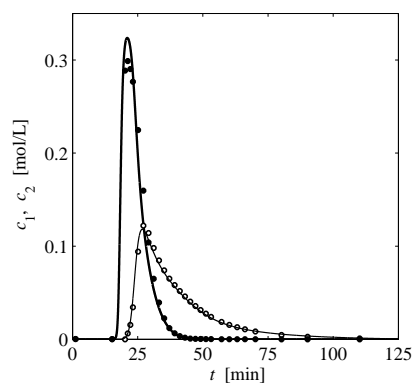
Figure 4: Model validation for an experimental chromatogram. Conditions – V_{inj}=26.5 mL, $c_{inj,1}$=0.214 mol/L, $c_{inj,2}$=0.180 mol/L, Q=2 mL/min. Symbol experiments, lines simulation. Filled symbol, thick line: cyclopentanone; open symbols, thin line: cyclohexanone. Simulation parameters for System 1 in Table 2.

Parameters were determined experimentally mainly on system 1. The porosity of the packing was measured based on a small injection of sodium chloride. Subsequently, small amounts of the two cycloketones were injected in order to determine the initial slopes of the single-component isotherms.

The axial dispersion coefficient, D_{ax} was calculated from the correlation by Chung and Wen (Chun1968) . The mass transfer coefficient, k_f, was subsequently found by fitting simulations with the transport-dispersive model, Eq. (7), to chromatograms

7

measured for small injections; i.e., under linear conditions. Overall, the system exhibits very strong dispersion – the total number of theoretical stages is about 30 only.

Table 2: Parameters determined for the two experimental systems.

Parameter	System 1	System 2
Column length l [cm]	10.2	
Column diameter d [cm]	1.5	
Porosity ϵ [-]	0.744	
Flow rate Q [mL/min]	2.0	
Axial dispersion D_{ax} [m^2/s]	$1.902 \cdot 10^{-7}$	
No. of theoretical stages, NTP	68	
Mass transfer $k_{f1} = k_{f2} = k_f$ [1/s]	0.105	0.035
Bi-Langmuir isotherms, Eq. (9):		
q_S^I [mol/L]	3.19	3.24
b_1^I [L/mol]	2.780	2.075
b_2^I [L/mol]	5.480	4.132
q_S^{II} [mol/L]	0.0533	0.2627
b_1^{II} [L/mol]	101.910	28.843
b_2^{II} [L/mol]	463.017	109.525

Finally, the adsorption isotherms of the two components were determined. In a first step, single-component loadings were obtained by frontal analysis; see, for instance, (Seidel-Morgenstern, 2004), and fitted to the bi-Langmuir model, Eq. (9). In a second step, strongly overloaded mixture injections were performed that resulted in only partially separated peaks. Samples were taken to determine the individual concentration profiles of these chromatograms. The competitive parameters of the bi-Langmuir adsorption isotherms were found by fitting simulated chromatograms to these data (inverse method or "peak fitting"). The single-component isotherms were used as starting values.

Table 2 gives a summary of all parameters determined experimentally. The determined values differ slightly for the two systems, which is probably due to different extra-column dispersion and the quality of the injection profile (the latter was assumed to be rectangular in all simulations). Figure 4 shows an example for the validation of the model. The agreement between simulation and an overloaded, fractionated chromatogram is considered very good.

5.3. SSR Experiments

Three different scenarios were considered in the MR-SSR experiments. Focus was set on validating the design method for high and low purity requirements as well as on the possibility to eliminate the startup period of the process. Note that arbitrary purity requirements were chosen that could be adjusted more easily in the experiments (i.e., rounded to whole seconds or minutes). All parameters and the results of the MR-SSR experiments are summarized in Table 3.

Figure 5 summarizes the first SSR experiment that was designed for high product purities (scenario 1 in Table 3). The design chromatogram (Fig. 5, left), was obtained by simulating an injection of fresh feed. From this the cut times where determined by the shortcut design method. The SSR process was operated for 15 cycles. Fig. 5 contains the evolution of

the detector signal (middle) and the product purities determined by off-line HPLC analysis (right) for all cycles. The purities approach the design specifications closely, both in the experiment and the simulation. It is noteworthy that the process rather slowly reaches steady state for these high purity requirements. The reason for this is found in the recycle fraction, which has a large volume and a composition significantly different from the fresh feed.

Figure 6 shows in an analogous manner the results for an SSR experiment designed for lower purity requirements (scenario 2 in Table 3). An important difference is here that the shortcut design method was applied directly to a fractionated experimental chromatogram (symbols in Fig. 6, left). It can be seen that the recycle fraction is rather small, and its composition is close to the fresh feed. Therefore, in this case the process approaches the steady state much faster than for high purities. An encouraging finding is that also in this case, which is designed without using any simulation data or measured parameters, a good agreement is obtained between design specification and experimental results.

In the third experiment (scenario 3 in Table 3) it is attempted to eliminate the startup phase of the process. As already observed in scenario 1 as well as in simulations, for high purity requirements many cycles are required before steady state is reached. This third experiment was designed again for high purities. The steady-state injection concentration was predicted by a full dynamic process simulation. A solution with this composition was used as initial filling of the injection reservoir in the experiment. As can be seen in Fig. 7, the process starts already very close to the steady state. However, the purity obtained for the first fraction is lower than required. It is assumed that here the second cut time, t_{AE}, is located on the shock layer discussed in the previous section. This would explain also the fluctuations of the purity for fraction A, which will occur already for small deviations of the shock layer position from cycle to cycle. Apart from that, the results confirm that the procedure is capable of eliminating the transient startup period of MR-SSR processes.

6. Influence of Column Efficiency on Process Performance

The design method presented above provides excellent estimates for the cut times required to operate an MR-SSR chromatography unit. This greatly simplifies numerical investigation of process performance, because only some fine tuning of the cut times t_{AE} and t_{BS} is required to match the purity constraints (cf. Section 4). In order to demonstrate the effect of column efficiency on process performance, a series of simulations were carried out with parameters of system 2 in Table 2. Purities of 97.5±0.01% for both product fractions were used as design constraints. Since the injection volume is the main operating parameter that can be optimized in MR-SSR chromatography, its influence on process performance is also investigated.

The results of the numerical simulations are shown in Fig. 8. The solid lines represent MR-SSR, whereas the filled circles on the left mark separations by batch chromatography that obtain

Table 3: Operating conditions and results of the three SSR experiments.

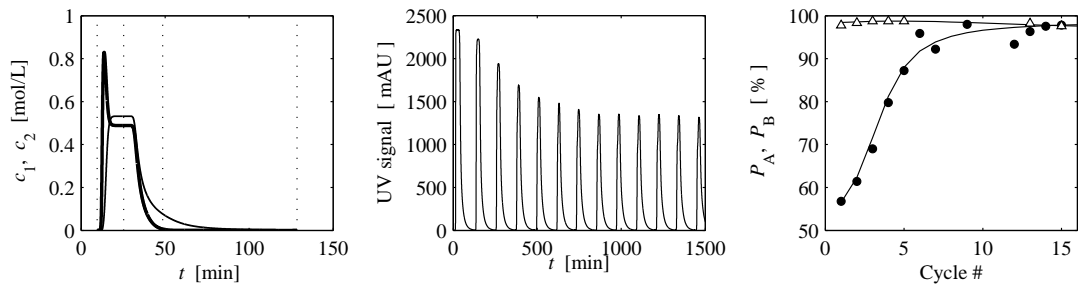|	Scenario 1	Scenario 2	Scenario 3
Experimental setup	System 1	System 2	System 2
Design chromatogram	simulated	experimental	simulated
Injection volume V_{inj} [mL]	50	60	60
Fresh feed conc. c_{F1}, c_{F2} [mol/L]	0.489, 0.532	0.109, 0.096	0.109, 0.097
Purities (required) $P_{A,req}, P_{B,req}$ [%]	98.8, 98.2	72.8, 82.9	95.6, 97.7
Cut times $t_{AS}, t_{AE}, t_{BS}, t_{BE}$ [min]	9.5, 25.37, 48.5, 128.5	11.3, 40.0, 47.28, 139.7	15.68, 36.51, 58.18, 144.18
Initial volume of injection tank V_{rec}^0 [mL]	51.3	63.0	65.0
Initial conc. in injection tank $c_{inj,1}^0, c_{inj,2}^0$ [mol/L]	fresh feed	fresh feed	0.055, 0.060
Purities (experimental) $P_{A,exp}, P_{B,exp}$ [%]	98.6, 98.2	72.0, 84.5	92.4, 98.3
Purities (simulated) $P_{A,sim}, P_{B,sim}$ [%]	98.3, 96.9	72.5, 84.6	90.3, 97.4

Figure 5: Design and results of the MR-SSR process for scenario 1 in Table 3. Thick lines/filled symbols: component 1 and fraction A, thin lines/open symbol: component 2 and fraction B. Left – design chromatogram, center – recorded UV signal, right – obtained and predicted product purities. The process is designed based on a simulated chromatogram (left) and started up with a fresh feed injection.

Figure 6: Design and results of the MR-SSR process for scenario 2 in Table 3. The process is designed based on an experimental chromatogram (left) and started up with a fresh feed injection. For symbols and lines see Fig. 5.
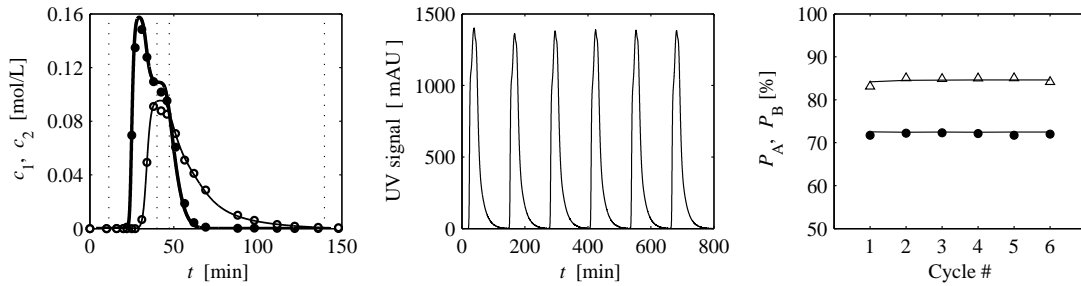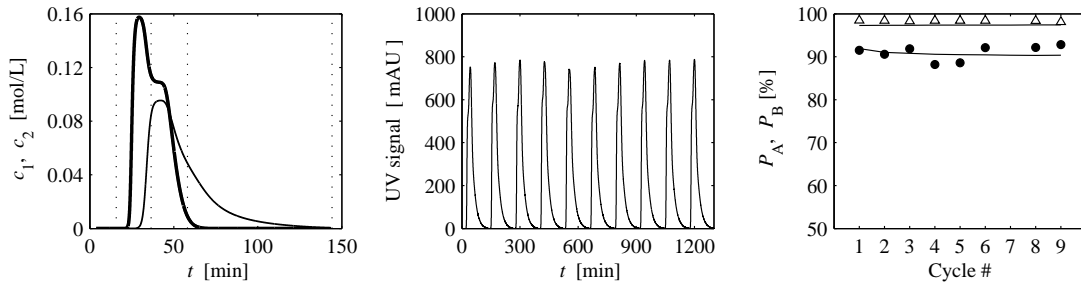

Figure 7: Design and results of the MR-SSR process for scenario 3 in Table 3. The process is designed based on a simulated chromatogram (left) and started up with the steady-state injection mixture predicted by simulation. For symbols and lines see Fig. 5.

the same yield as the SSR process (i.e. there are no waste frac- tions between the product fractions). In all cases the injection
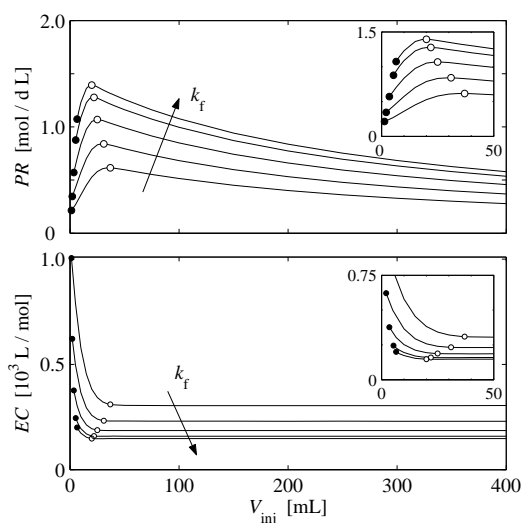
9

Figure 8: Performance of the MR-SSR process as a function of the mass transfer coefficient k_f and the total injection volume V_{inj} (simulation results). Process designed based on the shortcut method for 97.5% purity of both fractions. Top – productivity PR, bottom – eluent consumption EC. Open symbols – SSR operating points with maximum productivity. Filled symbols – operating points of batch chromatography for the same purity and yield (i.e., no waste fractions). Arrows indicate the direction of increasing k_f (k_f = 2, 3, 5, 10, 20 min^{-1}); for all other parameters see System 2 in Table 2.

intervals are optimized to achieve the desired stacked-injections scenario. As expected, the performance of both processes improves with increasing column efficiency (i.e. larger values of mass transfer coefficient k_f). It is more interesting to note that the productivity of SSR passes through a maximum as the total injection volume increases (open circles in the figure). Only for very large injection volumes the productivity of MR-SSR falls below that of batch (seen in Fig. 8 for $k_f \geq 5$ min^{-1}). In contrast to productivity, the specific eluent consumption reaches a constant minimum beyond a certain injection volume.

The performance of SSR at maximum PR is compared with that of optimized batch chromatography in Table 4. The lower is the column efficiency, the higher is the benefit of applying the MR-SSR concept in both PR and EC. It is further observed in Fig. 8 and Table 4 that the two process options behave qualitatively different with respect to the injection volume that gives the maximum productivity. In a low-efficiency column (e.g., k_f=2.0 min^{-1}), only a small injection can be processed in batch mode (V_{inj}=1.32 mL), whereas the SSR performs best with an almost 30 times larger injection (V_{inj}=37 mL). As the column efficiency increases, the optimum injection volumes approach each other. This is consistent with the results of the theoretical analysis by Sainio and Kaspereit (2009) , who showed that in the limit of infinite column efficiency (ideal conditions), the optimum injection volume of MR-SSR becomes equal to that of batch chromatography.

The results above demonstrate that, in contrast to ideal conditions, in the presence of dispersive effects productivity can be improved by recycling part of the elution profile. This can be explained by the following hypothetical consideration. In

batch chromatography, we demand that the purity constraints are matched without producing a waste fraction. The amount of fresh feed that can be processed per cycle is limited by both dispersive and thermodynamic effects. If part of the unresolved profile is recycled, but the amount of fresh feed per cycle is held constant, the purities of the product fractions increase above the design constraints. The purity constraints in recycling chromatography can thus be matched exactly only by rendering the separation thermodynamically more difficult, i.e. by simultaneously increasing the amount of fresh feed. Productivity increases by recycling if the relative increase in V_F is larger than the relative change in the cycle time ($t_{BE}-t_{AS}$).

Let us again use the case of $k_f = 2.0$ min^{-1} where $V_{inj} = 1.32$ mL in batch mode (see Table 4) as an example. The cycle time in batch mode is 127 min. Introducing a recycle fraction of 32.7 mL in volume requires increasing the fresh feed volume to 4.3 mL (+226% compared to batch) to match the purity constraints. The cycle time increases from 127 min only to 144.9 min (+14%). As a result, the specific productivity of MR-SSR is almost three times as high as in batch as indicated in the table.

It is also observed in Fig. 8 that EC is very close to its minimum when PR attains its maximum. This means that, for the model system studied here, no trade-off between productivity and eluent consumption need to be made when optimizing the MR-SSR. The largest difference was obtained with the lowest value of k_f, for which EC could be further improved by only 2% by using extremely large injection volumes.

7. Summary

A shortcut design method was developed for steady-state recycling processes in mixed-recycle mode (MR-SSR) under nonideal conditions with significant dispersive effects and convex-upward isotherms in general. The approach was derived based on an existing design method for ideal conditions. The new method does not require a dynamic process model, but can be applied directly to a single experimental chromatogram without knowledge of adsorption isotherm parameters.

The scope of the design method is to predict the four cut times required to achieve a given set of purity requirements in steady state. A model-based study revealed that the calculated cut times are very close to the required values. Furthermore, in all cases the purity of the second eluting product fraction was met with high accuracy. Minor refinements of the cut times are necessary only for very high purity requirements on the first product fraction.

The approach was validated successfully in an experimental study for a model system with significant dispersive effects and isotherm nonlinearity. Based on the numerical and experimental results, the proposed approach is considered an excellent starting point for the detailed design of MR-SSR processes.

Finally, it was shown in a simulation study that for separation problems with significant dispersion the MR-SSR concept outperforms significantly conventional batch chromatography in terms of productivity and solvent consumption.

Table 4: Comparison of the performance of MR-SSR and batch chromatography for the productivity optima marked in Fig. 8.

		Batch opt.			**S**SR opt (max *PR*)		**C**omparison	
k_f	V_inj	*PR*	*EC*	V_inj	*PR*	*EC*	Δ_{PR}	Δ_{EC}
[1/min]	[mL]	[mol/d/L]	[L/mol]	[mL]	[mol/d/L]	[L/mol]	[%]	[%]
2.0	1.32	0.214	1004.6	37	0.615	309.5	+187.9	−69.2
3.0	2.09	0.346	621.6	31	0.841	232.5	+143.3	−62.6
5.0	3.46	0.570	376.5	25	1.069	187.8	+ 87.3	−50.1
6.3	4.12	0.681	315.3	24	1.152	175.2	+ 69.1	−44.4
10.0	5.32	0.877	244.9	22	1.277	159.6	+ 45.6	−34.8
20.0	6.52	1.073	200.2	20	1.393	147.8	+ 29.8	−26.2

Acknowledgements

Notation

Symbols

b	Adsorption isotherm coefficient, Eqs. (8),(9), [L/mol]
c	Liquid phase concentration, [mol/L]
d	Column diameter, [cm]
D_ax	Axial dispersion coefficient [cm^2/min]
ϵ	Total porosity, [−]
EC	Eluent consumption, [L/mol]
F	Phase ratio, $F = (1 - \epsilon)/\epsilon$, [−]
k_f	Mass transfer coefficient, [1/min]
l	Column length, [cm]
m_{ij}	Amount of substance i in fraction j, [mol]
NTP	Number of theoretical stages
P_j	Purity of fraction j
PR	Specific productivity, [mol/d/L]
q	Solid phase loading of component i, [mol/L]
q_s	Saturation capacity, Eqs. (8),(9), [mol/L]
Q	Volumetric flow rate, [mL/min]
t	Time
t_0	Column holdup time $t_0 = \epsilon V/Q$, [min]
Δt_inj	Duration of an injection, $\Delta t_\mathrm{inj} = V_\mathrm{inj}/Q$, [min]
u	Interstitial fluid velocity, $u = Q/\left(\epsilon \frac{\pi}{4} d_c^2\right)$, [cm/min]
V	Volume, [mL]
Y_i	Overall recovery yield of component i, [-]
z	Spatial coordinate, [cm]

Subscripts

A	1st product fraction (weak adsorbing component 1)
B	2nd product fraction (strong adsorbing component 2)
E	End of a fraction
F	Fresh feed
inj	Injection
i	Component (1 - weak adsorbing, 2 - strong adsorbing)
j	Fraction, $j = A, B$
R	Recycle fraction
req	(Purity) requirement
S	Start of a fraction

Superscripts

I, II	Adsorption sites in bi-Langmuir model, Eq. (9)

Antos, D., 2003. Gradient techniques in preparative chromatography – Modelling and experimental realization. Oficyna Wydawnicza Politechniki Rzszowskiej, Rzeszw, Poland.

Antos, D., Seidel-Morgenstern, A., 2001. Application of gradients in simulated moving bed processes. Chemical Engineering Science 56 (23), 6667–6682.

Bailly, M., Tondeur, D., 1982. Recycle optimization in non-linear productive chromatography – I mixing recycle with fresh feed. Chemical Engineering Science 37 (8), 1199–1212.

Charton, F., Bailly, M., Guiochon, G., 1994. Recycling in preparative liquid chromatography. Journal of Chromatography A 687 (1), 13–31.

Chung, S., Wen, C., 1968. Longitudinal dispersion of liquid flowing through fixed and fluidized beds. AIChE Journal 14 (6), 857–866.

Grill, C. M., 1998. Closed-loop recycling with periodic intra-profile injection: a new binary preparative chromatographic technique. Journal of Chromatography A 796 (1), 101–113.

Grill, C. M., Miller, L. M., 2005. Preparative Enantioselective Chromatography. Blackwell Publishing, Ch. Steady-state recycling and its use in chiral separations, pp. 149–174.

Guiochon, G., Shirazi, D. G., Felinger, A., Katti, A. M., 2006. Fundamentals of Preparative and Nonlinear Chromatography, 2nd Edition. Academic Press, Boston.

Kaspereit, M., 2009. Advances in Chromatography. CRC Press, Taylor & Francis, Boca Raton/Fla, USA, Ch. Advanced operating concepts for Simulated Moving Bed Processes, pp. 165–192.

Kaspereit, M., Gedicke, K., Zahn, V., Mahoney, A. W., Seidel-Morgenstern, A., 2005. Shortcut method for evaluation and design of a hybrid process for enantioseparations. Journal of Chromatography A 1092 (1), 43–54.

Lee, J. W., Wankat, P. C., 2009. Optimized design of recycle chromatography to isolate intermediate retained solutes in ternary mixtures: Langmuir isotherm systems. Journal of Chromatography A 1216 (41), 6946 – 6956.

Rhee, H.-K., Aris, R., Amundson, N. R., 2001a. First-order Partial Differential Equations. Vol. I – Theory and Applications of Single Equations. Dover Publications.

Rhee, H.-K., Aris, R., Amundson, N. R., 2001b. First-order Partial Differential Equations. Vol. II - Theory and Applications of Hyperbolic Systems of Quasilinear Equations. Dover Publications.

Sainio, T., Kaspereit, M., 2009. Analysis of steady state recycling chromatography using equilibrium theory. Separation and Purification Technology 66 (1), 9–18.

Schlinge, D., Scherpian, P., Schembecker, G., 2010. Comparison of process concepts for preparative chromatography. Chemical Engineering Science 65 (19), 5373–5381.

Schmidt-Traub, H. (Ed.), 2005. Preparative chromatography of fine chemical and pharmaceutical agents. Wiley-VCH, Weinheim.

Seidel-Morgenstern, A., 2004. Experimental determination of single solute and competitive adsorption isotherms. Journal of Chromatography A 1037 (1-2), 255–272.

Seidel-Morgenstern, A., Keßler, L. C., Kaspereit, M., 2008. New developments in simulated moving bed chromatography. Chemical Engineering & Technology 31 (6), 826–837.

Siitonen, J., Sainio, T., Kaspereit, M., 2010. Theoretical analysis of steady state recycling chromatography with solvent removal. Separation and Purification Technology (subm.).

Contents lists available at ScienceDirect

Journal of Chromatography A

journal homepage: www.elsevier.com/locate/chroma

Effects of a strongly adsorbed additive on process performance in chiral preparative chromatography

P. Forssén [a], R. Arnell [b], M. Kaspereit [c], A. Seidel-Morgenstern [c,d], T. Fornstedt [a,*]

[a] *Department of Physical and Analytical Chemistry, BMC Box 577, SE-751 23 Uppsala, Sweden*
[b] *AstraZeneca Process R&D, SE-151 85 Södertälje, Sweden*
[c] *Max Planck Institute for Dynamics of Complex Technical Systems, D-39106 Magdeburg, Germany*
[d] *Otto-von-Guericke-University, D-39106 Magdeburg, Germany*

ARTICLE INFO

ABSTRACT

The shapes of elution profiles are often significantly influenced by the presence of strongly adsorbed additives in the mobile phase. This aspect needs to be considered in quantitative optimization of preparative chromatography. The theoretical study carried out here is based on available thermodynamic information for the enantiomers of three β-blockers, alprenolol, propranolol, and atenolol, on a teicoplanin chiral stationary phase (Chirobiotic T) using methanol/acetonitrile as the mobile phase and acetic acid/triethylamine as the additive. The properties of this strong additive made it possible to tune the binary elution profiles in any combination of the following apparent band shapes: anti-Langmuir/anti-Langmuir, anti-Langmuir/Langmuir and Langmuir/Langmuir. Optimization of the productivity and yield, when performing repetitive batch injections, was investigated using the equilibrium dispersive model. We show that it is important to consider the invisible additive perturbation peak when defining the cycle time and therefore a model-based optimization needs to take this into account. Furthermore, both productivity and yield could be improved for the two unusual shape combinations in comparison to the traditional Langmuir/Langmuir case.

© 2008 Elsevier B.V. All rights reserved.

1. Introduction

Since 1992 the US Food and Drug Administration (FDA) require that both optical isomers of chiral drugs are tested already at an early stage of drug development [1]. Usually hundreds, or thousands, of so-called candidate drugs are screened for the desired properties of the final drug. Therefore, fast methods for isolation of g to kg amounts of both optical isomers of the candidate drugs are of outmost importance for the pharmaceutical industry. Today, the best generic method for these amounts is preparative chromatography.

Many chiral stationary phases (CSPs) are available for the preparative chromatographic separation of chiral drugs [2–5]. Some of the more recently developed CSPs, that have large potential for several applications, are tartardiamide-based network-polymeric phases (Kromasil CHI) [6], phases immobilized with the macrocycles vancomycin [7], ristocetin A, teicoplanin [8], teicoplanin aglycone [9,10], and eremomycin [11]. The teicoplanin phase, named Chirobiotic T, is especially useful for the separation of the enantiomers of β-blockers [12].

A modern CSP has, because of its great specificity, generally a smaller capacity than a modern nonchiral column and so-called nonlinear effects with overloaded band profiles appear already at a moderate solute concentration in chiral preparative chromatography. Under non-linear conditions, the eluted bands of the components are strongly distorted and asymmetrical and strong band interactions and band contaminations appear [13,14]. Empiric estimation of optimal chromatographic operation conditions, when the bands interact with each other, is difficult and therefore effective optimization is harder in chiral preparative chromatography, but by using numerical simulation of the elution profiles with a suitable model one can predict the optimal experimental conditions and fractionation times [13].

For proper numerical optimization of a preparative chromatographic process it is important to consider (i) which objective functions should be used, (ii) which operating parameters should be optimized, and (iii) the constraints that will be imposed on the system (Chapter 18 in [13]). Typical operating parameters to be optimized are the amounts of feed injected, the velocity of the mobile phase, and the mobile phase composition including additive

type and level. Typical constraints are the yield and the degree of purity desired, sample solubility and maximum column backpressure. Normally, when the costs cannot be properly estimated, it is expedient to maximize the production rate using a yield constraint (Chapter 18 in [13]).

The main prerequisite for numerical optimization is knowledge of the competitive adsorption isotherms [13]. A considerable number of methods have been suggested to account for single-component liquid-solid equilibrium data, see, e.g., [14]. A reliable and very accurate technique is frontal analysis. However, in all chromatography processes of practical importance, we are dealing with multi-component cases and have to measure competitive adsorption isotherms. These are the very difficult to measure; multi-component frontal analysis, for instance, is very tedious and time-consuming and is often not applicable. A faster and more attractive method for acquisition of competitive adsorption data is the so-called inverse method (IM) [15–17]. There the adsorption isotherm parameters are estimated by iteratively minimizing the differences between experimentally determined elution profiles and profiles calculated using a suitable model.

Almost 15 years ago a remarkable band-shape phenomenon was investigated [18,19]. It was demonstrated that a band profile for a certain solute can have an anti-Langmuirian shape, i.e., diffuse front and sharp rear, although its adsorption isotherm is described by the simple Langmuir model that usually gives the traditional overloaded band shape with a sharp front and a diffuse rear. The first requirement for the unusual band shape to appear is that the additive, which is pumped through the column, has stronger adsorption strength than the solute. The second requirement is that the additive system peak elutes before the solute at the plateau level of additive. The first requirement is fulfilled if the retention factor of the additive, k_{add}, is larger than that of the solute, k_{sol}, when both components are injected into a column that contains only a weak solvent and not the additive, i.e., for the separation factor, α_0, between additive and solute it holds that $\alpha_0 = k_{add}/k_{sol} > 1$. The second requirement is fulfilled when the retention factor of the additive system peak, at a certain concentration-plateau of the additive, is smaller than that of the solute peak at the same plateau, i.e., $\alpha_P < 1$. Thus, the solute peak is anti-Langmuir-shaped if $\alpha_0 > 1$ and $\alpha_P < 1$ but Langmuir-shaped otherwise. The fundamental study was made on single-solute system especially designed to create these effects and was not intended for practical preparative separations. However, the effects can take place in any system fulfilling the requirements, or rule of thumb, outlined above. We refer to [12,18,19] for a more extended introduction to this rule. It is worth mentioning that in the case of Langmuir adsorption isotherms the above effects can be clearly explained on the basis of equilibrium theory, see, e.g. [13]. However, for the bi-Langmuir model to be applied here, the theory is not sufficiently developed. Therefore, here results will be discussed applying the above-mentioned straightforward rules.

It was recently demonstrated that these effects occur in modern systems aimed at chiral preparative separations of enantiomers [6,12] and one of these systems was investigated more thoroughly [12]. This system consisted of a teicoplanin stationary phase (Chirobiotic T) using a polar methanol/acetonitrile mobile phase with acetic acid/triethylamine forming the strongly adsorbing additive and the solutes were the β-blockers alprenolol, propranolol and atenolol. By using the inverse method the retention behaviour of the "invisible" additive (triethylamine) was considered by taking its influence on the solute peak shapes into account. An interesting shape of the binary elution profile occurs when (i) the two sharp sides point to each other, i.e., the first eluted peak is anti-Langmuir and the second eluted peak is Langmuir. Other shapes obtained were (ii) anti-Langmuir/anti-Langmuir, and (iii) the tra-

ditional Langmuir/Langmuir. The first situation allows baseline resolution at higher loads in contrast to the situation when both enantiomer peaks tail in the same direction [12].

The aim of this study is to investigate theoretically, how the yield and the productivity can be optimized in chromatographic systems where a strongly adsorbed additive is present and interferes with the two enantiomers of interest. For this purpose we used a standard column model capable of describing the migration behaviour of the solutes and the additive in the column using the adsorption isotherm parameters available from the previous experimental study [12]. Both the additive concentrations and the injection volumes were systematically varied. A further goal was to identify suitable cycle times for consecutive batch injections when taking the "invisible" concentration profiles of the additive into account. This study is of fundamental importance since normally displacement and tag-along effects only between the solutes are considered in optimizations.

2. Theory

In this study the equilibrium dispersion (ED) model was applied to describe the chromatographic process considered. The well-known components of this model; the mass balance equations, the standard boundary and initial conditions as well as the finite difference method of Rouchon used to solve the equations can be found in the literature [13]. The Rouchon method is numerically very efficient and is therefore particularly suited for systematic studies of problems that require very high stage numbers (as is the case here, see below). Further information on its numerical properties, e.g., stability, are given in [20]. If the model is used together with a suitable adsorption isotherm equation it is possible to generate quite reliable estimates for the elution profiles of the solutes and the additive. This information is required for a proper computer-assisted optimization of the production rate and the yield.

The most frequently considered performance criterion is the *production rate* (or *productivity*) which can be defined as

$$Pr_i = \frac{n_{coll,i}}{t_c}, \quad i = 1, \ldots, N. \tag{1}$$

The amounts collected $n_{coll,i}$ can be calculated according to

$$n_{coll,i} = F_V \int_{t_{start,i}}^{t_{end,i}} C_i(t)\, dt, \quad i = 1, \ldots, N. \tag{2}$$

where F_V is the volumetric flow rate (assumed to be constant), $C_i(t)$ are the component concentrations calculated at the column outlet at time t, and $t_{start,i}$ and $t_{end,i}$ are the cut or fractionation points for component i, i.e., the times between this component is collected. Often the productivity is related to a scale-relevant quantity, e.g., the volume of stationary phase.

The definition of the time between two consecutive injections, i.e., the cycle time t_c in Eq. (1), is of crucial importance to evaluate realistic production rates. Obviously, it is desirable to use a minimal cycle time in order to inject as frequently as possible and thereby achieve a higher production rate. Typically, the cycle time t_c is calculated as the difference between the time when the first eluting component exceeds a certain threshold concentration and when the elution profile of the last eluting component drops below this concentration. This is a traditional approach which has often been applied for separations of two enantiomers [13]. In contrast to these studies, here we also consider the elution profile of the additive which is, unfortunately, typically not detectable experimentally. The relevance of this aspect is demonstrated in Fig. 1, which also illustrates the elution order for the systems studied in this work. The elution profiles were predicted theoretically using the parameters
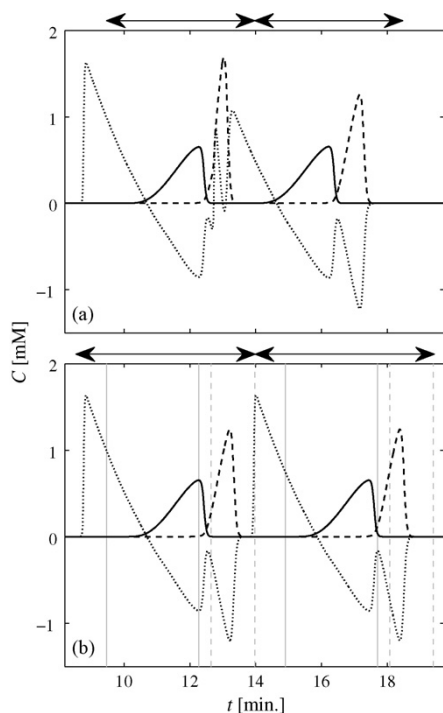
Fig. 1. Two consecutive injections when (a) the cycle time does not take the additive into account and when (b) the cycle time takes the additive into account (baseline for additive adjusted to 0 for clarity). Solid lines indicate enantiomer 1, dashed lines indicate enantiomer 2, dotted lines indicates the additive (TEA) and the arrows indicate the cycle start and stop times. In (b) the solid vertical lines are $t_{start,1}$, $t_{end,1}$ and the dashed vertical lines are $t_{start,2}$, $t_{end,2}$.

introduced below. Fig. 1a shows the chromatogram after two subsequent injections using a cycle time that resulted from considering only the threshold concentrations for the two enantiomers as determined from a single injection (or simulation). Due to the interference of the additive peak of the second elution profile, the shapes of the two consecutive elution profiles are not identical. In contrast, Fig. 1b shows a situation that result from considering the appearance of the additive peak for the start time, and the disappearance of the second eluting enantiomer for the end time, respectively. Although this approach leads to less frequent injections, it is preferred here, since it allows (i) for a practical treatment of invisible peaks (see below), and (ii) for a simplified optimization, since a single simulation suffices to predict the corresponding periodic operation.

In summary, an attractive and safe injection regime is based on assuring for consecutive injections that there is no overlap between the corresponding elution profiles, including the profile of the additive. Therefore, due to the specific elution order of the additive and the three solutes in this work the cycle time was determined as follows

$$t_c = t_{end,2} - t_{start,add}, \tag{3}$$

where $t_{start,add}$ is the time when the additive peak exceeds a certain threshold concentration and $t_{end,2}$ is when last eluted peak drops below this threshold. Finally, in order to manage invisible additive peaks in a practical application, it can be a valid approach to first determine the start and end times for the enantiomers, and then modify the resulting start and end times by safety factors, i.e.,

$$t_c = S_{end} t_{end,2} - S_{start} t_{start,1}, \tag{4}$$

where $(S_{end}, S_{start}) \geq 1$ are the safety factors. However, since in this work the threshold concentrations are known from the simulations, here we determined t_c using Eq. (3).
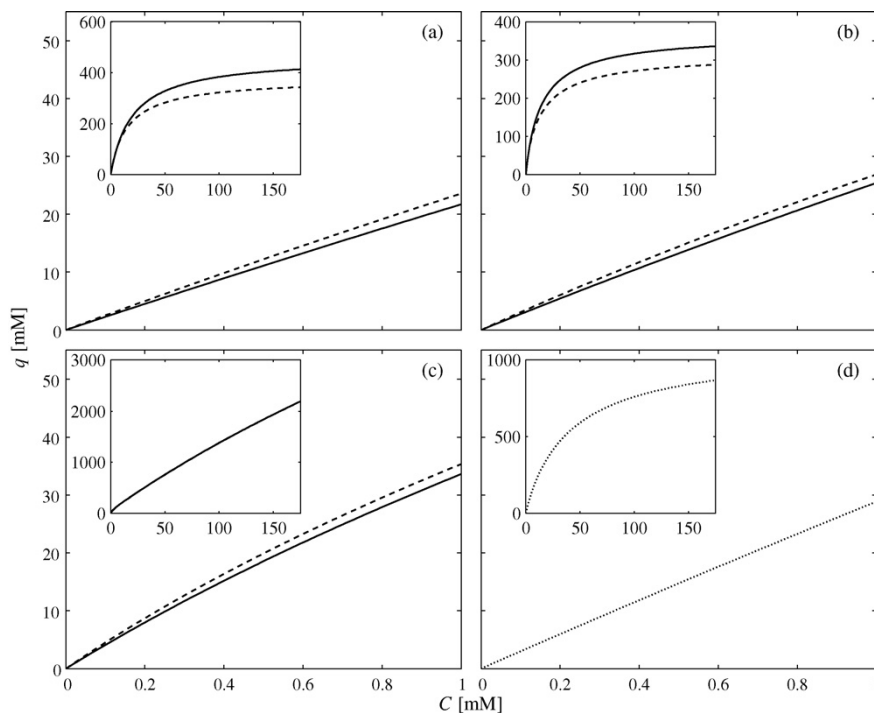
Fig. 2. The β-blocker enantiomers and the TEA additive single adsorption isotherms. The main figures display the adsorption isotherm up to 1 mM and the inset up to 175 mM of the solutes (a) alprenolol, (b) propranolol, (c) atenolol and (d) of the additive TEA. Solid lines indicate enantiomer 1 and dashed lines indicate enantiomer 2.

The *purity* of a fraction with respect to a component i, PU_i, is essential to identify the corresponding collection times, $t_{end,1}$ and $t_{start,2}$. Enantiomeric purity is defined as

$$PU_i = \frac{n_{coll,i}}{F_V \sum_{j=1}^{2} \int_{t_{start,i}}^{t_{end,i}} C_j(t)\, dt} \cdot 100\%, \quad i = 1, 2. \tag{5}$$

The recovery *yield* of component i, Y_i, is defined as

$$Y_i = \frac{n_{coll,i}}{n_{inj,i}}, \quad i = 1, \ldots, N, \tag{6}$$

where n_{inj} is the injected amount.

3. Experimental

The following conditions are the ones used in an earlier publication [12] and we will use the same for our analysis here. The column was a Chirobiotic T (250 mm × 4.6 mm; nominal particle size 5 μm). The mobile phase was a solution of methanol/acetonitrile/acetic acid/triethylamine (32.3/67.5/0.15/0.05/(v/v)). When the additive concentrations were changed, the volumetric ratio between HOAc and TEA was kept 3/1. The flow-rate was 1.50 ml/min and the total column porosity was 0.77. The average plate number of the column for the solutes and conditions considered was 11,250. The injected samples always had the same concentration of TEA as the mobile phase.

It is well known that higher productivities can be reached if the stationary phase is overloaded by concentration rather than volume. Consequently, the productivity of preparative chromatography is often the highest if the highest possible injection concentrations are used [13]. Therefore, saturated samples were assumed in all simulations in this study and the solubilities of the β-blockers in the solvent MeOH/ACN/HOAc/TEA 32.3/67.5/0.15/0.05 (v/v) were determined for each solute. The solubility was 1620 mM for alprenolol, 723 mM for propranolol and 694 mM for atenolol (always sum of enantiomers). The solubilities were found to be practically unchanged in the absence of additives in the mobile phase.

In the previous study [12] the equilibria of the systems under investigation were studied systematically on the Chirobiotic T stationary phase using the inverse method. The competitive isotherms of the additive TEA and of the two enantiomers of the three β-blockers could be successfully correlated using the following bi-Langmuir model

$$q_i = \frac{a_{I,i} C_i}{1 + b_{I,add} C_{add} + b_{I,1+2}(C_1 + C_2)} + \frac{a_{II,i} C_i}{1 + \sum_j b_{II,j} C_j},$$

$$i, j = 1, 2, \text{add}. \tag{7}$$

Table 1
Parameters of the adsorption isotherm model, Eq. (7).

Substance	a_I	b_I (M^{-1})	a_{II}	b_{II} (M^{-1})	α_0
TEA (add)	22.2	156	7.88	139	1
Alprenolol					
Enantiomer 1	8.99	43.6	13.8	54.0	1.31
Enantiomer 2	8.99	43.6	16.4	96.2	1.18
Propranolol					
Enantiomer 1	10.7	47.6	17	120	1.09
Enantiomer 2	10.7	47.6	20.5	230	0.96
Atenolol					
Enantiomer 1	14.8	1.22	27.4	454	0.71
Enantiomer 2	14.8	1.22	31.9	550	0.64

The *a* terms are related to the chromatographic retention factor and dictate adsorption under linear conditions. The *b* terms are the thermodynamic association constants for the respective binding sites. By taking the quotient, the saturation capacity, q_s, can be calculated for each site and for each component, by means of $q_{s,k,i} = a_{k,i}/b_{k,i}$. The first type of sites, or type I sites, include all molecular interactions responsible for non-enantioselective retention. Although their interaction energy is generally modest, these interactions contribute quite significantly to the overall retention, because of their large number. The second types of sites, or type II sites, include the selective interactions responsible for the separation of enantiomers [13]. Because the adsorption energy of the selective sites is high (related to the b_{II} values) and since they are relatively few, these sites are saturated at relatively low concentrations. Adsorption on the first site where considered to be not enantioselective by keeping $a_{I,1} = a_{I,2}$ and $b_{I,1} = b_{I,2}$ (denoted by $b_{I,1+2}$ above). The adsorption isotherm parameters for the additive and the enantiomers of the three β–blockers (see Experimental section for system details) are given in Table 1. Notice that the parameters
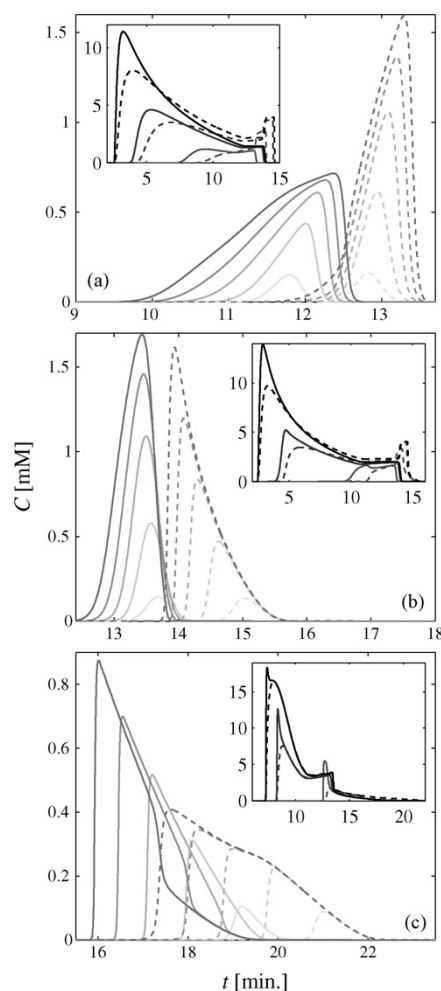
Fig. 3. The main figure shows the simulated chromatograms after injection of 0.1, 0.4, 0.8, 1.2, 1.6 μmol and the insets chromatograms after injection 8, 40 and 80 μmol when using saturated samples of (a) alprenolol, (b) propranolol and (c) atenolol racemic mixtures. Solid lines indicate enantiomer 1, dashed lines indicate enantiomer 2 and the darker the line the more substance injected.

in Table 1 are supposed to be valid for any TEA concentration in the mobile phase, provided that the HOAc/TEA ratio remains 3/1 (v/v) to keep pH constant. In Fig. 2 the corresponding adsorption isotherms are shown, in a–c for the β-blockers and in d for the TEA additive.

4. Results and discussion

There are many parameters to consider when optimizing preparative chromatography [13]. In order to analyse the effects of the additive on the production rates and yields of the batch process the (i) injection volumes and the (ii) additive concentrations were varied while keeping all other parameters constant.

In order to determine the production rates, Eq. (1), and yields, Eq. (6), the cut-points for the enantiomers, $t_{start,1}$, $t_{end,1}$, $t_{start,2}$, and $t_{end,2}$, have to be specified. To determine $t_{start,1}$ and $t_{end,2}$ a threshold concentration of 0.01 μM was applied. The same threshold was used to for $t_{start,add}$ and the cycle time t_c was calculated using Eq.

(3). The times $t_{end,1}$ and $t_{start,2}$ were determined by considering the purity of the collected fractions, Eq. (5). Here a purity of 99% was considered as the target value.

4.1. Elution profiles

At first, a series of elution profiles were generated for different injection volumes using the equilibrium-dispersion model and the isotherm model given above. Typical results are given in Fig. 3a–c. We already showed in the previous study [12] that the unusual peak shapes observed for β-blockers on the Chirobiotic T column are due to the properties of the strongly adsorbed triethylamine (TEA) additive. The profiles obtained show that system peak effects can cause even solute peak splitting. The insets show the remarkable binary band profiles resulting after the injections of saturated samples of the solutes, according to the solubility determinations (see above) at very high sample load. The lower and more realistic sample loads are presented in the main parts of Fig. 3a–c.
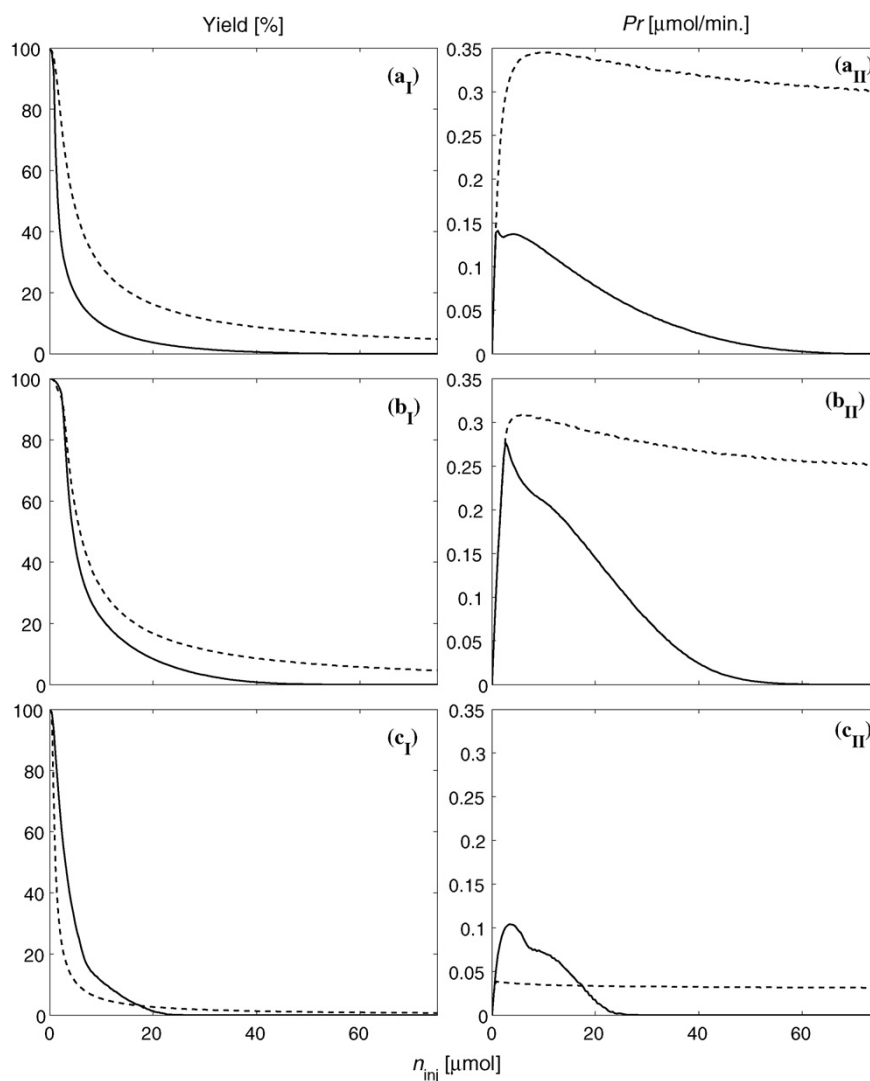

Fig. 4. Yield (I) and productivity (II) when varying the injected amount of the solutes (saturated samples used) for: (a) alprenolol, (b) propranolol and (c) atenolol, solid lines indicate enantiomer 1 and dashed lines indicate enantiomer 2. Concentration of the additive TEA, C_{add}, is 4.94 mM and the cycle times are calculated according to Eq. (3).

Both alprenolol enantiomers exhibit anti-Langmuirian band shapes with a diffuse front and a sharp rear (Fig. 3a). This case will be called anti-Langmuir/anti-Langmuir in the following text. Interestingly, the more retained isomer peak is sharper, and higher, than the less retained one. The diffuse front of the second peak bleeds into and contaminates the first peak, whereas the sharp rear of the first peak does not extend far into the second peak. Therefore, one might suspect that this anti-Langmuir/anti-Langmuir situation could be useful if the more retained enantiomer is the target component of the separation.

The propranolol enantiomer, Fig. 3b, peaks are quite different. The first eluting peak is anti-Langmuirian whereas the second one is Langmuirian with diffuse sides in opposite directions and sharp sides in between. Neither component bleeds into the other zone considerably, indicating that it should be possible to isolate both components with high purity at relatively large sample load. Note how efficiently the first peak is displaced by the second component: the rear of the first component actually elutes earlier at higher sample load (see Fig. 3b main figure).

Fig. 3c, finally, shows predicted peak shapes of the atenolol enantiomers. Both peaks are of the Langmuirian type, which is frequently the case in preparative chromatography. The first peak is always sharper than the second one. Furthermore, it can be seen in the main figure that the first component contaminates the second band severely at higher sample loads, whereas the first peak remains highly pure. This is in line with the common knowledge of preparative chromatographers that the desired component should preferably be eluted first.

4.2. Varying the injection volume

In order to study the effect of column overloading systematic simulations were performed for the three β-blockers varying the amounts injected for a constant additive concentration of 4.94 mM. In these calculations the concentrations of the injected samples were set at the specific saturation concentrations given above and the cycle time was set in accordance with Eq. (3). In Fig. 4 the yields and productivities at 99% purity, were plotted as a function of sample load. The yields decrease rapidly once a certain load has been exceeded, i.e., when baseline resolution is no longer obtained. Due to the specific thermodynamics of the three systems, there are quite different trends how the yields decrease with increasing sample load. For alprenolol, i.e., the anti-Langmuir/anti-Langmuir case, see. Fig. 4a$_I$, the second eluting enantiomer can be obtained with higher yields compared to the first eluting enantiomer in the whole loading range studied. This is because when the baseline resolution is lost and the sharp side of peak 1 interferes with the diffuse side of peak 2 the loss is smaller for the second enantiomer. Also for propranolol, i.e., the anti-Langmuir/Langmuir case, see Fig. 4b$_I$, the yield is higher for the second eluting enantiomer, but the difference is smaller compared to the previous case. For atenolol, i.e., the traditional Langmuir/Langmuir case, see Fig. 4c$_I$, the yield is instead higher for the first eluting enantiomer, up to moderately high loads and then the situation is the reverse. Here, when baseline resolution is lost, the diffuse side of peak 1 interferes with the sharp side of peak 2 so the loss is smaller for the first enantiomer. However at very high loads, when the bands almost completely overlap, a small pure fraction of enantiomer 2 can always be collected on the diffuse side of peak 2. This is the reason why the achievable yield for the two enantiomers reverse at high injected amounts in the atenolol case, see Fig. 4c$_I$.

Also with respect to productivity the three β-blockers behave very different, see Fig. 4, right. In all cases, the productivities increase initially linearly when the sample load is increased. Maxima of the productivity are found for all systems at about

5 μmol injected amount. The order of productivities for the two enantiomers corresponds to the order of the yields for all three compounds. The productivity maxima are higher for the second eluting enantiomer for both alprenolol, Fig. 4a$_{II}$, and propranolol, Fig. 4b$_{II}$. The absolute productivity values are the lowest for atenolol, Fig. 4c$_{II}$, which represents the traditional Langmuir/Langmuir case and here the maximum productivity is higher for the first eluting enantiomer. It should be noted that for atenolol, although the separation factors between the enantiomers are rather similar and the solubility is very close to that of propranolol, both productivity and yield are significantly lower than in the other two cases. This demonstrates the usefulness of achieving unusual band shapes for process optimisation.

4.3. Varying the additive concentration

A well known and popular way to adjust the productivity in situations where the cycle time is too long is to increase additive

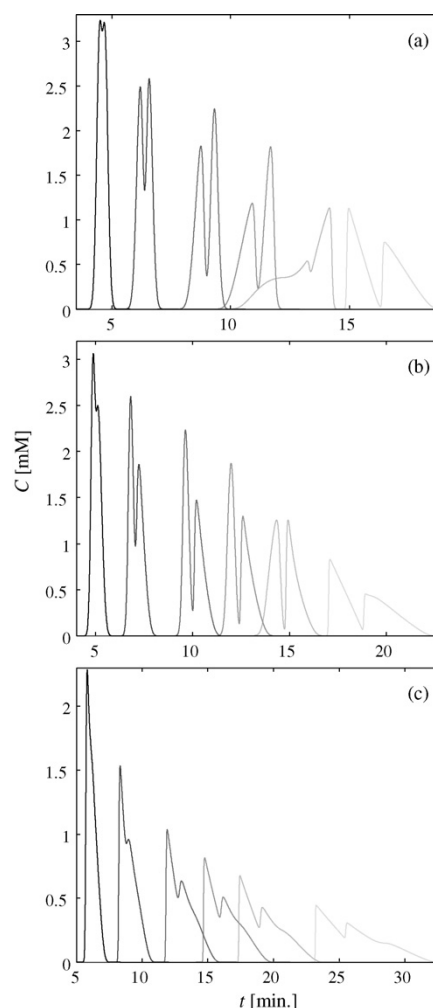**Fig. 5.** Chromatograms using 0, 4, 7, 12, 25, 50 mM concentrations of the additive TEA and 1.25 μmol injections of each enantiomer (50 μl of 25 + 25 mM samples). Lower retention times correspond to higher additative concentrations: (a) alprenolol, (b) propranolol, (c) atenolol. Solid lines indicate enantiomer 1, dashed lines indicate enantiomer 2 and the darker the line the higher the additive concentration.

concentrations in the mobile phase. To study this effect for the three β-blockers, further simulations were performed.

Fig. 5 illustrates the strong effect of the additive concentration, in a range between 0 and 50 mM, on the elution times and the shapes of the elution profiles. As expected, the atenolol peaks Fig. 5c are of the Langmuir type and elute closer to the void volume when the additive concentration is increased. In contrast, for alprenolol and propranolol, Fig. 5a and b, the binary peak shape symmetries change when the TEA concentration in the mobile phase is increased. The reason for this behaviour is the fact that the elution order of the additive perturbation and solute peaks change in this region. The solute peaks are actually of the Langmuir type for very low or zero additive concentration, i.e., when $\alpha_P > 1$. When the perturbation elutes very close to the solutes, the solute peaks become strangely deformed. Once the elution order has switched, i.e., $\alpha_P < 1$, and the additive perturbation elutes sufficiently long before the solutes, no further symmetry transformations occur. These observations are consistent with the rule of thumb given above. Fig. 5

illustrates that an intelligent adjustment of the additive concentrations offers a large potential to optimize a separation.

In order to study the influence of the additive concentration on the yield and productivity simulations were performed. The amount injected was fixed to be 1.25 μmol, using the specific saturation concentrations as the injection concentrations. In Fig. 6 the yield and productivity, for 99% purity, are plotted as a function of the additive concentrations for the two enantiomers. The results demonstrate the complex impact of the additive on the process performance. The initial minima observed for alprenolol and propranolol, Fig. 6a and b, are due to temporary loss of resolution associated with the switch of perturbation vs. solute elution order as discussed above. Obviously, the optimal additive concentrations differ significantly for each substance, target enantiomer and performance criterion.

The results shown in Figs. 4 and 6 clearly indicate that both the injected amount and the additive concentration have to be optimized simultaneously. Since it was not the primary goal of this
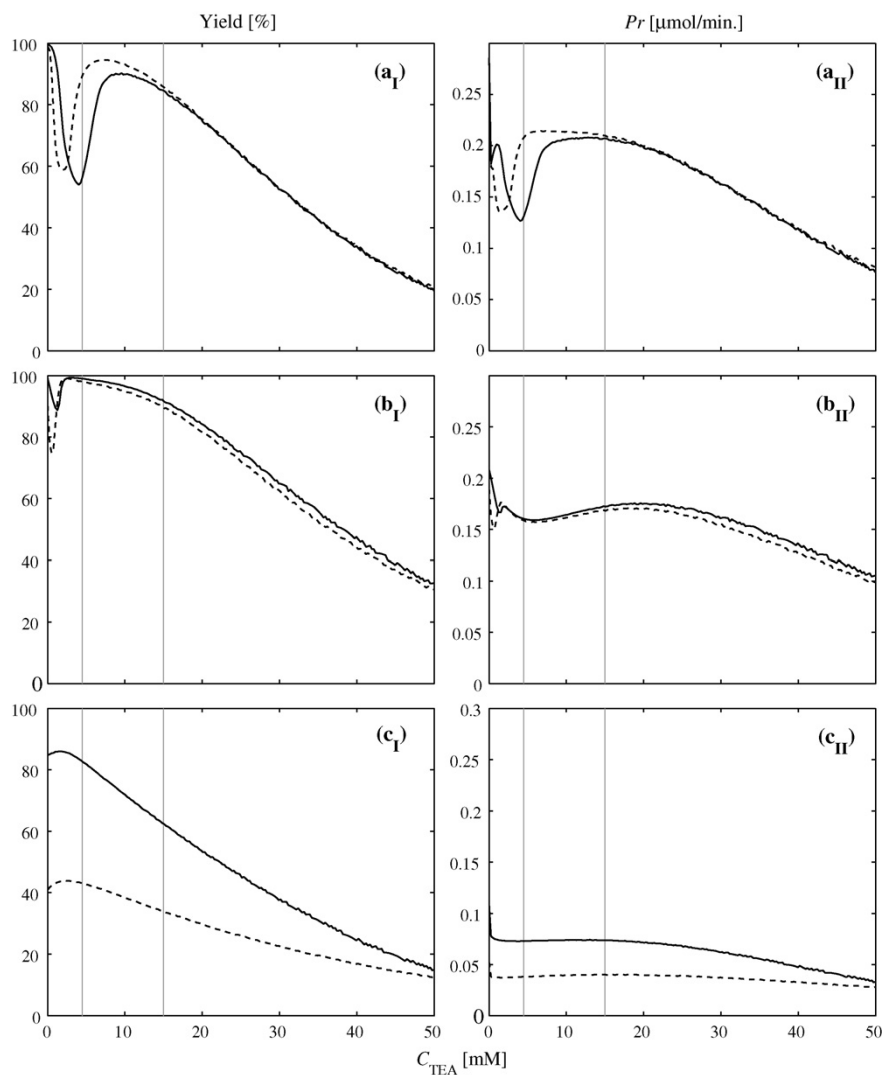
Fig. 6. Yield (I) and productivity (II) when varying the additative concentration and using 1.25 μmol injections of each enantiomer (50 μl of 25 + 25 mM samples): (a) alprenolol, (b) propranolol and (c) atenolol. Solid lines indicate enantiomer 1, dashed lines indicate enantiomer 2 and the vertical lines indicate C_{add} = 4.94 and 15 mM, see also Fig. 7.
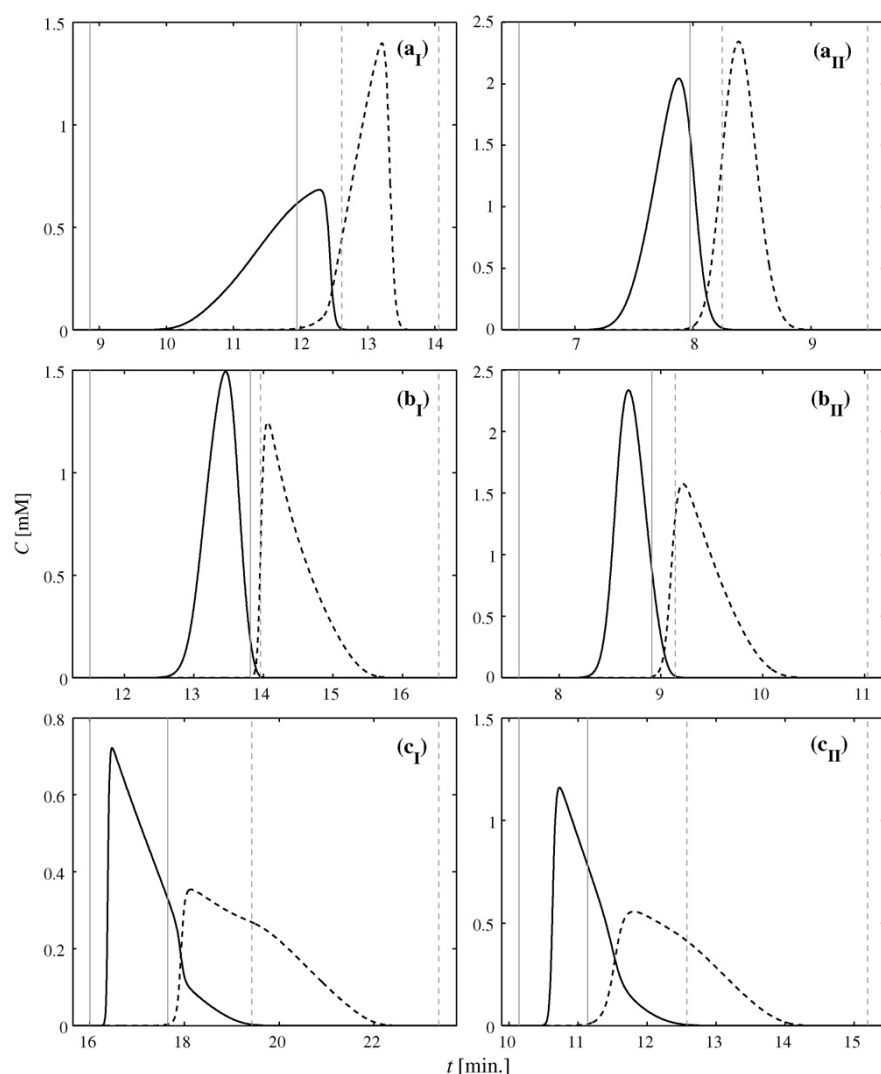
Fig. 7. Chromatograms and cut points for 99% purity injecting 1.25 μmol racemic mixture using saturated samples and additive concentration C_{add} = 4.94 mM (I) or 15 mM (II), see Fig. 6, (a) alprenolol, (b) propranolol, (c) atenolol. Solid lines indicate enantiomer 1 and dashed lines indicate enantiomer 2, solid vertical lines the cut points for enantiomer 1 and dashed vertical lines the cut points for enantiomer 2. The cycle times, t_c, are for (a$_I$) 5.4, (a$_{II}$) 5.1, (b$_I$) 7.7, (b$_{II}$) 6.7, (c$_I$) 14.0 and for (c$_{II}$) 10.6 min.

paper to perform a full optimization study, this straightforward but numerically expensive exercise was not undertaken here.

To further demonstrate the strong impact of the additive on the shape of the elution profiles, the corresponding elution profiles for two distinct values from Fig. 6, 4.94 and 15 mM (marked in the figure), are shown in Fig. 7. As expected, the β-blockers elute much earlier when the additive concentration is increased. The determined cut points to collect fractions of 99% purity are indicated by lines in the chromatograms. The most pronounced difference for these two additive concentrations occurs for alprenolol (Fig. 7a$_I$ vs. a$_{II}$). The higher productivity for the additive concentration 15 mM results from the much lower cycle time t_c, which can be clearly seen in the figure.

5. Conclusion

Based on available thermodynamic data for three specific chiral compounds, we quantified the effect on the performance of

preparative chromatography when a strongly adsorbing additive is present in the mobile phase. It was demonstrated that an optimization has to take the elution profile of the additive explicitly into account. Otherwise, unrealistically short and infeasible cycle times will be assumed and productivity will be overestimated. It was also demonstrated that both the injected solute amounts and the additive concentration have to be optimized simultaneously.

The study demonstrates that a considerable gain in terms of yield and productivity can be achieved if the concentration of the strong additive is tuned appropriately. An instructive result is the fact that for the examples investigated – which are characterized by similar solubilities – the performance is significantly higher for the systems with unusual band shapes in comparison to the classical Langmuir/Langmuir case. Thus, the quantitative incorporation of the effects of strongly adsorbed additive offers to exploit a new degree of freedom for optimizations of preparative liquid chromatography.

References

[1] US Food and Drug Administration (FDA), FDA's Policy Statement for the Development of New Stereoisomeric Drugs, US Food and Drug Administration (FDA), Rockville, MD, USA, 2001, http://www.fda.gov/cder/guidance/stereo.htm.
[2] E.R. Francotte, J. Chromatogr. A 906 (2001) 379.
[3] Y. Okamoto, Y. Kaida, J. Chromatogr. A 666 (1994) 403.
[4] Y. Yashima, Y. Okamoto, Bull. Chem. Soc. Jpn. 68 (1995) 3289.
[5] C.J. Welch, J. Chromatogr. A 666 (1994) 3.
[6] J. Lindholm, T. Fornstedt, J. Chromatogr. A 1095 (2005) 50.
[7] D.W. Armstrong, Y. Tang, S. Cheng, Y. Zhou, C. Bagwill, J.R. Chen, Anal. Chem. 66 (1994) 1473.
[8] D.W. Armstrong, Y. Liu, K.H. Ekborg-Ott, Chirality 7 (1995) 474.
[9] A. Berthod, X. Chen, J.P. Kullman, D.W. Armstrong, F. Gasparrini, I. D'Acquarica, C. Villani, Anal. Chem. 72 (2000) 1767.
[10] M. Bechtold, A. Felinger, M. Held, S. Panke, J. Chromatogr. A 1154 (2007) 277.
[11] K. Petrusevska, M.K. Kuznetsov, K. Gedicke, V. Meshko, S.M. Staroverov, A. Seidel-Morgenstern, J. Sep. Sci. 29 (2006) 1447.
[12] R. Arnell, P. Forssén, T. Fornstedt, Anal. Chem. 79 (2007) 5838.
[13] G. Guiochon, A. Felinger, D.G. Shirazi, A.K. Katti, Fundamentals of Preparative and Nonlinear Chromatography, 2nd ed., Elsevier Inc., San Diego, CA, 2006.
[14] A. Seidel-Morgenstern, J. Chromatogr. A 1037 (2004) 255.
[15] A. Felinger, A. Cavazzini, G. Guiochon, J. Chromatogr. A 986 (2003) 207.
[16] P. Forssén, R. Arnell, T. Fornstedt, J. Chromatogr. A 1099 (2005) 167.
[17] K. Kaczmarski, J. Chromatogr. A 1176 (2007) 57.
[18] T. Fornstedt, G. Guiochon, Anal. Chem. 66 (1994) 2116.
[19] T. Fornstedt, G. Guiochon, Anal. Chem. 66 (1994) 2686.
[20] G. Guiochon, B. Lin, Modeling for Prepaparative Chromatography, 1st ed., Academic Press, San Diego, CA, 2003.

Design of simulated moving bed processes under reduced purity requirements

Malte Kaspereit [a,*], Andreas Seidel-Morgenstern [a,b], Achim Kienle [a,c]

[a] *Max-Planck-Institut für Dynamik komplexer technischer Systeme, D-39106 Magdeburg, Germany*
[b] *Otto-von-Guericke Universität Magdeburg, Institut für Verfahrenstechnik, D-39106 Magdeburg, Germany*
[c] *Otto-von-Guericke Universität Magdeburg, Institut für Automatisierungstechnik, D-39106 Magdeburg, Germany*

Available online 24 February 2007

Abstract

The design of simulated moving bed chromatography under reduced purity requirements is investigated. A parametric study indicates that all internal flow rates should be considered as free parameters in process design. This is confirmed by systematic numerical optimisations of two different design scenarios. A restrictive scenario requires complete regeneration of liquid and solid phases. In contrast, in a non-restrictive design all flow rates are optimised. The latter leads to significantly improved process performance. On the basis of the obtained observations, a simple design method for simulated moving bed processes with desired outlet purity values is derived from equilibrium theory.
© 2007 Elsevier B.V. All rights reserved.

Keywords: Simulated moving bed; True moving bed; Design method; Reduced purity; Equilibrium theory; Langmuir adsorption isotherm

1. Introduction

Separations by simulated moving bed (SMB) chromatography are usually designed with the objective of maximising product purity. This is often a necessity in applications within the pharmaceutical and fine chemical industry. However, it is well known that the performance of SMB processes in terms of productivity, solvent consumption, and product concentration improves significantly with decreasing purity requirements (see, e.g., [1,2]). This circumstance can be exploited directly if products with only reduced purity are required. Alternatively, combining SMB chromatography with a complementary separation process allows to operate the SMB unit under reduced purity requirements. This, in turn, can allow for higher overall performance in comparison to a stand-alone SMB separation [1–6].

As far as a complete separation of components is concerned (i.e., pure products), useful design tools are available that allow for a direct prediction of necessary operating conditions; for example the 'standing wave analysis' [7,8] and the well-known 'triangle theory' [9,10]. The former accounts for both adsorption equilibria as well as dispersive effects and requires some

reconciliation using numerical models or experiments. The latter considers only the influence of the adsorption isotherms and provides explicit expressions for optimum operating parameters. It also specifies a range of adjustable operating parameters leading to pure products ('separation triangle'). The design method has been elaborated for most of the relevant types of adsorption isotherms [11–16].

Up to now there are no comparable methods available for an optimal design of SMB processes under reduced purity requirements. In the context of triangle theory, Storti et al. [9] indicate regions of operating parameters that lead to different outlet purities. A derivation of these regions was not given. Furthermore, complete regeneration of liquid and adsorbent phase was required in the corresponding zones of the SMB process.

Due to this lack of tools, up to now SMB processes with reduced product purity are designed on the basis of numerical simulations. Frequently, also here only the flow rates in the two separation zones are adjusted, while complete regeneration of solid and liquid phases is enforced; for example, by applying safety margins to the corresponding flow rates [2,17–19]. This appears contradictory, since reduced purity requirements should allow for a less restrictive process design. Due to the computational efforts related to optimising all internal flow rates of an SMB process, such optimisations were reported only recently. Different strategies have been applied; for example, genetic algorithms [20], sequential-quadratic programming (SQP) [4],

---

non-linear optimisation with full discretisation [21], a two-level approach [22], and the use of feedback control [23].

However, the behaviour of SMB processes under such conditions and, in particular, the role of the regeneration zones remain only partially understood. In this context, only few studies were performed in which parameter regions analogous to the mentioned separation triangle were determined numerically [2,5,24]. This approach was systematised by Rodrigues and co-workers, who suggested the concept of "separation volumes" [22,24–26]. The method was applied to linear and non-linear systems with mass transfer resistances and basically consists of a numerical parametric study to determine the influence of each regeneration zone on the feasibility-range of the remaining parameters. The obtained results will be included in the discussion below.

In this work, an optimisation study is performed for a true moving bed (TMB) process model using a synthetic set of parameters. It will be demonstrated that in an optimal design under reduced purity requirements no design restrictions must be applied to the regeneration zones and that, instead, all internal flow rates should be optimised. Furthermore, the role of the regeneration zones is investigated on the basis of a parametric study. Finally, based on the phenomenological observations obtained, local equilibrium theory is used to derive a method for the direct prediction of optimal design parameters for SMB processes under reduced purity requirements.

2. Theoretical background

2.1. Fundamentals and conventions

The principles of continuous chromatography are well-established. For details, the interested reader is referred to the standard literature on the topic; for example, [27,28].

In this work, we will apply the TMB concept as an approximation of the more complex SMB process. In order to introduce the notation to be used, Fig. 1 shows a scheme of a TMB process with internal concentration profiles. The less adsorbing solute 1 (solid line) is obtained at the raffinate port, while the stronger adsorbing component 2 (dashed line) is withdrawn at the extract port. The individual zones of the unit are denoted by $I \dots IV$. It should be noted that in the case of complete separation of the components, zones II and III are frequently denoted as separation zones, while zones I and IV are called regeneration zones.

The main design parameters for the process in Fig. 1 are the dimensionless zone flow rates, m^j. These are given by the ratios between liquid and solid flow rates in each zone j of the unit. The following definition holds and allows for a conversion between the flow rates in TMB and SMB processes, respectively [10]:

$$m^j = \frac{Q^j}{Q_S} = \frac{u^j}{\nu u_S} = \frac{Q^{j,\text{SMB}} t_S - \epsilon V}{V(1 - \epsilon)}, \quad j = (I \dots IV) \quad (1)$$

where Q^j denotes the liquid flow rate in zone j and Q_S the solid flow rate throughout the TMB unit, respectively; u^j and u_S are the corresponding interstitial velocities. The phase ratio is defined as $\nu = (1 - \epsilon)/\epsilon$. The right term in Eq. (1) holds for an analogous SMB process; here $Q^{j,\text{SMB}}$ stands for the liquid flow rate, t_S for the switching time, ϵ for the total column porosity, and V for the column volume, respectively.

The purity values for the raffinate, P^R, and the extract, P^E, are given by the steady-state concentrations at these outlets. They are defined with respect to their corresponding target components:

$$P^R = \frac{c_1^R}{c_1^R + c_2^R} \quad (2a)$$

$$P^E = \frac{c_2^E}{c_1^E + c_2^E} \quad (2b)$$

That is, component 1 should be obtained in excess at the raffinate port, and component 2 in excess at the extract port.

2.2. Modelling of countercurrent chromatography

In this work, two models for the TMB process in Fig. 1 are of relevance. These are the equilibrium model and an equilibrium-cell model. For more options concerning modelling of countercurrent chromatography see, for example, [29].

The equilibrium model for a countercurrent chromatographic process follows by neglecting any dispersive effects and assuming local adsorption equilibrium. Under these assumptions, the mass balances for an individual component i in a single TMB section j of the unit in Fig. 1 are given by [30]:

$$\frac{\partial}{\partial \tau}[c_i + \nu q_i(\bar{c})] + \frac{\partial}{\partial z}[m^j c_i - q_i(\bar{c})] = 0$$
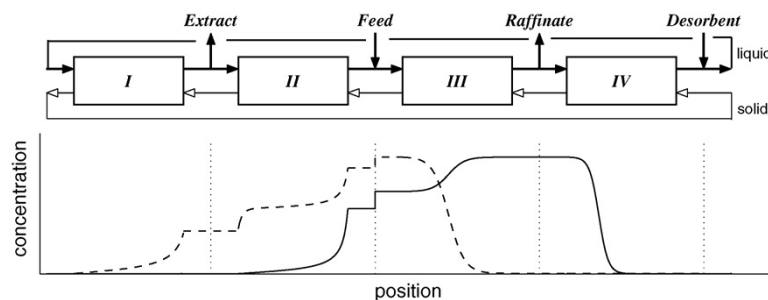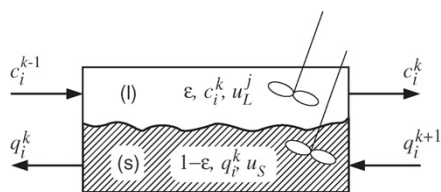$$i = (1, 2) \quad j = (I \dots IV) \quad (3)$$

Fig. 1. Schematic representation of a continuous chromatographic (TMB) process with internal concentration profiles. Solid line – less retained component 1; dashed line – stronger retained component 2.

Fig. 2. Single equilibrium cell k in section j of a TMB process.

where the liquid and solid phase concentrations are denoted by c and q, respectively. $\tau = (t\nu u_s)/L$ and $z = x/L$ are the dimensionless time and space variables. L is the section length, u_s the interstitial solid phase velocity, and $\nu = (1 - \epsilon)/\epsilon$ is the phase ratio that depends on the porosity ϵ. Please note that Eq. (3) is a set of homogeneous quasilinear partial differential equations. For this type of equations there is an elaborated theory available which allowed to derive solutions for different applications [30,31], and which was also used for the above-mentioned derivation of the triangle theory.

In most real chromatographic processes dispersion plays a significant role. In an numerical optimisation study to be presented later in this work, we account for this by using an equilibrium cell model. That is, each section j of the process in Fig. 1 is divided in N countercurrent equilibrium cells as shown in Fig. 2. The mass balances for a cell read

$$\frac{\partial}{\partial \tau}[\epsilon c_i^k + (1 - \epsilon)q_i^k(\bar{c}^k)] = m^j(c_i^{k-1} - c_i^k) + (q_i^{k+1} - q_i^k)$$

$$i = (1, 2) \quad j = (I \ldots IV) \quad k = (1 \ldots N) \tag{4}$$

Note, that in this case, $\tau = t Q_s/V$, with V being the volume of a cell.

In order to solve Eqs. (3) or (4), the dependence of the solid phase loading on the liquid phase concentration must be known; that is, the adsorption isotherms $q_i(\bar{c})$. Here we apply the competitive Langmuir adsorption isotherm model:

$$q_i = \frac{a_i c_i}{1 + \sum_{j=1}^{2} b_j c_j}, \quad i = (1, 2) \tag{5}$$

The equilibrium cell model, consisting of Eqs. (4) and (5), and the mass balances between the single sections, was implemented in the simulation environment DIVA [32]. Further details are given in [5].

3. Influence of the regeneration zones

In this section, a parametric study is performed to investigate the role of the two regeneration zones I and IV (see Fig. 1). In particular, processes with reduced purity requirements are considered.

The equilibrium cell TMB model, Eq. (4), is used together with a model system. All necessary parameters of that system are listed in Table 1. The table also contains the optimum flow rate ratios for 100% pure products, m_{100}^j, as calculated from the triangle theory [10].

Table 1
Parameters for the model system used in TMB calculations

Adsorption isotherms	$a_1 = 2$	$a_2 = 3$
	$b_1 = 0.02\,\text{l/g}$	$b_2 = 0.02\,\text{l/g}$
Feed concentrations	$c_1^F = c_2^F = 20\,\text{g/l}$	
Column dimensions	$20 \times 1\,\text{cm}$	
Stages per zone	100	
Porosity	$\epsilon = 0.7$	
Maximum zone flow rate	10 ml/min	
Opt. m-values (triangle theory, 100% purity)	$m_{100}^I = 3.0$	$m_{100}^{II} = 1.7423$
	$m_{100}^{III} = 2.0644$	$m_{100}^{IV} = 1.5799$

At first we consider the case of complete regeneration (i.e., in zone I all components are eluted from the solid phase, while in zone IV no breakthrough of the components towards zone I is permitted). For this purpose, "correction factors", β^j, are applied to the corresponding zones:

$$\beta^I = \frac{m^I}{m_{100}^I} \tag{6a}$$

$$\beta^{IV} = \frac{m_{100}^{IV}}{m^{IV}} \tag{6b}$$

In order to prevent any breakthrough of solutes from zone I to zone IV and *vice versa*, it is necessary that $(\beta^I, \beta^{IV}) \geq 1$.

A common tool for the design of SMB processes is the m^{II}–m^{III}-diagram. For the system investigated here, Fig. 3 contains a corresponding plot for the case of complete regeneration ($\beta^I = \beta^{IV} = 1.1$). The diagram was determined by calculating the steady state of the TMB process for different values of (m^{II}, m^{III}). These were given by an equidistant grid of about 1000 points within the diagram. Analysis of the results allows to derive the different regions shown in the figure. In each of them the purity of both outlets exceeds a certain value (between
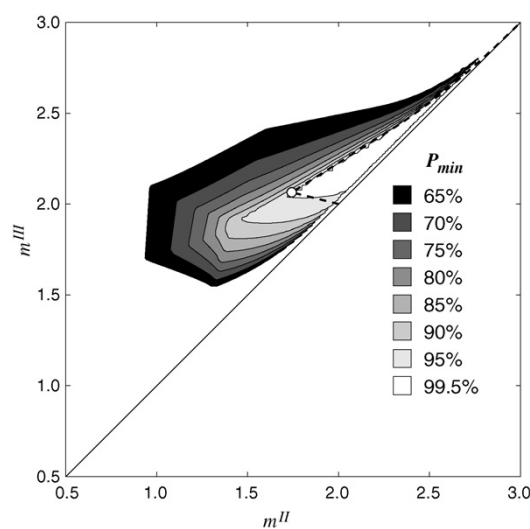

Fig. 3. Separation regions for different minimum values of outlet purity $(P^R, P^E) \geq P_{\min}$. Restrictive design of regeneration zones ($\beta^I = \beta^{IV} = 1.1$). Dashed line – region of complete separation, circle – optimum operating point according to triangle theory [10].
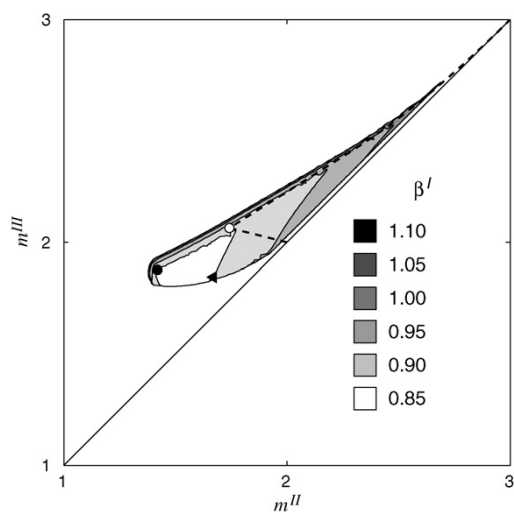
Fig. 4. Separation regions for outlet purity values P^R, $P^E \geq 90\%$ for a gradual decrease of the correction factor β^I ($\beta^{IV} = 1.1 = const.$). Symbols – example for the two vertices leading to identical purity, i.e. $P^R = P^E$; ● – vertex with high productivity, ◄ – vertex with low productivity.

65% and 99.5%). Compared to the region for complete separation given by the triangle theory (dotted line), the regions are significantly larger for lower purity requirements. Furthermore, their vertices move away from the diagonal. This indicates the possibility to increase the feed flow rate.

A different picture is obtained when abandoning the requirement of complete regeneration. This is achieved by lowering the correction factors. Figs. 4 and 5 show separation regions for at least 90% product purity at both outlets. The different regions result from decreasing stepwise one of the correction factors. In Fig. 4 β^I is varied while β^{IV} is kept at a "safe" value of 1.1. In Fig. 5 β^{IV} is varied while $\beta^I = 1.1$. In both figures the largest region is identical to the 90%-region in Fig. 3.
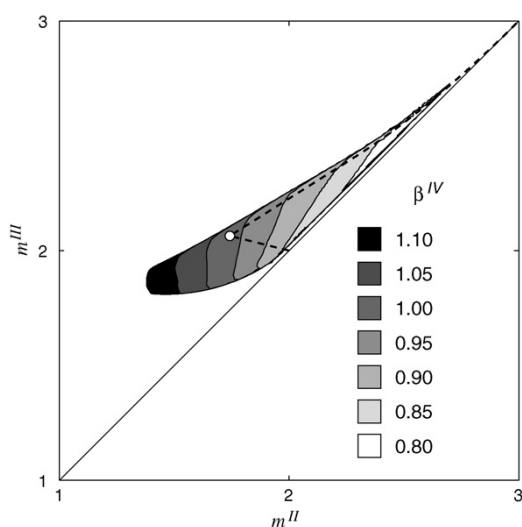

Fig. 5. Separation regions for outlet purity values P^R, $P^E \geq 90\%$ for a gradual decrease of the correction factor β^{IV} ($\beta^I = 1.1 = $ constant).

It can be seen from Fig. 4 that lowering β^I leads to a decreasing size of the separation region. Comparing the different areas, it can be observed that the region shrinks starting from the diagonal. This is caused by a breakthrough of the strong adsorbing solute from zone *I* into zone *IV*, which in turn decreases the raffinate purity. However, the effect is rather weak, since for Langmuir-type adsorption a dispersive wave is located in zone *I* and, thus, a decreased β^I leads to rather low concentrations to "wrap around" into zone *IV*. Only for $\beta^I \leq 0.8$ this effect is strong enough that the region vanishes completely (i.e., the minimum purity of 90% cannot be achieved anymore at one or both of the outlets). It should be noted that the position of the vertex of the regions remains almost constant for a rather wide range of β^I. This is important, since the m^I-value largely influences the pressure drop within an SMB unit and, thus, has a strong impact on productivity. Therefore, this almost constant vertex position indicates that the productivity can be increased (within certain limits) by lowering the correction factor β^I.

In contrast, when lowering β^{IV} (Fig. 5), the regions shrink starting from the "outside". The corresponding vertices move towards the diagonal. The effect is significant already for small deviations from $\beta^{IV} = 1.1$. This is caused by a breakthrough of the less adsorbing component from zone *IV* into zone *I*. Since for Langmuir adsorption isotherms in zone *IV* a shock wave is situated, such breakthrough immediately leads to a strong pollution of the extract. This effect is compensated only by operating points close to the diagonal, which are not attractive in terms of productivity. Ergo, a violation of the regeneration constraint in zone *IV* will entail a decrease of the productivity.

Similar observations were made by Rodrigues and co-workers [22,24–26], who suggested a design procedure based on systematic model-based scanning of the m^j-value parameter space. This approach certainly results in improved process performance, because it sets aside the constraint of complete regeneration. However, the application of the method is rather laborious and it remains uncertain whether optimal solutions are obtained. It will be shown in Sections 4 and 5 that all four zone flow rates can be optimised directly for two-component separations as considered here.

An interesting fact is that for violated constraints in zone *I* a second vertex develops at the lower border of the separation region (Fig. 4). The throughput for this point is much lower than for the upper vertex. Notably, in both points it holds $P^R = P^E$. This indicates that objective functions including conditions like (P^R, P^E) $\geq P_{min}$ (as was used in [2] and [33]) can cause convergence into suboptimal solutions.

4. Optimisation study

The results obtained from the parametric study above indicate that including the regeneration zones in the design procedure should allow for improving process performance. In particular, it might be beneficial to allow for a certain breakthrough of the strong adsorbing component from zone *I* into zone *IV*. In order to verify this assumption, below two different design scenarios will be investigated. In the first scenario, denoted as *restrictive design*, the flow rates in zones *II* and *III* are subject to numerical

optimisation, while complete regeneration in zones *I* and *IV* will be enforced. In the second, the *n* on-restrictive design, these restrictions are abandoned and all four flow rates are optimised.

4.1. Optimisation problem

For the optimisations, a sequential-quadratic programming (SQP) method available in DIVA is applied. SQP has already been used successfully by other authors for SMB optimisations; see, for example [34]. Optimisation variables are the four m^j-values. As the objective function *OF*, the ratio between desorbent flow rate and product mass flow is considered, which should simultaneously minimise eluent consumption and maximise productivity. The optimisation problem is then

$$OF = \frac{Q^D}{Q^R c_1^R + Q^E c_2^E + 1 \times 10^{-8}} \rightarrow \min$$
$$\text{s.t.} \quad P^R \geq P_{\min}^R \tag{7}$$
$$P^E \geq P_{\min}^E$$

The outlet purities P^R and P^E are considered as nonlinear constraints. The term 1×10^{-8} in Eq. (7) is introduced to prevent numerical difficulties if the remaining denominator becomes equal to zero. With respect to convergence, it was found useful to include also the following linear constraints:

$$m^I \geq m^{II} + \Delta m$$
$$m^{III} \geq m^{II} + \Delta m$$
$$m^{III} \geq m^{IV} + \Delta m$$
$$m^I \geq m^{IV} + \Delta m \tag{8}$$

These constraints prevent numerically expensive function evaluations at economically useless operating points (e.g., for extremely low feed flow rates). Furthermore, they guarantee for the proper direction of flows and prohibit flow rates equal to zero. For the isotherm parameters listed in Table 1, a value of $\Delta m = 10^{-2}$ was found appropriate.

In the following calculations, the flow rate in zone *I* will be set arbitrarily to $Q_L^I = 10.0$ ml/min, assuming that this corresponds to the highest tolerable flow rate within the unit and, thus, maximising the throughput for each obtained design point. It should be noted that this approach holds only if dispersive effects (here given by the number of equilibrium cells, *N*) can be assumed to be independent of the flow rate. The obtained results will be interpreted in terms of the following performance parameters. The average eluent consumption *EC* is given by the ratio of the flow rates of feed and desorbent, Q^F and Q^D, and the mass streams of the two products:

$$EC = \frac{Q^F + Q^D}{Q^R c_1^R + Q^E c_2^E} \tag{9}$$

The productivity *PR* is given by the sum of the two product mass fluxes:

$$PR = Q^R c_1^R + Q^E c_2^E \tag{10}$$

It should be noted, that this definition actually represents a throughput (rather than a productivity, which in chromatography is usually defined with respect to the volume of stationary phase). However, such definition can be misleading when applied to a TMB process. At any rate, the productivity of an analogous SMB process will be proportional to the values obtained from Eq. (10).

4.2. Results

Fig. 6 contains the optimisation results for the two design scenarios. For the restrictive design, complete regeneration was targeted by applying correction factors of $\beta^I = \beta^{IV} = 1.1$, while in the non-restrictive design all four zone flow rates were optimised. Optimisations were performed for different minimum purity values $P_{\min}$ between 60% and 99.8%. Both design scenarios were investigated for three different cases. The first case represents a symmetrical separation with equal raffinate and extract purity (i.e., $P^R = P^E = P_{\min}$; left column of Fig. 6). The other two cases are asymmetrical separations, in which either for the raffinate or for the extract a constant high purity of 95% was demanded, while the other outlet purity was varied. Such situations might be more relevant in practice than symmetrical purity adjustments.

Considering first the symmetrical case (Fig. 6, left), it becomes clear that for both design scenarios, the performance parameters productivity, eluent consumption, and product concentration improve significantly with lower purity requirements. For example, in case of the restrictive design (open symbols), the productivity and the raffinate concentration can be doubled by decreasing the purity constraints from 99.8% to 85%. Simultaneously, eluent consumption and extract concentration improve by approximately 30% and 20%, respectively. The results for the non-restrictive design (filled symbols) are even more promising; it introduces a significant additional benefit if compared to the restrictive design. Considering the numbers given above, productivity and eluent consumption can be further improved by 30%, while the extract concentration increases by 38%. The raffinate concentration (marked by triangles) increases only slightly.

A similar picture is obtained when analysing the results for the asymmetrical separations. For a constant raffinate purity and a variable extract purity (Fig. 6, middle), a significant benefit can be achieved. In this case also the raffinate concentration (filled triangles) can be increased (for $P^E \leq 90\%$). In contrast, the achievable gain is limited when keeping the extract purity constant and allowing lower values only at the raffinate port (Fig. 6, right). In this case, an improvement is found basically only with respect to the eluent consumption and the extract concentration. The raffinate concentration even slightly decreases with decreasing P^R. This is due to the increased concentration of the stronger adsorbing component at this outlet, which in turn accelerates the concentration fronts and necessitates unfavourable m^j-values.

Fig. 7 shows as an example the m^j-values obtained for the symmetrical case (corresponding to the results in the left column of Fig. 6). It can be seen that the different purity requirements
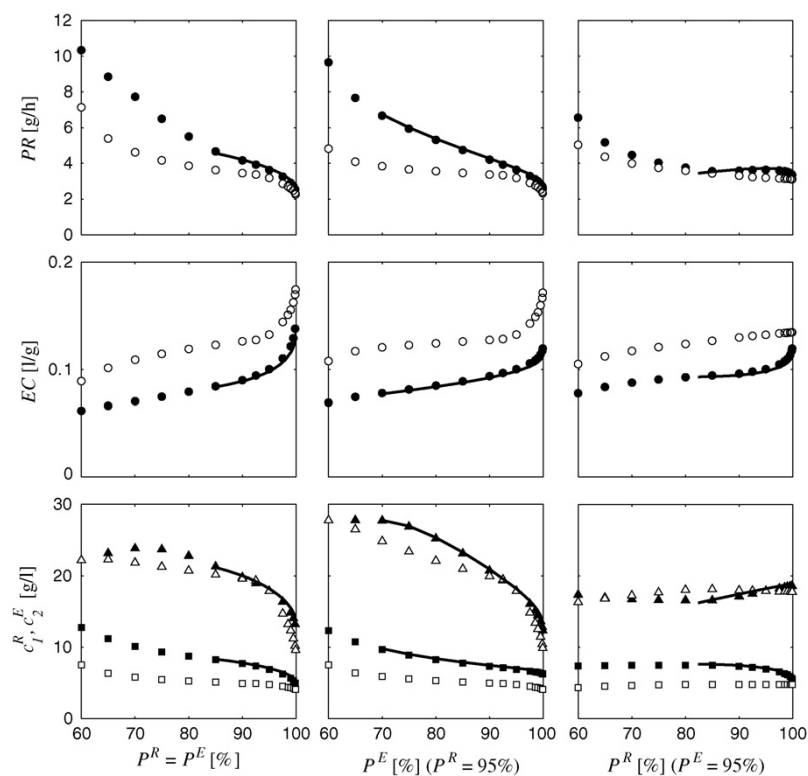
Fig. 6. Optimisation results for a restrictive (open symbols) and a non-restrictive design scenario (filled symbols), respectively. Left column – identical raffinate and extract purity; middle column – constant raffinate purity of 95%, variable extract purity; right column: variable raffinate purity, constant extract purity of 95%. Performance parameters as function of outlet purity: top row – productivity; middle row – eluent consumption; bottom row – outlet concentrations of target components at raffinate (triangles) and extract (squares), respectively. Lines – design prediction on the basis of equilibrium theory (see Section 5).
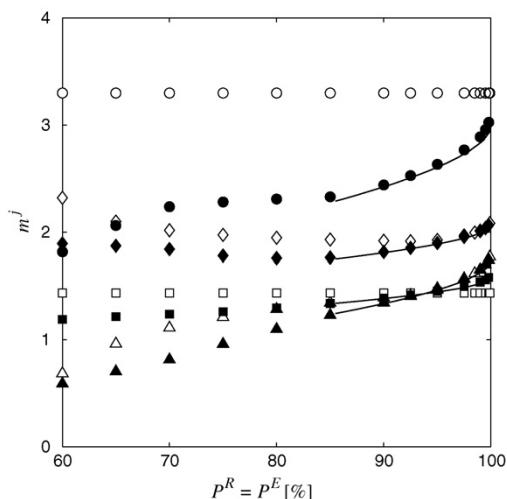
Fig. 7. Resulting m^j-values for the identical raffinate and extract purity (cf. Fig. 6, left). Open symbols – optimisation results for restrictive design ($\beta^I = \beta^{IV} = 1.1$). Filled symbols – optimisation results for non-restrictive design. Lines – design based on equilibrium theory. Circles – m^I, triangles – m^{II}, diamonds – m^{III}, squares – m^{IV}. Lines – prediction from equilibrium theory (see Section 5).

lead to very different optimal flow rates. More important, the two design scenarios lead to very different values for m^{II} and m^{III}. Surprisingly, in case of the non-restrictive design, the operating points move towards lower m^{III}-values, which would decrease the feed flow rates. However, at the same time the optimal m^{II}-values decrease more strongly than m^{III}. Therefore, overall the difference ($m^{III} - m^{II}$) and, thus, the feed flow rate, increases. Simultaneously, m^I (which is basically inversely proportional to the throughput) decreases significantly, while m^{IV} remains more or less constant. Summarising, the better performance of the non-restrictive design is caused by the changes of all m-values. It should be mentioned, that similar results for optimal m^j-values for reduced product purity have been reported in [20] and [21]. However, the scope of these works was somewhat different; thus, no comparison to a restrictive design or detailed discussion of the results was given.

The above results clearly emphasise that for the design of SMB processes under reduced purity requirements, all zone flow rates should be subject to optimisation. As already indicated by the solid lines in Figs. 6 and 7, equilibrium theory can be applied to predict the optimal operating conditions as a function of desired outlet purity. A corresponding simple design method is presented in Section 5.

4.3. Robustness of optimal operating points

An important issue for SMB separations is process robustness, i.e., the sensitivity of the process against disturbances. Basically any optimal operation point is sensitive and a slight deviation (e.g., of the flow rates) can lead to a decrease of product purity.

In the case of complete separation this problem can be addressed by adjusting each zone flow rate using a correction factor as defined in Eqs. (6). The m-values for zones I and II have to be increased, while those in zones III and IV have to be decreased. This ensures constant purity, but is at the expense of deteriorating all other performance parameters.

The case of reduced purity is more complex. Therefore, the effect of disturbances of the individual m^j-values on purity was quantified using by a sensitivity analysis. Steady state sensitivities of the raffinate and extract purity with respect to the flow rate ratios were calculated. For this purpose, the average deviations of P^R and P^E were calculated that result from a variation of each m-value. The corresponding normalised sensitivities are approximated numerically by

$$S_{P^k}^{m^j} = \frac{m_0^j}{P^k}\frac{\partial P^k}{\partial m^j} \approx \frac{m_0^j}{P^k}\frac{P_+^k - P_-^k}{m_+^j - m_-^j} \quad j = (I\ldots IV) \quad k = (E, R) \tag{11}$$

The index 0 represents an operating point obtained from the optimisations above. Terms with "+" and "−" denote values that result when deviating from the m^j-value by $+0.5\%$ and by -0.5%, respectively.

The results for the symmetrical separation (i.e., $P^E = P^R$) are shown in Fig. 8. The upper row refers to the restrictive design ($\beta^I = \beta^{IV} = 1.1$) and the lower row to the non-restricitive design.

In the restrictive design, the raffinate purity is easily disturbed while the extract purity appears more robust. This can be explained by the migration behaviour of the shock fronts within zones III and IV. For purities below approximately 93%, a strong increase of the sensitivity of the extract purity with respect to m^{IV} and m^{III} is observed. This due to the increasing concentration of the shock front in zone IV (and its correspondingly increasing migration velocity) with reducing the purity requirements. Eventually, a breakthrough of this shock into zone I occurs, causing a discontinuous increase of the sensitivity. Obviously, a correction factor β^{IV} higher than 1.1 would be necessary to prevent this.

In the non-restrictive design, the maximum sensitivities are lower than in the cases above. Furthermore, they are rather similar for most of the flow rates. m^{III} has the strongest impact on P^R, while m^{IV} influences mostly P^E. An encouraging aspect is that the sensitivities against m^I are low for both outlets.

In summary, an insensitive operation of SMB processes can be guaranteed only for complete separation with correction factors applied to all zones. This cannot be achieved for reduced purity. In a restrictive design, the use of inappropriate correction factors for the regeneration zones can lead to very sensitive operation. An encouraging finding is that the robustness of the non-restrictive design appears to be acceptable; in particular when considering the low sensitivities against the important flow rate in zone I.
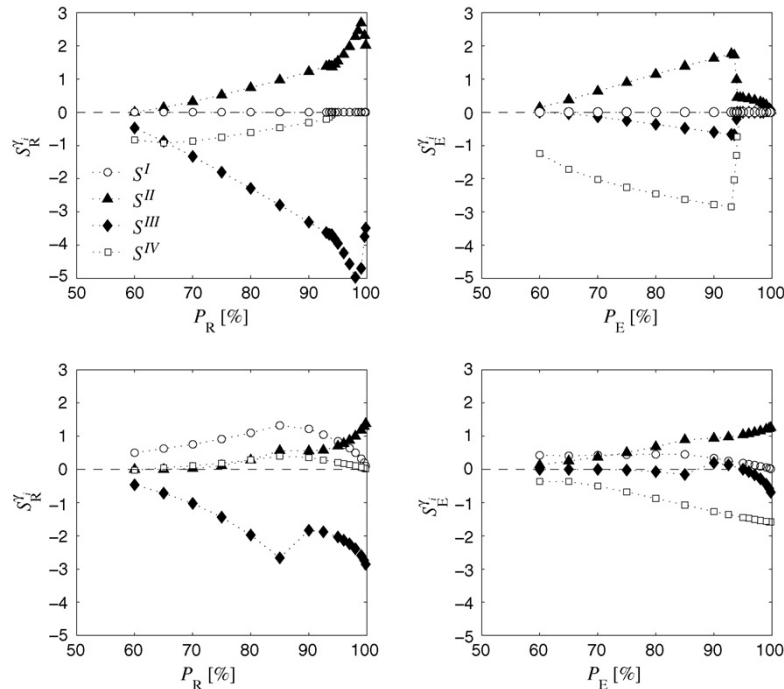

Fig. 8. Steady state sensitivities of raffinate and extract purity with respect to the four m^j-values (symmetrical separation with $P^E = P^R$; see Fig. 6, left). Comparison of optimised restrictive designs (top row) and non-restrictive designs (bottom row).
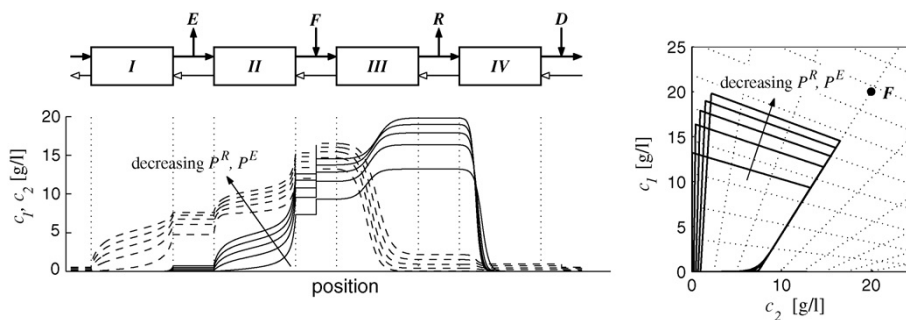
Fig. 9. Selected optimisation results for different values of the purity (non-restrictive design). Data for $P^R = P^E = 90, 92.5, 95, 97.5$, and 99.8%. Solid lines – less adsorbing component 1, dashed lines – strong adsorbing component 2. Left – concentration profiles vs. position, right – profiles in the hodograph space (c_1 vs. c_2). The path grid in the hodograph space (dotted lines) can be calculated *a priori* from the adsorption isotherms.

5. Development of a design method from equilibrium theory

Below a simple design method for SMB processes under reduced purity requirements will be derived using equilibrium theory. The problem to be solved is the following: given two values for the desired purity of the raffinate, P^R, and the extract, P^E, the four m^j-values should be found that correspond to a non-restrictive design as presented in Section 4.

Focus is on a demonstrative derivation of the method. Fundamental relations and the complete set of design equations are given in Appendixes A and B, respectively.

5.1. Derivation of design equations

At first, a closer look should be given to the results of the non-restrictive optimisations above. Fig. 9 (left) contains selected internal concentration profiles from these optimisations. The most important observation in all cases is a partial breakthrough of the dispersive wave of the stronger adsorbing component 2 (dashed lines) from zone *I* into zone *IV*. This effect determines the purity of the raffinate and, accordingly, becomes more pronounced the lower the required raffinate purity is. In contrast, the

shock fronts in zone *IV* are stationary there. The extract purity is therefore determined only by the dispersive waves of the two components that span over zone *I* and zone *II*. These findings are in accordance with the conclusions from the parametric study in Section 3.

Fig. 9 (right) shows the same concentration profiles in the hodograph space. This representation is an important tool in equilibrium theory. The diagram is constructed by plotting each value of c_1 against c_2 along each concentration–space profile. It can be seen that all concentration profiles have a very similar, distinct shape within this plot. The concentrations follow so-called characteristics. It is worth emphasising that these characteristics can be calculated explicitly and *a priori* from the adsorption isotherm parameters. For the Langmuir-type isotherms considered here, the characteristics are straight lines. Some fundamentals on this are given in Appendix A. An extensive theoretical treatment is given in [30,31].

If the four m^j-values are known, the equilibrium model, Eq. (3), can be solved to calculate the internal concentration profiles of a TMB process. This is demonstrated in Fig. 10 for two symmetrical separations with 100% purity (complete separation according to triangle theory, [10]) and 90% outlet purity (design method presented here), respectively. The profiles con-
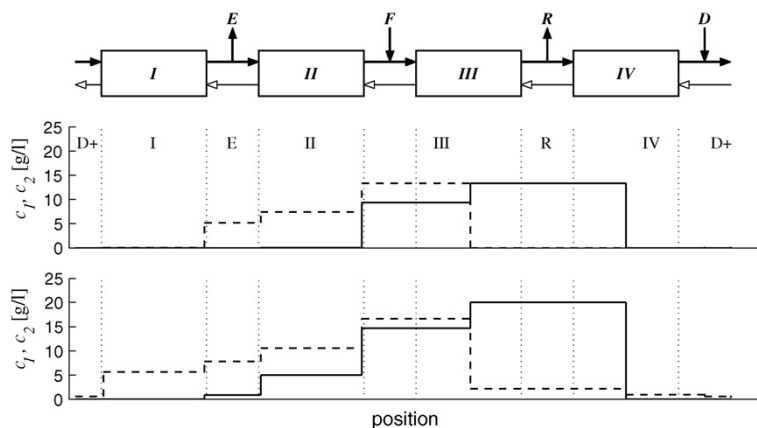

Fig. 10. Internal concentration profiles for complete separation (i.e., $P^E = P^R = 100\%$, top) and reduced purity (i.e., $P^E = P^R = 90\%$, bottom) resulting from equilibrium theory. m^j-values for 100% purity according to triangle theory [10], for 90% according to the design method described in this paper.
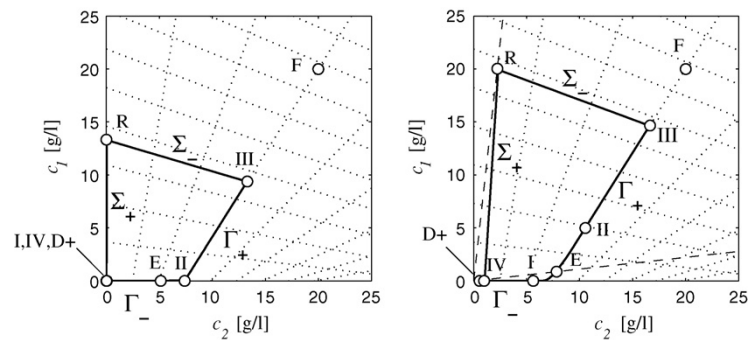
Fig. 11. Hodograph representations of the profiles in Fig. 10. Symbols – plateau concentrations as given in Fig. 10. Left – 100% purity (i.e., complete separation according to triangle theory). Right – 90% purity of extract and raffinate. Thick lines – numerical result obtained from the equilibrium cell model (see Fig. 7 for m^j-values). Dashed lines in the right are given by purity requirements.

sist of constant concentration plateaus which are connected by discontinuities. Fig. 11 shows these plateau concentrations as symbols in the hodograph space. The thick lines were calculated numerically using the equilibrium cell model. Obviously, both models are in very close agreement.

Comparing the hodographs in Fig. 11, one observes that for incomplete separation the two products are no longer situated on the two axes. Furthermore, also the state *II*, which for 100% is situated on the intersection of the "feed-characteristic" and the c_2-axis, is now moved along this characteristic in direction of the feed. Importantly, in both cases the state *III* lies on the intersection of two characteristics through *R* and *F*, respectively. From this follows that the states left and right of the feed are identical. In case of complete separation, a corresponding proof was given in [15]. Furthermore, this indicates that both scenarios lead to a maximum value of m^{III}.

The design task is now to calculate m^j-values (and all internal concentrations) that correspond to some given product purity and that simultaneously render the characteristic shape of the concentration profiles shown in Figs. 10 and 11(right). This problem can be solved by combining some fundamental relations from equilibrium theory and the phenomenological observations given above. In particular the following information are necessary:

(1) Relations for the wave velocity in each zone as a function of the corresponding concentrations. These expressions are known from equilibrium theory (see, for example, [30]).
(2) The characteristics in the hodograph space (also given by equilibrium theory).
(3) Mass balances for the two components between the plateaus (see Fig. 10).
(4) Observations derived from the optimisations as well as from Figs. 10 and 11. In particular:
(a) the concentration of component 1 in zones *I* and *IV* is zero,
(b) the raffinate *R* is situated on the intersection of a line given by the purity and the Σ_+-characteristic through state *IV*,
(c) the concentrations left and right of the feed are identical (state *III*); this state lies on the intersection of the Σ_--

characteristic through *R* and the Γ_+-characteristic through the feed *F*,
(d) the state in zone *II* is located on the Γ_+-characteristic through *F*,
(e) the extract is not situated on a characteristic but represents a so-called boundary discontinuity for zones *I* and *II*. This discontinuity lies on the corresponding line given by the extract purity.

The information above can be formulated as a system of nonlinear equations. Besides some auxiliary expressions, there are basically 16 equations for 16 unknowns (the four m^j-values and two concentrations for each of the plateaus *I, E, II, III, R* and *IV*; the state *D+* does not have to be considered). The equations can be re-arranged such, that only 3 implicit expressions remain. These can be solved by simple numerical methods. A summary of fundamental relations is given in Appendix A; a suggestion for an implementation of the equations is given in Appendix B.

The above procedure is largely analogous to the derivation of the triangle theory for complete separation (see, for example, [15]). However, for complete separation m^{II} and m^{III} are independent of the *m*-values in the regeneration zones. This is due to the requirement of complete regeneration. In fact, this allows the derivation of *i)* the region of complete separation (dashed line in Fig. 7), and *ii)* explicit expressions for the optimum operating point (the vertex of the region, see circle in Fig. 7).

In contrast, for incomplete separations as investigated here, the corresponding equations are not independent. They are coupled by the breakthrough of component 2 into zone *IV*. Therefore, the values for m^{II} and m^{III} depend on m^I and m^{IV}, and *vice versa*. It should be emphasised that due to this interdependency it is not useful to define an m^{II}–m^{III}-separation region for reduced purity. In fact, numerical simulations indicate that these regions shrink into a single point when applying a non-restrictive optimisation. This point corresponds to optimum performance and is predicted by the design method.

In order to verify the developed design approach, it was applied to the model system studied above. Figs. 6 and 7 contain a comparison between the equilibrium-design method (solid

lines) and the non-restrictive optimisation results (filled symbols). Obviously, the two methods predict the same operating parameters. The deviations between the two approaches is very small. This indicates the correct interpretation of the optimisation results in the frame of equilibrium theory.

5.2. Current limitations

The equilibrium-design method is currently limited with respect to some lower boundaries on the adjustable purity of the two outlets (i.e., P_{min}^R and P_{min}^E). As will be explained below, this limitation is related to the required shape of the concentration profiles.

The value for the minimum raffinate purity, P_{min}^R, depends on the actual value of P^E. Analogously, P_{min}^E is a function of P^R. It can be shown that for $P^R = P_{min}^R$ the concentration c_2 in zone *I* reaches a maximum. This value is determined by the intersection of the Γ_+-characteristic through *F* and the c_2-axis in Fig. 11. This leads to a maximum amount of stronger adsorbing solute 2 being transported from zone *I* into zone *IV*. Accordingly, this situation corresponds to $P^R = P_{min}^R$.

On the other hand, for $P^E = P_{min}^E$ the concentrations in zone *II* approach the feed composition (i.e., $c_i^{II} = c_i^{III} = c_i^F$). Due to the nature of the non-linear waves within the process, these are the highest concentrations that can be adjusted in this zone. Since the extract purity is controlled by the amount of weaker adsorbing solute 1 being transported leftwards through zone *II*, this minimises the extract purity.

Both values can be determined directly by a simple modification of the design equations in Appendix B. In this case, the expressions for c_2^I (for P_{min}^R) and/or c_i^{II} (for P_{min}^E) have to be replaced by the criteria given above. For the model system investigated here, it was found that $P_{min}^R = 86.91\%$ (achievable for $P^E = 100\%$), while $P_{min}^E = 67.46\%$ can be obtained if $P^R = P_{min}^R$.

6. Conclusions

In this work the design of SMB processes under reduced purity requirements was investigated. In general, reducing the purity requirements below 100% allows for significant improvement of performance parameters like higher productivity, lower eluent consumption, and higher product concentrations.

It was demonstrated that all four internal flow rates should be considered as free parameters in process design. A parametric study indicated that besides the two separation zones, in particular the flow rate in zone *I* provides for an optimisation potential. This was confirmed in a systematic optimisation study. Two design scenarios were compared. In the restrictive scenario, complete regeneration of liquid and solid phases was required in the corresponding zones. In contrast, in the non-restrictive design, all four zone flow rates were optimised. It was found that the latter allows for a significant further improvement of process performance.

Process robustness was investigated on the basis of a sensitivity analysis. The results confirm that – in contrast to safely operated complete separations – the process remains sensitive

towards disturbances. However, the magnitude of this effect appears to be within an acceptable range.

Finally, several phenomenological observations were used to derive a simple design method from equilibrium theory. The procedure requires the solution of a system of non-linear equations. Application of the approach provided an accurate reproduction of the non-restrictive optimisation results. The equilibrium-design method allows the direct prediction of optimal flow rates necessary to adjust desired purity values. Separation regions as defined by the well-known triangle theory for complete separation cannot be established, since the design parameters are not independent of each other.

Current work focuses on the limitation of the design method with respect to lower purity boundaries. Furthermore, since the presented design method is generally valid, its extension to other adsorption isotherm models will be investigated.

Acknowledgements

Appendix A. Fundamental relations

An extensive mathematical theory is available for the type of problem as given by the equilibrium model, Eq. (3). For details, the reader is kindly referred to, for example, [30,31]. For the purpose of this paper, it will be sufficient to know a few fundamentals.

The following explanations hold for two-solute systems ($n_s = 2$) with Langmuir-type adsorption isotherms according to Eq. (5). The design problem to be solved is to establish the characteristic concentration profiles as shown in Figs. 10 and 11. For this purpose, the *m*-value in each zone has to be adjusted such, that the velocity of the plateau concentrations or shock within that zone becomes zero.

For the velocity of a concentration value c_i holds in a dispersive wave (as found in zones *I* and *II*)

$$u_{c_i} = \frac{v u_S (dq_i/dc_i)|_{\bar{c}} - u_L}{1 + v(dq_i/dc_i)|_{\bar{c}}} \tag{A.1}$$

u_L and u_S denote the interstitial velocities of the liquid and the solid phase, respectively; $(\bar{c})$ stands for the mixture composition. In contrast, the velocity of a shock is given by

$$u_{c_i} = \frac{v u_s (\Delta q_i/\Delta c_i)|_{\bar{c}} - u_L}{1 + v(\Delta q_i/\Delta c_i)|_{\bar{c}}} \tag{A.2}$$

where Δq_i and Δc_i denote the differences of the solid and liquid phase concentrations across the shock. Now we require that the velocities given by Eqs. (A.1) and (A.2) are zero. Some rearrangement gives

$$m = \frac{dq_i}{dc_i}|_{\bar{c}} \tag{A.3}$$

for a dispersive wave, while for a shock front

$$m = \frac{\Delta q_i}{\Delta c_i}\big|_{\bar{c}} \tag{A.4}$$

The total derivative in Eq. (A.3) is obtained from the eigenvalues of the Jacobian matrix of the adsorption isotherms, Eq. (5). These eigenvalues are given by

$$\lambda_{1/2} = \frac{1}{2}[q_{11} + q_{22} \pm \sqrt{(q_{11} + q_{22})^2 + 4(q_{12}q_{21} - q_{11}q_{22})}] \tag{A.5}$$

where $q_{ij} = \partial q_i / \partial c_j$ denote the partial derivatives of the adsorption isotherms. Following the ideas given, for example, in [11,15], and [30], in zone I the smaller eigenvalue has to be used, while in zone II the larger value applies.

From the above we obtain for the m^j-values in the four zones:

$$m^I = \lambda_1(c_i{}^I) \tag{A.6a}$$

$$m^{II} = \lambda_2(c_i{}^{II}) \tag{A.6b}$$

$$m^{III} = \frac{q_i^{III} - q_i^{R}}{c_i^{III} - c_i^{R}} \tag{A.6c}$$

$$m^{IV} = \frac{q_i^{R} - q_i^{IV}}{c_i^{R} - c_i^{IV}} \tag{A.6d}$$

Another important information is the slope of the characteristics in the hodograph space (dotted lines in Fig. 11). It should be noted that these characteristics are time-invariant and do not depend on the operating conditions. Hence, they are identical for batch and TMB processes. Furthermore, they are straight lines for Langmuir systems and coincide for shocks and dispersive waves.

The slopes of the two characteristics that pass through a point in the hodograph plane is given by

$$\xi_{+/-} = \frac{q_{11} - q_{22}}{2q_{21}} \pm \sqrt{\frac{(q_{22} - q_{11})^2}{4q_{21}^2} + \frac{q_{12}}{q_{21}}} \tag{A.7}$$

As an example, the Γ_+-characteristic through the feed is given by

$$c_1(c_2) = c_1^{F} + \xi_+^{F}(c_2 - c_2^{F}) \tag{A.8}$$

where ξ_+^{F} is evaluated from Eq. (A.7) with $c_i = c_i^{F}$.

Besides the m-values and the characteristics, mass balances between the plateaus are required. Only the following balances are necessary for the set of design equations:

$$0 = m^I c_i{}^I - (m^I - m^{II})c_i^{E} - m^{II}c_i{}^{II} + q_i(\bar{c})^{II} - q_i(\bar{c})^{I} \tag{A.9a}$$

$$0 = m^{III}c_i{}^{III} - (m^{III} - m^{IV})c_i^{R} - m^{IV}c_i{}^{IV} + q_i(\bar{c})^{IV} - q_i(\bar{c})^{III} \tag{A.9b}$$

$$0 = m^{IV}c_i{}^{IV} - m^I c_i{}^I + q_i^{I} - q_i^{IV} \tag{A.9c}$$

$$0 = (m^{III} - m^{II})c_i^{F} - (m^{III} - m^{II})c_i^{R} - (m^I - m^{II})c_i^{E} \tag{A.9d}$$

In addition to the above, the observations listed under point 4) in Section 5.1 deliver some algebraic expressions. In particular, intersections of characteristics and purity lines were mentioned. The latter are given by Eq. (2a) as

$$c_1 = c_2 \frac{P^{E}}{1 - P^{E}} \tag{A.10a}$$

$$c_1 = c_2 \frac{1 - P^{R}}{P^{R}} \tag{A.10b}$$

The expressions resulting from the list will not be given in detail here. They can be derived by simple algebraic operations and are included in the re-arranged set of equations given in Appendix B.

The above equations result in a system of non-linear equations. It was found that the numerical solution can be complicated. However, the equations can be re-arranged such that only three implicit expressions remain. The system is then much easier to be solved. An according problem formulation is suggested in Appendix B.

Appendix B. Simple implementation of design equations

Below a viable implementation of the design equations is given. The three unknowns to be determined numerically are c_2^{I}, c_2^{II}, and c_2^{IV} (i.e., the concentrations of the strong adsorbing component in zones *I, II, IV*). The following equations should be used in the given order. The origin of each equation is reported with respect to the list given in Section 5.1.

Point 4a – zones *I* and *IV*:

$$c_1^{I} = 0 \tag{B.1}$$

$$c_1^{IV} = 0 \tag{B.2}$$

Point 4b – zone *IV* and raffinate *R*:

$$c_1^{R} = \frac{c_1^{IV} - \xi_+^{IV}c_2^{IV}}{1 - \xi_+^{IV}(1 - P^{R})/P^{R}} \tag{B.3}$$

$$c_2^{R} = \frac{1 - P^{R}}{P^{R}}c_1^{R} \tag{B.4}$$

Point 1 – wave velocity in zone *IV* (from Eq. (6d)):

$$m^{IV} = \frac{q_2^{R} - q_2^{IV}}{c_2^{R} - c_2^{IV}} \tag{B.5}$$

Point 4c – characteristics through *F* and *R* for state *III*:

$$c_2^{III} = \frac{c_1^{R} - c_1^{F} + \xi_+^{F}c_2^{F} - \xi_-^{R}c_2^{R}}{\xi_+^{F} - \xi_-^{R}} \tag{B.6}$$

$$c_1^{III} = c_1^{R} + \xi_-^{R}(c_2^{III} - c_2^{R}) \tag{B.7}$$

Point 1 – wave velocity in zone *III* (from Eq. (6c)):

$$m^{III} = \frac{q_1^{III} - q_1^{R}}{c_1^{III} - c_1^{R}} \tag{B.8}$$

Point 4d – zone *II* on characteristic:

$$c_1^{II} = c_1^{F} + \xi_+^{F}(c_2^{II} - c_2^{F}) \tag{B.9}$$

Point 1 – wave velocity in zone *II* and zone *I* (from Eq. (6b)):

$$m^{II} = \lambda_2(c_i^{II}) \tag{B.10}$$

$$m^{I} = \lambda_1(c_1^{I}, c_2^{I}) \tag{B.11}$$

Point 4e – extract. Follows from global mass balance, Eq. (A.9), and lies on purity line, Eq. (A.10):

$$c_1^{E} = c_2^{E} \frac{1 - P^{E}}{P^{E}} \tag{B.12}$$

$$c_2^{E} = \frac{(m^{III} - m^{II})c_2^{F} - (m^{III} - m^{IV})c_2^{R}}{m^{I} - m^{II}} \tag{B.13}$$

All solid phase concentrations q_i^{j} used above are in equilibrium values. The eigenvalues λ_1, λ_2 follow from Eq. (A.5), while the $\xi_\pm^{j}$ have to be calculated from Eq. (A.7).

Finally, plateau-to-plateau mass balances are required between zones *I* and *II* and between zones *IV* and *I*, respectively:

$$0 = m^{I}c_1^{I} - q_1^{I} - (m^{I} - m^{II})c_1^{E} - m^{II}c_1^{II} + q_1^{II} \tag{B.14a}$$

$$0 = m^{I}c_2^{I} - q_2^{I} - (m^{I} - m^{II})c_2^{E} - m^{II}c_2^{II} + q_2^{II} \tag{B.14b}$$

$$0 = m^{IV}c_2^{IV} - q_2^{IV} - m^{I}c_2^{I} + q_2^{I} \tag{B.14c}$$

The three Eq. (B.14) remain implicit and have to be solved numerically in order to determine the three unknowns (c_2^{I}, c_2^{II}, and c_2^{IV}).

References

[1] J. Blehaut, R.-M. Nicoud, Analusis Mag. 26 (1998) 60.
[2] M. Kaspereit, P. Jandera, M. Skavrada, A. Seidel-Morgenstern, J. Chromatogr. A 944 (2002) 249.
[3] K. Gedicke, W. Beckmann, A. Brandt, D. Sapoundjiev, H. Lorenz, U. Budde, A. Seidel-Morgenstern, Adsorption 11 (2005) 591.
[4] M. Kaspereit, K. Gedicke, V. Zahn, A.W. Mahoney, A. Seidel-Morgenstern, J. Chromatogr. A 1092 (2005) 43.
[5] M. Kaspereit, Separation of Enantiomers by a Process Combination of Chromatography and Crystallisation, Shaker, Aachen, 2006.
[6] M. Amanullah, M. Mazzotti, J. Chromatogr. A 1107 (2006) 36.
[7] Z. Ma, N.-H.L. Wang, AIChE J. 43 (1997) 2488.
[8] T. Mallmann, B.D. Burris, Z. Ma, N.-H.L. Wang, AIChE J. 44 (1998) 2628.
[9] G. Storti, R. Baciocchi, M. Mazzotti, M. Morbidelli, Ind. Eng. Chem. Res. 34 (1995) 288.
[10] M. Mazzotti, G. Storti, M. Morbidelli, J. Chromatogr. A 769 (1997) 3.
[11] G. Storti, M. Mazzotti, M. Morbidelli, S. Carrà, AIChE J. 39 (1993) 471.
[12] M. Mazzotti, G. Storti, M. Morbidelli, AIChE J. 40 (1994) 1825.
[13] M. Mazzotti, G. Storti, M. Morbidelli, AIChE J. 42 (1996) 2784.
[14] M. Mazzotti, G. Storti, M. Morbidelli, AIChE J. 43 (1997) 64.
[15] C. Migliorini, M. Mazzotti, M. Morbidelli, AIChE J. 46 (2000) 1384.
[16] M. Mazzotti, J. Chromatogr. A 1126 (2006) 311.
[17] T. Yun, G. Zhong, G. Guiochon, AIChE J. 43 (1997) 2970.
[18] L.S. Pais, J.M. Loureiro, A.E. Rodrigues, J. Chromatogr. A 827 (1998) 215.
[19] D.C.S. Azevedo, L.S. Pais, A.E. Rodrigues, J. Chromatogr. A 865 (1999) 187.
[20] Z. Zhang, M. Mazzotti, M. Morbidelli, Korean J. Chem. Eng. 21 (2004) 454.
[21] Y. Kawajiri, L.T. Biegler, J. Chromatogr. A 1133 (2006) 226.
[22] M. Minceva, A.E. Rodrigues, Comp. Chem. Eng. 29 (2005) 2215.
[23] H. Schramm, S. Grüner, A. Kienle, J. Chromatogr. A 1006 (2003) 3.
[24] D.C.S. Azevedo, A.E. Rodrigues, AIChE J. 45 (1999) 956.
[25] V. Silva, M. Minceva, A.E. Rodrigues, Ind. Eng. Chem. Res. 43 (2004) 4494.
[26] A.E. Rodrigues, L.S. Pais, Sep. Sci. Technol. 39 (2004) 245.
[27] G. Ganetsos, P.E. Barker (Eds.), Preparative and Production Scale Chromatography, Marcel Dekker, New York, 1993.
[28] D.M. Ruthven, Principles of Adsorption and Adsorption Processes, John Wiley, New York, 1984.
[29] G. Guiochon, D.G. Shirazi, A. Felinger, A.M. Katti, Fundamentals of Preparative and Nonlinear Chromatography, second ed., Academic Press, Boston, 2006.
[30] H.-K. Rhee, R. Aris, N. R. Amundson, First-order partial differential equations, Theory and Applications of Hyperbolic Systems of Quasilinear Equations, vol. II, Prentice-Hall, Englewood Cliffs, NJ, 1989.
[31] H.-K. Rhee, R. Aris, N. R. Amundson, First-order partial differential equations, Theory and Applications of Single Equations, vol. I, Prentice-Hall, Englewood Cliffs, NJ, 1986.
[32] M. Mangold, A. Kienle, E.D. Gilles, K.D. Mohl, Chem. Eng. Sci. 55 (2000) 441.
[33] G. Biressi, O. Ludemann-Hombourger, M. Mazzotti, R.M. Nicoud, M. Morbidelli, J. Chromatogr. A 876 (2000) 3.
[34] R.-M. Nicoud, in: G. Subramanian (Ed.), Bioseparation and Bioprocessing, vol. 1, Wiley-VCH, Weinheim, 1998.

Optimization and Analysis of Possible Column Arrangements for Multicomponent Separations by Preparative Chromatography

Javier García Palacios,[†] Malte Kaspereit,[†] Grzegorz Ziomek,[†] Dorota Antos,[‡] and Andreas Seidel-Morgenstern*[,†,§]

Max-Planck-Institut für Dynamik komplexer technischer Systeme, D-39106 Magdeburg, Germany, Department of Chemical Engineering, Rzeszów University of Technology, 35-959 Rzeszów, Poland, and Institut für Verfahrenstechnik, Otto-von-Guericke Universität Magdeburg, D-39106 Magdeburg, Germany

The optimal arrangement of eight identical chromatographic columns for the isolation of the intermediate adsorbing component of a ternary mixture is investigated theoretically. The arrangements considered are batch chromatography with columns connected in series and/or in parallel, cascades of two standard simulated moving bed (SMB) processes, and combinations of standard SMB units and batch columns. Based on standard column models, the productivity of each configuration was maximized by optimizing the relevant operating parameters using a modified simplex algorithm. The methodology applied allows us to evaluate all possible batch column arrangements on the basis of only eight different optimization runs. The results obtained reveal a significant dependency of the optimal process configuration on relevant aspects such as product purity, feed composition, and particle size of the adsorbent.

1. Introduction

Preparative chromatography is an important separation and purification technique within the pharmaceutical, biochemical, fine chemical, and food industries. The increasing interest in this technology continuously promotes the development of advanced operating modes and creates new challenges with respect to process understanding and optimization.

On an industrial scale, chromatographic separations are performed either discontinuously using batch columns, or continuously by the simulated moving bed (SMB) process (see, e.g., refs 1−3). Batch chromatography is a well-established and versatile operation capable of multicomponent separations. However, usually it is characterized by a strong trade-off between various performance parameters, for example, productivity and yield.[4] To improve the yield in batch processes, recycling techniques can be applied.[5−8] On the other hand, SMB chromatography often exhibits superior performance, but it is (in its standard configuration) limited to binary separation problems. Nowadays, the conventional SMB process is well understood and useful design methods are available for different requirements (see, e.g., refs 9−13).

It is emphasized that the availability of several identical columns represents a common situation for companies that regularly apply preparative chromatography, in particular for those who have to process varying feedstocks. Since many SMB systems are operated with two columns in each of the four zones, frequently exactly eight identical columns are available. An obvious question in this case is how to arrange these columns in an optimal way for a given separation problem.[14] Self-evident options are to arrange several batch columns in series or in parallel, or to apply them in an SMB setup. A previous study[15] addressed this issue for a binary separation using five identical chromatographic columns. In this work, the approach will be extended to a more complex situation, where a ternary mixture should be separated using eight columns. In addition to parallel and series arrangements, also more sophisticated schemes will also be investigated, for example, combinations of batch and SMB systems. In order to reflect typical practical challenges, the component with intermediate adsorptivity is the desired target product. It is expected that some results obtained from such a study might be extrapolated to mixtures with more than three components, from which an intermediate component should be isolated.

It should be noted that, besides the classical four-zone SMB units to be considered here, several SMB-based systems have been suggested for the separation of ternary mixtures. Examples are nine-zone SMB units and side stream SMBs,[16−21] or partially countercurrent modes[22,23] that can also incorporate modifier gradients.[24] However, these sophisticated schemes are subjects of current academic research; their evaluation is beyond the scope of this work.

The aim of this paper is to provide a detailed study of different continuous and discontinuous column arrangements that apply *eight* identical columns to produce the intermediately adsorbing component of a ternary mixture. Using a set of eight columns, several interesting schemes for ternary separations can be realized, which are of very different natures. This includes the straightforward option of a cascade of two standard SMB processes with four zones each.

The approach followed is to optimize—for a given set of adsorption isotherms—the productivity of the different schemes using standard column models. In a first step, optimization runs are performed for all possible parallel and series combinations of eight batch columns. Structural analogies between the different schemes are exploited in order to reduce computational efforts. The roles of important aspects are investigated, such as those of the feed concentration, the particle size of the packing material, the objective function, and the purity requirements. Subsequently, combinations of two standard SMB units are studied. Finally, the most promising connections between SMB units and batch arrangements are considered. A comparison of the results demonstrates that the optimal arrangement depends strongly on the above-mentioned parameters and constraints.

* To whom correspondence should be addressed. E-mail: anseidel@vst.uni-magdeburg.de.
† Max-Planck-Institut.
‡ Rzeszów University.
§ Otto-von-Guericke Universität.
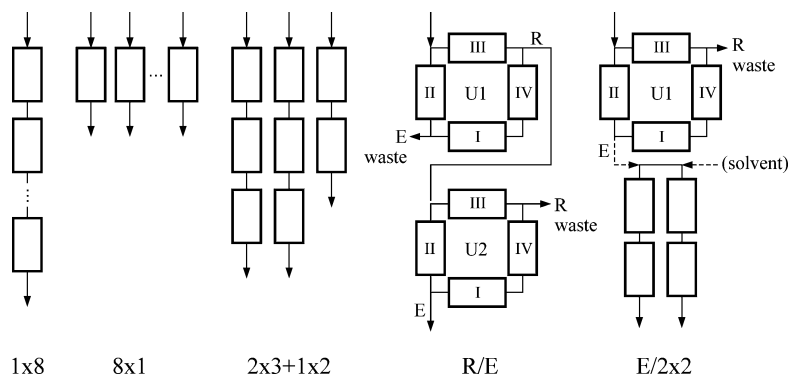
Figure 1. Selected arrangements of eight identical chromatographic columns. From left to right: series, parallel, and series/parallel connections of batch columns; combination of two SMB processes, and combination of an SMB unit with batch columns. See main text for more details.

2. Theory

2.1. Possible Column Arrangements. Figure 1 shows typical examples for the different possibilities that exist to arrange eight identical columns. The schemes shown reflect the general structural options: series, parallel, and series/parallel arrangements of batch columns, as well as combinations of two standard SMB units and of an SMB process followed by batch columns, respectively.

For the sake of brevity, we will use the following "$x \times y$" notation to describe a specific scheme. The factor x stands for the number of parallel trains that have y columns in series. The simplest schemes in Figure 1 are denoted by 1×8 (a train with eight columns in series) and 8×1 (eight single columns in parallel). More complicated are series−parallel systems, such as $2 \times 3 + 1 \times 2$, which indicates three parallel trains, two of which with 3 and one with 2 series columns. If SMB units are considered, the relevant product port ("E" for extract and "R" for raffinate, respectively) of each unit will be mentioned that delivers the desired intermediate component to the next SMB unit. Accordingly, the combination of two SMB units in Figure 1 is labeled as R/E. Finally, in the scheme E/2 × 2 the second unit has been replaced by a 2 × 2 arrangement of batch columns.

Note that we restrict ourselves here to classical SMB processes with a single column per zone. This is on one hand due to the large number of advanced SMB concepts (e.g., Varicol, Powerfeed, Modicon, PartialFeed, Partial Withdrawal, I-SMB, JO-SMB, etc.[3]). Combining these processes with additional batch columns leads to a multitude of process options, which could not be compared in a fair manner within this paper. On the other hand, the investigation of standard SMB units is interesting, since a cascade of two such units can be seen as the most straightforward SMB-based option to separate a ternary mixture.

The total number of possible column arrangements is rather large. For example, 22 configurations exist that involve only batch columns. It would be tedious to optimize each scheme individually. However, this combinatorial problem can be simplified to a certain extent. It will be shown in the next section that it is possible to evaluate all possible batch systems using only a few individual optimizations. Furthermore, as far as combinations of two standard SMB units are concerned that have four columns each, only two options (E/R and R/E) are capable of delivering the intermediate adsorbing solute. Finally, based on the obtained results, several promising SMB/batch combinations will be selected for detailed investigations.

2.2. Mathematical Model. Among the several possibilities to describe chromatographic processes, the equilibrium disper-

sive model is very often chosen since it gives a good approximation of wave propagation and dispersion effects and can be solved numerically efficient.[4] The model consists of the differential mass balances for the three components

$$\frac{\partial c_i^n}{\partial t} + \frac{1 - \varepsilon}{\varepsilon} \frac{\partial q_i^n(c_1, ..., c_N)}{\partial t} + u \frac{\partial c_i^n}{\partial x} = D_{ap} \frac{\partial^2 c_i^n}{\partial x^2} \quad (1)$$

where $i = 1, ..., 3$ and $n = 1, ..., N_{col}$ denote the ith component and the nth column; c_i and $q_i(c_1, ..., c_N)$ are the concentrations in the mobile phase and the solid phase, respectively. The total porosity is denoted by ε, u is the interstitial velocity, and D_{ap} is the apparent dispersion coefficient that accounts for mass transfer resistances and axial dispersion. N_{col} is the total number of columns (in this work, $N_{col} = 8$).

As initial conditions unloaded beds are assumed

$$c_i^n(x, t = 0) = 0; \qquad i = 1, ..., 3, \quad n = 1, ..., N_{col} \quad (2)$$

The boundary conditions must reflect the actual column configuration. For example, for k columns connected in series, a rectangular injection for the first column and a direct connection of the subsequent columns were assigned:

$$c_i^n(x = 0, t) = \begin{cases} c_{i,\text{inj}} & n = 1, \ 0 \leq t \leq t_{\text{inj}} \\ 0 & n = 1, \ t > t_{\text{inj}} \\ c_i^{n-1}\Big|_{x=L} & n = 1, ..., k \end{cases} \quad (3)$$
$$i = 1, ..., 3$$

where $c_{i,\text{inj}}$ denotes the injection concentrations. For SMB units, constant feed concentrations are assumed equal to the volume-averaged outlet concentrations of the preceding unit. An analogous assumption is used for the injection concentration of batch columns following an SMB unit. Note that the numerical solution methods used in this work do not require a second boundary condition.

In eq 1, thermodynamic equilibrium between concentrations in the two phases is assumed, which is described here using the classical competitive Langmuir adsorption isotherm model:

$$q_i = \frac{a_i c_i}{1 + \sum_{j=1}^{3} b_j c_j}, \quad i = 1, ..., 3 \quad (4)$$

The apparent dispersion coefficient in eq 1, D_{ap}, can be expressed for sufficiently efficient columns by the height equivalent of a theoretical plate, HETP:[4]

$$D_{ap} = \frac{u(\text{HETP})}{2} = \frac{uL}{2N} \tag{5}$$

where N is the stage number. Since the influence of the particle size of the packing material, d_p, is an important aspect of this work, HETP was modeled as a function of d_p. For the sake of simplicity HETP was taken as a linear function of the mobile phase velocity u. This is typically the case in preparative chromatography. Accordingly, the modified van Deemter equation reads as

$$\text{HETP} = Ad_p + Bd_p^2 u \tag{6}$$

where A and B are parameters. Furthermore, the pressure drop was determined from Darcy's equation

$$\Delta p = \eta \frac{uL'}{k_0 d_p^2} \tag{7}$$

with η as eluent viscosity and k_0 as the permeability of the packing.[4] Note that the effective length L' depends on the specific column arrangement.

To solve the model equations, we apply the so-called Rouchon algorithm.[25] In this method, the dispersion term in eq 1 is neglected. Instead, the time and space increments Δt and $\Delta x = L/N$ are chosen such that the resulting numerical error matches the physical dispersion quantified by eqs 5 and 6.

While the Rouchon algorithm could be applied to systems that include SMB units (the corresponding implementation is given in ref 26), for batch column systems the wide range of parameters covered in the optimization leads to stability problems. These could be overcome by using the classical Craig stage model,[27] which is more robust but computationally somewhat less efficient. It assumes that a transport of equilibrated mobile phase occurs at discrete time points. This can be expressed as[28]

$$c_{i,j}^{k+1} - c_{i,j-1}^k + \frac{1 - \varepsilon}{\varepsilon}(q_{i,j}^{k+1} - q_{i,j}^k) = 0 \tag{8}$$

$$i = 1, ..., 3, \quad k = 1, ..., n_t, \quad j = 1, ..., N_{\text{Craig}}$$

for component i and stage j. The superscript k denotes the exchange time points, which follow from the residence time per stage. In order for the two models to give identical results, a different stage number N_{Craig} must be used in the Craig model. The corresponding conversion rule is

$$\frac{N_{\text{Craig}}}{N} = \frac{F\bar{a}}{1 + F\bar{a}} \tag{9}$$

where $F = (1 - \varepsilon)/\varepsilon$ is the phase ratio and $\bar{a}$ is the average of the a_i parameters in eq 4.[4]

Both the Craig model and the equilibrium dispersive model are well-established in modeling preparative chromatographic processes.[4] When following the conversion rule eq 9, numerical solutions obtained from both models are basically identical and will not affect the trends reported in this work. In-depth discussions regarding their analogy and implementation are given in refs 4 and 29.

2.3. Optimization Problem. 2.3.1. General. A comparison of different column arrangements requires optimization of the operating conditions for each scheme. A suitable objective function is required for this. In specific applications this would be a detailed cost function that includes many factors that are in conflict or mutually related, such as productivity, solvent consumption, recovery, market prices, labor, and investment costs. Alternatively, different options exist to use one or more of the performance indicators as an objective function, while applying constraints on others. An example is to minimize specific solvent consumption for a given throughput, while requiring minimum values for the yield and product purity. However, in either case, such analysis will lead to rather specific results.

Since the focus of this work is on methodology, we use—as an example—the productivity as the main objective function; the only constraint is applied to the product purity. This allows for a certain generalization of the findings and an easier understanding of the approach. Besides this, such an optimization problem is typical for situations where limited amounts of a substance have to be provided in a short time (such as during the development of a new drug). However, it is emphasized that the approach presented here can be used with any other objective function and constraints.

The specific productivity, Pr, is often considered as the key parameter in preparative chromatography.[4,30,31] Pr is defined here as the mass flow rate of the intermediate target component of the complete column arrangement, $\dot{m}_{2,\text{tot}}$, divided by the volume of stationary phase contained in the N_{col} columns:

$$\text{Pr} = \frac{1}{N_{\text{col}}}\frac{\dot{m}_{2,\text{tot}}}{(1 - \varepsilon)V} \tag{10}$$

where V is the volume of a single column. For the given number of columns $N_{\text{col}} = 8$, the optimization problem in this work can be written as

$$\dot{m}_{2,\text{tot}} \rightarrow \max \tag{11}$$

s.t.

$$\text{Pu} \geq \text{Pu}_{\min}, \quad \Delta p \leq \Delta p_{\max}, \quad \dot{V} \leq \dot{V}_{\max}$$

The constraints in eq 11 account for practical conditions; i.e., upper limits are assumed for the pressure drop, eq 7, and for the pump flow rate(s) $\dot{V}$. Product quality is ensured by a lower limit for the product purity Pu at all product outlets, defined as

$$\text{Pu} = \frac{\dot{m}_{2,\text{out}}(k)}{\sum_{i=1}^{3} \dot{m}_{i,\text{out}}(k)} \tag{12}$$

where k denotes the corresponding product outlet. Note that, for selected interesting schemes, additionally the recovery yield, Y, was considered as part of the objective (see section 3.2.4). This parameter is particularly important for expensive products. The yield Y is defined as

$$Y = \frac{\dot{m}_{2,\text{tot}}\Delta t_c}{\sum_k V_{\text{inj}}(k)c_{2,\text{inj}}} \tag{13}$$

where the index k denotes all solute inlets and Δt_c denotes the cycle time (i.e., the time between two consecutive injections).

The key in the optimization runs is to determine the total product stream $\dot{m}_2^{\text{tot}}$. When inspecting the structures illustrated in Figure 1, it becomes clear that this is generally a combination of the different streams from parallel and/or series arrangements. While for a set of eight columns only a few different SMB arrangements could be realized, the number of possible batch column arrangements is much larger. Their evaluation requires a more detailed explanation.

In *series arrangements* of k batch columns (e.g., the 1×8 setup in Figure 1), the product is obtained at the outlet of the last (i.e., kth) column. For each of the possible $k = 1, ..., N_{col}$ series connections the product flux is given by

$$\mathbf{\dot{m}}_{2,out}(k) = \frac{\dot{V}\bar{c}_{2,out}(k)}{\Delta t_c} = \frac{\dot{V}}{\Delta t_c} \int_{t_S}^{t_E} c_{2,out}(k,t)\,dt \qquad (14)$$

where $\bar{c}_{2,out}(k)$ is the time-averaged outlet concentration of the kth column (i.e., the last in the column series; $k = 1$ for a single column). t_S and t_E are the start and end times of the fractionation interval (see next section for their determination).

In *parallel arrangements*, such as the schemes 8×1 or $2 \times 3 + 1 \times 2$ in Figure 1, the total product flux $\dot{m}_{2,tot}$ in eq 10 obviously corresponds to the sum of the different parallel product streams $\dot{m}_{2,out}(k)$ as determined from eq 14.

It is important to realize that the performance of *any possible arrangement* of columns possible can be evaluated if the optimization results for the different series systems with $k = 1, ..., N_{col}$ columns are known. In this case, the combined product stream of a column setup can be evaluated from

$$\dot{m}_{2,tot} = \mathbf{n} \cdot \dot{\mathbf{m}}_{2,out}^T = \sum_{k=1}^{N_{col}} \mathbf{n}(k)\,\dot{m}_{2,out}(k) \qquad (15)$$

with

$$N_{col} = \sum_{k=1}^{N_{col}} k\mathbf{n}(k)$$

In these expressions, $\dot{\mathbf{m}}_{2,out}$ is a vector that contains the optimization results for all series arrangements with $k = 1, ..., N_{col}$ columns. The vector $\mathbf{n}$ defines the structure of the complete scheme. It specifies how many systems are present with exactly k columns in series. For example, for the $2 \times 3 + 1 \times 2$ system in Figure 1, it holds $\mathbf{n} = [0\ 1\ 2\ 0\ 0\ 0\ 0\ 0]$. The last expression in eq 15 simply restricts the number of columns to the available quantity.

The total number of possible schemes with batch columns follows from the partition function $p(n)$. This tabulated function defines the number of options to write the integer n as a sum of integers.[32] The number increases significantly with increasing n: $p(2) = 2$, $p(5) = 7$, $p(10) = 42$, $p(20) = 627$, etc. For a total column number of $N_{col} = 8$ it holds $p(8) = 22$. Hence, there exist 22 different arrangements of batch columns (i.e., 22 different vectors $\mathbf{n}$).

It is emphasized that the mathematical representation introduced above allows for a straightforward treatment of all possible batch column arrangements. The performance of the 22 different structures can be evaluated by performing only eight optimizations for the possible series connections.

2.3.2. Specific Optimization Problems. Systems with Batch Columns. The optimized variables in batch systems are the flow rate, $\dot{V}$, the injection volume V_{inj}, and the cycle time, Δt_c, which corresponds to the time between two consecutive injections. Below more specific details are given. A summary of the optimization problem and the applied algorithm can be found in section 2.3.3.

The focus of this work is on process performance in *periodic steady state*. In order to maximize productivity (i.e., minimizing the cycle time, Δt_c), we allow for an overlap of the profiles resulting from consecutive injections. Due to interactions of neighboring profiles, generally a certain number of cycles will be required until a periodic steady state is reached. In the cases studied here, it was found that already after the elution of the
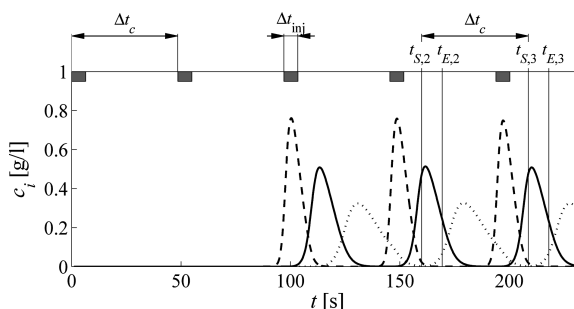
Figure 2. Evaluation of batch chromatography during optimizations. The elution profiles of the second and third injections were used to estimate the periodic performance. Bars denote injections. The example shows the optimization result for a single column with $d_p = 15\ \mu m$ and $Pu_{min} = 95\%$.

second profile no significant changes occur. Thus, in order to limit computational efforts, only the first three elution profiles were evaluated. However, for systems with stronger nonlinearity, it would be more accurate to determine the cyclic steady state by comparing the profiles of consecutive injections.

Figure 2 exemplifies this situation for one of the optimization results. Note that all elution profiles are influenced by their neighboring injections. In the example shown already five injections were performed when the third cycle has been eluted.

The fractionation interval for the kth cycle, ($t_{S,k}$ and $t_{E,k}$, $k = 2, 3$), which is required to calculate the mass flux in eq 11, is determined from the following straightforward procedure. The start times $t_{S,k}$ are fixed if the *current* purity at the outlet $\widetilde{Pu}(t_{S,k})$, starts to exceed the required product purity, Pu_{min}:

$$\widetilde{Pu}(t_{S,k}) = \frac{c_{2,out}(t_{S,k})}{\sum_{i=1}^{3} c_{i,out}(t_{S,k})} = Pu_{min}, \quad k = 2, 3 \qquad (16)$$

The end times, $t_{E,k}$, are found if the *integral* purity of the fraction collected so far, eq 12, just reaches Pu_{min}:

$$Pu(t_{E,k}) = \frac{\int_{t_{S,k}}^{t_{E,k}} c_{2,out}(t)}{\sum_{i=1}^{3} \int_{t_{S,k}}^{t_{E,k}} c_{i,out}(t)} = Pu_{min}, \quad k = 2, 3 \qquad (17)$$

As an additional, practically relevant constraint for batch systems, a lower bound for the product collection interval was applied:

$$\Delta t_{frac} = t_{E,k} - t_{S,k} \geq \Delta t_{min}, \quad k = 1, ..., 3 \qquad (18)$$

As already mentioned, upper limits were applied for the flow rates ($\dot{V}_{max}$) and the pressure drop (Δp_{max}). Note that, for n columns in series, Δp is determined from eq 7 using an effective length of $L' = nL$.

Systems with SMB Units. For the sake of simplicity, we only consider SMB processes with four columns (i.e., a single column per zone). The most commonly used design parameters of SMB processes, the dimensionless flow rate ratios, m_k, in the four zones k (see, e.g., ref 9), were optimized:

$$m_k = \frac{\dot{V}_k t^* - \varepsilon V}{(1 - \varepsilon)V}, \quad k = I, ..., IV \qquad (19)$$

Additionally, the flow rate $\dot{V}_I$ was optimized, which—for Langmuir adsorption isotherms—corresponds to the highest flow

Table 1. Summary of the Optimization Problem for the Different Arrangements

scheme		variables	remarks
batch (series)	3	Δt_c, V_{inj}, $\dot{V}$	$\Delta t_{frac} \geq \Delta t_{min}$ (three cycles evaluated)
SMB/SMB	9	m_I^{U1}, ..., m_{IV}^{U1}, m_I^{U2}, m_{II}^{U2}, m_{III}^{U2}, $\dot{V}_I^{U1}$, $\dot{V}_I^{U2}$	m_{III}^{U2} from coupling
SMB/batch	7	Δt_c, m_I, ..., m_{IV}, $\dot{V}_I$, $\dot{V}$	$V_{inj} = \Delta t_c \dot{V}_{out}^{U1}$, $\dot{V}_{out}^{U1} = (\dot{V}_E, \dot{V}_R)$, $\Delta t_{frac} \geq \Delta t_{min}$

rate in the unit. The switching time (times), t^*, follows (follow) from m_I and $\dot{V}_I$ when applying eq 19 to the SMB unit(s). Note that, for combinations of two SMB units, the flow rate in zone III of the second unit, m_{III}^{U2}, is fixed by the outlet stream of the preceding SMB. For example, for the system shown in the right of Figure 1, it holds $\dot{V}_{III}^{U2} = \dot{V}_{II}^{U2} + (\dot{V}_{III}^{U1} - \dot{V}_{IV}^{U1})$.

For SMB/batch schemes, additionally the flow rate of the batch arrangement and the cycle time Δt_c were optimized. Note that in this case the injection volume for the batch columns is fixed by the cycle time and the outlet flow rate of the SMB unit (see next section).

The limits $\dot{V}_{max}$ and Δp_{max} were also applied to SMB systems. The pressure drop was calculated for each zone of the SMB unit(s) using $L' = L$ in eq 7. The highest value obtained (occurring here most frequently in zone I) was compared to the constraint. Note that the pressure drop of a given SMB system will depend on the actual pump and zone configuration. Corresponding values could be obtained from the m-values as reported in the results below.

2.3.3. Summary of Optimization Problems. Table 1 gives an overview of the optimization problem and the number of variables for the three general types of column arrangements studied here.

All optimizations were carried out using a derivative-free simplex method based on the Nelder−Mead algorithm.[33] Since this algorithm cannot handle constraints, we apply penalty factors to suppress constraint violations as described in ref 15. In order to avoid being "trapped" in local optima, the method was combined with a stochastic optimization algorithm (a random search procedure) as described in ref 15.

3. Results and Discussion

3.1. Summary of Investigated Problem Parameters. The model parameters used correspond to a theoretical separation problem. They represent a typical situation and were chosen such that the values describing the component's properties and the column efficiency closely match the separation problem investigated in ref 15.

Table 2 contains all parameter values together with the variables and constraints that were used to generate the results of the following sections.

3.2. Batch Arrangements. Below, the influence of the feed concentration, the particle size of the packing material, and the purity requirement on the optimal arrangement of batch columns will be investigated with the requirement to maximize the overall productivity.

3.2.1. Role of Feed Concentration. Typically, the highest productivity in preparative chromatography is achieved at maximum feed concentration. However, other aspects also need to be considered, such as solubility constraints, nonlinearity of adsorption isotherms, process stability, and efforts for preconcentration and downstream processing. Therefore, the feed concentration should be regarded as an operational degree of freedom.

Here we apply equal injection concentrations for all three components and consider the three different levels given in Table 2. The purity requirement is chosen as $Pu_{min} = 95\%$.

Table 2. Summary of Parameters, Variables, and Constraints As Applied in the Optimization

Parameters			
Langmuir adsorption isotherms, eq 4	a_i		4.18, 5.45, 6.89
	b_i	[L/g]	0.1, 0.16, 0.21
separation factors	α		1.30, 1.26
van Deemter, eq 6, with $[u]$ = m/s, $[d_p]$ = m	A		4.167
	B	[s/m²]	2.5×10^4
pressure drop, eq 7	k_0		0.0012
	η	[mPa s]	0.904
column length	L	[cm]	15
column diameter	D	[cm]	1
Investigated Variables			
feed concentrations	$c_{i,inj}$	[g/L]	0.2, 0.5, 1.0 (each)
particle size	d_p	[μm]	5, 9, 12, 15, 20
purity requirements	Pu_{min}	[%]	95, 99
Constraints			
pressure drop, eq 7	Δp_{max}	[bar]	100
maximum pump flow rates	$\dot{V}_{max}$	[mL/min]	500
minimum fractionation interval, eq 18	Δt_{min}	[s]	10

Table 3 contains the optimization results for different series connections of batch columns for a feed concentration of $c_{i,inj}$ of 1.0 g/L. The following trends are readily observed. Due to the increased capacity of the system, the optimal injection volume V_{inj} increases steadily the more columns are connected in series. The optimal flow rate first increases and then reaches a maximum for three columns in series. Longer arrangements have a higher number of stages and achieve the same separation at a higher flow rate and higher productivity. However, once the pressure drop (cf. eq 7) hits the constraint boundary, the values of the optimal flow rate decrease with increasing length of the system. This is observed here for all arrangements with more than two columns in series (see Table 3). Finally, the cycle time Δt_c increases, mainly due to the increased injected volumes.

Figure 3 shows the optimized values for $\dot{m}_{2,out}$ obtained from eq 14 for the different feed concentrations. The figure demonstrates that the interplay of the above trends results in a clear maximum for the product mass flux, $\dot{m}_{2,out}$. For all values of $c_{i,inj}$, the most productive individual series arrangement is found to be three columns in series (3 × 1). The figure also confirms the expected increased product streams for increasing feed concentrations.

As already mentioned, the optimization results for the series setups allow for determining the total product flux $\dot{m}_{2,tot}$ for all possible arrangements. The latter is found by applying eq 15 to combine properly the different optimized product streams $\dot{m}_{2,out}$. As a simple example, the filled symbols in Figure 3 represent the product fluxes for all parallel arrangements that have only *single* columns in parallel (i.e., 2 × 1, 3 × 1, etc.). For N_{col} single columns this corresponds to using the N_{col}-fold of the throughput of a single column. This corresponds to using $\mathbf{n}(1) = N_{col}$ and $\mathbf{n}(i) = 0$ for $i > 1$ in eq 15.

The application of eq 15 for the 22 different values that exist for $\mathbf{n}$ with $N_{col} = 8$ corresponds to evaluating all valid combinations of the data shown in Figure 3. Table 4 shows the performance obtained in this way for selected series/parallel batch schemes. The most productive schemes have four parallel
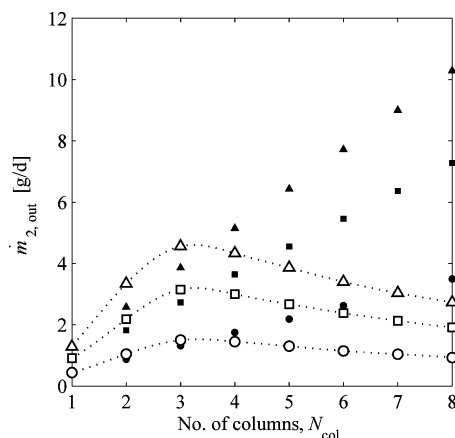
Table 3. Optimization Results for the Eight Possible Series Connections of Batch Columns for $c_{i,inj} = 1.0$ g/L, $d_p = 15$ μm, and $Pu_{min} = 95\%$

N_{col}	$\dot{V}$ [(mL)/(min)]	V_{inj} [mL]	Δt_c [min]	$\dot{m}_{2,out}$ [g/d]	Y [%]	Δp [bar]
1	10.95	1.16	0.808	1.29	62.1	14.6
2	23.49	2.54	0.729	3.34	66.7	62.7
3	24.99	4.18	0.977	4.56	74.0	100.0
4	18.72	6.21	1.728	4.33	83.6	100.0
5	15.00	8.04	2.636	3.86	87.9	100.0
6	12.50	9.80	3.770	3.40	90.8	100.0
7	10.71	11.54	5.041	3.03	92.0	100.0
8	9.37	13.16	6.461	2.73	93.1	100.0

Table 4. Selected Schemes That Combine Series and Parallel Systems for $d_p = 15$ μm and $Pu_{min} = 95\%$[a]

scheme	Pr [g/d/L]	Y [%]	rank[b]
4×2	708.9	66.7	1
$3 \times 2 + 2 \times 1$	668.1	65.7	2
$1 \times 3 + 2 \times 2 + 1 \times 1$	664.6	68.6	3
8×1	545.8	62.1	11
1×8	144.8	93.1	22

[a] The productivity is determined from eqs 10 and 15. [b] Ranked with respect to Pr.

Figure 3. Optimization results for series and parallel arrangements of N_{col} batch columns for different feed concentrations ($d_p = 15$ μm and $Pu_{min} = 95\%$). Symbols: $c_{i,inj} = 1.0$ g/L (triangles), 0.5 g/L (squares), and 0.2 g/L (circles). Open symbols: optimized product streams for the eight possible series connections. Filled symbols: total product mass flux from eq 15 for parallel arrangements of *single* columns. Lines are guides to the eye.

trains, each with two columns in series (4×2). It is interesting to note that this setup does not contain the most productive individual series scheme (three columns in series, see Figure 3). Although being a coincidental result, the "symmetrical" 4×2 scheme appears also to be attractive with respect to process design and control, since identical operating parameters hold for the four parallel trains. The next two, more-complex systems in Table 4 provide slightly lower productivities. The achievable yield is limited for the four first, rather "short" systems. This should be considered with respect to "fully parallel" setups, which are often used in practice. Interestingly, the productivity of the corresponding scheme (8×1) ranks only 11 of 22. In this context it is worth mentioning that the same performance will be achieved by a single column that has the same length, but an 8-fold cross-sectional area. Such a system would have the same interstitial velocity, which corresponds to a scale-up approach common in preparative chromatography. The second straightforward approach with eight columns in series (1×8) even ranks last, but achieves the highest yield.

While the productivity obviously depends strongly on the arrangement (in Table 4, Pr is about 5 times higher for 4×2 than for 1×8), their ranking is not influenced very strongly

by the feed concentration (at least not for the parameters used here). For $c_{i,inj} = 0.5$ g/L and $c_{i,inj} = 0.2$ g/L, the only change is that the second-best option in Table 4 is replaced by the similar $2 \times 3 + 1 \times 2$ setup. Another indication for the weak influence of $c_{i,inj}$ is that it does not affect the position of the maxima for $\dot{m}_{2,out}$ in Figure 3. Different observations might be made for adsorption isotherms with more pronounced nonlinearity, or for significantly higher feed concentrations.

3.2.2. Role of Particle Size. Generally, low particle sizes d_p result in higher column efficiency (i.e., a higher number of theoretical plates), as is reflected by eq 6. On the other hand, small particles lead to a higher pressure drop and, thus, to lower maximum flow rates. The flow rates, in turn, affect also the stage number, as can be seen in eqs 5 and 6.

In order to investigate these opposite trends, here we consider values for d_p between 5 and 20 μm. Figure 4 shows the optimized product streams as a function of the number of series columns for different particle sizes.

Figure 4 reveals that, with increasing particle diameter, the maxima shift toward higher column numbers. This is due to the lower pressure drop for larger particles, which allows us to connect more columns in series before the pressure drop limit $\Delta p_{max} = 100$ bar is reached. In fact, the pressure drop constraint $\Delta p \leq \Delta p_{max}$ becomes active at the maximum and for all longer arrangements. Shorter systems operate below this limit. Note that for small particles the pressure drop limit was already reached for a single column (5 μm) or two columns in series (9 μm), respectively. Performance of these systems cannot be improved by longer column arrangements. Since optimizations for such small particles and low flow rates are numerically very expensive, no further calculations were performed for these two cases.

Table 5 shows the most productive schemes obtained from the data in Figure 4 and eq 15. Obviously, the particle size has a significant impact on the optimal structure. For smaller
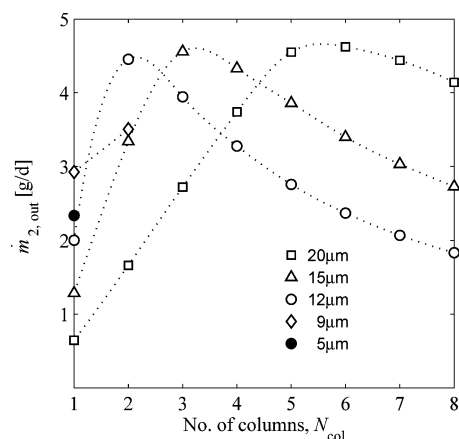
Figure 4. Optimization results for series connections for different particle sizes. Injection concentration $c_{i,inj} = 1.0$ g/L; purity requirement, 95%. Lines are guides to the eye.
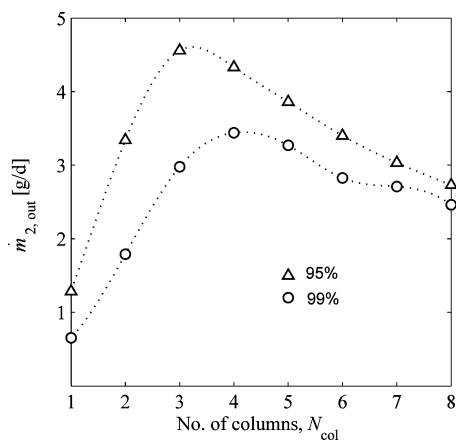
Figure 5. Optimization results for series connections and two different purity requirements. Injection concentration $c_{i,inj} = 1.0$ g/L; particle size $d_p = 15$ μm; injection. Lines are guide to the eye.

particles, parallel arrangements are more productive, while larger particles require longer setups. The reason for this is the interplay between column efficiency and pressure drop. For increasing particle size, the stage number calculated from eqs 5 and 6 decreases, while the throughput increases due to a lower Δp from eq 7. Furthermore, it is observed that larger particles lead to a decrease of the yield, which is a result of the same trade-off.

The highest productivity is found for $d_p = 9$ μm (eight columns in parallel, 8×1). Although an optimization of the particle size itself is beyond the scope here, the data in Table 5 imply that such an optimum lies between 5 and 12 μm, and that the best column arrangement would be an 8×1 (which is the fully parallel setup often used in practice) or a 4×2 system.

3.2.3. Role of Purity Requirement. Productivity typically decreases for higher purity demands. In order to investigate the role of this aspect, in addition to above cases with $Pu_{min} = 95\%$, also the more demanding case with $Pu_{min} = 99\%$ is considered.

Figure 5 shows the corresponding results for a given feed concentration and particle size. It can be expected that the increased purity requirement necessitates a higher column efficiency. Correspondingly, the optimizations lead to longer arrangements and lower flow rates. The latter cause the pressure drop constraint to become active only at higher column numbers.

For the given particle size of 15 μm and 95% purity the best arrangement found earlier was 4×2 (four parallel trains, each with two columns in series, see Table 4). In contrast, the optimum for 99% purity is the somewhat longer setup $2 \times 3 + 1 \times 2$ (see Figure 1, center). It achieves a productivity of Pr = 410.9 g/d/L, which is about 42% less than for 95%. The yield of $Y = 67.1\%$ is very similar to the case for 95% (see Table 4).

3.2.4. Role of the Objective Function. In addition to the parameters investigated above, the definition of the objective function itself has an impact on the optimal process configuration. So far, the productivity Pr was used as the objective, which is of obvious importance for preparative separations.

Table 5. Optimal Multicolumn Arrangements for Different Particle Sizes

d_p [μm]	optimal scheme	Pr [g/d/L]	Y [%]
5	8×1	991.5	91.5
9	8×1	1241.7	82.9
12	4×2	945.3	73.2
15	4×2	708.9	66.7
20	2×4	396.9	65.0

Table 6. Optimal Multicolumn Arrangements for the Modified Objective Function (Pr)Y as a Function of Particle Size

d_p [μm]	optimal scheme	(Pr)Y [g/d/L]	Pr [g/d/L]	Y [%]
12	4×2	788.4	910.4	86.6
15	$2 \times 3 + 1 \times 2$	523.9	638.1	82.1
20	2×4	303.5	378.0	80.3

However, in industrial applications total separation costs have to be minimized, which depend on a rather large number of aspects (see section 2.3.1). A correspondingly detailed cost function will not be used here, since it would lead to highly specific results.[4] In-depth discussions of this can be found in refs 4, 31, and 34.

The new objective function applied here is (Pr)Y, which was suggested in ref 34. This corresponds to multiplying the product flux $\dot{m}_{2,tot}$ in eq 10 with Y. Note that, since the product flux and the yield are mutually related, the new objective corresponds to a stronger weighting of the yield than in the investigations above.

Using the new objective, the optimization was repeated for all batch schemes and different particle sizes (cf. section 3.2.2). Table 6 lists the obtained optimal schemes together with the values for Pr and Y. In comparison with the earlier results in Table 5, a certain trend toward longer configurations can be observed (i.e., for $d_p = 15$ μm, 4×2 is replaced by $2 \times 3 + 1 \times 2$). As regards process performance, Y increases significantly by about 22% (averaged value). This is in line with the expectation that higher yields require systems with higher column efficiencies, which are achieved by (i) longer column arrangements and (ii) lower flow rates. Due to the latter, the productivity decreases. However, the decrease is less significant (about 6%), since it is counterbalanced by the increased yield.

3.3. SMB/SMB Arrangements. A viable alternative to the batch column schemes studied above is to arrange the given set of columns as a simulated moving bed (SMB) process. It appears interesting to investigate whether SMB setups or batch column arrangements are suited better for a ternary separation problem. Note that we will neglect any additional costs for SMB arrangements (i.e., investment costs for pumps and a valve setup to perform column switching).

Multicomponent separations could be performed using sophisticated SMB arrangements, typically with more than four zones and internal recycles.[16-19] Such complex schemes will not be considered here due to their complexity. The focus here is on straightforward series connections of two conventional four-zone SMB units (see, for example, refs 20 and 21), each with a single column per zone. Only two feasible options exist for a ternary separation: In the first (denoted as R/E in Figure 1), the intermediate target component is obtained at the raffinate of the first SMB process (port R of U1 in Figure 1). This stream serves as feed for the second SMB, which then delivers the product through its extract (port E of U2). In the second option (E/R configuration), the target component is obtained via the extract E of unit U1 and the raffinate port R of unit U2.

The optimization of such SMB/SMB connections is numerically more expensive than those for batch chromatography. As shown in Table 1, there are nine free variables (in comparison with only three for batch chromatography). This led to significantly higher calculation times.

Before discussing the results, it is useful to introduce a measure for the quality of the separation achieved by the first SMB unit. We define the residual of the nondesired component in the connecting stream between the two SMB units, $\bar{R}_{co}$, as

$$\bar{R}_{co} = \frac{\bar{c}_{j,k}^{U1}}{\sum_{i=1}^{3} \bar{c}_{i,k}^{U1}} \qquad (20)$$

where $k = $ (R, E) denotes the outlet of U1 and j marks the undesired solute (i.e., $j = 1$ for $k = $ E and $j = 3$ for $k = $ R). Concentrations are time-averaged values as obtained in the periodic steady state. A residual of 0% means a complete removal of the third solute by the first SMB process (i.e., a "sharp split"). In contrast, a value of 33% corresponds to the original feed (i.e., no separation can be observed with respect to the connecting stream).

The optimization results for the two setups are listed for different particle sizes in Table 7, together with the operational parameters. The residuals for all schemes are close to zero, which indicates that the first SMB unit achieves a sharp split.

The productivity for E/R schemes is significantly lower than that for R/E systems. Also the residuals (eq 20) are slightly higher for E/R. The reason for this is the high extract flow rate of the first unit and the corresponding product dilution (which is always the case for Langmuir-type adsorption isotherms). This limits the throughput of the second SMB systems. This can be almost fully compensated for by an intermediate removal of all excess solvent from the connecting stream. This was assumed in the scheme E/R*, where the concentration of the higher concentrated component in the connecting stream was readjusted to the original value of 1.0 g/L.

With respect to particle size, the same trends are observed as found for batch arrangements: Small particles allow for more efficient separation, but cause a higher pressure drop. As a consequence, the highest productivity is achieved by SMB systems with intermediate particle sizes. When comparing the results in Table 7 to those for batch systems in Table 5, the performance of SMB/SMB setups is clearly lower than the best batch arrangement with a particle size of $d_p = 9 \mu m$ (see Table 5). However, for increasing particle sizes, the performance of both options becomes similar. This trend will continue for a further increase of d_p. Eventually, the SMB-based systems will outperform batch arrangements with the same particle size. This underlines the lower demands of SMB chromatography with respect to column efficiency, which was already noted earlier.[35,36] On the other hand, the productivity of E/R setups is in all cases significantly lower than that of batch column arrangements.

Note that the productivities listed in Table 7 hold for the case that the pressure drop constraint can be applied to each single zone. If a different pump configuration is applied, the values for Pr have to be recalculated from the given m-values. For example, in systems with a single recycle pump, the total pressure drop typically corresponds to the sum of the contributions of the individual zones. In such cases, the possible productivity will be significantly lower.

3.4. SMB/Batch Arrangements. As a final variant, different combinations were studied that combine SMB chromatography with subsequent batch columns. In the selected schemes either the extract or the raffinate port of the SMB unit was connected to a 4×1, 2×2, or 1×4 setup, respectively. An example (E/2×2) is shown in Figure 1.

As indicated by the dashed lines in Figure 1, it is assumed that the product from the SMB process is stored and then injected into the batch columns, which operate at an independent flow rate. Using this type of connection, only one degree of freedom is lost. Out of the three variables for batch systems (flow rate, injection volume, and cycle time) the injection

volume was determined from the outlet of the SMB such that all material is processed. In summary, seven variables remain to be optimized (see Table 1).

Table 8 summarizes the optimization results. In general, lower productivities are obtained than those obtained for batch arrangements or similar to those obtained for SMB/SMB systems. The highest value is found for the configuration R/2 $\times$ 2, which corresponds to a connection of the more "favorable" raffinate port of the SMB unit and the best possible four-column batch arrangement (see Table 3 and Figure 3). Configurations via the extract port lead to very low productivities.

A closer inspection of the residuals $\bar{R}_{co}$ in Table 8 reveals that the performance of "raffinate SMBs" is poor. The residuals range from 13% to 21% (in comparison with about 1% for SMB/SMB connections, see Table 7). Even more drastically, "extract SMBs" do not perform a separation of the mixture delivered toward the trains of batch columns: the residual of about 33.3% corresponds to that of the original feed solution. These systems just serve as a bypass with additional dilution. The optimization runs for this type of setup basically identify the optimal batch arrangement that is capable of processing a given amount of a diluted ternary mixture. A removal of excess solvent before the injections into the batch columns leads to a performance similar to that for the systems with raffinate connections (not shown).

The reason for this seems to be a certain "incompatibility" of the two processes. The connection between an SMB unit and a batch arrangement reduces the number of free parameters to optimize. As a consequence, an optimal injection volume for the batch arrangement rarely corresponds to an optimal operation of the SMB unit and vice versa. For the parameters used, the objective function appears to be more sensitive to the variables related to the batch columns than to the design parameters of the SMB unit. Therefore, the optimization determines optimal batch schemes. This leads, in turn, to a suboptimal performance of the SMB units. An indication for this is that the two different types of chromatographic units achieve their optimal performance at different particle sizes (15 μm for SMB systems, 9 μm for batch columns; see sections 3.2.2 and 3.3, respectively). The authors believe that an optimal SMB/batch arrangement will require the independent optimization of SMB and batch units with respect to, for example, the particle size. This is beyond the methodology of this work, but certainly deserves to be studied in further investigations. In this context, it would be interesting to investigate an approach that is often recommended for practical use. In this method, the target peak is first split at its maximum by batch chromatography. Subsequently, the target is isolated from both fractions by SMB chromatography.

4. Summary and Conclusions

The chromatographic separation of a ternary mixture was investigated for a broad range of possible column arrangements using eight identical chromatographic columns. The optimal column arrangement was determined for maximizing the specific productivity by model-based optimization for batch chromatography, standard SMB processes, and combinations thereof.

A methodology was established that allows for a straightforward evaluation of batch chromatography systems. It was shown that it is sufficient to optimize eight different series connections in order to evaluate all 22 possible column arrangements.

The role of relevant parameters was investigated with respect to the resulting structure of the optimal arrangement. Different trade-offs could be demonstrated to exist between design

Table 7. Optimization Results for the Two Different Connections of SMB Processes for Different Particle Sizes ($c_{i,inj} = 1.0$ g/L, $Pu_{min} = 95\%$)[a]

scheme	d_p [μm]	Pr [g/d/L]	Y [%]	$\bar{R}_{co}$ [%]	m_I^{U1}	m_{II}^{U1}	m_{III}^{U1}	m_{IV}^{U1}	m_I^{U2}	m_{II}^{U2}	m_{IV}^{U2}	$\dot{V}_I^{U1}$ [mL/min]	$\dot{V}_I^{U2}$ [mL/min]
R/E	12	258.1	65.5	1.02	6.925	3.553	4.938	4.054	6.182	3.723	4.336	40.8	33.9
R/E	15	368.9	78.8	1.02	7.556	4.093	5.126	4.307	5.620	3.787	3.409	68.7	62.3
R/E	20	325.1	72.3	1.31	7.578	4.006	5.069	4.202	5.592	4.007	3.725	64.3	75.6
E/R	12	187.8	75.7	4.06	4.601	3.189	4.097	2.022	7.621	4.601	4.884	30.8	46.3
E/R	15	205.2	70.1	1.50	4.538	3.480	4.147	2.798	7.191	4.646	2.880	49.1	54.1
E/R	20	114.5	43.8	2.10	4.801	3.489	4.361	3.320	8.050	4.041	4.651	34.6	36.2
E/R*	15	310.4	86.4	1.79	5.066	3.529	4.214	3.059	7.936	4.548	3.137	62.4	62.8

[a] The R/E scheme is shown schematically in Figure 1; the E/R scheme is defined correspondingly. E/R* denotes a special case where excess solvent is removed from the connecting extract stream.

Table 8. Optimization Results for Connections between an SMB Process and Different Batch Arrangements via Extract (E) and Raffinate (R) Ports of the SMB Unit, Respectively ($c_{i,inj} = 1.0$ g/L, $d_p = 15$ μm, and $Pu_{min} = 95\%$)

scheme	Pr [g/d/L]	$\bar{R}_{co}$ [%]	Y [%]	m_I	m_{II}	m_{III}	m_{IV}	$\dot{V}_I^{U1}$ [mL/min]	$\dot{V}$ [mL/min]	V_{inj} [mL]	Δt_c [min]
R/4 × 1	407.4	12.96	71.2	7.609	2.314	5.026	3.983	67.7	10.4	1.20	0.790
R/2 + 2	429.6	20.73	72.5	6.955	4.198	5.755	4.363	63.7	23.4	2.79	0.678
R/1 × 4	272.6	13.58	75.5	6.285	4.145	5.269	4.334	45.6	17.9	7.31	1.760
E/4 × 1	279.4	33.33	59.5	5.675	1.284	6.546	5.659	68.6	11.0	1.18	0.746
E/2 + 2	237.0	29.87	71.6	3.624	1.026	3.919	3.218	52.8	13.4	3.55	1.457
E/1 × 4	226.0	33.33	84.8	4.414	1.478	4.945	4.405	55.4	19.7	5.65	1.586

parameters (feed concentration, flow rates, particle size), dependent system properties (column efficiency and pressure drop), and the objective function. For the parameters studied, a change of the feed concentration has no significant effect on the optimal setup. This might well be the case for more nonlinear adsorption isotherms. In contrast, the particle size has a stronger influence due to the pronounced interplay between column efficiency and pressure drop. In turn, there is an optimal particle size for a given length of the arrangement. Large particles lead to longer optimal arrangements. The same holds when increasing the purity requirements, or when including the yield in the objective function.

Direct continuous combinations of two standard SMB processes were found to achieve a higher throughput if the connection between them is established via the raffinate stream of the first unit. SMB schemes connected by the extract port suffer from stronger product dilution. In either case, productivity increases when including an intermediate desorbent removal. Furthermore, the SMB processes can be operated using larger adsorbent particles than in batch arrangements. Such stationary phases are typically less expensive.

However, for the ternary separation problem and the given parameter values, it was found that the throughput of cascades of standard SMB units is lower than that attainable by a system of optimally arranged batch columns. A general statement cannot be derived from this, but the results indicate that a flexible multicolumn batch system is an interesting option for multicomponent separations. Simple sequences of powerful *binary* separation processes (i.e., standard SMB units) will not automatically be more effective. This might be different for more sophisticated SMB-based systems that are designed specifically for ternary separations (see, e.g., refs 16−23).

In comparison with batch or combinations of two SMB processess, an intermediate performance is found for connections of SMB units with subsequent batch columns. Similar to SMB/SMB systems, these perform better when using the raffinate port of the SMB unit as input for the batch column arrangement. For the system considered here, the determined operating parameters seem optimal rather for the batch system, than for the SMB unit.

Generally, the optimal setup for a given set of columns will differ significantly for each particular separation problem. In this context, the concept suggested for optimization of batch chromatography appears particularly attractive, since it requires only few optimization runs to assess all possible arrangements. The method could be useful in industrial sectors that apply the same type of equipment to frequently changing separation problems. This is the case, for example, in pharmaceutical development facilities and companies that perform custom separations. The flexibility achievable by optimizing the arrangement of a set of identical columns can be a powerful alternative to a suboptimal exploitation of existing single columns or investment in new equipment.

Acknowledgment

Literature Cited

(1) Broughton, D. B.; Gerhold, C. G. Continuous sorption process employing fixed bed of sorbent and moving inlets and outlets. U.S. Patent 2,985,589, 1961.

(2) Ruthven, D. M.; Ching, C. B. Counter-current and Simulated Counter-current Adsorption Separation Processes. *Chem. Eng. Sci.* **1989**, *44*, 1011.

(3) Seidel-Morgenstern, A.; Kessler, L. C.; Kaspereit, M. New Developments in Simulated Moving Bed Chromatography. *Chem. Eng. Technol.* **2008**, *31*, 826.

(4) Guiochon, G.; Shirazi, D. G.; Felinger, A.; Katti, A. M. *Fundamentals of Preparative and Nonlinear Chromatography*, 2nd ed.; Academic Press: Boston, 2006.

(5) Bombaugh, K.; Dark, W.; Levangie, R. High Resolution Steric Chromatography. *J. Chromatogr. Sci.* **1969**, *7*, 42.

(6) Seidel-Morgenstern, A.; Guiochon, G. Theoretical Study of Recycling in Preparative Chromatography. *AIChE J.* **1993**, *39*, 809.

(7) Charton, F.; Bailly, M.; Guiochon, G. Recycling in Preparative Liquid Chromatography. *J. Chromatogr., A* **1994**, *687*, 13.

(8) Grill, C. M. Closed-loop Recycling With Periodic Intra-profile Injection: A New Binary Preparative Chromatographic Technique. *J. Chromatogr., A* **1998**, *796*, 101.

(9) Mazzotti, M.; Storti, G.; Morbidelli, M. Optimal Operation of Simulated Moving Bed Units for Nonlinear Chromatographic Separations. *J. Chromatogr., A* **1997**, *769*, 3.

(10) Mallmann, T.; Burris, B. D.; Ma, Z.; L. Wang, N.-H. Standing Wave Design of Nonlinear SMB Systems for Fructose Purification. *AIChE J.* **1998**, *44*, 2628.

(11) Storti, G.; Masi, M.; Carrà, S.; Morbidelli, M. Optimal Design of Multicomponent Countercurrent Adsorption Separation Processes Involving Nonlinear Equilibria. *Chem. Eng. Sci.* **1989**, *44*, 1329.

(12) Storti, G.; Mazzotti, M.; Morbidelli, M.; Carrà, S. Robust Design of Binary Countercurrent Adsorption Separation Processes. *AIChE J.* **1993**, *39*, 471.

(13) Kaspereit, M.; Seidel-Morgenstern, A.; Kienle, A. Design of Simulated Moving Bed Chromatography Under Reduced Purity Requirements. *J. Chromatogr., A* **2007**, *1162*, 2.

(14) Mann, G. Bayer-Schering Pharma AG, personal communication, 2006.

(15) Ziomek, G.; Antos, D.; Tobiska, L.; Seidel-Morgenstern, A. Comparison of Possible Arrangements of Five Identical Columns in Preparative Chromatography. *J. Chromatogr., A* **2006**, *1116*, 179.

(16) Wooley, R.; Ma, Z.; Wang, N. H. L. A Nine-zone Simulating Moving Bed for the Recovery of Glucose and Xylose from Biomass Hydrolyzate. *Ind. Eng. Chem. Res.* **1998**, *37*, 3699.

(17) Kessler, L. C.; Seidel-Morgenstern, A. Theoretical Study of Multicomponent Continuous Countercurrent Chromatography Based on Connected 4-zone Units. *J. Chromatogr., A* **2006**, *1126*, 323.

(18) Beste, Y. A.; Arlt, W. Side-Stream Simulated Moving-Bed Chromatography for Multicomponent Separation. *Chem. Eng. Technol.* **2002**, *25*, 956.

(19) Kim, J. K.; Zang, Y. F.; Wankat, P. C. Single-cascade Simulated Moving Bed Systems for the Separation of Ternary Mixtures. *Ind. Eng. Chem. Res.* **2003**, *42*, 4849.

(20) Wankat, P. C. Simulated Moving Bed Cascades for Ternary Separations. *Ind. Eng. Chem. Res.* **2001**, *40*, 6185.

(21) Nicolaos, A.; Muhr, L.; Gotteland, P.; Nicoud, R. M.; Bailly, M. Application of Equilibrium Theory to Ternary Moving Bed Configurations (Four Plus Four, Five Plus Four, Eight and Nine Zones) I. Linear Case. *J. Chromatogr., A* **2001**, *908*, 71.

(22) Hur, J. S.; Wankat, P. C. New Design of Simulated Moving Bed (SMB) for Ternary Separations. *Ind. Eng. Chem. Res.* **2005**, *44*, 1906.

(23) Paredes, G.; Abel, S.; Mazzotti, M.; Morbidelli, M.; Stadler, J. Analysis of a Simulated Moving Bed Operation for Three-Fraction Separations (3F-SMB). *Ind. Eng. Chem. Res.* **2004**, *43*, 6157.

(24) Ströhlein, G.; Aumann, L.; Mazzotti, M.; Morbidelli, M. A Continuous, Counter-current Multi-column Chromatographic Process Incorporating Modifier Gradients for Ternary Separations. *J. Chromatogr., A* **2006**, *1126*, 338.

(25) Rouchon, P.; Schonauer, M.; Valentin, P.; Guiochon, G. Numerical Solution of Band Propagation in Nonlinear Chromatography. *Sep. Sci. Technol.* **1987**, *22*, 1793.

(26) Seidel-Morgenstern, A.; Bümel, C.; Kniep, H. Efficient Design of the SMB Process Based on a Perturbation Method to Measure Adsorption Isotherms and on a Rapid Solution of the Dispersion Model. In *Fundamentals of Adsorption*; Meunier, F., Ed.; Elsevier: Paris, 1998; pp 303−308.

(27) Craig, L. C. Identification of Small Amounts of Organic Compounds by Distribution Studies. II. Separation By Counter-current Distribution. *J. Biol. Chem.* **1944**, *155*, 519–534.

(28) Shan, Y.; Seidel-Morgenstern, A. Analysis of the Isolation of a Target Component Using Multicomponent Isocratic Preparative Elution Chromatography. *J. Chromatogr., A* **2004**, *1041*, 53–62.

(29) Czok, M.; Guiochon, G. The Physical Sense of Simulation Models of Liquid Chromatography: Propagation Through a Grid or Solution of the Mass Balance Equation. *Anal. Chem.* **1990**, *62*, 189–200.

(30) Felinger, A.; Guiochon, G. Optimizing Experimental Conditions in Overloaded Gradient Elution Chromatography. *Biotechnol. Prog.* **1996**, *12*, 638–644.

(31) Heuer, C.; Kniep, H.; Falk, T.; Seidel-Morgenstern, A. Comparison of Various Process Engineering Concepts of Preparative Chromatography. *Chem. Eng. Technol.* **1998**, *21*, 469–477.

(32) Weisstein, E. W. *CRC Concise Encyclopedia of Mathematics*; Chapman & Hall: Boca Raton, FL, 1999.

(33) Nelder, J.; Mead, R. A. Simplex Method for Function Minimization. *Comput. J.* **1965**, *7*, 308–313.

(34) Felinger, A.; Guiochon, G. Optimizing Preparative Separations at High Recovery Yield. *J. Chromatogr., A* **1996**, *752*, 31–40.

(35) Charton, F.; Nicoud, R.-M. Complete Design of a Simulated Moving Bed. *J. Chromatogr., A* **1995**, *702*, 97–112.

(36) Biressi, G.; Ludemann-Hombourger, O.; Mazzotti, M.; Nicoud, R.; Morbidelli, M. Design and Optimisation of a Simulated Moving Bed Unit: Role of Deviations from Equilibrium Theory. *J. Chromatogr., A* **2000**, *876*, 3–15.

Contents lists available at ScienceDirect

Separation and Purification Technology

Theoretical analysis of steady state recycling chromatography with solvent removal

Jani Siitonen [a], Tuomo Sainio [a,*], Malte Kaspereit [b]

[a] Lappeenranta University of Technology, Skinnarilankatu 34, FI-53850 Lappeenranta, Finland
[b] Max Planck Institute for Dynamics of Complex Technical Systems, Sandtorstrasse 1, D-39106 Magdeburg, Germany

ARTICLE INFO

ABSTRACT

The possibility to enhance the process performance of steady state recycling (SSR) chromatography by removing solvent was investigated in the framework of the equilibrium theory. A method was developed to choose *a priori* the relevant cut times corresponding to arbitrary purity constraints and to predict the steady state of the process without performing dynamic simulations. The amount of fresh feed introduced per cycle and the injection width were identified as the only free operating parameters. A relationship was derived between the amount of fresh feed and the solvent removal capacity required to achieve the chosen purities.

The performance of three different process configurations was analyzed: solvent removal applied to (I) the fresh feed, (II) the recycle fraction, and (III) their mixture. It was found that solvent removal facilitates treating more fresh feed per cycle than is possible in a conventional SSR process. In addition, it was shown that the three SSR-SR configurations have identical performance with the same operating parameters. In contrast, the configurations differ with respect to the maximum amount of fresh feed that can be processed per cycle, as well as to the range of feasible injection widths.

It was shown that SSR with solvent removal can yield higher productivity and lower eluent consumption than an optimized batch chromatography process that employs solvent removal.

© 2011 Elsevier B.V. All rights reserved.

1. Introduction

Preparative chromatography is a highly developed technique in the pharmaceutical and fine chemical industries and is used for the separation and purification of a wide range of substances. Single-column batch chromatography and multi-column simulated moving bed (SMB) chromatography are the most common process schemes. The batch mode usually suffers from high eluent consumption and low productivity but is versatile, provides multiple product fractions, and allows rapid method development. As to the SMB, high productivity and low eluent consumption are counterbalanced by high investment costs and a high degree of complexity. For these reasons, there is room for simple, compact, yet efficient chromatographic processes.

The idea of enhancing the separation by recycling the chromatogram partially or as a whole is not new, but has recently received considerable attention. Many recycling methods have been suggested, such as closed loop recycling [1–3], peak shaving [2], and steady state recycling (SSR) chromatography [4–15]. In an SSR process, the pure leading and trailing sections of the

chromatogram are collected, while the unresolved remainder is recycled back to the inlet of the column. In addition, a constant amount of fresh feed is added to the recycled fraction, which eventually causes the process to attain a periodic steady state. The process can be operated in different modes depending on the injection method. In the closed-loop mode (CL-SSR) [4–9], the recycle fraction and the fresh feed are introduced separately in order to preserve the already achieved partial separation. In the mixed-recycle mode (MR-SSR) [10–15], the recycle fraction is mixed with fresh feed before injection.

The optimal design of SSR chromatography is challenging due the dynamic character of the process. The limiting case of complete separation under ideal conditions was studied by Bailly and Tondeur [10–12] and Charton [13] for binary Langmuir systems by using the equilibrium theory. Sainio and Kaspereit [15] extended this approach to the case of arbitrary purity requirements, and provided a detailed analysis of MR-SSR. In addition, Sainio and Kaspereit developed a method for the *a priori* calculation of fractionation times that guarantee the fulfillment of arbitrary purity or yield constraints at the steady state. The method requires the isotherm parameters only and does not employ dynamic simulations.

In an SSR process, the recycle fraction is typically more dilute than the fresh feed. It seems plausible that process perfor-

mance could be enhanced by concentrating the recycle fraction by removing some of the solvent. In the case of multi-column chromatography systems, this kind of solvent removal from the internal process stream has been used successfully. In SMB operation, a portion of the extract stream can be concentrated and re-injected at the same point of the unit [16]. Under certain circumstances, a high concentration of the more retained compound intensifies the displacement effect on the less retained compound and improves the process performance. This technique is called M3C [17] or enriched extract SMB (EE-SMB) [16,18]. However, solvent removal from the recycle fraction in SSR has not been theoretically investigated before, and no analysis or design principles of such a process concept have been presented.

The objective of the present work is to investigate the possibility to enhance the mixed-recycle SSR performance by introducing a solvent removal unit into the chromatographic separation process. The process concept will henceforth be abbreviated as SSR-SR. Solvent removal could be applied to (I) the fresh feed, (II) the recycle fraction, or (III) the actual feed solution (which is obtained by mixing the fresh feed and the recycle fraction). A theoretical framework will be provided for the analysis of the characteristic features of these process configurations and for the optimal design of SSR-SR chromatography. The approach will be based on the so-called equilibrium theory, where mass-transfer resistance and axial dispersion are neglected, and will be limited to binary systems that follow the competitive Langmuir adsorption isotherm model. This means that the proposed theory will be most applicable for systems of high efficiency. It should be also noted that, in practice, the extent of solvent removal would be limited by for example the solubility of the components or the viscosity of the solution. Here we focus on developing the theoretical background of steady state recycling chromatography with solvent removal, and such limitations are beyond the scope of this work.

A short summary of the analysis and design of the conventional MR-SSR process developed by Sainio and Kaspereit [15] will be presented. After that, the theoretical framework concerning the SSR-SR process will be developed, and a method to predict the steady state of the SSR-SR process will be provided. The method allows choosing the operating parameters such that, in the steady state, arbitrary purity and yield constraints will be satisfied. It will be shown that different SSR-SR process configurations will lead to exactly the same steady state and thus have identical performance when the operation parameters (*i.e.* the injection volume and the volume of fresh feed processed during each cycle) as well as purity constraints are same. However, the range of feasible injection volumes and the maximum amount of fresh feed that can be processed per cycle are not identical. Finally, the method will be used to investigate the performance of different SSR-SR process configurations.

2. Theory of SSR chromatography

The analysis and design of SSR with solvent removal requires understanding of the corresponding principles of a conventional SSR process. For this reason, the basic theory and the design method for the mixed-recycle SSR chromatography developed by Sainio and Kaspereit [15] are briefly described in the following sections (Sections 2.1–2.3).

The design method, based on the equilibrium theory, allows for the direct prediction of the steady state for systems with competitive Langmuir adsorption isotherms. The steady state can be obtained on the basis of adsorption isotherm parameters only without performing dynamic simulations. The operating parameters (in this case, the cut times t_{A1}, t_{A2}, t_{B1} and t_{B2} shown in Fig. 1 and the injection volume V_{inj}) can be chosen such that, in the steady state,

arbitrary purity and yield constraints are satisfied. With respect to Fig. 1b, the purities are defined as follows:

$$p^A = \frac{m_1^A}{m_1^A + m_2^A} = \frac{\int_{t_{A1}}^{t_{A2}} c_1 \, dt}{\int_{t_{A1}}^{t_{A2}} (c_1 + c_2) \, dt} \tag{1}$$

$$p^B = \frac{m_2^B}{m_1^B + m_2^B} = \frac{\int_{t_{B1}}^{t_{B2}} c_2 \, dt}{\int_{t_{B1}}^{t_{B2}} (c_1 + c_2) \, dt} \tag{2}$$

where m_i^j denotes the mass of component $i = (1, 2)$ in the product fraction $j = (A, B)$. It is assumed that component 1 is the less adsorbed one and is the target compound in product fraction A.

As an alternative to the specifications of the desired purities, the yields of the components can be given. However, since the SSR (and SSR-SR) process represents a binary separation without a waste stream, the purity and yield constraints are interchangeable [19]:

$$Y_1 = \frac{m_1^A}{m_1^{FF}} = \frac{p^A}{p^{FF}} \frac{p^{FF} + p^B - 1}{p^A + p^B - 1} \tag{3}$$

$$Y_2 = \frac{m_2^B}{m_2^{FF}} = \frac{p^B}{1 - p^{FF}} \frac{p^A - p^{FF}}{p^A + p^B - 1} \tag{4}$$

where p^{FF} is defined as the purity of component 1 in fresh feed: $p^{FF} = c_1^{FF}/(c_1^{FF} + c_2^{FF})$. In other words, by specifying any two of the four quantities, the remaining two are also determined.

2.1. Equilibrium theory for binary Langmuir adsorption isotherm system

In the ideal model, column efficiency is assumed to be infinite. The material balance, which can be written in matrix form as follows in Eqs. (5) and (6), governs the propagation of the concentration states in the column.

$$\mathbf{A} \frac{\partial \mathbf{c}}{\partial t} + u \frac{\partial \mathbf{c}}{\partial x} = 0, \tag{5}$$

where

$$\mathbf{A} = \begin{bmatrix} 1 + F(\partial q_1/\partial c_1) & F(\partial q_1/\partial c_2) \\ F(\partial q_2/\partial c_1) & 1 + F(\partial q_2/\partial c_2) \end{bmatrix}, \qquad \mathbf{c} = \begin{bmatrix} c_1 \\ c_2 \end{bmatrix} \tag{6}$$

and q is the stationary phase concentration, F is the phase ratio, x is the space coordinate, t is time, and u is the interstitial velocity. According to the competitive Langmuir adsorption isotherm, the stationary phase concentration is given by

$$q_i = \frac{q_{m,i} b_i c_i}{1 + b_1 c_1 + b_2 c_2} \quad \text{(for } i = 1, 2) \tag{7}$$

where $q_{m,i}$ is the saturation capacity of the adsorbent for species i, and b_i is its Langmuir parameter.

Because of the competitive behavior of the phase equilibrium, the model forms a coupled system of two partial differential equations which has no analytical solution when the space coordinate x and time t are the independent variables. However, using the concentrations c_1 and c_2 as the independent variables, Eq. (5) can be solved analytically with the method of characteristics. This is the basis of the so-called equilibrium theory, which is described extensively in the literature [20,21]. Here, only its most relevant aspects will be explained.

When a rectangular pulse of a mixture of two components is injected at the inlet of a clean column, two simple wave transitions and two shock transitions are composed. The solution of Eq. (5) consists of describing the movement of these waves and their interactions along the column. The solution at the column outlet can be constructed in the so-called hodograph plane. An example of hodograph representation and corresponding chromatograms
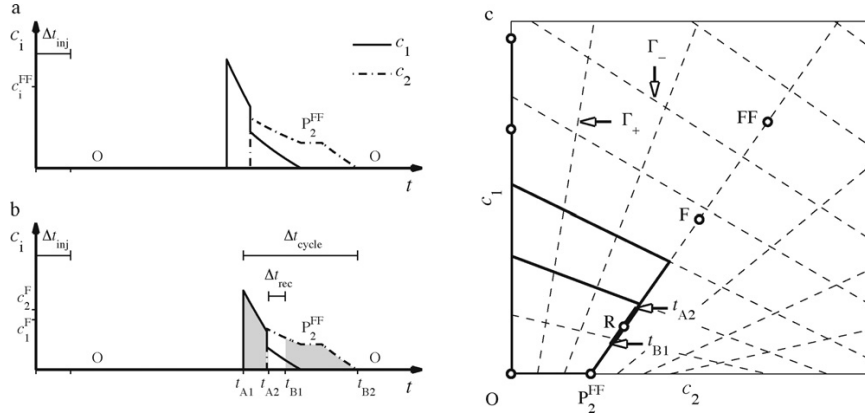
Fig. 1. Steady state recycling chromatography in the mixed-recycle mode. (a) Chromatogram for the first injection (injection of fresh feed with concentrations c_i^{FF}). (b) Chromatogram at the steady state (injection with concentrations c_i^F). (c) Corresponding hodograph representations.

are given in Fig. 1. In the case of Langmuir isotherms, simple waves correspond on the hodograph plane to segments on straight lines, which are called characteristics. The characteristics with a positive slope dc_1/dc_2 are referred to as Γ_+ characteristics and those with a negative slope as Γ_- characteristics. The slopes can be calculated explicitly from the right eigenvectors of the coefficient matrix **A** in Eq. (6), and therefore depend on the isotherm parameters only. The propagation velocities of simple waves can be obtained from the eigenvalues of **A**.

For Langmuir isotherms, the images of shock transitions (called Σ_+ and Σ_- shocks) also fall into the characteristics. The propagation velocities of shock waves are given by the mass balance across the discontinuity. In addition, if the injection is wide enough, the chromatographic profile includes concentration plateaus between simple and shock waves. On these plateaus, c_1 and c_2 are constant. Consequently, these regions are represented on the hodograph plane by single points.

2.2. Determination of cut times and steady state feed composition

In the conventional SSR process, the steady state feed composition F in the hodograph plot is always located in the Γ_+ characteristic that passes through the fresh feed composition FF [15]. In addition, as long as the SSR process is operated such that the purity constraints are fulfilled, the rear of the elution profile remains unaltered even if the feed plateau or the first component plateau erodes during elution. For this reason, we can first determine the cut times t_{B1} and t_{B2}. Obviously, the cut time t_{B2} should be chosen such that it matches the time of the complete elution of the injection. For the Langmuir system, t_{B2} is given by the following equation:

$$t_{B2} = \Delta t_{inj} + t_0(1 + F\,q_{m,2}b_2) \tag{8}$$

The injection time Δt_{inj} refers to the width of the pulse that is fed into the column after mixing the recycle fraction and the fresh feed, and t_0 is the elution time of a non-retained component.

Next, the cut time t_{B1} is chosen so that the purity constraints of product fraction B are fulfilled. An explicit expression for t_{B1} can be obtained, but it is rather complex. A more convenient option is to exploit the numerical technique and use some type of search algorithm to find the lower integration limit that satisfies Eq. (2). The required analytical expressions for $c_i(t)$ given by Guiochon et al. [20] are presented in Appendix A.

Once t_{B1} and t_{B2} are obtained, the volume of fresh feed that can be processed per cycle V^{FF} and the cut time t_{A2} can be solved with given purity constraints as follows [15]:

$$V^{FF} = \frac{\int_{t_{B1}}^{t_{B2}} c_2\,dt}{c_2^{FF}Y_2}\dot{V} = \frac{p^A + p^B - 1}{(c_1^{FF} + c_2^{FF})(p^A - p^{FF})p^B}\int_{t_{B1}}^{t_{B2}} c_2\,dt\,\dot{V} \tag{9}$$

$$t_{A2} = t_{B1} - \Delta t_{inj} + \frac{V^{FF}}{\dot{V}} \tag{10}$$

where $\dot{V}$ is the volume flow rate. Consequently, the steady state feed composition can be solved from the mass balance around the feed node

$$c_i^F = \frac{\int_{t_{A2}}^{t_{B1}} c_i\,dt + (c_i^{FF}V^{FF}/\dot{V})}{\Delta t_{inj}} \quad (\text{for } i = 1, 2) \tag{11}$$

As the last step, the remaining cut time t_{A1} should be equal to the elution time of the pure component 1 shock that corresponds to the steady state feed concentration. In the case of a large injection width, the plateau P_1^F in the front of the elution profile is not eroded during elution, and the analytical solution for the cut time t_{A1} is given by:

$$t_{A1} = t_0\left(1 + F\frac{q_1\left(c_1^{PF}, 0\right)}{c_1^{PF}}\right) \tag{12}$$

where the height of the plateau P_1^F is obtained from the intersection of the c_1 axis and the Γ_- characteristic passing though the steady state feed on the hodograph plane. In contrast, for sufficiently small injections, the pure component 1 plateau erodes completely, and a numerical approach to solve t_{A1} is needed. Several methods have been presented in the literature for solving this problem, for example by Guiochon et al. [20] and by Rhee et al. [21].

2.3. Performance of mixed-recycle SSR chromatography

In addition to developing the design method, Sainio and Kaspereit [15] have analyzed the performance of mixed-recycle SSR chromatography. The results can be summarized as follows:

1. The amount of fresh feed introduced to the process per cycle is independent of the total injection width (obtained by mixing the fresh feed and the recycle fraction).
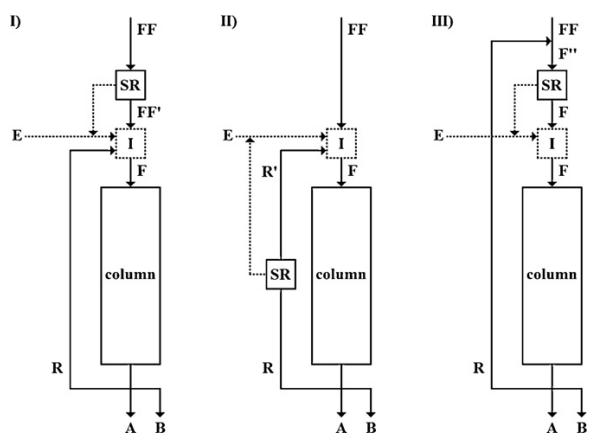
Fig. 2. Schematic representations of alternative SSR-SR configurations. (I) Solvent removal from fresh feed. (II) Solvent removal from recycle fraction. (III) Solvent removal from mixed fraction. *FF*, fresh feed; *FF'*, concentrated fresh feed; *R*, recycle fraction; *R'*, concentrated recycle fraction; *F'*, mixed fraction; *F*, column feed; *E*, eluent; *SR*, solvent removal unit; *I*, injection port; *A*, product fraction *A* (weaker adsorbing component 1); *B*, product fraction *B* (strong adsorbing component 2).

2. The cycle time always increases as the injection width increases.
3. The productivity of SSR decreases with the increasing injection width and is always lower than that of a batch process which is optimized so that no gap exists between successive chromatographic cycles.
4. The eluent consumption decreases with an increasing injection width for small injections, but is independent of the injection width for large injections. In terms of eluent consumption, SSR chromatography always outperforms batch chromatography.
5. The concentration of product fraction *A* increases with the injection width for small injections, but is independent of the injection width for large injections. With respect to the concentration of the product fraction *A*, an SSR process always outperforms an optimized batch process.
6. The concentration of the product fraction *B* is independent of the injection width and always the same as in batch chromatography.

As will be seen later, these findings can also be exploited to some extent in investigating the characteristic features of SSR-SR chromatography.

3. Theory of SSR chromatography with solvent removal

As mentioned in Section 1, there are basically three alternative configurations for applying solvent removal in a steady state recycling chromatography process. These are illustrated in Fig. 2. Either the fresh feed (option I) or the recycle fraction (option II) can be concentrated before they are mixed together and introduced to the column. Alternatively, solvent can be removed from their mixture (option III). The removed solvent can be used as eluent and thus reduce the consumption of fresh eluent.

Similarly to a conventional MR-SSR chromatography process (Fig. 1), the steady state operation of these three process options is conveniently presented in the hodograph plane as shown in Fig. 3. The relative composition of a solution is not changed in an ideal solvent removal unit. Therefore, the *operating line of the solvent removal unit* is a straight line on the hodograph plane, and solvent removal corresponds to moving upwards on it. As seen in Fig. 3, the operating line passes through the origin and has a slope equal to c_1/c_2 of the solution treated.

In process option I (Fig. 3I), solvent removal is applied to the fresh feed *FF*. The operating line thus passes through the origin and *FF*, and the resulting composition maps onto point *FF'*. On every cycle, a recycle fraction is collected between cut times t_{A2} and t_{B1}. The volume-average composition of the recycle fraction is presented on the hodograph plane as *R*. When the recycle fraction *R* is mixed with the concentrated fresh feed *FF'*, the actual feed composition *F* is obtained. When the SSR process operates at the steady state, the feed point *F*, and thus also the recycle point *R*, must be located on the Γ_+ characteristic that passes through the concentrated fresh feed *FF'*. It will be shown below that the steady state of the process is uniquely determined by specifying (in addition to the purity/yield constraints) the injection volume and one of the following: (1) the amount of fresh feed introduced per cycle, (2) the amount of solvent removed per cycle, or (3) the relative volumes of fresh feed and removed solvent.

In process option II (Fig. 3II), solvent removal is applied to the recycle fraction *R* instead of the fresh feed *F*. In that case, the operating line of the solvent removal unit passes through the origin and the recycle fraction *R*. The resulting composition maps onto point *R'*. Mixing the concentrated recycle fraction *R'* and the fresh feed *FF* together, the actual feed composition *F* is obtained. According to the lever rule, *F* must be located on the line segment between *FF* and *R'*. At steady state, the feed point *F* does not move on the hodograph plane from cycle to cycle, and is located on the same Γ_+ characteristic as the steady state recycle fraction composition *R*. It will be shown below that the performance of option II is identical to option I within certain limits.

In process option III (Fig. 3III), the fresh feed *FF* and the recycle fraction *R* are mixed before solvent removal. The mixture, referred to as *F''*, is located on the line segment between *FF* and *R*. Since solvent is removed from the mixture, the operating line passes through the origin and *F''*. The resulting feed composition maps onto point *F*. Similarly to configurations I and II, the steady state feed composition *F* and the steady state recycle fraction *R* are located on the same Γ_+ characteristic. It will be shown below that option III is the most versatile with respect to the amount of fresh feed that can be processed or the amount of solvent that can be removed per cycle.

The aim of solvent removal is to enhance process performance through increasing the volume of fresh feed that can be fed to the column in each cycle. The question arises, which of these SSR-SR process concepts yields the best process performance? In the following sections, we will investigate the operation of different options. At first, in sections 3.1 and 3.2, the dependency between the volume of fresh feed, the volume of removed solvent and the composition of the steady state feed are considered generally. In section 3.3, a method is presented for predicting the steady state of an SSR-SR process without performing dynamic simulations. At the same time, it will be shown that all SSR-SR options have equal performance when the injection width as well as the volume of fresh feed introduced to the column during each cycle are the same. Finally, in section 3.4, the operation limits of different configurations are compared.

3.1. Dependency between V^{FF} and steady state feed composition

In conventional SSR chromatography, the steady state feed composition and the fresh feed composition are located on the same Γ_+ characteristic on the hodograph plane [15]. Consequently, specifying the purity requirements determines the volume of fresh feed V^{FF} that can be processed per cycle. When solvent removal is applied, the steady state feed composition is no longer located on the same Γ_+ characteristic as the fresh feed (see Fig. 3). The following questions arise: (1) is the volume of fresh feed per cycle in this case fixed by specifying the purities, or is it an independent variable, and (2)
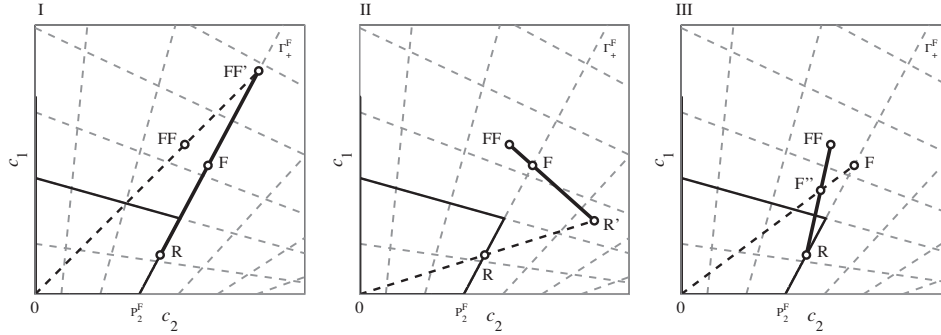
Fig. 3. Schematic representations of alternative SSR-SR configurations in the hodograph plane. (I) Solvent removal from fresh feed. (II) Solvent removal from recycle fraction. (III) Solvent removal from mixed fraction.

if V^{FF} is not fixed, how do it and the location of the steady state feed composition on the hodograph plane depend on each other?

As opposed to the conventional SSR process, the volume of fresh feed is *not* fixed when solvent is removed. This can be shown by considering the amounts of components 1 and 2 in the product fraction *B*. Evidently, the specification of the fresh feed composition, the volume of fresh feed per cycle and purity requirements fixes the masses m_1^B and m_2^B. On the other hand, those masses can be obtained by integrating the rear part of the steady state chromatogram from the cut time τ_{B1} to τ_{B2} [15]:

$$m_1^B = \frac{(1-p^B)(p^A - p^{FF})}{p^{FF}(p^A + p^B - 1)}c_1^{FF}V^{FF} = \left(\int_{\tau_{B1}}^{\tau_{B2}} c_1 \, dt \right) \dot{V} \tag{13}$$

$$m_2^B = \frac{p^B(p^A - p^{FF})}{(1-p^{FF})(p^A + p^B - 1)}c_2^{FF}V^{FF} = \left(\int_{\tau_{B1}}^{\tau_{B2}} c_2 \, dt \right) \dot{V} \tag{14}$$

Time here is presented relative to the end of the injection ($\tau = t - \Delta t_{inj}$) in order to emphasize that the obtained results are independent of the injection width. Explicit expressions for the integral terms are given in Appendix A. Their values depend on the integration limits (τ_{B1}, τ_{B2}) as well as on which Γ_+ characteristic the point *F* is located. Let us denote the characteristic in question by, its slope by Γ_+^F, and the intersection between the characteristic and the c_2 axis by c_2^{PF}. Physically, c_2^{PF} corresponds to the height of the pure component 2 plateau in the tail of the chromatogram. The relationship between ξ_+^F and c_2^{PF} is given by [20]:

$$\xi_+^F = \frac{\alpha - 1 - b_2 c_2^{PF}}{\alpha b_1 c_2^{PF}} \tag{15}$$

When the cut time τ_{B2} is set equal to the time of complete elution of component 2, its value is obtained directly from the adsorption isotherm parameters (see Eq. (8)). Hence, the composition of the product fraction *B* depends on the cut time τ_{B1} and the concentration c_2^{PF} only. These values can be solved from the pair of Eqs. (13) and (14), which has at most one solution (see Appendix B for uniqueness of solution). This means that for every V^{FF} there can be only one characteristic Γ_+^F on which the steady state feed composition can be located. Accordingly, since Γ_+^F is not fixed in the SSR-SR process, neither can V^{FF}. Moreover, if an SSR-SR process is designed by specifying the volume of fresh feed (in addition to purity requirements), the steady state feed composition *F* will always map onto a certain characteristic Γ_+^F irrespective of the injection width.

Let us next investigate how Γ_+^F changes with the amount of fresh feed. As seen in Eq. (B.9), the higher c_2^{PF} is, the shorter τ_{B1} has to be in order to fulfill the purity requirements. In addition, when τ_{B1} is constant, m_2^B increases with the increasing c_2^{PF} (Eq. (B.2)) and, when c_2^{PF} is constant, m_2^B increases with the decreasing τ_{B1} (Eq. (B.5)). This

means that m_2^B, and thus the volume of fresh feed, must increase with the increasing c_2^{PF} with the given purity requirements

$$\left. \frac{\partial V^{FF}}{\partial c_2^{PF}} \right|_{p^B} > 0 \Leftrightarrow \left. \frac{\partial c_2^{PF}}{\partial V^{FF}} \right|_{p^B} > 0 \tag{16}$$

By applying the chain rule to Eqs. (B.9) and (16), it is observed that the cut time τ_{B1} decreases as V^{FF} increases:

$$\left. \frac{\partial \tau_{B1}}{\partial V^{FF}} \right|_{p^B} = \left. \frac{\partial \tau_{B1}}{\partial c_2^{PF}} \right|_{p^B} \left. \frac{\partial c_2^{PF}}{\partial V^{FF}} \right|_{p^B} < 0 \tag{17}$$

In practice, this means that the larger the amount of fresh feed that is introduced to the column during each cycle, the higher a c_2^{PF} and the shorter a τ_{B1} are needed to fulfill the purity requirements. We shall use this information in Section 3.4 to derive operation limits for the various SSR-SR configurations.

3.2. Dependency between V^{FF} and V^{SR}

Let us next analyze how the volume of fresh feed V^{FF} and the volume of removed solvent V^{SR} depend on each other. For all configurations shown in Fig. 3 (in other words, regardless of the position of the solvent removal unit), the following equation holds for the injection width:

$$V_{inj} = V^{FF} + V^R - V^{SR} \tag{18}$$

Because solvent removal does not affect the amounts of components 1 and 2 in the treated fraction (*i.e.* the fraction to which the solvent removal is applied), the two mass balances around the feed node are given by

$$V_{inj}c_1^F = V^{FF}c_1^{FF} + V^R c_1^R \tag{19a}$$

$$V_{inj}c_2^F = V^{FF}c_2^{FF} + V^R c_2^R \tag{19b}$$

In addition, since the steady state feed composition *F* and the steady state recycle fraction composition *R* are located on the same Γ_+ characteristic on the hodograph plane, we can write

$$c_1^F = \xi_+^F(c_2^F - c_2^{PF}) \tag{20a}$$

$$c_1^R = \xi_+^F(c_2^R - c_2^{PF}) \tag{20b}$$

and solve the injection volume by eliminating the steady state feed composition from Eqs. (19a), (19b) and (20a):

$$V_{inj} = \frac{\xi_+^F(V^{FF}c_2^{FF} + V^R c_2^R) - (V^{FF}c_1^{FF} + V^R c_1^R)}{\xi_+^F c_2^{PF}} \tag{21}$$
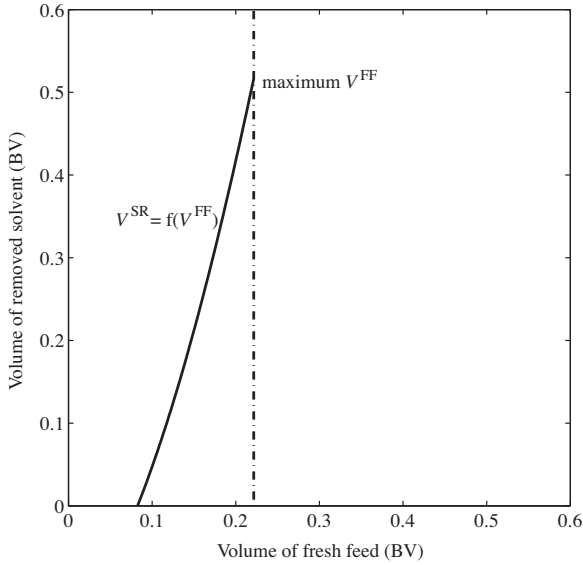
Fig. 4. Effect of fresh feed volume on the required solvent removal capacity as bed volumes in a mixed-recycle SSR-SR process. The calculation method used is described in Section 3.3. Parameters: $c_1^{FF} = c_2^{FF} = 10$ g/L; $F = 1/3$; $q_{m,1} = q_{m,2} = 100$ g/L; $b_1 = 0.02$ L/g; $b_2 = 0.025$ L/g. Purity constraints $p^A = p^B = 0.9$. The dash-dotted line shows the upper limit of V^{FF} that can be achieved (see Section 3.4).

The volume of solvent removed per cycle can now be solved by combining Eqs. (18), (20b) and (21):

$$V^{SR} = V^{FF} \left(1 + \frac{c_1^{FF}}{\xi_+^F c_2^{PF}} - \frac{c_2^{FF}}{c_2^{PF}} \right) \tag{22}$$

As seen in the equation, the volume of the solvent removed during each cycle is independent of the injection width. This means that specifying the volume of fresh feed uniquely fixes the amount of removed solvent.

In addition, it is interesting to note that V^{SR} increases with an increasing V^{FF}. This can be observed by substituting ξ_+^F from Eq. (15) into Eq. (22) and differentiating the resulting equation with respect to c_2^{PF}:

$$\frac{\partial (V^{SR}/V^{FF})}{\partial c_2^{PF}} = \frac{c_1^{FF} \alpha b_1 b_2}{(\alpha - 1 - b_2 c_2^{PF})^2} + \frac{c_2^{FF}}{(c_2^{PF})^2} > 0 \tag{23}$$

By applying the chain rule to Eqs. (16) and (23), we can note that the ratio V^{SR}/V^{FF} must increase with an increasing V^{FF}

$$\frac{\partial (V^{SR}/V^{FF})}{\partial V^{FF}} = \frac{\partial (V^{SR}/V^{FF})}{\partial c_2^{PF}} \frac{\partial c_2^{PF}}{\partial V^{FF}} > 0 \tag{24}$$

and, thus also V^{SR} must increase with an increasing V^{FF}

$$\frac{\partial V^{SR}}{\partial V^{FF}} > 0 \tag{25}$$

Eq. (25) means that the dependency between V^{FF} and V^{SR} is single-valued also the other way around: specifying V^{SR} uniquely fixes V^{FF} with which the desired purity requirements can be satisfied. Moreover, if the process is designed by specifying the ratio V^{FF}/V^{SR}, both parameters are fixed, as can be seen from Eq. (24).

An example of the dependency between the volume of fresh feed and the volume of removed solvent is shown in Fig. 4. As seen in the figure, the more fresh feed is introduced to the column per cycle, the more solvent must be removed. The trend is the same as predicted in Eq. (25). In addition, the curve is convex downward. This means that the solvent removal capacity that is required to

operate an SSR-SR process increases faster than the amount of fresh feed that can be processed per cycle (see Eq. (24)).

Using the findings above, it can also be observed that the volume of the recycle fraction must increase linearly with an increasing injection width. Since both V^{FF} and V^{SR} are independent of V_{inj}, we can differentiate Eq. (18) with respect to the injection width and obtain

$$\frac{\partial V^R}{\partial V_{inj}}\bigg|_{V^{FF}} = 1 \tag{26}$$

Finally, it should be emphasized that these results are also valid when $V^{SR} = 0$, which of course corresponds to the conventional MR-SSR process. By setting $V^{SR} = 0$ in Eq. (22), it is observed that the steady state feed composition must be located on the Γ_+ characteristic passing through the fresh feed composition. This is congruent with the findings by Sainio and Kaspereit [15].

3.3. Method for predicting the steady state of SSR-SR

The previous analysis of dependency between the volume of fresh feed, the volume of removed solvent and the steady state feed composition provides the basis for designing the SSR-SR process. Next, the method by Sainio and Kaspereit [15] to predict the steady state of the conventional SSR process without performing dynamic simulations will be extended to SSR chromatography with solvent removal. The goal is to find the cut times (t_{A1}, t_{A2}, t_{B1} and t_{B2}) such that, in the steady state, arbitrary purity constraints are satisfied.

The main difference between designing SSR processes with and without solvent removal is that there is one more independent variable in the latter case. In the conventional SSR process, the injection width is the only freely chosen operating parameter [15] when the fresh feed composition and the purity requirements are given. In the case of SSR-SR, however, one of the following can be chosen in addition to V_{inj}: (1) the volume of fresh feed per cycle V^{FF}, (2) the volume of solvent removed per cycle V^{SR}, or (3) the ratio V^{SR}/V^{FF} (see Section 3.2). As will be shown below, this choice affects the method for the prediction of the steady state.

Since the fresh feed and the steady state feed compositions are not located on the same Γ_+ characteristic on the hodograph plane, the first step in designing an SSR-SR process is to determine the Γ_+ characteristic passing through the steady state feed composition. The method for determining the parameter Γ_+^F depends on the parameter used as the design criterion. The simplest alternative is to select the ratio between V^{SR} and V^{FF} as a starting point. In that case, the slope ξ_+^F of Γ_+^F is obtained analytically from Eq. (22). The resulting equation is a second order polynomial with respect to ξ_+^F and has only one positive root. When V^{FF} or V^{SR} is used as a design parameter, determining Γ_+^F is somewhat more complicated. c_2^{PF} is solved form the pair of Eqs. (13) and (14) when V^{FF} is specified, and from the set of Eqs. (13), (14) and (22) when V^{SR} is specified. As seen in those equations, an analytic solution is no longer practical (even if possible). The most convenient way is to use a numerical technique for root finding.

When the desired Γ_+^F characteristic has been obtained, the rear part of the chromatogram is known and the cut times (t_{A1}, t_{A2}, t_{B1} and t_{B2}) as well as the steady state feed composition can be solved. The procedure is very similar to the conventional SSR process. At first, the cut time t_{B2} can be obtained from Eq. (8) and t_{B1} should be chosen such that the purity constraints of product fraction B are fulfilled. When calculating the cut time t_{A2}, the volume of the removed solvent V^{SR} has to be taken into account:

$$t_{A2} = t_{B1} - \Delta t_{inj} + \frac{V^{FF} - V^{SR}}{\dot{V}} \tag{27}$$

If V^{FF} or V^{SR} are not used as a design criterion, their values must be solved from Eqs. (9) and (22), respectively, before applying Eq.

(27). It is worth noting that, similarly to conventional MR-SSR, t_{A2} is independent of V_{inj} (since $\tau_{B1} = t_{B1} - \Delta t_{inj}$ is independent of V_{inj}).

The steady state feed composition can be solved from the mass balance around the feed node, Eq. (11). As in the case of conventional MR-SSR, it is independent of the injection width when t_{A2} is located on the injection plateau (*i.e.* for large injection volumes). This can be observed by rewriting Eq. (11) as

$$c_i^F = \frac{\int_{\tau_P}^{\tau_{B1}} c_i d\tau + c_i^{FF}(t_{A2} - \tau_{B1} + (V^{SR}/\dot{V}))}{t_{A2} - \tau_P} \tag{28}$$

where τ_P denotes the elution time of the end of the injection plateau relative to the end of the injection and thus depends on c_i^F and isotherm parameters only.

Finally, the remaining cut time t_A should be equal to the elution time of the pure component 1 shock for minimizing the cycle time. The solution is analogous to that outlined in Section 2.2 for the conventional SSR process.

It is important to note that the previous approach is independent of the process configuration (I–III) concerned. This means that all process options with the same injection width and fresh feed volume per cycle must lead to exactly the same steady state. Consequently, the process performance with the same operating parameters is also identical.

3.4. Feasible range of operation parameters for different SSR-SR configurations

The conclusion above concerning the identical performance of various SSR-SR configurations requires that the same operating parameters can be used for all options. However, this is not always possible. As will be shown shortly, the configurations differ with respect to the amounts of fresh feed that can be processed per cycle, as well as the range of feasible injection widths. Especially the limits for the maximum fresh feed volume and the minimum injection width are not identical. The minimum fresh feed volume, however, is the same for all configurations. In addition, there is no upper limit for the injection volume since the volume of the recycle fraction can be increased without any limits. The limits for different configurations are illustrated in Fig. 5 and can be derived as follows.

Let us first consider the lower limit for the fresh feed volume. As mentioned before, the volume of fresh feed always increases with an increasing volume of removed solvent. This means that the minimum V^{FF} for all three configurations is achieved when $V^{SR} = 0$. Obviously, this corresponds to the operation of the *conventional SSR process*. Since V^{FF} is independent of the injection volume for a certain V^{SR}, the limit is a straight vertical line in Fig. 5 (limit A). The corresponding V^{FF} can be obtained from Eq. (9).

3.4.1. Specific limits for configuration I

In configuration I (solvent removal from fresh feed), the minimum injection volume for a certain V^{FF} is achieved when $V^R = 0$ (limit B in Fig. 5). This can be observed by considering that V_{inj} always increases with an increasing V^R (see Eq. (26)). The condition corresponds to *batch chromatography with solvent removal*. The limit can be constructed in Fig. 5 by giving the ratio V^{SR}/V^{FF} goes upward from 0 (more exactly from 0 to 1, as will be shown shortly) and solving the corresponding V^{FF} and V^{SR} values with the design method described in Section 3.3. The desired V_{inj} values are then obtained from Eq. (18) by setting V^R to 0, which yields $V_{inj,I} = V_I^{FF} - V_I^{SR}$.

The upper limit for the fresh feed volume originates from the fact that V^{SR} can never be larger than the fraction to which the solvent removal is applied. In the case of configuration I, this means that the volume of solvent removed has to be less than the volume of
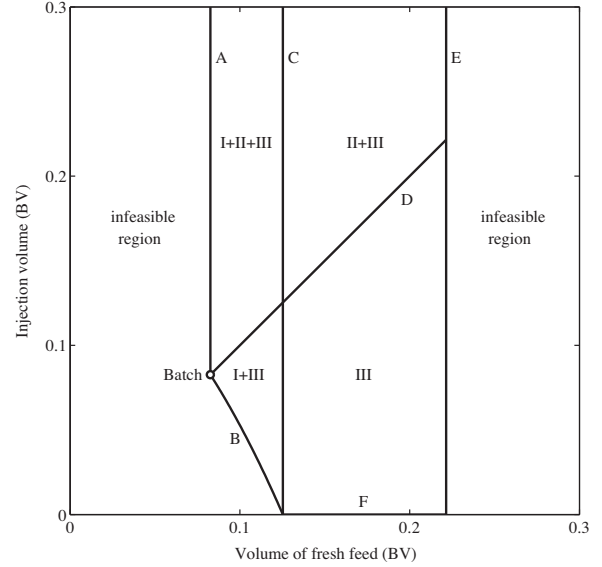

Fig. 5. Regions of feasible operating parameters for different SSR-SR configurations. Limit A: $V^{SR} = 0$ (conventional SSR chromatography), limit B: $V^R = 0$ (batch chromatography with solvent removal), limit C: $V^{SR} = V^{FF}$, limit D: $V^{SR} = V^R$, limit E: $t_{A2} = t_0$, limit F: $V_{inj} = 0$. Feed concentrations, isotherm parameters and purity constraints are the same as in Fig. 4.

fresh feed:

$$V_I^{SR} < V_I^{FF} \tag{29}$$

Hence, the maximum is achieved when $V_I^{SR} = V_I^{FF}$ (*i.e.* $V_I^{SR}/V_I^{FF} = 1$). On the hodograph plane, this corresponds to the situation where the *operating line of the solvent removal unit is parallel to* Γ_+^F. As for Fig. 5, the limit is a vertical line (limit C), the V^{FF} coordinate of which can be obtained by setting $V_I^{SR}/V_I^{FF} = 1$ to Eq. (22), solving the corresponding c_2^{PF}, and finally calculating V^{FF} from Eq. (9).

3.4.2. Specific limits for configuration II

Let us next consider the case of solvent removal from the recycle fraction (option II in Fig. 3). The volume of removed solvent must be less than the volume of the recycle fraction:

$$V_{II}^{SR} < V_{II}^R \tag{30}$$

In addition, V^R increases linearly with an increasing V_{inj}, as mentioned before. This means that the lower limit for the injection width is achieved when $V_{II}^{SR} = V_{II}^R$. Obviously, this corresponds to $V_{inj} = V^{FF}$, and hence in Fig. 5 the limit is a straight line with slope 1 (limit D).

Since solvent removal does not constrain V_{II}^{FF} but V_{II}^{SR} (compare Eqs. (29) and (30)), the volume of fresh feed in option II can be larger than in option I. Of course, this requires that the injection volume is large enough. On the hodograph plane, this means that the steady state feed composition F can be located on a characteristic Γ_+, the slope of which is smaller than c_1^{FF}/c_2^{FF}. However, there is an upper limit for V^{FF} also in option II. This condition is obtained by considering that the cut time t_{A2} must be larger than the elution time of a non-retained component t_0

$$t_{A2} = \tau_{B1} + \frac{V^{FF} - V^{SR}}{\dot{V}} > t_0 \tag{31}$$

It can be shown that the left hand side of the inequality decreases monotonically with an increasing c_2^{PF} and approaches minus infinity when c_2^{PF} approaches its maximum value, the so-called watershed point. This means that there has to be a maximum

V^{FF}, which does not fulfill the condition above (limit E in Fig. 5). The value can be solved numerically by searching for a V^{FF} with which t_{A2} corresponds to t_0.

3.4.3. Specific limits for configuration III

In process option III (solvent removal from the mixed fraction before injection), the volume of the mixed fraction $V^{F''}$ must be larger than the volume of removed solvent V^{SR}

$$V_{III}^{SR} < V_{III}^{F''} = V_{III}^{FF} + V_{III}^{R} \tag{32}$$

In practice, this means that the injection volume must always be positive $V_{inj} > 0$ (limit F in Fig. 5). However, the volume of the recycle fraction cannot be negative in this case, either. For this reason, when $V^{SR}/V^{FF} < 1$ the lower limit of V_{inj} for configuration III is the same as for configuration I (limit B).

As to the upper limit of V^{FF}, configuration III is equal to configuration II (limit E). This means that configuration III is the most flexible one with respect to the injection width and the volume of fresh feed. As can been seen from Fig. 5, there exists no combination of operating parameters V_{inj} and V^{FF} that allows the operation of configuration I or II but not configuration III.

4. Performance evaluation of SSR-SR process

As usual in designing separation processes, it is important to find the operating parameters that lead to optimal process performance. In the present case, the most interesting performance parameters are (1) specific productivity, (2) specific eluent consumption, and (3) the average product concentrations. The productivity and the eluent consumption are here defined for component 1 (and analogously for component 2) as follows:

$$PR_1 = \frac{m_1^A}{\Delta t_{cycle}} = \frac{Y_1 c_1^{FF} V^{FF}}{\Delta t_{cycle}} \tag{33}$$

$$EC_1 = \frac{\dot{V}\Delta t_{cycle} - V_{inj} - V^{SR}}{Y_1 c_1^{FF} V^{FF}} \tag{34}$$

As seen in the latter equation, it is assumed that the removed solvent can be used as eluent in the process. Evidently, this reduces the need for fresh eluent. The average concentration of product fraction A is defined with respect to component 1 and the average concentration of product fraction B with respect to component 2:

$$\bar{c}_1^A = \frac{m_1^A}{(t_{A2} - t_{A1})\dot{V}} = \frac{1}{t_{A2} - t_{A1}} \int_{t_{A1}}^{t_{A2}} c_1 dt \tag{35}$$

$$\bar{c}_2^B = \frac{m_2^B}{(t_{B2} - t_{B1})\dot{V}} = \frac{1}{t_{B2} - t_{B1}} \int_{t_{B1}}^{t_{B2}} c_2 dt \tag{36}$$

To predict the optimum performance of different SSR-SR configurations, the system is assumed to operate in "stacked injections" mode. This means that injection times are chosen so that no gaps exist between fraction B and fraction A of the following cycle. Hence, the cycle time is

$$\Delta t_{cycle} = t_{B2} - t_{A1} = \Delta t_{inj} + \tau_{B2} - t_{A1} \tag{37}$$

Since τ_{B2} is always independent of the injection width, the effect of V^{FF} on the cycle time depends only on the behavior of t_{A1}. According to our understanding, the derivative $\partial t_{A1}/\partial \Delta t_{inj}$ is always non-negative but less than unity, which yields

$$0 < \left.\frac{\partial \Delta t_{cycle}}{\partial \Delta t_{inj}}\right|_{V^{FF}} = 1 - \left.\frac{\partial t_{A1}}{\partial \Delta t_{inj}}\right|_{V^{FF}} \leq 1 \tag{38}$$

The behavior is similar to the case of conventional SSR. The equality sign refers to large injections with witch the pure component 1 plateau is not eroded and the cut time t_{A2} is located on

the injection plateau. This can be seen considering that in this case the steady state feed composition and thus also the cut time t_{A1} are independent of the injection width. On the other hand, when small injection volumes are applied, no closed form expression for derivative $\partial t_{A1}/\partial \Delta t_{inj}$ can be given. However, a parametric analysis using the approach by Guiochon et al. [20] for the calculation of t_{A1} and applying small and large separation factors, low and high purities as well as weakly and strongly non-linear adsorption isotherms implied that the inequality above is valid also when solvent removal is applied.

4.1. Effect of injection volume on performance parameters

When evaluating the performance of the SSR-SR process, the valuable findings concerning conventional SSR chromatography can be exploited (see Section 2.3). Obviously, the SSR-SR configuration I is equivalent to a conventional SSR chromatography process (no solvent removal) if the feed concentration of the latter is

$$c_{SSR}^{FF} = \frac{V_I^{FF}}{V_I^{FF} - V_I^{SR}} c_{SSR-SR}^{FF} \tag{39}$$

In addition, in Section 3.3 it was shown that all three SSR-SR options have identical performance when the same operating parameters are used. This means that the results obtained by Sainio and Kaspereit [15] are valid for all SSR-SR configurations as far as they are operated in region which is feasible for configuration I (see Fig. 5). Consequently, for a certain solvent removal capacity (i.e. also for a certain V^{FF}) productivity always decreases with an increasing injection volume. Moreover, eluent consumption decreases and average concentrations in product fraction A increase with an increasing injection width until they level off as the injection volume becomes sufficiently large. The limit is achieved when t_{A2} is located on the injection plateau. Average concentrations in product fraction B are, in contrast, always independent of the injection width. Comparing the SSR-SR process with optimized batch chromatography with the same V^{SR} (i.e. $c_{batch}^{FF} = c_{SSR}^{FF}$ from Eq. (39)), the recycling scheme is always better in terms of the specific eluent consumption and concentration of the first product fraction. As to the specific productivity, batch chromatography is better.

The results above concerning the operation area of configuration I can be easily extended also to other regions. By differentiating Eqs. (33)–(36) with respect to the injection volume and accepting the empirical inequality in Eq. (38), the following expressions are obtained:

$$\left.\frac{\partial PR_1}{\partial \Delta t_{inj}}\right|_{V^{FF}} = -\frac{Y_1 c_1^{FF} V^{FF}}{(\Delta t_{cycle})^2} \left.\frac{\partial \Delta t_{cycle}}{\partial \Delta t_{inj}}\right|_{V^{FF}} < 0, \tag{40}$$

$$\left.\frac{\partial EC_1}{\partial \Delta t_{inj}}\right|_{V^{FF}} = \frac{\dot{V}}{Y_1 c_1^{FF} V^{FF}} \left(\left.\frac{\partial t_{cycle}}{\partial \Delta t_{inj}}\right|_{V^{FF}} - 1 \right) \leq 0, \tag{41}$$

$$\left.\frac{\partial \bar{c}_1^A}{\partial \Delta t_{inj}}\right|_{V^{FF}} = \left.\frac{\partial}{\partial \Delta t_{inj}} \left(\frac{Y_1 c_1^{FF} V^{FF}}{(t_{A2} - t_{A1})\dot{V}} \right)\right|_{V^{FF}}$$
$$= \frac{Y_1 c_1^{FF} V^{FF}}{(t_{A2} - t_{A1})^2 \dot{V}} \left.\frac{\partial t_{A1}}{\partial \Delta t_{inj}}\right|_{V^{FF}} \geq 0, \tag{42}$$

$$\left.\frac{\partial \bar{c}_2^B}{\partial \Delta t_{inj}}\right|_{V^{FF}} = \left.\frac{\partial}{\partial \Delta t_{inj}} \left(\frac{Y_2 c_2^{FF} V^{FF}}{(t_{B2} - t_{B1})\dot{V}} \right)\right|_{V^{FF}} = 0 \tag{43}$$

As can be seen, these are equivalent with the findings above. In addition, the same results for productivity and eluent consumption are obtained if the analysis is carried out for component 2.

Regions for optimal operation conditions concerning different performance parameters are presented in Fig. 6. The curve line G
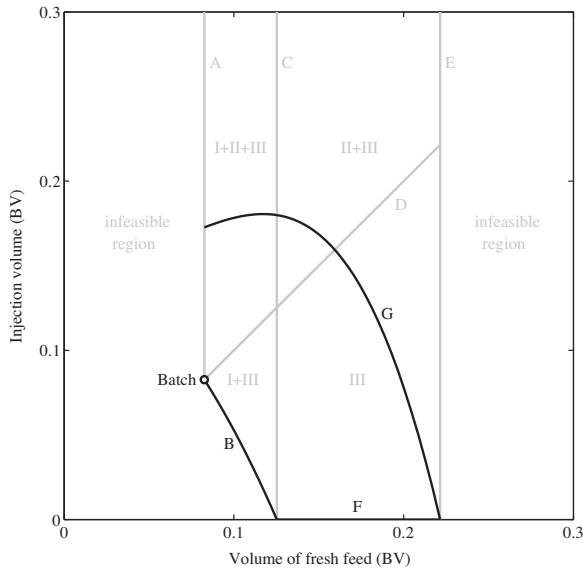
Fig. 6. Limits of optimal operating parameters for the SSR-SR process. For a certain V^{FF}, maximum productivity is obtained at the limits B and F. Minimum eluent consumption and maximum product concentrations in fraction A are obtained at the limit G and above it. Gray background: regions of feasible operating parameters for different SSR-SR configurations (see Fig. 5). Feed concentrations, isotherm parameters and purity constraints are the same as in Fig. 4.

corresponds to the maximum injection width with which the injection plateau is not recycled. As can be seen in Eqs. (41) and (42), the minimum eluent consumption and maximum product concentrations of fraction A for a certain V^{FF} are obtained at this limit and above it. In contrast, as to the productivity, the optimum is always achieved with the smallest possible injection width (see Eq. (40)). In Fig. 6, this corresponds on limits B and F.

As seen from Fig. 6, for a certain V^{FF} the process option I can be operated both at the point of maximum productivity and in the region of the minimum eluent consumption. However, the maximum fresh feed volume that can be obtained is lower than in other cases, as mentioned already in Section 3.4. In configuration II, the value chosen for V^{FF} can be more flexible, but the maximum productivity is never achieved. All this means that the optimum operating point, which is naturally a trade-off between different performance parameters as well as the required solvent removal capacity, may be located in a region where only the process scheme III can be operated. Such calculations are beyond the scope of this work, however.

4.2. Simulation of process performance with a generic example

The design method presented above can be used to compare the performance of different SSR-SR process configurations. In particular, the effect of the operating parameters V^{FF} and V_{inj} on the specific productivity, the specific eluent consumption, and the average product concentrations were of interest here. The simulations were carried out with a generic model system. The feed concentrations
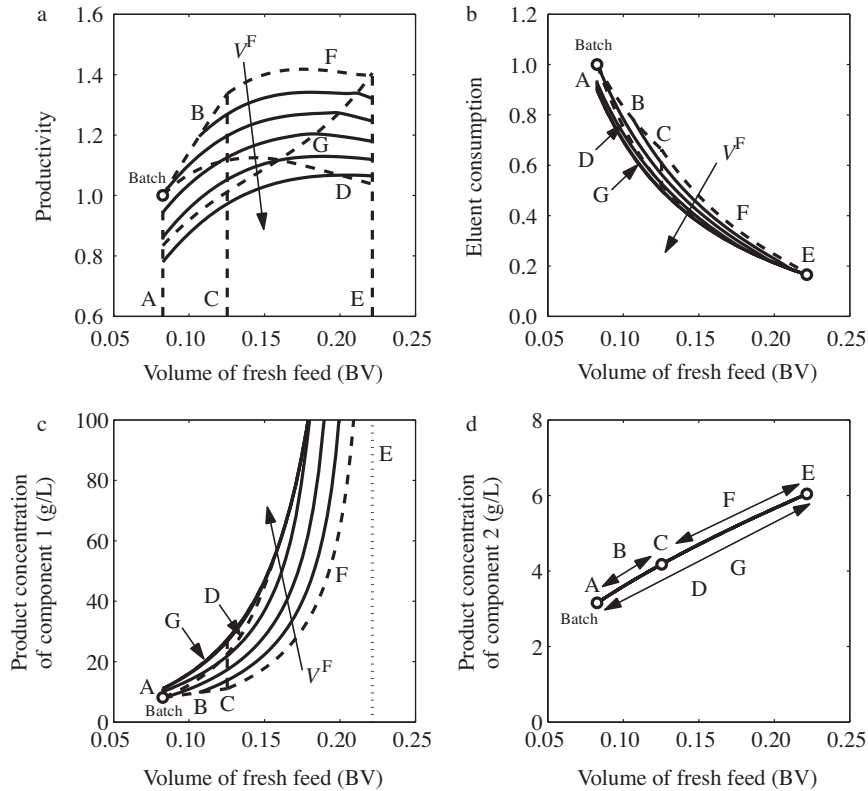
Fig. 7. Effect of volume of fresh feed and injection volume on the performance of mixed-recycle SSR chromatography with solvent removal. The direction of increasing injection volume (0.04, 0.08, 0.12, 0.16 and 0.20 BV) is indicated with an arrow. Feed concentrations and isotherm parameters are given in the text. Circles: batch chromatography without solvent removal; dashed lines: operation limits of SSR-SR configurations (limits A–G in Figs. 5 and 6).

were $c_1^{FF} = c_2^{FF} = 10$ g/L, the phase ratio $F = 1/3$, and the parameters of Langmuir isotherms, Eq. (7), $q_{m,1} = q_{m,2} = 100$ g/L, $b_1 = 0.02$ L/g and $b_2 = 0.025$ L/g. The purity constrains of both product fractions were set equal to 0.9.

The dependence of the performance parameters on the volume of fresh feed and the injection volume is displayed in Fig. 7. Because the same feed concentrations and purity requirements were used for both components, the productivities and eluent consumptions behave identically. The white circles in the subfigures represent the performance of batch chromatography without solvent removal and the dashed lines the operation limits of various SSR-SR configurations (limits A–G in Figs. 5 and 6).

It is observed in Fig. 7a that productivity increases with an increasing V^{FF}. It is interesting to note that an SSR-SR process can achieve a higher productivity than an optimized batch chromatography process that also employs solvent removal (line B in Fig. 7a). In this respect, SSR-SR is fundamentally different from conventional SSR. However, this condition requires that the volume of removed solvent is larger than the volume of fresh feed (see also Fig. 5, limit C). In other words, the SSR-SR must operate in an area that is not feasible for batch chromatography with solvent removal or for the SSR-SR configuration I. Considering that the solvent removal capacity required to operate SSR-SR increases rapidly with V^{FF} (see Fig. 4), the economic optimum might not be where the productivity is the highest. As mentioned before, such calculations are beyond the scope of this work, however.

It can also be observed from Fig. 7a that productivity decreases with an increasing V_{inj} (direction of the arrows). This effect is the same as predicted in Eq. (40) and can be explained in a similar way as in the case of a conventional SSR process [15]. When the volume of fresh feed is constant, the volume of the recycle fraction increases rapidly with the increasing injection volume. Hence, less fresh feed is introduced compared to the size of the recycle fraction, and the operation is less efficient. This means that when the ratio V^{SR}/V^{FF} is less than 1 (Fig. 5, limit C), batch chromatography with solvent removal always outperforms SSR-SR chromatography in terms of productivity. When the ratio V^{SR}/V^{FF} is at least 1, the optimum injection volume (with respect to productivity) is zero.

In Fig. 7b, it is seen that the eluent consumption decreases with an increasing volume of fresh feed. The trend originates from two different causes. Firstly, the amounts of components in the product fractions increase as V^{FF} increases. This means that the denominator in Eq. (34) increases, and thus the specific eluent consumption decreases. Secondly, the more fresh feed is introduced into the column, the more solvent has to be removed. As mentioned before, the removed solvent can be used as eluent, and less fresh eluent is needed.

The effect of the injection volume on the eluent consumption is congruent with Eq. (41) and the findings by Sainio and Kaspereit [15]. The eluent consumption decreases with an increasing injection volume until it levels off as the injection volume becomes sufficiently large. The limit is achieved when the injection plateau is recycled.

Using a larger volume of fresh feed also results in higher concentrations of components 1 and 2 in product fractions A and B, respectively (Fig. 7c and d). It is interesting to note that when the volume of fresh feed approaches its maximum value (limit E), the product concentrations in fraction A approach infinity. However, the concentrations in fraction B remain finite. Similarly to conventional SSR, the injection volume has no effect on the average concentrations in the product fraction B, as predicted in Eq. (43). Moreover, the average concentrations in the product fraction A become independent of the injection volume when t_{A2} is located on the injection plateau (see Eq. (42)).

5. Conclusions

Operation and performance of mixed-recycle SSR chromatography with solvent removal was analyzed theoretically in the framework of the equilibrium theory. A method was developed to choose *a priori* the cut times for fractionating the outlet stream of the chromatography column so that the user-given purity and/or yield specifications are fulfilled. With this approach, the steady state is obtained on the basis of adsorption isotherm parameters only, without performing dynamic simulations. The amount of fresh feed introduced per cycle and the injection width were identified as the only free operating parameters. A relationship was derived between the amount of fresh feed and the solvent removal capacity required to achieve the chosen purities.

The following three process configurations were investigated: (I) solvent removal is applied to the fresh feed, (II) solvent removal is applied to the recycle fraction, and (III) solvent removal is applied after mixing the recycle fraction and the fresh feed. It was shown that, due to solvent removal, it is possible to treat more fresh feed in each cycle in an SSR-SR process than in the conventional SSR concept. In addition, it was demonstrated that specifying the volume of fresh feed (together with the purity requirements) fixes the volume of solvent that has to be removed. The solvent removal capacity was shown to increase rapidly with the amount of fresh feed introduced to the column per cycle.

The theoretical analysis also revealed that all three SSR-SR configurations have identical performance when the same operating parameters, *i.e.* injection volume and fresh feed volume, are used. However, the maximum amounts of fresh feed that can be processed per cycle, as well as the range of feasible injection widths, are not identical. With respect to the considered process performance parameters, the configuration where solvent removal is applied after mixing the recycle fraction with the fresh feed is the most flexible one and can provide the highest performance.

SSR-SR chromatography was shown to have a lower eluent consumption and higher concentration of the first product fraction compared to batch chromatography with the same solvent removal capacity. As to the productivity, the optimized batch operation with solvent removal outperforms SSR-SR when solvent is removed from the fresh feed. However, when the solvent removal in SSR-SR is applied to the mixed fraction, higher productivity can be achieved than in the optimized batch operation.

Finally, it should be reminded that the theory presented in this work is based on the equilibrium theory of chromatography with assumption of infinite column efficiency. For this reason, the approach is most applicable for high performance systems, while some conclusions may not be valid for systems of moderate or low efficiency. However, we believe that the proposed approach can be used in many real industrial applications to predict the preliminary operating parameters which can be later optimized by detailed simulations. In practice, solvent removal in a chromatographic process has also some limitations that were not considered here. The solubility of the solutes or the viscosity of the concentrated solution may limit the amount of solvent that can be removed.

Nomenclature

A	coefficient matrix in Eq. (5)
a	coefficient of the Langmuir isotherm
b	Langmuir parameter (L/mol or L/g)
c	concentration (mol/L or g/L)
$\bar{c}$	average concentration in a product fraction (mol/L or g/L)
F	phase ratio

EC   eluent consumption
m mass (g)
p^j purity of fraction j with respect to a target component
P_i pure component plateau in a chromatogram with constant concentration of i
PR   productivity
q stationary phase concentration (mol/L or g/L)
q_m saturation capacity of the adsorbent (mol/L or g/L)
t time relative to beginning of cycle (min)
t_0 elution time of a non-retained component (min)
u interstitial velocity (m/min)
V volume (L or BV)
$\dot{V}$ volume flow rate (L/min)
x space coordinate (m)
Y yield with respect to a target component

Greek symbols
α separation factor
Γ characteristic of a simple wave
γ auxiliary parameter in Eqs. (A.1)–(A.5)
ξ slope of the characteristic in the hodograph plane
Σ shock wave
τ time relative to the end of injection (min)
τ_R^0 retention time at infinite dilution relative to the end of injection (min)

Subscripts
1, 2   components to be separated
I, II, III   type of SSR-SR process configuration
A1   beginning of product fraction A
A2   end of product fraction A
B1   beginning of product fraction B
B2   end of product fraction B
cycle   cycle of an SSR process
E1   end of mixed zone
E2   end of elution profile
I   end of pure component 2 plateau
inj   injection
P   end of injection plateau
+   faster wave or shock
−   slower wave or shock

Superscripts
A   product fraction A
B   product fraction B
F   steady state feed
F′   steady state feed before solvent removal
FF   fresh feed before solvent removal
FF′   fresh feed after solvent removal
P   pure component plateau
R   recycle fraction before solvent removal
R′   recycle fraction after solvent removal
SR   solvent removal

Appendix A. Integral terms in Eqs. (13) and (14)

In this appendix, analytical expressions for the integral terms in Eqs. (13) and (14) are given. The elution profiles of components 1 and 2 as a function of time are given by Guiochon et al. [20] for the mixed wave as in Eqs. (A.1) and (A.2):

$$c_1 = \frac{1}{b_1 + b_2/(\alpha \xi_+^F)} \left[\sqrt{\frac{\gamma}{\alpha} \frac{\tau_{R,1}^0 - t_0}{\tau - t_0}} - 1 \right] \tag{A.1}$$

$$c_2 = \frac{1}{b_2 + \alpha b_1 \xi_+^F} \left[\sqrt{\gamma \frac{\tau_{R,2}^0 - t_0}{\tau - t_0}} - 1 \right] \tag{A.2}$$

and for the pure component 2 wave as in Eq. (A.3):

$$c_2 = \frac{1}{b_2} \left[\sqrt{\gamma \frac{\tau_{R,2}^0 - t_0}{\tau - t_0}} - 1 \right] \tag{A.3}$$

The following parameters are used in Eqs. (A.1)–(A.3). The initial slope of the Langmuir isotherm is $a_i = b_i q_{m,i}$, the separation factor $\alpha = a_2/a_1$, the retention time at infinite dilution $\tau_{R,i}^0 = t_0(1 + Fa_i)$, and an auxiliary parameter $\gamma = \alpha/(1 + b_2 c_2^{PF})$.

The integration limits are the end time of the mixed zone, Eq. (A.4), the end time of the pure component 2 concentration plateau, Eq. (A.5), and the end time of the elution profile, Eq. (A.6).

$$\tau_{E1} = t_0 \left(1 + \frac{\gamma Fa_1}{\alpha} \right) \tag{A.4}$$

$$\tau_I = t_0 \left[1 + Fa_2 \left(\frac{\gamma}{\alpha} \right)^2 \right] \tag{A.5}$$

$$\tau_{E2} = t_0(1 + Fa_2) \tag{A.6}$$

By employing these equations, the integral term in Eq. (13) can be integrated analytically to give

$$\int_{\tau_{B1}}^{\tau_{B2}} c_1 \, dt = \int_{\tau_{B1}}^{\tau_{E1}} c_1 \, dt = \frac{\alpha - 1 - b_2 c_2^{PF}}{b_1(\alpha - 1)} \left[\tau_{B1} + t_0 \left(\frac{Fa_1}{1 + b_2 c_2^{PF}} - 1 \right) \right. $$
$$\left. - 2 \sqrt{\frac{t_0 Fa_1}{1 + b_2 c_2^{PF}} (\tau_{B1} - t_0)} \right] \tag{A.7}$$

and the integral term in Eq. (14) to give

$$\int_{\tau_{B1}}^{\tau_{B2}} c_2 \, dt = \int_{\tau_{B1}}^{\tau_{E1}} c_2 \, dt + \int_{\tau_{E1}}^{\tau_I} c_2 \, dt + \int_{\tau_I}^{\tau_{E2}} c_2 \, dt = \frac{c_2^{PF}}{(\alpha - 1)} \left[\tau_{B1} \right.$$
$$\left. + t_0 \left(\frac{(2\alpha - 1)Fa_1}{1 + b_2 c_2^{PF}} - 1 \right) - 2\alpha \sqrt{\frac{t_0 Fa_1}{1 + b_2 c_2^{PF}} (\tau_{B1} - t_0)} \right]$$
$$+ t_0 Fa_1 c_2^{PF} \left[\frac{\alpha}{(1 + b_2 c_2^{PF})^2} - \frac{1}{1 + b_2 c_2^{PF}} \right]$$
$$+ \frac{t_0 Fa_2}{b_2} \left(1 - \frac{1}{1 + b_2 c_2^{PF}} \right)^2 \tag{A.8}$$

Appendix B. Uniqueness of solution to pair of Eqs. (13) and (14)

An essential intermediate result in the analysis of SSR-SR is the fact that specifying V^{FF} (in addition to purity or yield requirements) determines the characteristic Γ_+^F onto which F will map in the steady state. This characteristic is independent of the injection width. This holds true if the pair of Eqs. (13) and (14) has a unique solution, which can be shown as follows.

If we determine the cut time τ_{B1} as a function of c_2^{PF} so that the purity p^B matches a design constraint, we get a strictly decreasing curve. The same applies if we determine τ_{B1} as a function of c_2^{PF} so that the mass m_1^B, given on the left in Eq. (13), is correct. In contrast, when we determine τ_{B1} so that m_2^B is correct, a strictly increasing curve is obtained. This can be observed as follows.

When the cut time τ_{B1} is held at a fixed value but c_2^{PF} is increased (*i.e.* the height of the pure component 2 plateau increases), the amount m_1^B decreases (due to enhanced displacement) and m_2^B increases:

$$\left.\frac{\partial m_1^B}{\partial c_2^{PF}}\right|_{\tau_{B1}} < 0 \tag{B.1}$$

$$\left.\frac{\partial m_2^B}{\partial c_2^{PF}}\right|_{\tau_{B1}} > 0 \tag{B.2}$$

Thus, the purity of the product fraction B must also increase with an increasing c_2^{PF}:

$$\left.\frac{\partial p^B}{\partial c_2^{PF}}\right|_{\tau_{B1}} > 0 \tag{B.3}$$

In addition, for a constant c_2^{PF} but a decreasing τ_{B1} (*i.e.* the increasing length of product fraction B along a chosen Γ_+ characteristic), m_1^B and m_2^B both increase, whereas p^B decreases.

$$\left.\frac{\partial m_1^B}{\partial \tau_{B1}}\right|_{c_2^{PF}} < 0 \tag{B.4}$$

$$\left.\frac{\partial m_2^B}{\partial \tau_{B1}}\right|_{c_2^{PF}} < 0 \tag{B.5}$$

$$\left.\frac{\partial p^B}{\partial \tau_{B1}}\right|_{c_2^{PF}} > 0 \tag{B.6}$$

By applying the triple product rule to Eqs. (B.1) and (B.4), to Eqs. (B.2) and (B.5) and to Eqs. (B.3) and (B.6), we can determine the sign of the partial derivatives of τ_{B1} with respect to c_2^{PF} in the case of a constant m_1^B, m_2^B, and p^B, as shown in Eqs. (B.7)–(B.9). These are equivalent to our statements above:

$$\left.\frac{\partial \tau_{B1}}{\partial c_2^{PF}}\right|_{m_1^B} < 0 \tag{B.7}$$

$$\left.\frac{\partial \tau_{B1}}{\partial c_2^{PF}}\right|_{m_2^B} > 0 \tag{B.8}$$

$$\left.\frac{\partial \tau_{B1}}{\partial c_2^{PF}}\right|_{p^B} < 0 \tag{B.9}$$

Evidently, the solution of the equation pair (13) and (14) can be found from the intersection of the curves $\tau_{B1} = f(c_2^{PF})_{m_1^B}$, $\tau_{B1} = f(c_2^{PF})_{p_2^B}$ and $\tau_{B1} = f(c_2^{PF})_{p^B}$. Because strictly increasing and strictly decreasing curves can have only one intersection, also the pair of Eqs. (13) and (14) has only one solution.

References

[1] K.J. Bombaugh, W.A. Dark, R.F. Levangie, High-resolution steric chromatography, J. Chromatogr. Sci. 7 (1969) 42–47.
[2] A. Seidel-Morgenstern, G. Guiochon, Theoretical study of recycling in preparative chromatography, AIChE J. 39 (1993) 809–819.
[3] C. Heuer, A. Seidel-Morgenstern, P. Hugo, Experimental investigation and modeling of closed-loop recycling in preparative chromatography, Chem. Eng. Sci. 50 (1995) 1115–1127.
[4] C.M. Grill, Closed-loop recycling with periodic intra-profile injection: a new binary preparative chromatographic technique, J. Chromatogr. A 796 (1998) 101–113.
[5] C.M. Grill, L. Miller, Separation of a racemic pharmaceutical intermediate using closed-loop steady state recycling, J. Chromatogr. A 827 (1998) 359–371.
[6] C.M. Grill, L. Miller, T.Q. Yan, Resolution of a racemic pharmaceutical intermediate. A comparison of preparative HPLC, steady state recycling, and simulated moving bed, J. Chromatogr. A 1026 (2004) 101–108.
[7] J. Kennedy, M. Belvo, V. Sharp, J. Williams, Comparison of separation efficiency of early phase active pharmaceutical intermediates by steady state recycle and batch chromatographic techniques, J. Chromatogr. A 1046 (2004) 55–60.
[8] T.Q. Yan, C. Orihuela, Rapid and high throughput separation technologies-Steady state recycling and supercritical fluid chromatography for chiral resolution of pharmaceutical intermediates, J. Chromatogr. A 1156 (2007) 220–227.
[9] J.W. Lee, P.C. Wankat, Comparison of recycle chromatography and simulated moving bed for pseudobinary separations, Ind. Eng. Chem. Res. 48 (2009) 7724–7732.
[10] M. Bailly, D. Tondeur, Recycle optimization in nonlinear productive chromatography. I. Mixing recycle with fresh feed, Chem. Eng. Sci. 37 (1982) 1199–1212.
[11] M. Bailly, D. Tondeur, Reversibility and performances in productive chromatography, Chem. Eng. Process. 18 (1984) 293–302.
[12] D. Tondeur, M. Bailly, in: P. Barker, G. Ganetsos (Eds.), Preparative and Production-scale Chromatography, Chromatographic Science Series, vol. 61, Marcel-Dekker, New York, 1993, pp. 79–109.
[13] F. Charton, Optimisation des coupes et recyclages en chromatographie préparative industrielle, PhD thesis, Institut National Polytechnique de Lorraine, Nancy, 1995.
[14] F. Charton, M. Bailly, G. Guiochon, Recycling in preparative liquid chromatography, J. Chromatogr. A 687 (1994) 13–31.
[15] T. Sainio, M. Kaspereit, Analysis of steady state recycling chromatography using equilibrium theory, Sep. Purif. Technol. 66 (2009) 9–18.
[16] M. Bailly, R.-M. Nicoud, A. Philippe, O. Ludemann-Hombourger, Method and device for chromatography comprising a concentration step, U.S. Patent Application No. WO204039468, 2004.
[17] S. Abdelmoumen, L. Muhr, M. Bailly, O. Ludemann-Hombourger, The M3C process: a new multicolumn chromatographic process integrating a concentration step. I—the equilibrium model, Sep. Sci. Technol. 41 (2006) 2639–2663.
[18] G. Paredes, H.-K. Rhee, M. Mazzotti, Design of simulated-moving-bed chromatography with enriched extract operation (EE-SMB): Langmuir isotherms, Ind. Eng. Chem. Res. 45 (2006) 6289–6301.
[19] M. Kaspereit, K. Gedicke, V. Zahn, A.W. Mahoney, A. Seidel-Morgenstern, Shortcut method for evaluation and design of a hybrid process for enantioseparations, J. Chromatogr. A 1092 (2005) 43–54.
[20] G. Guiochon, D.G. Shirazi, A. Felinger, A.M. Katti, Fundamentals of Preparative and Nonlinear Chromatography, Academic Press, Boston, 2006.
[21] H.-K. Rhee, R. Aris, N.R. Amundson, First-order Partial Differential Equations Theory and Applications of Hyperbolic Systems of Quasilinear Equations, vol. II, Dover Publications, Mineola, N.Y., 2001.

Thermal effects in reactive liquid chromatography

T. Sainio[a,*], M. Kaspereit[b], A. Kienle[b,c], A. Seidel-Morgenstern[b,c]

[a]*Lappeenranta University of Technology, Skinnarilankatu 34, FIN-53850 Lappeenranta, Finland*
[b]*Max-Planck-Institut für Dynamik komplexer technischer Systeme, Sandtorstrasse 1, D-39106 Magdeburg, Germany*
[c]*Otto-von-Guericke-Universität, Universitätsplatz 2, D-39106 Magdeburg, Germany*

Abstract

Thermal effects in unsteady-state liquid phase chromatographic reactors were investigated experimentally in a thermally insulated column. In the case of an exothermic esterification reaction catalyzed by an acidic ion-exchange resin, a self-amplifying positive thermal wave was found to develop in the reactor. This improved the reactor performance considerably when compared to isothermal conditions: both conversion of reactants and the mole ratio of the desired and undesired products in a product fraction increased. The heat of reaction, enthalpy of adsorption, and heat of mixing all contribute to the thermal behavior of the reactor. The coupling between the concentration fronts and thermal waves was elucidated by means of numerical simulations. The solid phase to fluid phase heat capacity ratio was found to be an important parameter because it affects the magnitude and propagation velocities of the thermal waves.
© 2007 Elsevier Ltd. All rights reserved.

Keywords: Chromatographic reactor; Non-isothermal reactor; Thermal effects; Process intensification; Ion-exchange resin; Esterification

1. Introduction

In reactive chromatography, chemical reactions and chromatographic separation of the products are combined into a single unit operation. The aim of the method is to increase conversion of the reactants and product purity. Characteristic to reactive chromatographic processes is their transient behavior. When carried out batchwise in a single column unit, pulses of reactants are eluted through the reactor. In a continuous simulated moving bed reactor (Mazzotti et al., 1996), periodic switching of the inlet and outlet ports in the direction of fluid flow generates a periodic, quasi-steady state with moving concentration fronts in each column.

Owing to the dynamic nature of the process, there is continuous generation or consumption of heat due to enthalpies of adsorption, chemical reaction, and mixing. In addition, thermal effects can also originate from viscous heat dissipation, especially in HPLC columns packed with fine particles (Brandt et al., 1997). Such phenomena should be taken into account in scale-up of the reactor concept because increasing the column

diameter eventually renders the system nearly adiabatic. Until recently (Sainio, 2005), thermal effects in liquid phase chromatographic reactors have been overlooked and the literature is limited to isothermal conditions. Meurer (1999) briefly discussed the factors involved in non-isothermal operation, but thermal effects were considered to be small and no experimental or numerical investigation was carried out. This is in contrast with reactive gas–solid separation processes, where thermal effects are commonly included in mathematical modeling (Yongsunthon and Alpay, 1999; Xiu et al., 2002).

The aim of this work is to demonstrate how thermal effects can significantly affect conversion and separation in non-isothermal liquid phase chromatographic reactors. Experimental results for esterification of acetic acid with ethanol, catalyzed by an acidic ion-exchange resin, are shown. Influences of adsorption and mixing enthalpies on the thermal behavior of the reactor are illustrated with data from non-reactive experiments. Numerical simulations are presented to further elucidate the coupling between concentration and temperature waves in the reactor. The results demonstrate that—analogous to gas–solid reactors (Glöckler et al., 2003)—the solid phase to fluid phase heat capacity ratio is a major factor in non-isothermal unsteady-state liquid phase chromatographic reactors.

* Corresponding author. Tel.: +358 5 6212269; fax: +358 5 6212199.
 E-mail address: tuomo.sainio@lut.fi (T. Sainio).

2. Materials and methods

A sulfonated poly(styrene-*co*-divinylbenzene) cation-exchange resin in H^+ form was used as the stationary phase in the chromatographic reactor experiments. KEF76 resin (Finex Oy, Finland) has a mesoporous structure and a moderate level of cross-linking (see Table 1). Esterification of acetic acid with ethanol served as a model reaction. Reagent grade chemicals were used as received in all experiments. The properties of the chemicals, shown in Table 2, yield a reaction heat $\Delta_{rxn}H = -4.6\,kJ/mol$ and a reaction Gibbs energy change $\Delta_{rxn}G = -6.5\,kJ/mol$.

A glass column (inner diameter 2.6 cm), covered with a 3 cm layer of rock wool for thermal insulation, was used as the reactor. Six thermocouples were fitted into the column such that the first was located 4.7 cm from the inlet and the others 6.8 cm from each other. Experiments under isothermal conditions were carried out as a reference in a jacketed reactor of the same size.

Chemical analysis of the effluent stream was carried out with an in-line FT-IR spectrophotometer (Bomem MB155S) at the near infra-red region. A multivariate PLS calibration model for the spectrometer consisted of approximately 70 multicomponent samples with non-stoichiometric compositions, enabling determination of the mole fractions of all four chemical components independently. In order to validate the FT-IR analysis, part of the liquid phase samples were analyzed also with a gas chromatograph (HP 5890 series II) using a thermoconductive detector. The average relative difference between the two methods was approximately 5%.

The column was packed with the resin from a water suspension and equilibrated with ethanol prior to the esterification reaction experiments. Displacement of water was carried out with top-bottom flow at $5.0\,cm^3\,min^{-1}$. The feed concentration was changed from 94 wt% EtOH to 99.5 wt% after 50 min.

In the initial state of the reaction experiments, the height of the resin bed was 47.5 cm, and the upper flow distributor was adjusted to remove dead volume formed during displacement and so that the bed was under slight axial compression. In the reaction experiments, an equimolar mixture of ethanol and acetic acid was continuously fed into the column at a flow rate of $5.0\,cm^3\,min^{-1}$ at a temperature of 293 K. Regeneration of the column was not investigated.

3. Experimental results and discussion

An important design objective for the esterification of acetic acid with ethanol in a chromatographic reactor is to minimize the water content in the product fraction containing ethyl acetate. Typical experimental results, as are displayed in Fig. 1, show that the application of a chromatographic reactor facilitates this objective. Analysis of the concentration profiles in similar experiments under isothermal conditions has been given by Mazzotti et al. (1997) and is not repeated here.

As seen in Fig. 1, the non-isothermal reactor yields considerably higher maximum concentration of ethyl acetate during the non-steady-state phase than the isothermal reactor (293 K). Moreover, the amount of EtOAc collected during the non-steady-state operation increases by approximately 20% (from 1.10 mol for the isothermal case to 1.34 mol) and the EtOAc to water mole ratio in the product fraction by 90 % (from 2.0 to 3.8).

The improvement of reactor performance (i.e., increased conversion and ester to water mole ratio in the product fraction) under non-isothermal conditions originates from increased temperature in the reactor and thus increased reaction rate. This appears plausible when considering the relatively large activation energy of $62\,kJ\,mol^{-1}$ reported by Sainio (2005) for this esterification reaction with the KEF76 ion-exchange resin.

Experimental temperature histories at six locations inside the non-isothermal reactor are shown in Fig. 2. As seen in the figure, the developing thermal wave has a self-amplifying nature: it grows stronger as it travels through the reactor. This indicates that the temperature front moves with approximately the same velocity as the reaction front.

The maximum temperature increase of circa 20 K seen in Fig. 2 is high considering that the esterification reaction is only weakly exothermic ($\Delta_{rxn}H = -4.6\,kJ\,mol^{-1}$ at 298 K) and that the reactor is not perfectly insulated. Indeed, when the

Table 1
Properties of the KEF76 ion-exchange resin in H^+ form

Property	
Manufacturer	Finex Oy
Cross-link density, wt%	7.0
Particle size in water, mm	0.3
Porosity in Na^+ form, vol%	7
Ion-exchange capacity, equiv kg^{-1}	5.1
Degree of functionalization, %	95

Table 2
Properties of the chemicals

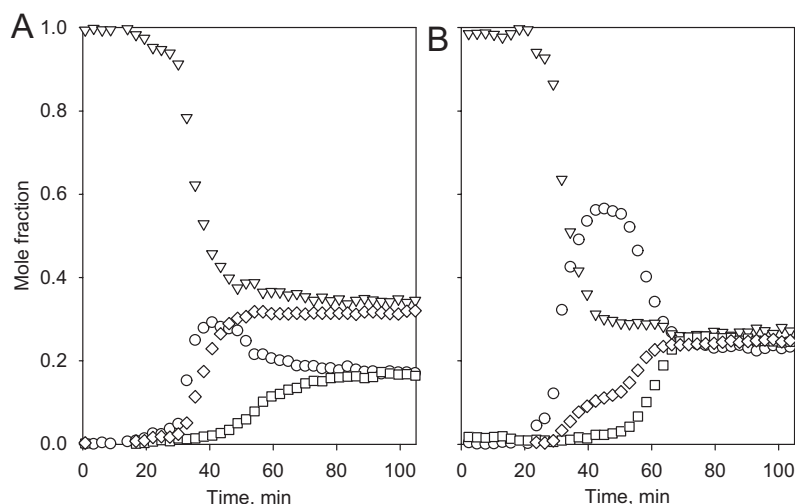| Property	Acetic acid	Ethanol	Ethyl acetate	Water
Molar mass, $kg\,mol^{-1}$	0.0601	0.0461	0.0881	0.0180
Density (293 K), $kg\,m^{-3}$	1004.5	785	900	998.3
Molar volume, $cm^3\,mol^{-1}$	57.57	58.73	97.89	18.05
Gibbs energy of formation[a], $kJ\,mol^{-1}$	−388.8	−174.4	−332.4	−237.3
Enthalpy of formation[a], $kJ\,mol^{-1}$	−484.2	−277.0	−480.0	−285.8
Molar heat capacity[a], $J\,mol^{-1}\,K^{-1}$	123.1	112.55	170.6	75.29

[a]TRC Thermodynamic Tables (1996).

Fig. 1. Ethyl acetate synthesis in (A) isothermal and (B) non-isothermal chromatographic reactor. Stationary phase: KEF76 ion-exchange resin. Initial temperature: 293 K. Bed height: 47.5 cm. Initial state: EtOH, feed: equimolar mixture of HOAc and EtOH. Bottom up flow at $u_{fluid} = 0.94 \, \text{cm} \, \text{min}^{-1}$ (bottom–top). Symbols: (∇) = EtOH, ($\Diamond$) = HOAc, ($\square$) = water, ($\bigcirc$) = EtOAc.
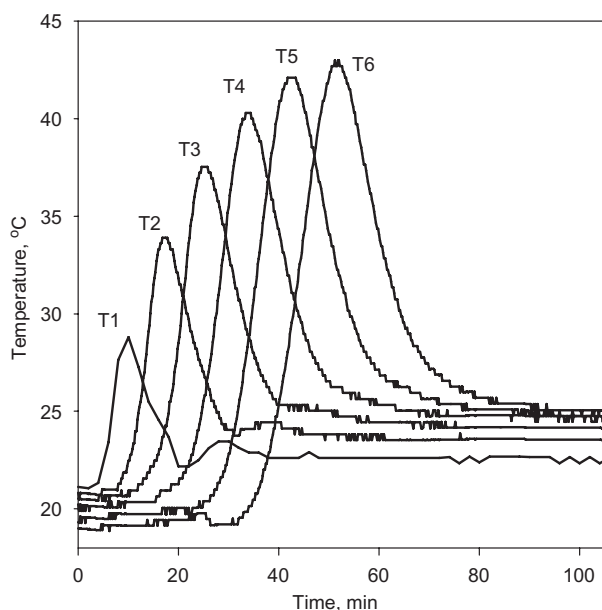

Fig. 2. Temperature profiles in a non-isothermal chromatographic reactor. Experimental conditions are as in Fig. 1. Numbering of the temperature measurement points (T1, T2, etc.) ascending from the reactor inlet.

thermally insulated column was operated as a conventional fixed-bed reactor at steady state (not shown), the temperature increase in the reactor was only approximately 5 K. This is somewhat lower than the adiabatic temperature rise of approximately 9 K calculated with the values given in Table 2 and the experimentally obtained steady-state conversion.

When using another ion-exchange resin catalyst that is characterized by an approximately 50% lower overall reaction rate at room temperature (Amberlyst 15, Rohm & Haas), the tem-

perature increase in the thermal wave remained approximately half of that observed with KEF76 (not shown). This suggests that the main cause for the development of the thermal waves is the reaction heat. However, also the contributions of mixing enthalpies and adsorption enthalpies should be assessed.

3.1. Enthalpy of mixing and heat of adsorption

The enthalpy of mixing in the present multicomponent system is a complex function of composition. Non-reactive displacement of water by ethanol, shown in Fig. 3, demonstrates the effects of mixing and adsorption enthalpies on the development of the thermal waves. More information can be extracted from such displacement experiments if the feed concentration is increased stepwise rather than changing from pure water to pure ethanol at once. Therefore, the displacement was carried out in two steps, and the vertical dashed line in the figure marks the time when ethanol concentration in the feed was increased from 94 to 99.5 wt%.

Three transitions are observed in the temperature data in Fig. 3 at each axial measurement point. In absence of calorimetric data for the EtOH–water–KEF76(H$^+$) system, the results can be discussed only on a qualitative level. Firstly, there is a sharp negative thermal peak that originates from desorption of water from the resin, which is an endothermic process. This temperature decrease is mostly overcome by exothermic mixing of water and ethanol, which occurs in both phases. The width of this thermal wave corresponds roughly to the width of the ethanol front in the breakthrough curve.

The third transition, a broad negative thermal wave, is observed only after the EtOH concentration in the feed is increased to 99.5 wt%. The main cause of this phenomenon is desorption of water tightly bound to the sulfonic acid groups (solvation shell) from the resin. The enthalpy of desorption is here larger than in the first negative transition.
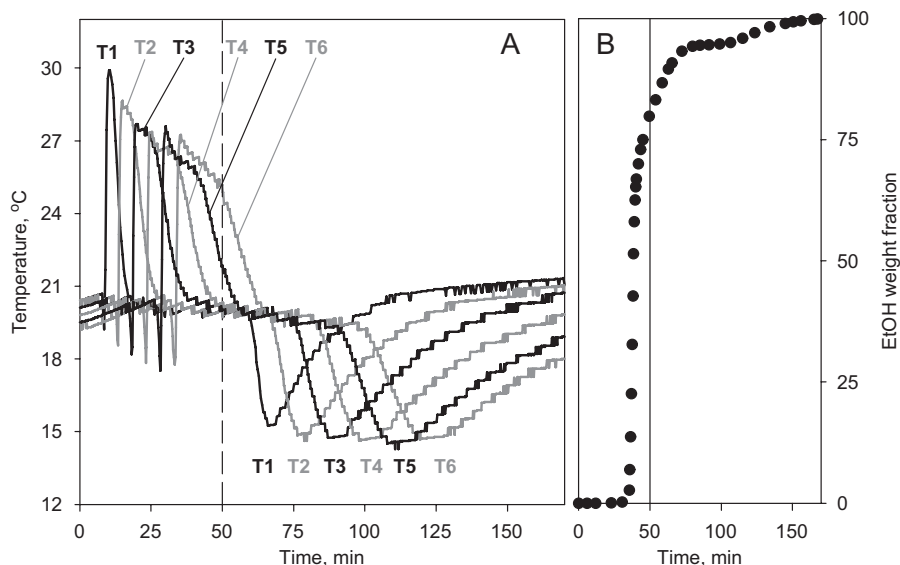
Fig. 3. Non-reactive displacement of water by ethanol in a thermally insulated column. (A) Temperature in the resin bed. (B) Composition of the effluent stream. Feed concentration switched from 94 wt% EtOH to 99.5 wt% at $t = 50$ min.

4. Theory

The dynamic behavior of a non-isothermal chromatographic reactor is best analyzed by mathematical modeling. However, the phase equilibrium behavior of the esterification reaction mixture in presence of an elastic ion-exchange resin is complex, and several temperature and concentration-dependent parameters would be required to describe it accurately. In addition, the heat of mixing in such a non-ideal multicomponent system is difficult to estimate. The aim here is to demonstrate the coupling between the concentration fronts and thermal waves as well as to identify parameters that influence the reactor performance. Therefore, the following theoretical discussion and numerical simulations consider a hypothetical system with linear adsorption isotherms and no heat of mixing in the liquid phase.

Equilibrium theory provides a useful theoretical framework for analyzing the role of thermodynamics in column separation processes (Rhee et al., 1989). It has also been applied to reactive separations, such as reactive distillation and reactive chromatography, at the limit of chemical and phase equilibrium (Grüner and Kienle, 2004). On the other hand, feasibility studies based on the equilibrium theory should be combined with numerical simulations with finite reaction rates in order to assess the influence of practical constraints, e.g. column length (Vu Dinh et al., 2005). Since here we limit the discussion to systems with relatively slow reaction kinetics, we solve the governing equations shown below numerically.

Assuming local phase equilibrium, thermal equilibrium, and plug flow, the material balance for component k in a differential volume element in a chromatographic reactor is

$$\frac{\partial c_k}{\partial t} + F \frac{\partial q_k}{\partial t} = -u \frac{\partial c_k}{\partial z} + v_k r^L + F v_k r^S. \tag{1}$$

If the enthalpy of mixing is neglected, the energy balance for a differential volume element in an adiabatic chromatographic reactor becomes

$$(\rho^L C_p^L + F \rho^S C_p^S) \frac{\partial T}{\partial t} = -u \rho^L C_p^L \frac{\partial T}{\partial z} - F \sum_{j=1}^{N} \Delta_{\mathrm{ads}} H_j \frac{\partial q_j}{\partial t}$$
$$- \Delta_{\mathrm{rxn}} H (r^L + F r^S). \tag{2}$$

Under non-isothermal conditions, the propagation velocities of concentration and temperature fronts are coupled through the enthalpies of adsorption. It is well known that in non-reactive chromatography a non-isothermal N-component system is mathematically equivalent to an isothermal $N + 1$ component system (Rhee et al., 1989). The same applies for reactive systems as well if the heat of reaction is considered as an analogue of the stoichiometric coefficients, and a new variable is defined as $v_{N+1} = -\Delta_{\mathrm{rxn}} H$. By using transformed variables defined in Eqs. (3) and (4)

$$c_{N+1} = \rho^L C_p^L (T - T^{\mathrm{ref}}), \tag{3}$$

$$q_{N+1} = \rho^S C_p^S (T - T^{\mathrm{ref}}) + \sum_{j=1}^{N} \Delta_{\mathrm{ads}} H_j q_j, \tag{4}$$

the governing equations can be written (in dimensionless coordinates) without a separate energy balance as shown in Eq. (5).

$$\left(1 + F \frac{\partial q_k}{\partial c_k}\right) \frac{\partial c_k}{\partial \tau} + F \sum_{\substack{j=1 \\ j \neq k}}^{N+1} \frac{\partial q_k}{\partial c_j} \frac{\partial c_j}{\partial \tau} + \frac{\partial c_k}{\partial \xi}$$
$$- v_k \frac{L}{u_{\mathrm{fluid}}} (r^L + F r^S) = 0, \quad k = 1, 2, \ldots, N+1. \tag{5}$$

The physical interpretations of the variables defined in Eqs. (3) and (4) are thermal energy contents per unit volume of liquid and solid phases, when compared to a reference state (Rhee et al., 1989).

It is worthwhile noting that Eq. (5) can be rearranged to yield expressions for the velocities of pure thermal waves and single-component concentration fronts in the reactor. The propagation velocity of a single component concentration wave, u_C, depends on the local slope of the adsorption isotherm as shown in Eq. (6). As seen in Eq. (7), the propagation velocity of a pure thermal wave, u_T, is governed by the ratio of the volumetric heat capacities of liquid and solid phases that typically depend only weakly on temperature.

$$u_C = \frac{u_{\text{fluid}}}{1 + F \partial q / \partial c},$$ (6)

$$u_T = \frac{u_{\text{fluid}}}{1 + F \rho^S C_p^S / \rho^L C_p^L}.$$ (7)

In order to study the non-isothermal reactor behavior in a parametric study, a reversible reaction $A \rightleftharpoons B + C$ and linear isotherms are considered here. Adsorbed amounts depend on temperature, and this dependency is often described with a van't Hoff type of relation by using the enthalpy of adsorption. In the case of a linear adsorption isotherm, the phase equilibrium relation can be written as

$$q_i = K_i c_i, \quad K_i = K_i^{\text{ref}} \exp\left(\frac{-\Delta_{\text{ads}} H_i}{R}\left(\frac{1}{T} - \frac{1}{T^{\text{ref}}}\right)\right).$$ (8)

The reaction rate is here described with a simple power law expression in terms of the solid phase concentrations

$$r^S = k_+ \left(q_A - \frac{1}{K_a} q_B q_C\right).$$ (9)

The effect of temperature on the chemical reaction rate is calculated according to the Arrhenius equation and that on the equilibrium constant according to the van't Hoff relation similar to Eq. (8).

5. Numerical results and discussion

The aim here is to demonstrate the coupling between the concentration fronts and thermal waves as well as to identify parameters that influence the reactor performance. For this purpose, a reversible reaction $A \rightleftharpoons B + C$ and linear isotherms are considered. The eluent is regarded inert and non-adsorbing. It is further assumed that the reactant A is eluted between the products B and C, and that separation of the products is possible. Although complete conversion and separation is possible also with other elution orders (Vu Dinh et al., 2005), the one chosen here is considered most suitable for practical purposes.

Values of $K_A = 1.0$, $K_B = 0.7$, $K_C = 1.3$ at 300 K were used for the adsorption isotherms. Further, a reaction rate constant of $k_+ = 10^{-4} \, \text{s}^{-1}$ at 300 K and an activation energy of $E_{\text{act}} = -60 \, \text{kJ/mol}$ were chosen. The heat capacity ratios for the liquid and solid phases were $\rho^L C_p^L = \rho^S C_p^S = 4.0 \, \text{kJ L}^{-1} \, \text{K}^{-1}$ that correspond roughly to pure water and a water-swollen ion-exchange resin. These parameters result in incomplete
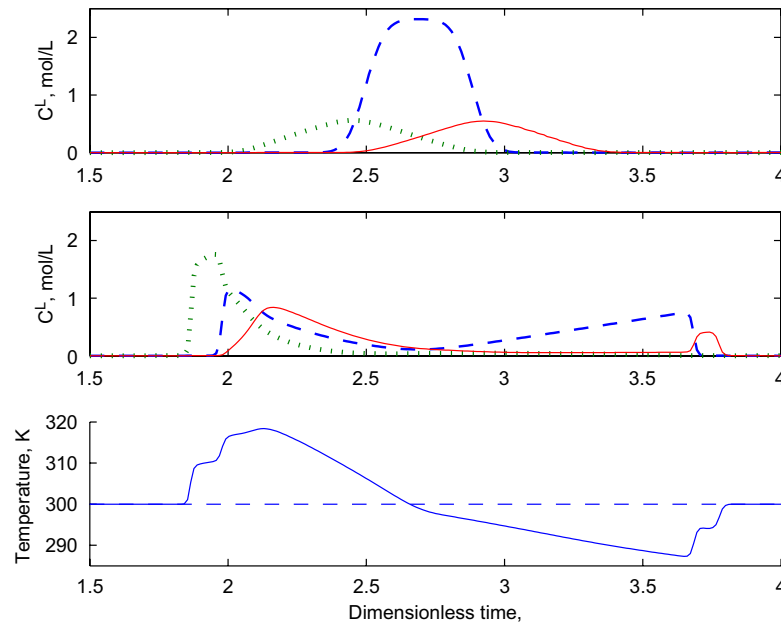
Fig. 4. Reversible reaction $A \rightleftharpoons B + C$ in a chromatographic reactor under isothermal (top) and non-isothermal (middle) conditions. Concentration profiles: dashed line = A, dotted line = B, solid line = C. Temperature profiles in (bottom): dashed line = isothermal, solid line = non-isothermal. Linear adsorption isotherms, $\Delta_{\text{ads}} H = -20 \, \text{kJ/mol}$, $\Delta_{\text{rxn}} H = -10 \, \text{kJ/mol}$, $\rho^S C_p^S = \rho^L C_p^L = 4.0 \, \text{kJ L}^{-1} \, \text{K}^{-1}$.
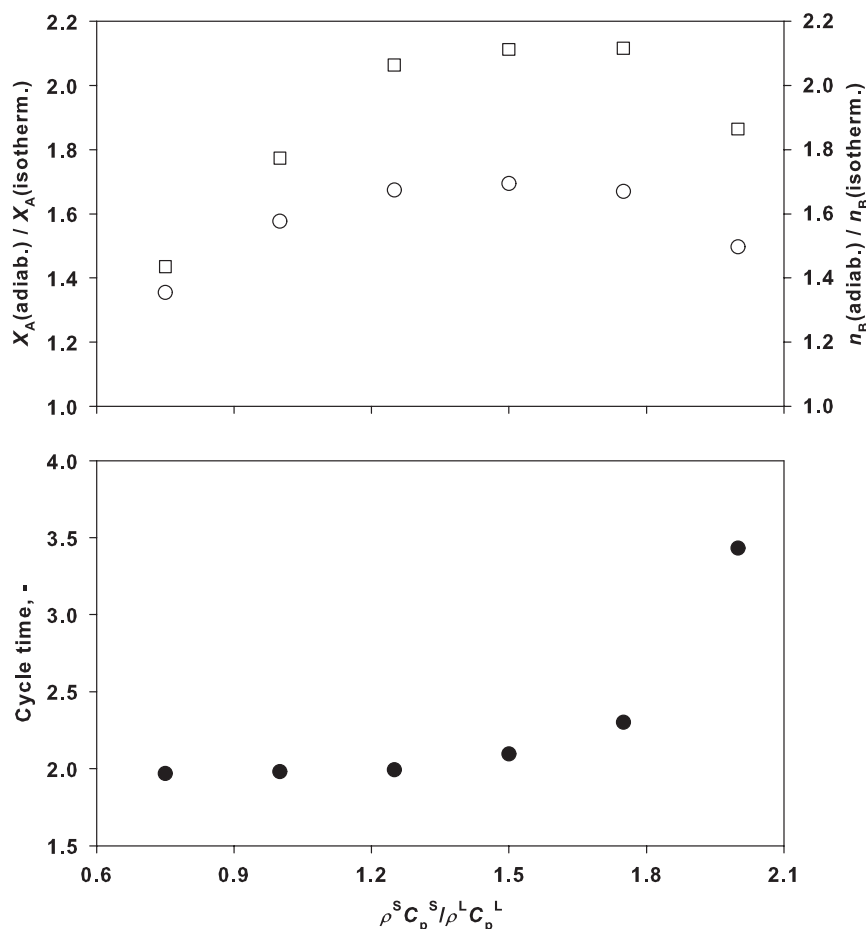
Fig. 5. Effect of heat capacity ratio on chromatographic reactor performance. Top: increase in productivity parameters due to non-isothermal operation when compared to isothermal operation. ($\square$) = amount of pure product B collected; ($\bigcirc$) = conversion of reactant A. Bottom: cycle time is defined as the dimensionless time elapsed between the first eluted front and the last eluted front for a pulse injection.

conversion and separation under isothermal conditions and thus allow studying the influence of thermal effects on the reactor performance.

Concentration and temperature profiles for a pulse injection of 0.384 dimensionless time units with a feed concentration $c_A^{\text{feed}} = 3.0 \, \text{mol} \, \text{L}^{-1}$ are shown in Fig. 4. Under isothermal conditions (top), the propagation velocities of the chemical species are constant and independent of each other. Due to a relatively low reaction rate, the conversion of reactant A is only 22.8%.

Under non-isothermal conditions (middle and bottom of Fig. 4), the concentration profiles are totally different from the isothermal case. This is a direct consequence of the coupling of thermal and concentration fronts, which is clearly seen when comparing the graphs in middle and bottom of Fig. 4.

In contrast with isothermal chromatography, it is observed in Fig. 4 that thermal effects can cause self-sharpening fronts even when the adsorption isotherms are linear with respect to concentrations. An increase in temperature (due to negative enthalpies of adsorption and heat of reaction) decreases the slope of the adsorption isotherms as shown in Eq. (8). Consequently,

the concentration waves at higher temperature are accelerated because the value of the denominator in Eq. (6) decreases, and a shock front is formed.

Increased temperature also increases the reaction rate (activation energy $E_{\text{act}} = -60 \, \text{kJ/mol}$), and the conversion of A in the non-isothermal reactor is 35.5%. The molar amount of B collected in the pure product fraction (i.e., before A and B breakthrough from the reactor) is 43.6% higher under non-isothermal conditions than under isothermal conditions.

In the rear part of the concentration profiles, severe tailing and even formation of so-called double peaks are observed. The tailing originates from decreasing temperature due to desorption of the species by the eluent and the consequent increase in the slopes of the adsorption isotherms, which leads to decreasing migration velocity of the corresponding concentration waves. Furthermore, the local reaction rate decreases below that observed in the isothermal reactor, which gives rise to a disperse profile of unreacted reactant A.

In the above, adsorption of the eluent was neglected. It should be mentioned that in cases where the eluent is adsorbed

significantly, the behavior of the non-isothermal reactor will change (not shown). Firstly, the increase in temperature at the front of the first eluted species *B* would decrease due to the heat of desorption of the eluent molecules. Similarly, the decrease in temperature at the rear part of the profile would be diminished because the heat of desorption of species *A* and *C* would be partly covered by the heat of adsorption of the eluent. Summarizing, adsorption of the eluent would lead to weakening of both the desired increase of conversion and the undesired tailing effects.

It is worth noting that the propagation velocities of the temperature and concentration fronts are closer to each other in liquid–solid systems than in gas–solid systems (Eigenberger, 1992), and, therefore, it is more probable in the present case that a thermal wave becomes self-amplifying. This is due to the fact that the volumetric heat capacities are of the same order in magnitude (see Eqs. (6) and (7)). The effect of the heat capacity ratio on selected performance parameters is shown in Fig. 5. The ratio was varied by changing $\rho^S C_p^S$ while keeping $\rho^L C_p^L$ equal to $4.0 \, \text{kJ} \, \text{L}^{-1} \, \text{K}^{-1}$.

It is seen in Fig. 5 that the conversion of *A* is always higher in the non-isothermal reactor than in the isothermal reactor. Also the amount of product *B* collected in the pure product fraction is larger in the adiabatic reactor. It is interesting to note that the improvement of the performance of the non-isothermal reactor, when compared with the isothermal reactor, has a maximum at a certain value of $\rho^S C_p^S / \rho^L C_p^L$. With low values of this parameter, the increase in temperature at the front of the concentration profiles is high, which favors the reaction, but the decrease in temperature at the rear is also large, which leads to severe tailing. As the value of $\rho^S C_p^S$ increases beyond the maximum in the curves, the temperature increase at the reaction front becomes smaller, and the improvement of the performance is not very high. This is because the heat capacity of the system is larger (small increase in temperature) and because a pure thermal wave would lag behind the concentration fronts, eliminating the self-amplifying nature of the thermal wave.

It is also seen in the bottom of Fig. 5 that increased conversion and amount of pure product *B* compared to the isothermal reactor at 300 K only come with a price of increased cycle time. Cycle time is here taken as the width of the breakthrough profiles for the pulse injection. Under isothermal conditions, the cycle time is 1.4 dimensionless time units (see Fig. 4). As seen in Fig. 5, the cycle time is always higher than this under non-isothermal conditions due to severe tailing, and increases with increasing solid phase heat capacity.

These results indicate that this type of process is relatively sensitive to the heat capacity ratio. Although this parameter cannot be easily varied in practice—the choice of stationary phase is based on its catalytic activity and separation properties—it is important to acknowledge that a favorable heat capacity ratio could improve the process performance.

6. Conclusion

It was shown experimentally that a moving, self-amplifying thermal wave can develop in a liquid phase chromatographic re-

actor under adiabatic conditions. For an exothermic reaction the thermal wave is positive (i.e., higher temperature result compared to the initial state) and can significantly enhance the reactor performance when it moves together with the reactive front. An increase of 90% in the ethyl acetate to water mole ratio was observed when the chromatographic reactor was operated under near-adiabatic conditions instead of isothermal conditions.

The experimental results obtained suggest that the main cause for the development of the thermal waves is the reaction heat. However, it was shown by non-reactive displacement experiments that also the enthalpies of mixing of the solvent components, as well as mixing the solvents and the functionalized polymer (i.e., sorption enthalpies), can result in similar thermal waves.

Coupling of the propagation of concentration and thermal waves in a chromatographic reactor was illustrated by numerical simulations. The results obtained suggest that the reactor performance can be improved by modifying the volumetric heat capacity of the solid phase.

Thermal effects in chromatographic reactors can also be disadvantageous. As an example, radial temperature gradients would give rise to increased axial dispersion through radial gradients in the propagation velocities of the species. On the other hand, the self-amplifying nature of the thermal wave could increase the risk of thermal runaway in chromatographic reactors, which should be considered in the case of strongly exothermic reactions.

The results obtained in this work emphasize the necessity to account for thermal effects in reactive chromatography, in particular when aiming at scale-up of the process. Moreover, these results indicate that non-isothermal operation of an adiabatic simulated moving bed reactor will give rise to several interesting theoretical and practical questions. As an example, it should be investigated whether an SMB process could possibly overcome the disadvantageous tailing predicted under non-isothermal conditions and whether the moving thermal wave can be captured in the reaction zone to increase the conversion.

Notation

c	liquid phase concentration, $\text{mol} \, \text{m}^{-3}$
C_p	heat capacity, $\text{J} \, \text{kg}^{-1} \, \text{K}^{-1}$
C_{pm}	molar heat capacity, $\text{J} \, \text{mol}^{-1} \, \text{K}^{-1}$
E_{act}	activation energy, $\text{kJ} \, \text{mol}^{-1}$
F	phase ratio, dimensionless
$\Delta_{rxn} G$	Gibbs energy of reaction, $\text{kJ} \, \text{mol}^{-1}$
$\Delta_{ads} H$	enthalpy of adsorption, $\text{kJ} \, \text{mol}^{-1}$
$\Delta_{rxn} H$	enthalpy of reaction, $\text{kJ} \, \text{mol}^{-1}$
K	slope of linear adsorption isotherm, dimensionless
K_a	reaction equilibrium constant, $\text{mol} \, \text{m}^{-3}$
k_+	forward reaction rate constant, s^{-1}
L	column length, m
M	molar mass, $\text{kg} \, \text{mol}^{-1}$
n_B	molar amount of product *B* in a pure product fraction, mol
q	solid phase concentration, $\text{mol} \, \text{m}^{-3}$

r	chemical reaction rate, mol m^{-3} s^{-1}
R	gas constant, 8.314 J mol^{-1} K^{-1}
t	time, s
T	temperature, K
u_{fluid}	linear velocity of the fluid, m s^{-1}
V_m	molar volume, cm^3 mol^{-1}
X_A	conversion of reactant A
z	axial distance, m

Greek letters

v	stoichiometric coefficient, dimensionless
ξ	dimensionless distance, $\xi = z/L$, dimensionless
ρ	density, kg m^{-3}
τ	dimensionless time, $\tau = tu_{\text{fluid}}/L$, dimensionless

Subscripts

C	single-component concentration wave
j, k	index
T	pure thermal wave

Superscripts

feed	feed stream into the reactor
L	liquid phase
ref	reference state
S	solid phase (resin phase)

References

Brandt, A., Mann, G., Arlt, W., 1997. Temperature gradients in preparative high-performance liquid chromatography columns. Journal of Chromatograpy A 769, 109–117.

Eigenberger, G., 1992. Fixed bed reactors. Ullmann's Encyclopedia of Industrial Chemistry, vol. B4. VCH-Weinheim, pp. 199–238.

Glöckler, B., Kolios, G., Eigenberger, G., 2003. Analysis of a novel reverse-flow reactor concept for autothermal methane steam reforming. Chemical Engineering Science 58, 593–601.

Grüner, S., Kienle, A., 2004. Equilibrium theory and nonlinear waves for reactive distillation columns and chromatographic reactors. Chemical Engineering Science 59, 901–918.

Mazzotti, M., Kruglov, A., Neri, B., Gelosa, D., Morbidelli, M., 1996. A continuous chromatographic reactor: SMBR. Chemical Engineering Science 51, 1827–1836.

Mazzotti, M., Neri, B., Gelosa, D., Morbidelli, M., 1997. Dynamics of a chromatographic reactor: esterification catalyzed by acidic resins. Industrial & Engineering Chemistry Research 36, 3163–3172.

Meurer, M., 1999. Dynamische Simulation chromatographischer Simulated-Moving-Bed Flüssigphasen-Reaktoren. VDI-Verlag, Düsseldorf.

Rhee, H.-K., Aris, R., Amundson, N.R., 1989. First-order partial differential equations. Theory and Application of Hyperbolic Systems of Quasilinear Equations, vol. II. Prentice-Hall, New Jersey.

Sainio, T., 2005. Ion-exchange resins as stationary phase in reactive chromatography. Acta Universitatis Lappeenrantaensis 218, Diss. Lappeenranta University of Technology

TRC Thermodynamic Tables: Non-hydrocarbons, 1996. Thermodynamics Research Center, Texas A&M University, College Station, TX

Vu Dinh, T., Seidel-Morgenstern, A., Grüner, S., Kienle, A., 2005. Analysis of ester hydrolysis in a chromatographic reactor using equilibrium theory and a rate model. Industrial & Engineering Chemical Research 44, 9565–9574.

Yongsunthon, I., Alpay, E., 1999. Design of periodic adsorptive reactors for the optimal integration of reaction, separation, and heat exchange. Chemical Engineering Science 54, 2647–2657.

Xiu, G., Li, P., Rodrigues, A.E., 2002. Sorption-enhanced reaction process with reactive regeneration. Chemical Engineering Sciecne 57, 3893–3908.

Javier García Palacios[1]
Malte Kaspereit[1]
Achim Kienle[1,2]

[1] Max-Planck-Institut für Dynamik komplexer technischer Systeme, Magdeburg, Germany.

[2] Otto-von-Guericke Universität Magdeburg, Lehrstuhl Automatisierungstechnik/ Modellbildung, Magdeburg, Germany.

Research Article

Conceptual Design of Integrated Chromatographic Processes for the Production of Single (Stereo-)Isomers

Dedicated to Prof. Dr.-Ing. Gerhart Eigenberger on the occasion of his 70th birthday

A fundamental investigation is performed for integrated processes that combine continuous chromatography and isomerization reactions to produce a single (stereo-)isomer. The focus is on the conceptual design of different process concepts and their theoretical analysis. The investigated process variants include reactor-separator-recycle systems, schemes with side reactors, and chromatographic reactors. As a new option, continuous chromatographic reactors with internally distributed functionalities are suggested. Using parameters of a model system, the performance of the processes is compared based on optimizations of corresponding models. The results reveal the potential and the limits of the different approaches under various conditions. It is found that the suggested new options can allow for significantly enhanced process performance.

1 Introduction

Integrated processes that combine chemical reaction and separation are an attractive approach to improve yield, selectivity, or productivity of chemical productions. One possible option among the different variants is the chromatographic reactor. Chromatographic reactors are particularly useful if separation of the components is very difficult, or if products are sensitive to harsh conditions [1]. They have been considered mainly to enhance equilibrium-limited conversions for reversible reactions with the stoichiometry $A \rightleftarrows B + C$ or $A + B \rightleftarrows C + D$ [1]. These hold for the well-studied esterifications and ester hydrolyses (e.g., [2–4]), and the synthesis of acetals [5].

The production of a single isomer from its counter isomer (or from a mixture of both) is a frequent task in the manufacturing of hydrocarbons, sugars, fine chemicals, pharmaceuticals, etc. As will be discussed below, it is more difficult to devise integrated chromatographic processes for the corresponding stoichiometry $A \rightleftarrows B$. A challenging example in this context is enantiomers, which serve as a reference case in this

work. These stereoisomers are of great importance in the production of pharmaceuticals, agrochemicals, and fine chemicals. They have identical physicochemical properties, but can have different physiological effects. Therefore, typically only one enantiomer is desired as the product. For economic reasons, they are often produced by classical non-selective syntheses that deliver the 1 : 1 mixture ("racemate"). From the latter, the desired form is isolated by means of chromatography or crystallization. The achievable yield of such an approach is only 50 %. However, for many enantiomeric systems, this value could be increased by incorporating an isomerization reaction ("racemization") into the production process.

The process concepts that combine continuous chromatography and isomerizations fall mainly into three general categories, as illustrated in Fig. 1. The first approach (see Fig. 1, left) is a conventional flow sheet where reaction and separation are performed sequentially and non-converted educt is recycled. So far, this has been studied for only a few enantiomeric systems. These combine an enzymatic or thermal racemization with simulated moving bed (SMB) chromatography [6–8]. The second option (see Fig. 1, center) has been most frequently considered for isomerizations. In this concept, which was suggested by Hashimoto et al. [9], side reactors are distributed spatially along a non-reactive chromatographic unit. This aims at confining the reaction to positions where it is not affecting product purity. Most investigations were de-

Correspondence: Dr.-Ing. Malte Kaspereit (kaspereit@mpi-magdeburg.mpg.de), Max-Planck-Institut für Dynamik komplexer technischer Systeme, Sandtorstraße 1, D-39106 Magdeburg, Germany.

Continuous chromatographic reactors   1393
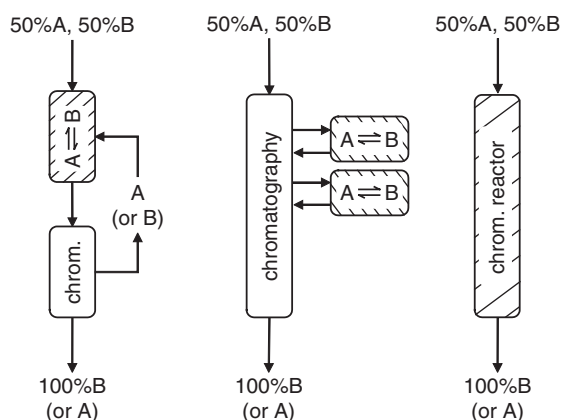
Figure 1. General concepts for producing a single isomer by chromatography and isomerization reactions. Left – flow sheet-integrated process (reactor-separator-recycle). Center – semi-integrated process with side reactors. Right – fully integrated process (reactive separator).

voted to the isomerization of glucose to fructose [7, 9–12]. The only enantiomeric problem considered so far is the thermal racemization of Tröger's base [7]. It should be noted that the investigated examples share several very specific properties. Typically, the desired component is stronger adsorbing, it is obtained at only limited purity and/or conversion, and one or both components exhibit a peculiar adsorption behavior characterized by so-called unfavorable isotherms. The last option (see Fig. 1, right) is a fully integrated SMB reactor where reaction and separation occur simultaneously throughout the unit. The approach was applied, for example, to esterifications [13–16] and different enzymatic productions [17, 18]. As regards isomerization reactions, only a case with low purity requirements was studied [19]. Several theoretical investigations were devoted to this concept [20–23]. In addition to the concepts discussed above, more sophisticated continuous schemes were also suggested with alternating reactive and non-reactive columns [24–26]. However, these schemes include purge and vent streams which limit conversion and yield.

Only few studies attempt a comparison of the different concepts. Borren [7, 12] evaluated several processes for the two mentioned examples, glucose/fructose and Tröger's base, and suggested more complex extensions of the Hashimoto concept. Tylko [27] discussed spatially distributed functionalities in

view of the Hashimoto concept. Fricke [28] investigated theoretically the role of different reaction rates in the zones of a continuous reactive chromatographic process under linear conditions. However, for the realization, he suggested the Hashimoto concept.

Summarizing the above, the concepts developed so far were designed mostly for very specific cases. The typical application is characterized by limited product purity, the stronger adsorbing component being the target component, and specific types of adsorption equilibria. Against this background, we aim here at a more fundamental investigation of the possibility to integrate continuous chromatography and isomerization reactions. For this purpose, existing and new process options will be investigated on a conceptual level in order to evaluate their potentials and limits.

This paper is organized as follows. At first, different processes – including new approaches – are defined based on the three general options shown in Fig. 1. Subsequently, the mathematical model and the optimization method are explained. Afterwards, the performance of the processes is optimized under various conditions that reflect typical practical aspects. The investigations will be extended beyond the typical applications discussed above by applying more rigorous requirements on product purity and conversion, by using more common types of adsorption equilibria, and by considering both the stronger and the weaker adsorbing component as the possible target product. While the challenging production of a single enantiomer will serve as a reference case, the results are readily applicable to other isomerization problems.

2 Investigated Processes

Based on the three general options shown in Fig. 1, the five different process concepts shown in Fig. 2 were selected for detailed investigations. For computational reasons, we apply true moving bed (TMB) units (i.e., a continuous countercurrent is assumed between the solid and the fluid). In contrast to most of the existing literature, the processes in Fig. 2 are designed to obtain the weaker adsorbing component *B* as product. Setups for the stronger adsorbing solute *A* are obtained easily by "inverting" these schemes. Since one goal of this work is to maximize the conversion and yield of each process, the schemes shown have only a single product outlet and no waste streams.

The first option (process 1) is a classical reactor-separator-recycle system with a four-zone TMB process. The weaker ad-
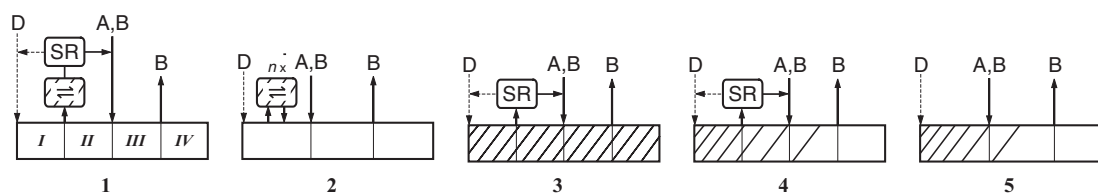
Figure 2. Investigated processes for the production of the weaker adsorbing component *B*. (1) Classical flow sheet-integrated process with a separation by TMB chromatography, isomerization reactor, recycle, and intermediate solvent removal (SR). (2) Three-zone TMB process with *n* side reactors ("Hashimoto concept"). (3) Four-zone TMB reactor with recycle and solvent removal. (4) Four-zone TMB reactor with *internally distributed* reaction, recycle, and solvent removal. (5) Three-zone TMB reactor with *internally distributed* reaction.

sorbing product B is obtained at the so-called raffinate port while the unconverted educt A is transported towards the reactor. As also applied in [7], an intermediate removal of excess solvent (SR) is included to counter-balance the typically strong dilution. The removed solvent could be re-used. The next processes correspond to the previously mentioned Hashimoto concept (2) and a fully integrated TMB reactor (3), respectively. The latter also has a solvent removal. The last two processes are new suggestions. They combine the spatial distribution attempted by the Hashimoto approach and the reduced flow sheet complexity of a fully integrated process. In both schemes, it is assumed that the reaction rate can be "distributed" optimally within the unit. The four-zone version (4) contains a recycle and solvent removal. In contrast, the simple three-zone system (5) requires no external devices.

It is emphasized that it is beyond the scope of this work to suggest detailed practical implementations for the schemes in Fig. 2. However, the spatial functionality distribution in processes 4 and 5 deserves some remarks. Since it is more or less impossible to realize a TMB process in practice, such an integrated process will rely on the SMB concept. However, due to the periodic column switching, the desired internal distribution of the reaction can hardly be achieved by incorporating reactive columns into an SMB process. A useful alternative here is to introduce gradients of operating conditions, which is a well-known approach in non-reactive SMB processes. The most promising ideas in this context appear to be:

(i) the manipulation of adsorption behavior by gradients of solvent strength, salts, pH, etc. (see [29–31]) or temperature (see [16, 32]);

(ii) the use of gradients of a homogeneous catalyst, e.g., of the pH value (see [33]) (note that racemization can be triggered for many enantiomers by changing the pH value);

(iii) the use of gradients of inhibitors that suppress the reaction in some part of the unit, e.g., by reversibly adsorbing to an active center;

(iv) combinations of the above.

This list reveals that, in general, both functionalities (reaction and adsorption) could be spatially distributed. For the sake of simplicity, in the following we will only consider a distribution of the chemical reaction.

3   Mathematical Model and Optimization

The large number of optimizations carried out in this work requires a flexible and numerically efficient model. Here, we use an equilibrium stage model for the TMB process, which consists of the mass balances for the two components in the fluid and solid phases within each stage:

$$\varepsilon V \frac{dc_i^{k,n}}{dt} + (1-\varepsilon)V \frac{dq_i^{k,n}}{dt} = Q^n(c_i^{k-1,n} - c_i^{k,n}) + Q_s(q_i^{k+1,n} - q_i^{k,n}) + \varepsilon V v_i r^{k,n} \tag{1}$$

where the indices $i = A, B$ denote the component, $k = 1, ..., N_s$ the stage, and $n = I, ..., N_z$ the zone of the TMB process (see Fig. 2), respectively. c_i and q_i are the liquid and solid phase

concentrations, V is the volume of a stage and ε the porosity. Q and Q_s are the volumetric flow rates of the fluid and the solid phase, respectively. The axial dispersion is adjusted by the number of stages, N_s.

The last term in Eq. (1) describes the chemical reaction with v_i as the stoichiometric coefficient and r as the reaction rate. In this work, we consider a reversible (*i.e.* equilibrium-limited) isomerization $A \rightleftarrows B$. Unless otherwise stated, the reaction is assumed to occur in the fluid phase. Thus, the reaction equilibrium constant is given by

$$K_{eq} = \frac{c_B}{c_A} = \frac{k_f}{k_b} \tag{2}$$

with k_f and k_b as rate constants of the forward and backward reaction, respectively. From Eq. (2) follows for the reaction rate in Eq. (1)

$$r^{k,n} = k_f \left(c_A^{k,n} - \frac{c_B^{k,n}}{K_{eq}} \right) \tag{3}$$

The design variables to be optimized in this work are the dimensionless zone flow rate ratios, m^n, and the Damköhler number, Da^n, for each zone n:

$$m^n = \frac{Q^n}{Q_s} \tag{4}$$

$$Da^n = \varepsilon \tau_s k_f^n \tag{5}$$

where $\tau_s = V/Q_s$ is the residence time of the solid within a single stage. Using these definitions and Eq. (3), we can rewrite Eq. (1) for the reactive TMB process as

$$\varepsilon \tau_s \left(\frac{dc_i^{k,n}}{dt} + F \frac{dq_i^{k,n}}{dt} \right) = m^n(c_i^{k-1,n} - c_i^{k,n}) + q_i^{k+1,n} - q_i^{k,n} + v_i Da^n \left(c_A^{k,n} - \frac{c_B^{k,n}}{K_{eq}} \right) \tag{6}$$

with $i = (A, B)$, $k = 1, ..., N_s$, $n = I, ..., N_z$
where $F = (1 - \varepsilon)/\varepsilon$ is the phase ratio. Using corresponding values for Da^n, Eq. (6) allows for a simple modeling of both non-reactive chromatographic processes (i.e., $Da^n = 0$ for all n), as well as of reactive processes with or without distribution of the reaction within the unit (i.e., $Da^n \neq 0$ for selected n).

The relation between the solid and the liquid phase concentrations in Eq. (6) is given by the adsorption equilibrium. Here, bi-Langmuir adsorption isotherms apply, which are most frequently used for enantiomeric systems:

$$q_i = \frac{q_{s,1} b_{i,1} c_i}{1 + b_{A,1} c_A + b_{B,1} c_B} + \frac{q_{s,2} b_{i,2} c_i}{1 + b_{A,2} c_A + b_{B,2} c_B}, \quad i = (A, B) \tag{7}$$

Eq. (7) describes competitive adsorption of the two solutes (A, B) on two different types of adsorption sites of the solid (1, 2); $q_{s,1}$ and $q_{s,2}$ are the corresponding saturation capacities. For these isotherms, a separation factor (valid for infinite dilution) can be defined as:

$$a = \left. \frac{q_{s,1} b_{A,1} + q_{s,2} b_{A,2}}{q_{s,1} b_{B,1} + q_{s,2} b_{B,2}} \right|_{c_1 = c_2 = 0} \tag{8}$$

The external devices connected to the TMB units shown in Fig. 2 were modeled as follows. The reactors in processes 1 and 2 are described as continuously stirred tank reactors (CSTR) with an infinite reaction rate and negligible volume. The devices for solvent removal (SR) were assumed to instantaneously adjust the mixture concentrations such that the higher concentrated component has the same concentration as in the feed.

The following objective function was applied in the optimizations to evaluate the different process schemes:

$$OF = \frac{Q^D}{Q^{out} c_i^{out}} = \frac{Q^D}{Pr} \tag{9}$$

where Q^D and Q^{out} are the flow rates of the desorbent and product ($out = R$ for raffinate, $out = E$ for extract port), respectively. c_i^{out} is the concentration of the desired component in this stream. The term $Pr = Q^{out} c_i^{out}$ is the productivity of the process. Note that for calculating Q^D, a possible re-use of the removed solvent (as indicated in Fig. 2) was not considered. Eq. (9) is the most frequently used objective function for continuous chromatography, since it simultaneously minimizes solvent consumption and maximizes productivity. The optimization problem can be summarized as:

$$OF(m^n, Da^n) \to \min$$
$$s.t. \tag{10}$$
$$Pu^{out} = \frac{c_i^{out}}{c_A^{out} + c_B^{out}} \geq Pu_{min}$$

where Pu^{out} denotes the purity of product i at the corresponding outlet. If the weaker adsorbing component B is the target product, for the indices in Eqs. (9)–(11) holds $i = B$, $j = A$, and $out = R$. Correspondingly, if the stronger adsorbing component A is desired, $i = A$, $j = B$, and $out = E$.

Note that no additional constraint for the conversion is required because the processes in Fig. 2 have only a single outlet. From the mass balances around the unit, it can be shown that, for such processes, the following relation between purity and conversion holds:

$$X_i = \frac{Pu^F + Pu^{out} - 1}{Pu^F} \tag{11}$$

where the purity of the feed is defined with respect to component j.

The model was implemented in the simulation environment DIVA [34]. All optimizations were performed using a sequential quadratic programming (SQP) algorithm available in DIVA.

4   Results

4.1   Optimizations for a Reference Case

In order to provide a basis for further discussions, we optimize the performance of the processes shown in Fig. 2 for a reference case. The optimized parameters are the flow rate ratios m^n, Eq. (4), and – where applicable – the Damköhler numbers

Da^n, Eq. (5). The enantiomers of chlorthalidone are considered as a model system. For this substance, experimental parameters are available in [8]. For enantiomeric systems, the reaction equilibrium constant in Eq. (2) holds $K_{eq} = 1$. The feed is considered to be racemic (i.e., $c_A^F = c_B^F$). Tab. 1 summarizes the parameter values and conditions used for the reference case.

Table 1. Properties of the model system as taken from [8] and parameters of the reference case.

Parameter	Symbol		Values
Bi-Langmuir adsorption isotherms, Eq. (7)	$q_{s,1}$	[mg/mL]	94.175
	$q_{s,2}$	[mg/mL]	0.224
	$b_{i,1}$	[mL/mg]	0.207 0.141
	$b_{i,2}$	[mL/mg]	6.395 3.192
Porosity	ε	[–]	0.796
Stage volume	V	[mL]	1.0
Number of stages per zone	N_s	[–]	50
Reference parameters			
Feed concentration	c_i^F	[mg/mL]	0.2
Equilibrium constant	K_{eq}	[–]	1.0
Separation factor	α	[–]	1.496
Purity requirement	Pu_{min}	[%]	90

Firstly, we apply a moderate purity requirement of $Pu_{min} = 90\%$, which corresponds to a conversion of $X = 80\%$ (see Eq. (11)). Tab. 2 contains the optimization results for the case that the weaker adsorbing component B is desired. The table lists the optimized parameters, the values of the objective func-

Table 2. Optimization results for the processes shown in Fig. 2 for the reference case. The target product is the weakly adsorbing component B, which is obtained at the raffinate port at a purity requirement of $Pu^R \geq 90\%$. Note that the purity of the recycle stream, Pu^{rec}, is (if present) defined with respect to component A.

Process	OF	Pr	Q^D	Pu^{rec}	m^I Da^I	m^{II} Da^{II}	m^{III} Da^{III}	m^{IV} Da^{IV}
1	5.30	1.12	5.94	78.44	19.466 –	11.182 –	18.669 –	13.530 –
2[a)]	5.98	0.67	4.02	–	17.275 –	19.140 –	13.259 –	– –
3	24.79	0.40	9.93	77.93	21.839 0.03	0.534 0.03	19.039 0.03	11.410 0.03
4	2.88	1.14	3.29	50.02	16.369 10^2	11.311 10^{-4}	18.468 10^{-8}	13.078 10^{-8}
5	4.37	0.81	3.56	–	16.630 10^2	18.892 10^{-8}	13.072 10^{-8}	– –

a) For five side reactors.

tion, and the performance indicators productivity, *Pr*, and the desorbent stream, Q^D (see Eq. 10). The purity of the recycle stream (if present), Pu^{rec}, is also indicated.

Obviously, all processes are capable of delivering the product at the required purity of 90 %. The conventional reactor-separator-recycle scheme (process 1 in Fig. 2) achieves an average performance. An interesting aspect is that the recycle stream (i.e., the extract) has a purity of $Pu^{rec} \approx 78$ %. This indicates that, under optimal conditions, a complete separation of the components is not required. It should be mentioned that a simple design method exists for continuous chromatography for such a scenario [35], which could be applied directly to design process 1 for adsorption isotherms of the Langmuir type.

The performance of a partially integrated process with five side reactors (process 2 in Fig. 2) is slightly worse than for process 1. While the productivity is about 40 % lower, this is partially compensated by a 32 % lower desorbent flow rate Q^D. The latter is due to the lower optimal m^I value, which indicates an easier regeneration of zone *I*. It is emphasized that the performance of process 2 depends strongly on the number of side reactors. This will be discussed in more detail in the next section, together with the reason for the easier desorption.

The fully integrated process 3 affords only an inferior performance (*OF* is about five times higher than for process 1). This is due to the "omnipresence" of the forward and backward reaction throughout the unit. As a consequence, the purity requirement can only be achieved by having a low Damköhler number. In turn, this requires a very high recycle ratio through the reactor, as is indicated by the low value of m^{II}. Interestingly, the purity of the recycle stream is very similar to the value found for process 1.

The four-zone process with an internally distributed reaction (process 4 in Fig. 2) achieves the best performance of all concepts. As expected, the optimizer determines a high optimal reaction rate in zone *I* (i.e., Da^I), which is the only zone that is not adjacent to the product port. In the other zones, very low *Da* values are found, which cause basically no conversion (note that Da^{III} and Da^{IV} are equal to the lower limits allowed in the optimizations). The favorable value for *OF* (almost 50 % lower than for process 1) is mainly due to a significantly lower solvent requirement. Q^D decreases strongly due to lower m^I values. Obviously, the high reaction rate in zone *I* facilitates an easier desorption of the components within this zone. We denote this effect as *reaction-assisted regeneration* and will analyze it in the subsequent section.

Finally, the performance of the simple three-zone scheme with an internally distributed reaction (process 5) ranks second for the given purity requirement. This is also caused by a reaction-assisted regeneration in zone *I*. This is an encouraging finding because this simple process requires no additional unit operation like a solvent removal (see Fig. 2).

The optimizations were repeated for the stronger adsorbing component *A* as the target product. Tab. 3 summarizes the results. The performance of most schemes is rather similar in comparison to the case that the weaker adsorbing *B* is desired (see Tab. 2). Exceptions are processes 2 and 4 which require higher desorbent flow rates. This is due to the reaction-assisted regeneration now taking place in zone *IV*, where it is less effec-

Table 3. Optimization results for the reference case for corresponding processes that deliver the stronger adsorbing component *A* with a purity of $Pu^E \geq 90$ %. The purity of the recycle stream, Pu^{rec}, is (if present) defined with respect to component *B*.

Process	OF	Pr	Q^D	Pu^{rec}	m^I Da^I	m^{II} Da^{II}	m^{III} Da^{III}	m^{IV} Da^{IV}
1	5.01	0.96	4.82	72.77	18.022 –	12.573 –	19.943 –	13.199 –
2[a]	7.75	0.96	7.44	–	20.849 –	12.740 –	13.408 –	– –
3	24.16	0.41	9.81	89.36	23.370 0.043	14.069 0.043	17.600 0.043	13.588 0.043
4	3.62	1.04	3.75	50.07	19.291 10^{-8}	13.041 10^{-8}	20.560 10^{-8}	15.541 10^2
5	4.15	1.02	4.22	–	19.905 10^{-8}	12.852 10^{-8}	15.682 10^2	– –

a) For five side reactors.

tive for the type of adsorption isotherms used here (see also next section).

The purity requirement of 90 % used so far might be sufficient in certain cases. For many applications (e.g., in the production of a single, pharmaceutically active enantiomer), more restrictive demands hold with respect to product purity and conversion. To address this aspect, the calculations were repeated for a purity of $Pu^{min} = 99.9$ % (corresponding to $X = 99.8$ %). Tab. 4 lists the optimization results for the two schemes that are capable of performing this task. Out of the five schemes, only processes 1 and 4 are capable of delivering this required purity. Process 1 achieves an acceptable performance despite the comparably low number of theoretical stages used (50 per zone). The new process 4 again outperforms this for the production of the weaker adsorbing *B* (upper part of Tab. 4), but not for the production of the stronger adsorbing *A* (lower part of the table). Process 4 in both cases profits from the reaction-assisted regeneration, as

Table 4. Optimization results for processes 1 and 4 shown in Fig. 2 and Pu^{out} 99.9 %. The target products are the weakly adsorbing component *B* (upper part of the table) and the strongly adsorbing component *A* (lower part).

| Process	OF	Pr	Q^D	Pu^{rec}	m^I Da^I	m^{II} Da^{II}	m^{III} Da^{III}	m^{IV} Da^{IV}
1	11.69	0.87	10.22	79.24	23.458 –	11.427 –	17.344 –	13.224 –
4	8.56	0.87	7.44	50.06	19.699 10^2	11.690 10^{-4}	17.239 10^{-8}	12.260 10^{-8}
1	9.66	0.74	7.11	73.67	19.345 –	14.712 –	20.435 –	12.236 –
4	10.37	0.81	8.41	50.53	23.382 10^{-8}	14.958 10^{-8}	20.750 10^{-3}	14.971 10^2

indicated by the lower m^I or the higher m^{IV} when producing B or A, respectively. However, in the second case, the positive effect on m^{IV} is outbalanced by a higher value of m^I. In process 1, a partial breakthrough of component A from zone I to zone IV enhances performance. This is similar to earlier observations [35]. In contrast, such breakthrough is detrimental in process 4. The reason for this appears to be that any component A entering zone IV decreases the driving force of the isomerization within this zone. The conversion would be reduced by this, which would require more restrictive internal flow rates. This is also supported by independent calculations, which indicate that this can be overcome by suppressing the reaction in the rightmost parts of zone IV.

The other process schemes (2, 3, 5) are not capable of obtaining a product with 99.9 % purity for the number of stages used. Obviously, process 3 would require an extremely high stage number to resolve this task. In contrast, doubling the stage number for process 5 already leads to a similar performance as achieved here by process 1.

4.2 Analysis of Reaction-Assisted Regeneration

In the previous section, the superior performance of processes with an internally distributed reaction was explained by an effect denoted as reaction-assisted regeneration. Here, we will analyze this effect.

First of all, the optimized internal concentration profiles in steady state should be compared for the four-zone processes 1 and 4. These are shown in Fig. 3. The first aspect to be noted is that, in both cases, the purity of the raffinate is determined by concentration waves originating from zones III and zone I, respectively. This indicates that it is not necessary to fully regenerate zone I, as was already observed above and discussed in [35]. The second, more important, observation concerns
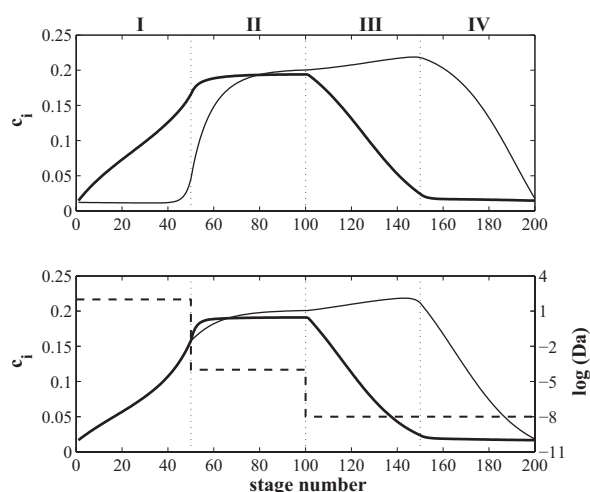
the profiles in the regeneration zone I. In the non-reactive process 1 (see Fig. 3, top) the concentration fronts of the two components are stationary at different positions. In contrast, for process 4 (bottom), the fast reversible isomerization leads to a common concentration front for both components. As already indicated, a lower flow rate (i.e., m^I) suffices to stabilize this front. This can be explained when considering that the reaction converts stronger adsorbing molecules into weaker adsorbing ones. These, in turn, are desorbed more easily and will migrate with the liquid before being converted again. An analogous effect is observed in zone IV if the stronger adsorbing solute A is desired, although here the benefits observed are slightly lower.

This effect can be analysed on the basis of an equilibrium theory, i.e., by assuming an instantaneous reaction and adsorption equilibrium throughout the process. In this case, it is possible to determine the flow rate ratios m^I and m^{IV} that are necessary to achieve complete regeneration of the corresponding zones. Such analysis was performed for homogeneous and heterogeneous reactions. For the sake of brevity, it was performed for adsorption isotherms of the Langmuir type. The results are summarized in Appendix A. Such derivations can also be performed for the bi-Langmuir model, Eq. (7). They reveal analogous trends but would require a too detailed treatment, being out of the scope of this manuscript.

The expressions given in Tab. 5 can be used for basic design purposes. Furthermore, they allow the quantification of the required regeneration efforts in each particular case. As an example, Fig. 4 shows the flow rates required for the complete regeneration of zone I for three cases: non-reactive separation, homogeneous reaction, and heterogeneous reaction. The values in the figure were scaled with respect to the non-reactive separation. The abscissa is the separation factor α, which can be easily substituted into the expressions for m^I. These expressions as a function of α are included in Appendix A in Eq. (A-12). The figure underlines that the effect of a reaction-assisted regeneration increases significantly the easier the separation. This holds in particular for a heterogeneous reaction. For example, for $\alpha = 3$, the flow rate in zone I could be reduced by 30 or 50 %, depending on whether the reaction is homogeneous or heterogeneous. These numbers translate directly into a reduced solvent requirement.

Figure 3. Steady-state concentration profiles for the four-zone processes 1 (top) and 4 (bottom) under optimized conditions. The target product is the weaker adsorbing component B. $K_{eq} = 1.0$, $Pu_{min} = 90\%$. Lines: components A (thick) and B (thin), Damköhler number, Da (dashed).

Table 5. Minimum m^I and maximum m^j, ($j = III$ or IV) for complete regeneration of the corresponding zones. Values hold for Langmuir adsorption isotherms and infinite reaction and adsorption rates.

	m^I_{min}	m^j_{max} , $j = (III, IV)$
Non-reactive	$q_s b_A$	$\dfrac{q_s b_B}{1 + b_B c^j_B}$
Homogeneous reaction	$\dfrac{q_s b_A + q_s b_B K_{eq}}{1 + K_{eq}}$	$\dfrac{q_s b_A + q_s b_B K_{eq}}{1 + K_{eq} + b_A C^j + b_B K_{eq} C^j}$
Heterogeneous reaction	$\dfrac{q_s b_A (1 + K_{eq})}{1 + K_{eq}\frac{b_A}{b_B}}$	$\dfrac{q_s b_A (1 + K_{eq})}{\left(1 + K_{eq}\frac{b_A}{b_B}\right)\left[1 + b_B c^j_B\left(\frac{1 + K_{eq}}{K_{eq}}\right)\right]}$
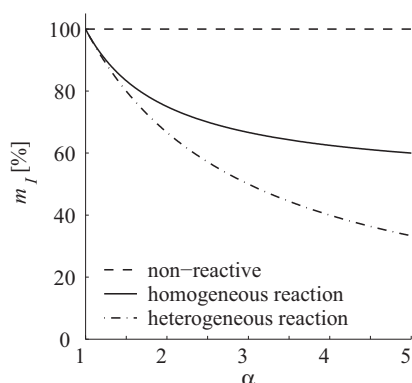
Figure 4. Flow rates required for the regeneration of zone *I* as a function of the separation factor α. Calculated for Langmuir isotherms using the expressions given in Tab. 5 ($K_{eq} = 1$). Values are scaled with respect to the non-reactive case.

An obvious question is to which extent the beneficial effect of a reaction-assisted regeneration can be accomplished by the well-investigated Hashimoto concept. Fig. 5 compares the performance of this approach (process 2 in Fig. 2) for different numbers of side reactors to that of a similar process with an internally distributed reaction (process 5). Process 2 is clearly outperformed as long as the number of side reactors is lower than the number of stages (here: 50 per zone). Obviously, in the implementation used here, the Hashimoto process represents a special case of process 5. Furthermore, the results imply that an efficient SMB-based realization will require a high number of side reactors and columns within zone *I* (or zones *III* or *IV* for obtaining the other isomer). For a detailed discussion of this, it is necessary to analyze SMB systems instead of TMB processes, which will be the subject of a later contribution.
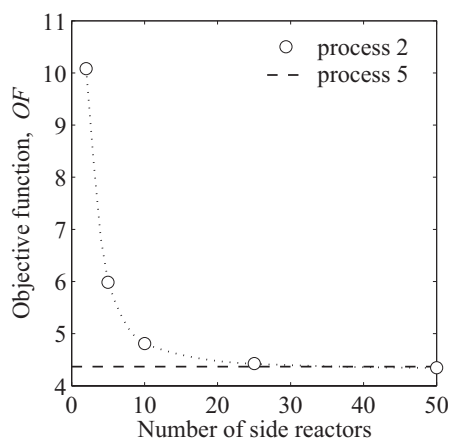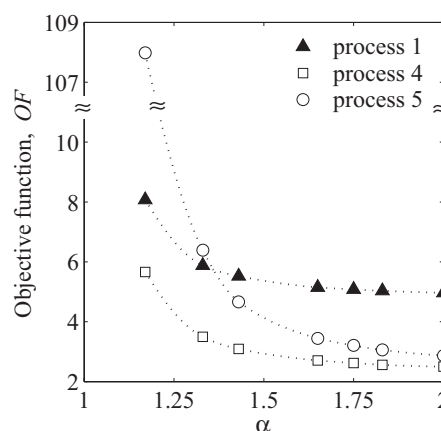
4.3   Role of Relevant Aspects

We will now extend the investigations beyond the reference case. Enantiomeric systems are characterized by low separation factors, α, and a reaction equilibrium constant of $K_{eq} = 1$ (as studied above). Below, the two corresponding functionalities, "adsorption" and "reaction", will be addressed, as well as their optimal spatial distribution.

The results above indicate that fully integrated processes (process 3) are not suitable for isomerization problems. Furthermore, the Hashimoto concept (process 2) can be regarded as a special case of three-zone systems with an internally distributed reaction (process 5). Therefore, in the following, we focus on the remaining processes 1, 4, and 5 shown in Fig. 2.

4.3.1   Separation Factor

The separation factor, α, plays a major role in any separation process. As demonstrated in Fig. 4, α also plays an important role with respect to the effectiveness of the reaction-assisted regeneration. The question to be answered here is whether different values for α will change the ranking of processes 1, 4 and 5 with respect to their performance.

It is difficult to vary the separation factor for the bi-Langmuir model in Eq. (7) in a useful manner without significantly affecting the nonlinear properties of the isotherms. The reason is the high number of parameters that determine α (see Eq. (8)). It can be expected, however, that similar trends will be obtained by using the Langmuir isotherms, Eq. (A-1), which were already used for the analysis in the previous section. Therefore, the parameters of the Langmuir model were adjusted such that the bi-Langmuir isotherms in Tab. 1 are matched closely ($q_s = 100$, $b_A = 0.20$, $b_B = 0.14$, and $\alpha = 1.43$).

Figure 5. Comparison of the performance of the three-zone set-up with a distributed reaction (process 5, dashed line) and the Hashimoto concept (process 2, circles) with different numbers of side reactors. The target product is the weaker adsorbing component *B*. $K_{eq} = 1.0$, $Pu_{min} = 90\%$.
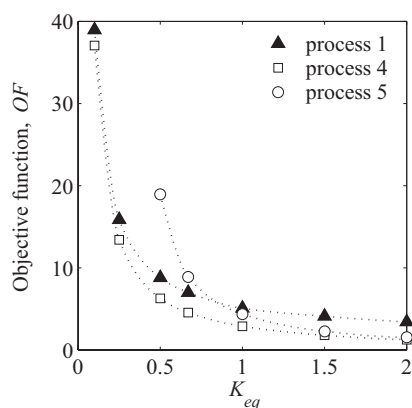

Figure 6. Performance as a function of the separation factor α, Eq. (8) for Langmuir isotherms. The target product is the weaker adsorbing component *B*. $K_{eq} = 1.0$, $Pu_{min} = 90\%$. Lines are guide to the eye.

Fig. 6 shows the optimization results for the weaker adsorbing component B obtained at a purity of 90 % (for other parameters than the isotherms, see Tab. 1). In the calculations, α was varied by increasing b_A and decreasing b_B in Eq. (A-2) by the same factor. As could be expected, the performance of all processes improves with increasing α. Process 4 has the best performance for the whole range studied. This is a consequence of the fact that process 4 has four zones and, thus, the highest number of free variables. This superiority is more pronounced for easier separations (high α values). For α = 2.0, the performance of process 4 is 200 % of that of process 1. While for difficult separations, the conventional process 1 achieves an 'intermediate' value for the objective function, it is also outperformed by process 5 for easier separations. The latter achieves a similar performance as process 4 for sufficiently large values of α. This is a promising aspect, since the simple process 5 requires no additional external operations.

4.3.2 Reaction Equilibrium

While for enantiomeric systems K_{eq} = 1 always holds, this stoichiometry is usually not found in other isomerizations. Therefore, we will investigate the three processes 1, 4, and 5 for different values of K_{eq}.

Fig. 7 shows the results obtained (i.e., the objective function OF versus K_{eq}). Again, the weaker adsorbing component B was the target product, obtained at a purity of 90 % (for the applied bi-Langmuir isotherms and other parameters, see Tab. 1). Very similar trends are observed in comparison to the influence of α (see Fig. 6). Again, process 4 is the best performing setup. For low values of K_{eq}, which correspond to an unfavorable reaction equilibrium (see Eq. 2), the performance of process 1 is lower than that for process 4. The objective function for process 5 improves significantly for favorable reaction equilibria and achieves a similar performance as process 4 for sufficiently large values of K_{eq}.


Figure 7. Performance as a function of the reaction equilibrium constant K_{eq}, Eq. (2) (bi-Langmuir isotherms). The target product is the weaker adsorbing component B. Pu_{min} = 90 %. Lines are guide to the eye.

4.3.3 Distribution of the Functionalities

In the schemes investigated above, the "reaction functionality" was distributed along the TMB unit by adjusting a single value for the Damköhler number, Da (Eq. 5), for each zone. In order to gain more insight into an optimal spatial distribution and its dependency on other aspects, optimizations were performed for a finer distribution with five different values for Da within each TMB zone.

Since it achieves the best performance, process 4 will be considered as an example. The results for this process are shown in Fig. 8. The upper part of the figure shows the optimized spatial profiles for Da for three different values of the product purity (Pu^R = 90, 95 and 99.9 %). Obviously, the higher the purity demand, the more stages are required to perform the separation task and, consequently, the lower the number of reactive stages. Furthermore, it can be seen that Da only changes within zone II. The values in the other zones are constant and correspond either to the upper (zone I) or to the lower limit (zones III and IV), respectively. It should be mentioned that the finer distribution of the functionalities does not result in a significant improvement in performance. For the example of Pu_{min} = 90 %, the value of the objective improves by only 1 % (OF = 2.87) in comparison to the results in Tab. 2.
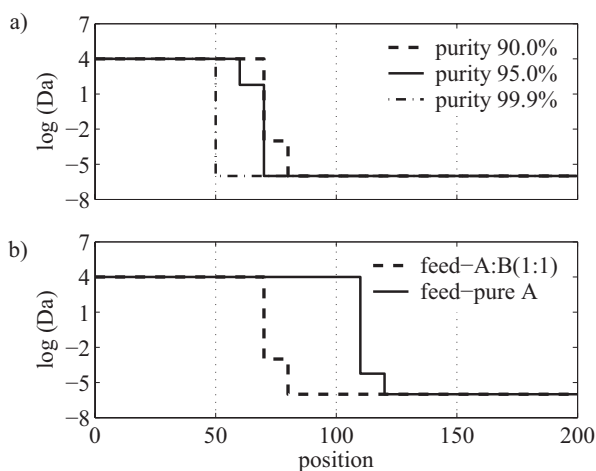
Figure 8. Optimal distribution of the functionalities for a reactive four-zone TMB unit (process 3 in Fig. 2) as a function of (a) the purity requirement and (b) the feed composition for Pu_{min} = 90 %. In the optimizations, five different values for the Damköhler number, Da, were adjusted within each zone. The target product is the weaker adsorbing component B with Pu_{min} = 90 %.

The lower part of the figure was obtained for two different values of the relative feed composition. In the first case, B is to be produced from a 1 : 1 mixture of A and B. This corresponds to the situation that was assumed so far. In the second case, B should be obtained from pure A fed into the unit. This is the case, for example, in the processing of waste streams, or if the synthesis of a counter-isomer is easier than of the desired form. As could be expected, in the latter case a larger proportion of the unit is required for the chemical reaction because a

higher conversion is required (i.e., $X = 90\%$ instead of 80%; see Eq. 11).

5   Conclusions

A systematic and fundamental theoretical study was performed with respect to the possibility of devising integrated reactive separations that combine continuous chromatography and isomerization reactions. A particularly important field of application for such processes is the production of single enantiomers.

Different process schemes were derived from the general options existing for process integration. The performance of the processes was compared using model-based optimizations. A new process concept was suggested that utilizes an internal spatial distribution of the functionalities. The results indicate that such a process could outperform conventional reactor-separator-recycle systems. It was found that the observed benefits mainly originated from the easier regeneration of the corresponding zones of the chromatographic process. This effect, denoted as reaction-assisted regeneration, was analyzed on the basis of equilibrium theory. In this context, some of the limitations of existing process concepts could be explained.

Furthermore, the performance of the different schemes was evaluated in view of selected relevant aspects. It was found that the concept of internally distributing the functionalities could be an attractive option, in particular under favorable conditions with respect to reaction equilibrium and/or separation difficulty. In such cases, the performance of a simple three-zone setup without any external unit operations is superior to that of more complex conventional process structures.

Future work will be devoted to the application of the results to practically feasible processes based on SMB systems.

Acknowledgement

Appendix A: Analysis of Reactive Regeneration in TMB Reactors

For countercurrent chromatographic processes, equilibrium theory can be applied to derive analytical solutions under linear and nonlinear conditions for Riemann problems (i.e., piecewise constant boundary and initial conditions). Furthermore, the theory can also be applied to isomerizations with finite rates of adsorption or reaction. The interested reader is referred to the elaborate treatment given in [22].

Here, we will summarize the application of the theory to the regeneration zones of non-reactive TMB processes. Subsequently, we will extend this to reactive systems with established adsorption and reaction equilibria in order to derive expressions that quantify the effect of reaction-assisted regeneration. For this purpose, we will apply the straightforward theoretical framework presented in [36]. For the sake of brevity, the bi-Langmuir model (Eq. 7) will be replaced by the simpler Langmuir-type adsorption isotherms:

$$q_i = q_s \frac{b_i c_i}{1 + b_A c_A + b_B c_B} \quad i = (A, B) \tag{A–1}$$

In analogy to Eq. (8), the separation factor for Langmuir isotherms is given by

$$a = \frac{b_A}{b_B} \tag{A–2}$$

In the non-reactive case, the mass balances for a single zone are given by the following system of first-order partial differential equations:

$$\frac{\partial}{\partial \tau}[c + Fq(c)] + \frac{\partial}{\partial x}[c - \mu q(c)] = 0$$
$$\text{with } x = \frac{z}{L}, \quad \tau = \frac{v_f t}{L}, \quad \mu = \frac{v_s}{v_f} F = \frac{1}{m} \tag{A–3}$$

where v_f and v_s are the liquid- and solid-phase velocities (which are assumed to be constant), z refers to the spatial coordinate, and L is the total length. Eq. (A-3) is a homogeneous system of quasilinear equations that describes wave phenomena. The system is reducible for isotherms of the Langmuir type (when, like in this case, q_s is equal for both components) and thus allows for analytical solutions by, for example, the method of characteristics [22].

In order to design continuous chromatographic processes, the propagation velocity, λ_k, for each concentration value within the unit must be known. For simple (i.e., spreading) waves in non-reactive systems, this is given by:

$$\lambda_k = \frac{1 - \mu \sigma_k}{1 + F \sigma_k} \tag{A–4}$$

where the subindex k denotes different ranges of the solution. σ_k is given by the eigenvalues of the Jacobian matrix of the adsorption isotherm. For shock waves, σ_k has to be replaced by the relation $\Delta q / \Delta c$.

Of main interest in this work are the zones where the reaction occurs. These zones are responsible for the regeneration of the solid (zone *I*) and the liquid phase (zone *III* or *IV*), respectively. For a complete regeneration, the corresponding waves have to be stabilized. Therefore $\lambda_k = 0$ in Eq. (A-4). In the non-reactive case, the following conditions for the required flow rate ratios m can be derived from Eq. (A-4):

$$m^I = \frac{1}{\mu} = \frac{\partial q_A}{\partial c_A}\bigg|_{c_A = 0} \tag{A–5}$$

For the shock waves in zones *III* or *IV* holds

$$m^j = \frac{\Delta q_B}{\Delta c_B}\bigg|_j, \quad j = (III, IV) \tag{A–6}$$

For reactive systems, it is somewhat more difficult to obtain explicit solutions, because the underlying mass balances (one for each component) are no longer homogeneous:

$$\frac{\partial}{\partial \tau}[c + Fq(c)] + \frac{\partial}{\partial x}[c - \mu q(c)] = r$$

$$\text{with } r = \begin{cases} r(c) & : \text{ homogeneous reaction} \\ r(q) & : \text{ heterogeneous reaction} \end{cases} \tag{A–7}$$

However, by assuming an infinite reaction rate, this system can be reduced to a homogeneous one (see [36]). Under this assumption, the concentrations of the two components are related, and the system of two differential equations can be reduced, for binary mixtures, to a single homogeneous partial differential equation. For the stoichiometry used here, this equation is also reducible:

$$\frac{\partial}{\partial \tau}[C + FQ(C)] + \frac{\partial}{\partial x}[C - \mu Q(C)] = 0$$

$$\text{with } C = c_A + c_B, \quad Q = q_A + q_B \tag{A–8}$$

where C and Q are transformed variables defined according to the stoichiometry of the reaction [36]. In analogy to Eqs. (A-5) and (A-6), one finds for the flow rate ratios m that are necessary for complete regeneration:

$$m^{\mathrm{I}} = \left.\frac{\partial Q}{\partial C}\right|_{C=0} \tag{A–9}$$

and

$$m^{\mathrm{j}} = \left.\frac{\Delta Q}{\Delta C}\right|_{\mathrm{j}}, \quad j = (III, IV) \tag{A–10}$$

In order to solve Eqs. (A–9) and (A–10), additional information is required to specify $Q(C)$ (*cf.* Eq. (A–8)). These are given by the equilibria of adsorption, Eq. (A–1), and reaction. For the latter holds, in the case of a homogeneous reaction, Eq. (2), while for a heterogeneous reaction, this is given by

$$K_{\mathrm{eq}} = \frac{q_B}{q_A} \tag{A–11}$$

Tab. 5 contains the resulting m values necessary for the complete regeneration of zones *I* and *IV* for the three considered cases: non-reactive, homogeneous reaction, and heterogeneous reaction. The table holds for the Langmuir isotherm model. Note that the concentrations that appear in the rightmost column of the table can be calculated from simple mass balances.

The expressions in Tab. 5 can be simplified further. For example, in order to investigate the impact of the reaction-assisted regeneration, the separation factor a can be substituted into the corresponding terms. For the particular case of enantiomers ($K_{eq} = K'_{eq} = 1$), this leads to the following ratios of the flow rates in zone *I* required for complete regeneration in reactive and non-reactive cases, respectively:

$$\frac{m^{\mathrm{I}}}{m^{\mathrm{I}}_{\mathrm{non-reactive}}} = \begin{cases} 1 & : \text{ no reaction} \\ \frac{a+1}{2a} & : \text{ homogeneous reaction} \\ \frac{2}{a+1} & : \text{ heterogeneous reaction} \end{cases} \tag{A–12}$$

An analogous analysis as above can be performed for bi-Langmuir isotherms. However, the derivation is more detailed and will be explained in a future contribution. Finally, note

that for more complicated reaction mechanisms than assumed here, it might not be possible to derive explicit solutions.

Symbols used

b	[mL/mg]	isotherm parameter
c	[mg/mL]	liquid-phase concentration
Da	[–]	Damköhler number
F	[–]	phase ratio
K_{eq}	[–]	equilibrium constant
K_f	[min^{-1}]	kinetic constant for the forward reaction
K_b	[min^{-1}]	kinetic constant for the backwards reaction
m	[–]	dimensionless flow rate
OF	[–]	objective function
Pr	[mg/min]	productivity
Pu	[%]	purity
Q	[mL/min]	volumetric flow rate
q	[mg/mL]	solid-phase concentration
q_S	[mg/mL]	saturation capacity
r	[mg/mL]	reaction term
t	[min]	time
V	[mL]	stage volume
X	[–]	conversion

Greek symbols

a	[–]	separation factor
ε	[–]	porosity
υ	[–]	stoichiometric coefficient

Subscripts/superscripts

i	component
k	stage
n	zone
s	solid phase
l	liquid phase
D	desorbent
E	extract
F	feed
R	raffinate

References

[1] *Integrated Chemical Processes* (Eds: K. Sundmacher, A. Kienle, A. Seidel-Morgenstern), Wiley-VCH, Weinheim **2005**.

[2] M. Sardin, J. Villermaux, *Chem. Eng. J.* **1985**, *30 (2)*, 91.

[3] D. Gelosa, M. Ramaioli, G. Valente, M. Morbidelli, *Ind. Eng. Chem. Res.* **2003**, *42 (25)*, 6536.

[4] T. D. Vu, A. Seidel-Morgenstern, S. Grüner, A. Kienle, *Ind. Eng. Chem. Res.* **2005**, *44 (25)*, 9565.

[5] G. K. Gandi, V. M. T. M. Silva, A. E. Rodrigues, *Chem. Eng. Sci.* **2007**, *62 (4)*, 907.

[6] M. Bechtold, S. Makart, M. Heinemann, S. Panke, *J. Biotechnol.* **2006**, *124 (1)*, 146.

[7] T. Borren, *Ph.D. Thesis*, Universität Dortmund **2006**.

[8] M. Kaspereit, J. García Palacios, T. Meixús Fernández, A. Kienle, in *Computer-Aided Chemical Engineering (Vol. 25) – 18th Europ. Symp. on Comp. Aided Process Eng.* (Eds: B. Braunschweig, X. Joulia), Elsevier, Amsterdam **2008**.

[9] K. Hashimoto, S. Adachi, H. Noujima, Y. Ueda, *Biotechnol. Bioeng.* **1983**, *25 (10)*, 2371.

[10] K. Hashimoto, S. Adachi, Y. Shirai, in *Preparative and Production Scale Chromatography* (Eds: G. Ganetsos, P. E. Barker), Marcel Dekker, New York **1993**.

[11] Y. Zhang, K. Hidajat, A. Ray, *Biochem. Eng. J.* **2004**, *21 (2)*, 111.

[12] T. Borren, J. Fricke, *Preparative Chromatography of Fine Chemicals and Pharmaceutical Agents*, Wiley-VCH, Weinheim **2005**, Ch. Chromatographic Reactors.

[13] M. Kawase, T. Suzuki, K. Inoue, K. Yoshimoto, K. Hashimoto, *Chem. Eng. Sci.* **1996**, *51 (11)*, 2971.

[14] D. C. S. Azevedo, A. E. Rodrigues, *Chem. Eng. J.* **2001**, *82 (1–3)*, 95.

[15] G. Ströhlein, M. Mazzotti, M. Morbidelli, *Chem. Eng. Sci.* **2005**, *60 (6)*, 1525.

[16] T. Sainio, M. Kaspereit, A. Kienle, A. Seidel-Morgenstern, *Chem. Eng. Sci.* **2007**, *62 (18–20)*, 5674.

[17] M. Kawase, Y. Inoue, T. Araki, K. Hashimoto, *Catal. Today* **1999**, *48 (1–4)*, 199.

[18] M. Kawase, A. Pilgrim, T. Araki, K. Hashimoto, *Chem. Eng. Sci.* **2001**, *56 (2)*, 453.

[19] A. Toumi, S. Engell, *Chem. Eng. Sci.* **2004**, *59 (18)*, 3777.

[20] B. K. Cho, R. Aris, R. W. Carr, *Proc. R. Soc. Lond. A* **1982**, *383 (9)*, 147.

[21] T. Petroulas, R. Aris, R. Carr, *Chem. Eng. Sci.* **1985**, *20 (12)*, 2233.

[22] H.-K. Rhee, R. Aris, N. Amundson, First-Order Partial Differential Equations. Vol. II. Theory and Application of Hyperbolic Systems of Equations, Prentice-Hall, Englewood Cliffs, NJ **1989**.

[23] M. Sardin, D. Schweich, J. Villermaux, in *Preparative and Production Scale Chromatography* (Eds: G. Ganetsos, P. E. Barker), Marcel Dekker, New York **1993**.

[24] A. K. Ray, R. W. Carr, R. Aris, *Chem. Eng. Sci.* **1994**, *49 (4)*, 469.

[25] A. K. Ray, R. W. Carr, *Chem. Eng. Sci.* **1995**, *50 (19)*, 3033.

[26] M. C. Bjorklund, R. W. Carr, *Catal. Today* **1995**, *25 (2)*, 159.

[27] M. Tylko, *Ph.D. Thesis*, Universität Dortmund **2008**.

[28] J. Fricke, *Ph.D. Thesis*, Universität Dortmund **2005**.

[29] T. Jensen, T. Reijns, H. Billiet, L. van der Wielen, *J. Chromatogr. A* **2000**, *873 (2)*, 149.

[30] D. Antos, A. Seidel-Morgenstern, *Chem. Eng. Sci.* **2001**, *56 (23)*, 6667.

[31] S. Abel, M. Mazzotti, M. Morbidelli, *J. Chromatogr. A* **2004**, *1026 (1/2)*, 47.

[32] D. Ruthven, C. B. Ching, *Chem. Eng. Sci.* **1989**, *44 (5)*, 1011.

[33] N. Gottschlich, S. Weidgen, V. Kasche, *J. Chromatogr. A* **1996**, *719 (2)*, 267.

[34] R. Köhler, K. D. Mohl, H. Schramm, M. Zeitz, A. Kienle, M. Mangold, E. Stein, E. D. Gilles, in *Adaptative Method of Lines* (Eds: A. V. Wouwer, P. Saucez, W. E. Schiesser), CRC, Chapman and Hall, London **2001**.

[35] M. Kaspereit, A. Seidel-Morgenstern, A. Kienle, *J. Chromatogr. A* **2007**, *1162 (1)*, 2.

[36] S. Grüner, A. Kienle, *Chem. Eng. Sci.* **2004**, *59 (4)*, 901.

Javier García Palacios[1]
Malte Kaspereit[1]
Achim Kienle[1,2]

[1] Max-Planck-Institut für Dynamik komplexer technischer Systeme, Magdeburg, Germany.

[2] Otto-von-Guericke Universität Magdeburg, Lehrstuhl Automatisierungstechnik/ Modellbildung, Magdeburg, Germany.

Research Article

Integrated Simulated Moving Bed Processes for Production of Single Enantiomers

Based on the assumption of true moving bed processes it was demonstrated that integration of a racemization reaction into a continuous chromatographic process can improve the production of single enantiomers. In view of possible practical implementations, the analysis is extended to more realistic simulated moving bed (SMB) processes. Superstructures of SMB-based systems are defined that reflect the three general concepts of flow sheet, partial, and total process integration. Process candidates are generated by simultaneously optimizing process structure and operating conditions. Optimal process setups are determined under idealized conditions as a function of the purity requirement. The best performance is achieved by fully integrated processes. These are compared under more realistic conditions to units with side reactors. The results indicate that a simple fully integrated SMB system with three zones is a particularly promising new process option. The new concept is investigated in detail to identify relevant practical aspects.

1   Introduction

Enantiomers are stereoisomers structured like mirror images. They play an important role in pharmaceutical industry. Frequently, only one enantiomer has the desired physiological effect. The other form can be ineffective or might even be harmful. On an industrial scale, producing single enantiomers by selective synthesis is often unfeasible or too expensive due to long development times. Thus, often the 50/50 mixture of both enantiomers is produced by conventional chemical synthesis. In this case, a subsequent separation step is required. Techniques such as chromatography, crystallization, or kinetic resolution are usually applied to recover the desired enantiomeric form. However, the achievable yield by this approach is inherently limited to 50 %.

The focus of this work is on increasing the yield of such productions to basically 100 % by devising processes that combine continuous chromatographic separation by simulated moving bed (SMB) chromatography with a racemization (isomerization) reaction. The investigated processes should be capable of delivering the target enantiomer at high purity and simultaneously interconvert the undesired form into the desired one.

Possible approaches to combine SMB chromatography with an isomerization reaction fall into three categories [1]: (i) conventional separator-reactor-recycle systems, (ii) partially integrated processes with side reactors, and (iii) fully integrated processes which perform reaction and separation within the same unit.

The conventional combination of SMB chromatography with an interconversion reactor in a recycle has rarely been studied in detail. Bechtold et al. investigated its potential with respect to enzyme-catalyzed racemizations to produce amino acids [2, 3]. Zhang et al. [4] evaluated it for the production of high-fructose syrup. Bergeot et al. [5] described this combination for isomerization of C8 aromatics. In this and previous works we consider such recycle systems as reference case [1, 6].

An alternative concept based on partial integration has been proposed by Hashimoto et al. [7]. Here, side reactors are spatially distributed along an SMB unit with three zones to produce the stronger adsorbing isomer. The advantage of this more complex process allows deciding where the reaction should take place. The approach was studied mainly for sugar applications and several modifications have been proposed, including recycle streams and systems with four zones [4, 5, 8–11]. Applications to the production of the stronger adsorbing enantiomer of Troeger's base were reported in [8, 9, 12].

Correspondence: Dr. M. Kaspereit (kaspereit@mpi-magdeburg.mpg. de), Max-Planck-Institut für Dynamik komplexer technischer Systeme, Sandtorstraße 1, 39106 Magdeburg, Germany.

First theoretical investigations on the third concept, where an isomerization reaction is fully integrated into a countercurrent chromatographic reactor, were reported in [13, 14]. The reaction was allowed to take place uniformly within all columns. Mathematical evidence was provided that an isomer can be produced at high purity for specific ratios of adsorption and reaction kinetics. Corresponding three-zone systems were investigated, e.g., for glucose isomerization [15] and gas phase reactions [16, 17].

It is important to note that the mentioned works on partially and fully integrated processes consider exclusively the production of the stronger adsorbing isomer and focus on products with limited purity. The only exception was presented by Ray et al. [16], who obtained the weaker adsorbing component at high purity. However, they studied a markedly favorable case with a reaction equilibrium constant greater than 100 and a separation factor of 4. As was already found in [1] and will be elucidated further in this work, side reactor-based systems achieve rather poor performance when producing the weaker adsorbing species, in particular when aiming at high product purity.

Recently, a more general evaluation of the fundamental concepts discussed above was presented and several new process candidates were suggested for both the weak- and strong-adsorbing component as target product [1]. It was concluded that integration of the chemical reaction into the chromatographic unit can improve the overall process performance if the reaction is spatially distributed such that it is confined to the regeneration zone. This is due to an effect denoted as reaction-assisted regeneration. The investigation utilized simplified process models that assume a true moving bed (TMB).

In view of a practical implementation, the objective of this work is to extend the analysis in [1] to more realistic SMB processes. It will be shown that the periodic switching in SMB processes can cause a different behavior than found for the corresponding TMB-based schemes. This has to be taken into account in process design. Furthermore, finding optimal SMB configurations is more complex, since the number of columns, reactors, and chromatographic reactors, as well as their position, are degrees of freedom. This problem is solved here by defining superstructures which are then subjected to a mixed-integer nonlinear programming (MINLP). Against the background discussed above, the focus is on difficult scenarios that are typical for enantioseparations: high purity requirements, low separation factors, and both forms can represent the target product.

Based on initial calculations and the results in [1], superstructures were defined which reflect the three general concepts for process integration. Fig. 1 shows five of them dedicated to obtain the less retained enantiomer B. Process 1 is the reference case of a classical reactor-separator-recycle system (flow-sheet integration). Here, the SMB unit performs the separation of A and B. The undesired component A is recovered and reconverted into the racemic mixture in an external reactor. An intermediate removal of solvent (SR) is included to counterbalance the typical dilution caused by the SMB system.

Schemes 2 to 5 represent superstructures subject to optimization where R^1 to R^5 are used as decision variables determining if these positions should hold the reaction. Scheme 2 subsumes possible partially integrated processes. It is based on a four-zone SMB setup and performs a solvent removal (SR) in the recycle stream. The superstructure has five relevant degrees
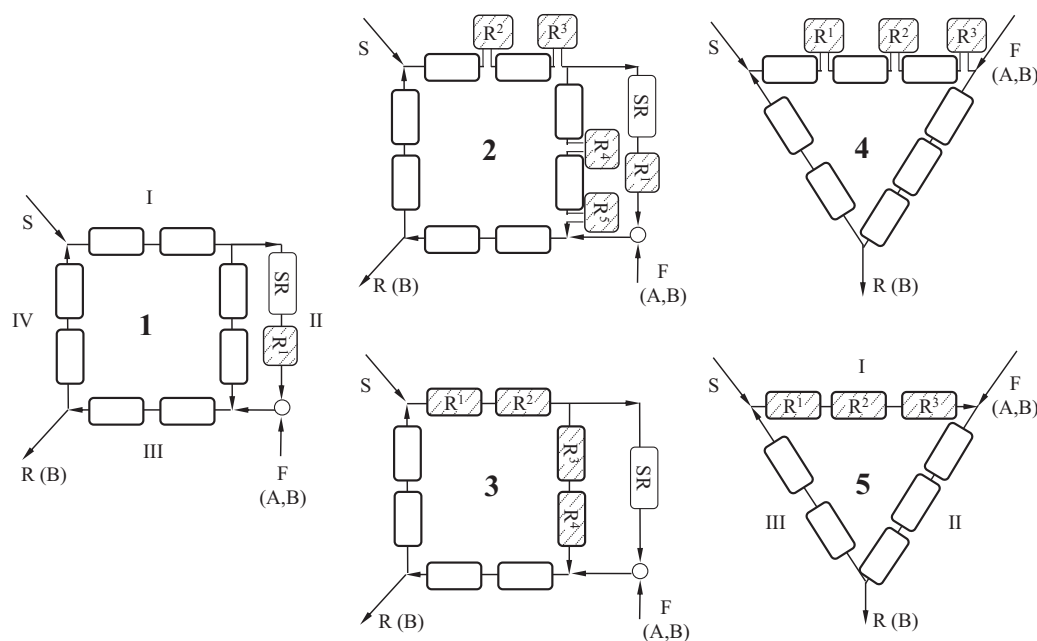
Figure 1. Process schemes for producing the less retained enantiomer B by integrating SMB chromatography and isomerization reactions (raffinate setups). (1) Conventional flow sheet-integrated SMB process (reactor-separator-recycle; fixed structure) with a solvent removal device (SR); (2) semi-integrated four-zone SMB with side reactors; (3) fully integrated four-zone SMB; (4) semi-integrated three-zone SMB with side reactors (Hashimoto concept); (5) fully integrated three-zone SMB.

of freedom: A reactor can be placed in the recycle (R^1), while four more reactors (R^2 through R^5) can be located along zones I and II. Note that in total this allows for 2^5 (i.e., 32) different reactor arrangements (subsets). In principle, many more reactor positions could be studied. However, to limit the structural complexity of the optimization problem, the reaction is allowed only in certain positions corresponding to the finding in [1] that the optimal location of the reaction is left of the feed point.

Scheme 3 is a completely integrated device where the reaction takes place in columns that are reactive only when they are located at specific positions within the SMB unit. Due to the switching of columns this will require that during operation the reaction in these beds is periodically switched on and off. This is possible by applying reactive gradients as will be discussed below. Superstructure 3 has four degrees of freedom (R^1 to R^4) corresponding to 16 (2^4) possible subsets, depending on in which of the four columns the reaction is permitted.

Schemes 4 and 5 in Fig. 1 represent similar concepts like processes 2 and 3 but contain an SMB unit with only three zones. These configurations are simpler since they do not require recycle streams or devices for solvent removal. As already mentioned, previous studies of process 4 concluded that its performance decreases rapidly for high purity demands [12, 18]. As will be demonstrated below, process 5 can be an attractive alternative that achieves better performance. Each of the structures 4 and 5 have a degree of freedom of three, resulting in 8 (2^3) subsets in each case. It is worth mentioning that process 5 has been successfully validated experimentally by using a step gradient of the pH value to trigger the reaction at the desired locations [19].

Fig. 2 illustrates analogous schemes for producing the more retained component A. As in Fig. 1, schemes 2 to 5 represent superstructures subject to optimization where R^1 to R^5 are used as decision variables determining if these positions should hold the reaction. According to the findings in [1], again the racemization reaction is confined to certain positions. It is worth mentioning that process 4 represents the classical Hashimoto concept. Furthermore, structure 2 inherits also an extended process suggested by Borren et al. [8, 9] where reactors are placed at the positions R^1, R^4, and R^5, as well as, e.g., the setups considered in [5] and [10].

The superstructures presented above subsume in total 130 possible process candidates. It would be tedious to define a model and subsequently optimize the operating conditions for each of them. Therefore, to allow for a fair comparison, dynamic SMB models were defined for each superstructure and an MINLP approach was applied to identify simultaneously the optimal operating conditions and the optimal process setup for the general approaches reflected by these superstructures. Note that in the calculations the number of columns in the systems in Figs. 1 and 2 is kept constant (eight for each process). Only the reactivity of a side reactor or chromatographic reactor is turned on or off by the optimization.

The paper is organized as follows. First, the mathematical model and the optimization method are explained. Then, the performance of the resulting structures is compared and discussed as a function of the purity requirements. The differences with respect to process performance and dynamic behavior between partially and fully integrated processes are elaborated. Finally, the interesting new integrated process concept with three zones is analyzed in detail.
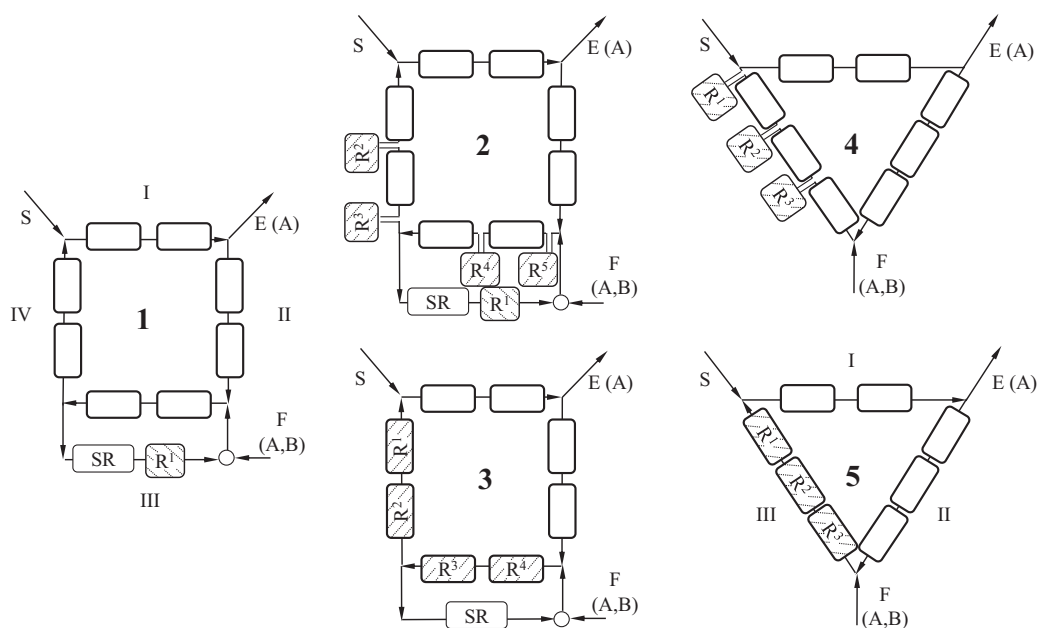
Figure 2. Process schemes for producing the more retained enantiomer A by integrating SMB chromatography and isomerization reactions (extract setups). (1)–(5) as described in Fig. 1.

2   Mathematical Model and Optimization

The MINLP optimization approach used in this work requires a numerically efficient process model. A conventional equilibrium stage model is applied to describe the migration of the two components within the columns. The mass balances for the two species within each stage are given by

$$\frac{dc_i^{k,n}}{dt} + F\frac{dq_i^{k,n}}{dt} = \frac{Q^z}{V\varepsilon}(c_i^{k-1,n} - c_i^{k,n}) + R^j v_i r^{k,n} \tag{1}$$

where indices $i = A$, B denote the component, $k = 1...N_s$ is the stage index, $n = 1...N_c$ is the stage index of the column, and $z = I...N_z$ marks the corresponding zone of the SMB unit. c_i and q_i are the liquid and solid phase concentrations, Q is the volumetric flow rate of the fluid phase, V is the stage volume, and $F = (1-\varepsilon)/\varepsilon$ is the phase ratio, respectively. The axial dispersion is adjusted by the number of stages, N_s [20].

The last term in Eq. (1) describes the chemical reaction with r as the reaction rate and v_i as the stoichiometric coefficient. The decision variables $R^j \in \{0, 1\}$ describe whether the chemical reaction is allowed in the column at position $j = 1...N_r$, or not, i.e., if $R^j = 1$, the corresponding column is a chromatographic reactor, for $R^j = 0$ it is a conventional column. N_r is the number of columns where the reaction can take place, and depends on the particular superstructure (see Figs. 1 and 2). In this work, a reversible isomerization $A \Delta B$ that occurs in the fluid phase was considered. The reaction equilibrium constant is

$$K_{eq} = \frac{c_B}{c_A} = \frac{k}{k_b} \tag{2}$$

with k and k_b as rate constants of the forward and backward reaction, respectively. For the specific case of racemization $k = k_b$ and thus $K_{eq} = 1$. From Eq. (2) follows for the reaction rate in Eq. (1):

$$r^{k,n} = k\left(c_A^{k,n} - \frac{c_B^{k,n}}{K_{eq}}\right) \tag{3}$$

The relation between the solid and the liquid phase concentrations in Eq. (1) is given by the adsorption equilibrium. Here, competitive bi-Langmuir adsorption isotherms are applied that are used frequently for enantiomers [21]:

$$q_i = \frac{q_{s,1}b_{i,1}c_i}{1 + b_{A,1}c_A + b_{B,1}c_B} + \frac{q_{s,2}b_{i,2}c_i}{1 + b_{A,2}c_A + b_{B,2}c_B}$$

with $i = (A, B)$ \hfill (4)

Eq. (4) describes competitive adsorption of the two solutes (A, B) on two different types of adsorption sites of the solid (1, 2). The two different saturation capacities are denoted by $q_{s,1}$ and $q_{s,2}$.

The following mass balances define the connections among the columns in the four-zone SMB units

$$\text{if } n = 8 \quad : \quad Q^{IV}c_i^{N_s,n} + Q^S c_i^S = Q^I c_i^{0,1}$$

$$\text{if } n = 4 \quad : \quad Q^{II}c_i^{N_s,n} + Q^{Rec}c_i^{Rec} + Q^F c_i^F = Q^{III}c_i^{0,n+1} \tag{5}$$

$$\forall n \neq \{4, 8\} \quad : \quad c_i^{N_s,n} = c_i^{0,n+1}$$

where positions 8 and 4 correspond to the columns upstream of the desorbent and the feed points, respectively. $c_i^{0,n}$ is the concentration entering column n and Rec is the recycle stream in the four-zone systems (see Figs. 1 and 2).

For the three-zone systems, similar balances hold for the raffinate setups (see Fig. 1)

$$\text{if } n = 8 \quad : \quad Q^{III}c_i^{N_s,n} + Q^S c_i^S = Q^I c_i^{0,1}$$

$$\text{if } n = 3 \quad : \quad Q^I c_i^{N_s,n} + Q^F c_i^F = Q^{II}c_i^{0,n+1} \tag{6}$$

$$\forall n \neq \{3, 8\} \quad : \quad c_i^{N_s,n} = c_i^{0,n+1}$$

and for the extract schemes in Fig. 2, the indices {3, 8} in the last line of Eq. (6) have to be replaced by {5, 8}.

The continuous design variables to be optimized in this work are the dimensionless zone flow rate ratios m_z for each zone z (e.g., [22]):

$$m^z = \frac{Q^z t^* - \varepsilon V_c}{(1 - \varepsilon)V_c} \tag{7}$$

with V_c as the volume of a chromatographic column. t^* is the switching time of the SMB system.

The external devices connected to the SMB units in Figs. 1 and 2 are modeled as follows. The side reactors represent continuously stirred tank reactors (CSTRs)

$$\frac{dc_i^{0,n+1}}{dt} = \frac{Q^z}{\varepsilon V_r}\left(c_i^{N_s,n} - c_i^{0,n+1}\right) + R^j v_i r^j \tag{8}$$

where V_r is the volume of the side reactor. The decision variable R^j decides whether the reactor is active or not. The devices for solvent removal (SR) are assumed to instantaneously adjust the mixture concentrations such that the higher concentrated component has the same concentration as in the feed.

The specific solvent consumption is applied as the objective function in the optimizations to evaluate the different process schemes:

$$\text{OF} = \frac{Q^S}{Q^{out}c_d^{out}} = \frac{Q^S}{\text{Pr}} = P^{-1} \tag{9}$$

In Eq. (9), the performance indicator P is introduced as the reciprocal of the objective OF. This is mainly to simplify later graphical representations. Q^S and Q^{out} are the flow rates of the desorbent and the product (out = R for processes in Fig. 1, out = E for Fig. 2), respectively. c_d^{out} is the concentration of the desired component d in this stream. The term $\text{Pr} = Q^{out}c_d^{out}$ is the throughput of the process. Eq. (9) is a frequently used objective function for continuous chromatography, since it simultaneously aims at minimizing solvent consumption and maximizing productivity. The optimization problem can be summarized as:

$$\text{OF}\left(m^z, R^j\right) \rightarrow \min$$

s.t.

$$\text{Pu}^{\text{out}} = \frac{c_d^{\text{out}}}{c_A^{\text{out}} + c_B^{\text{out}}} \geq \text{Pu}_{\min} \qquad (10)$$

with $z = 1...N_z$, $j = 1...N_r$, $d = (\text{A, B})$

In Eq. (10), Pu^{out} denotes the product purity and $\text{Pu}_{\min}$ is the purity demand. Note that no additional constraint for the conversion is required because the processes in Figs. 1 and 2 have only a single outlet. In such case, purity and conversion are related by the global mass balance [1].

The dynamic simulation of the SMB systems are performed using the simulation environment with DIVA [23, 24]. For the periodic switching a Petri net routine is implemented. The dynamic simulations reach a cyclic steady state (CSS) after a certain number of cycles, which can vary significantly depending on the external devices and the operating parameters. A stopping criterion based on a Poincaré map [25] is used to identify the CSS in each simulation. Typically, around 15 complete cycles are required. A conventional evolutionary algorithm [26] is applied to solve the MINLP problem that consists of determining the values for m^z and R^j in Eq. (10). Calculation times on a modern quad core PC are in the range of 2 min for systems with 200 total stages and up to 20 min for 800 stages.

For our model system, we choose the adsorption isotherm parameters of the chlorthalidone enantiomers [6]. The feed is considered to be racemic, i.e., the feed concentrations of A and B are equal. Tab. 1 summarizes the model parameters and conditions used. Note that in the calculations a switching time of $t^\star = 1$ min has been applied (cf. Tab. 1). In a real process, this arbitrary choice would be replaced, e.g., by specifying an internal flow rate according to a pressure drop constraint. It is emphasized that $t^\star$ has no effect on the value of the objective function as long as the reaction rate is infinite, since it is cancelled out when substituting the m^z-values into Eq. (10). An effect is observed only for systems with finite reaction kinetics as studied in Section 3.2. In these cases, the objective function is

also rendered independent of $t^\star$ by using in the model a ratio of kinetic constants rather than individual rate constants.

3 Results

The structure and performance of an optimal process depend strongly on the specific requirements on the separation or production task. Besides fulfilling fundamental constraints on, e.g., purity requirements, obvious objectives are high performance and low process complexity.

In Section 3.1 MINLP optimization was applied to find the optimal subprocesses of the superstructures depicted in Figs. 1 and 2 for different purity requirements. The identified process alternatives are compared with respect to their performance. To alleviate the analysis, we assume in this first step reaction equilibrium corresponding to an infinitely fast reaction and negligible volume of the external devices. In Section 3.2 the effect of finite volumes of the external devices is investigated, which reveals some fundamental differences between TMB and SMB systems. Finally, in Section 3.3, the role of finite reaction kinetics is addressed for an attractive three-zone process identified in the previous sections in view of its practical feasibility.

3.1 Process Synthesis and Optimization

Idealized conditions were applied that correspond to an established reaction equilibrium (adjusted by a very high reaction rate constant of $k = 10^5 \, \text{min}^{-1}$) and a negligible volume of possible side reactors ($V_r = 0$).

3.1.1 Moderate Purity Requirements

The production of pure enantiomers is generally carried out through successive separation stages. Often, chromatographic separations are followed by crystallization steps which increase the product quality. Moderate purity requirements for the SMB can result advantageous due to the existing interplay between productivity and purity. Correspondingly, relaxed purity demands can be of interest since they may lead to an increased overall performance of combined separation processes [27].

Tab. 2 contains the optimization results of the superstructures shown in Fig. 1 as raffinate setups. The purity requirements of 90 % and 95 % are considered moderate. Low efficiency columns ($N_s = 25$) are used in this case for the SMB units. Note that $R^j = 1$ means that a column is reactive, i.e., reaction and adsorption occur simultaneously. $R^j = 0$ denotes a conventional chromatographic column. Similarly, a value of 1 indicates that a side reactor is active, while 0 denotes an inactive one.

The performance of the fixed structure 1 – a conventional reactor-separator-recycle process – will be used as a reference for comparison with the other optimized processes. On average, schemes 2 through 5 allow for a performance improvement of about 31 % in comparison to this reference case. The optimal structure of the side reactor process 2 contains in this case all five side reactors (R^1 to R^5). The fully integrated scheme 3

Table 1. System parameters and constant operating conditions. Properties of the model system CTD as taken from [6].

Parameters	Symbol	Unit	Value	
bi-Langmuir adsorption isotherms, Eq. (4)	$q_{s,1}$	[g L^{-1}]	94.175	
	$q_{s,2}$	[g L^{-1}]	0.224	
	$b_{i,1}$	[L g^{-1}]	0.207	0.141
	$b_{i,2}$	[L g^{-1}]	6.395	3.192
Reaction equilibrium	K_{eq}	[–]	1.0	
Column length	L_c	[dm]	2.0	
Column diameter	d_c	[dm]	0.04	
Porosity	ε	[–]	0.796	
Feed concentration	c_i^F	[g L^{-1}]	0.2	
Switching time	$t^\star$	[min]	1.0	

Table 2. Optimization results for the schemes depicted in Fig. 1 (raffinate setups). Moderate purity requirements with low efficiency columns ($N_s = 25$).

Process	OF	Pu^R	m^I	m^{II}	m^{III}	m^{IV}	R^1	R^2	R^3	R^4	R^5
1	5.284	90.00	19.727	8.234	18.936	14.160	–	–	–	–	–
	6.026	95.00	19.941	10.731	18.404	13.196	–	–	–	–	–
2	3.607	90.00	17.838	8.632	19.031	13.479	1	1	1	1	1
	4.183	95.00	17.810	8.538	18.419	13.323	1	1	1	1	1
3	3.444	90.02	17.674	10.887	19.263	13.194	1	1	1	1	–
	3.941	95.00	17.633	9.401	18.226	13.432	1	1	1	0	–
4	3.465	90.00	16.569	19.062	13.461	–	–	1	1	1	–
	5.258	95.00	17.171	19.263	12.992	–	–	1	1	1	–
5	3.108	90.00	16.210	18.731	13.389	–	–	1	1	1	–
	4.115	95.00	16.731	19.033	13.131	–	–	1	1	1	–

based on chromatographic reactors outperforms both systems 1 and 2 for both purity requirements. Here, the optimal structure changes with increasing purity requirement from four ($Pu^R = 90\%$) to three ($Pu^R = 95\%$) reactive columns. This can be explained by the trade-off between separation and reaction functionalities. As a result of the higher purity demand, the reaction volume is reduced in favor of the separation. The three-zone system 4 with side reactors also outperforms the classical approach 1, but does not reach the performance of 2 and 3. Structure 5 obtains the best performance out of all options for $Pu^R = 90\%$ and the second best for $Pu^R = 95\%$. This is an encouraging finding since this new process setup is a rather simple three-zone SMB system.

A closer look at the m-values in Tab. 2 allows identifying the source of the differences in process performance. The simultaneous reaction and separation can strongly support the regeneration within SMB units, which was denoted as reaction-assisted regeneration in [1]. The integrated systems require lower m^I-values to regenerate zone I when the reaction is placed within this zone. This decreases the solvent consumption and, thus, improves the overall performance.

Tab. 3 summarizes the optimization results for the extract setups in Fig. 2. Similar trends can be observed compared to the schemes in Fig. 1. The average improvement over the reference process 1 is with 26% slightly lower than for the raffinate setups, but still significant. It is interesting to note that the three-zone systems work better for the production of the more re-

tained component at reduced purity demands than processes with four zones. For a purity requirement of 90%, the best performance is obtained for process 5 followed by option 4. Indeed, most of the studies related to process 4 focused specifically on the production of the stronger retained component, e.g., [7, 9, 28] at rather low product purity. At slightly higher purity demands $Pu^E = 95\%$, the totally integrated system 3 obtains the best result, which is due to the higher degree of freedom for this process. The optimal configuration constrains the reaction to the second and third columns within the SMB unit, i.e., in this case for process 3 in Fig. 2 holds $R^1 = R^4 = 0$ and $R^2 = R^3 = 1$ in Eq. (1).

The better performance of the integrated schemes is based again due to the reaction-assisted regeneration. In these cases, the effect takes place in the last zone of the SMB in structures 2 to 5. There, we obtain higher optimal m-values when the reaction occurs (see Tab. 3). These high m-values permit a greater recycle of the solvent, reducing its consumption.

3.1.2 High Purity Requirements

In this section, the production under high purity requirements is discussed. The purity requirement is set equal to $Pu^{out} = 99.9\%$, typical for pharmaceuticals products like enantiomers. For these high purity requirements, more efficient columns with a higher stage number will be required.

Table 3. Optimization results for the schemes depicted in Fig. 2 (extract setups). Moderate purity requirements with low efficiency columns ($N_s = 25$).

Process	OF	Pu^E	m^I	m^{II}	m^{III}	m^{IV}	R^1	R^2	R^3	R^4	R^5
1	4.982	90.00	17.939	12.301	19.684	12.940	–	–	–	–	–
	6.490	95.00	19.300	13.851	18.860	13.582	–	–	–	–	–
2	4.133	90.00	20.386	12.440	21.448	15.405	1	1	1	1	1
	4.949	95.00	20.033	12.987	20.209	14.863	1	1	1	1	1
3	3.955	90.00	20.435	12.445	21.070	15.682	1	1	1	1	–
	4.146	95.02	19.803	12.959	21.034	15.197	0	1	1	0	–
4	3.588	90.00	19.837	12.364	15.625	–	–	1	1	1	–
	4.838	95.00	21.020	12.749	15.663	–	–	1	1	1	–
5	3.577	90.00	19.898	12.457	15.709	–	–	1	1	1	–
	4.543	95.00	20.700	12.859	15.733	–	–	1	1	1	–

Chem. Eng. Technol. **2011**, 34, No. 5, 688–698

© 2011 WILEY-VCH Verlag GmbH & Co. KGaA, Weinheim

www.cet-journal.com

As an example, the influence of the number of stages on the performance P of the different systems as introduced in Eq. (9) is shown in Fig. 3 for the raffinate setups. As expected, in all cases P improves (i.e., it increases) with increasing number of stages. This increase is more pronounced for the three-zone schemes 4 and 5 in Fig. 1, since three-zone schemes have only a single zone responsible for the separation. Since in enantioseparation typically columns with very high efficiency are applied, for the further investigations a total number of 800 stages was chosen corresponding to 100 stages per column.
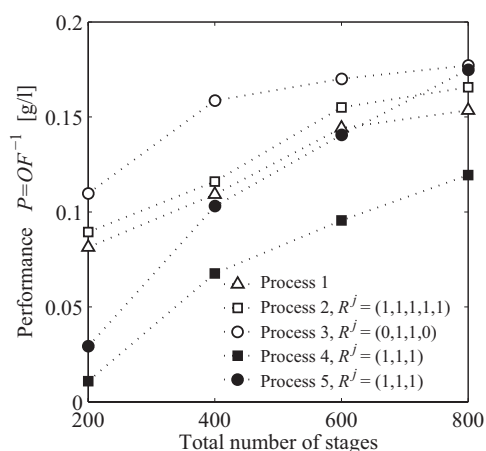
Figure 3. Performance of the process schemes in Fig. 1 (raffinate setups) vs. total number of theoretical plates (NTP) of the SMB unit. For the superstructures (2)–(5) the optimal configuration (in brackets) was found to be independent of the NTP in the range studied.

Detailed results for the production of pure B are reported in Tab. 4. The totally integrated process 3 obtains the best performance out of all the considered options. The optimal structure corresponds to the use of two reactive columns in the second and third positions. As already expected from the results in Fig. 3, there exist large differences of the performance between the partially and fully integrated three-zone systems. Both schemes require a lower m^I-value than the purely separative SMB. However, the effect of the reaction-assisted regeneration in system 5 is more significant, increasing its overall performance. Under the idealized conditions assumed here, this trend confirms the observations reported in [1].

Analogously, Tab. 5 contains the optimization results obtained for the production of pure A. Here, similar trends are observed for the performance compared to the case with moderate purity demands (see Tab. 3). Process 1 is outperformed by

all superstructures. The best performance corresponds to the completely integrated superstructure 3, followed by process 5, the integrated three-zone SMB process.

Summarizing, the integrated processes investigated in this section represent alternatives to the conventional reactor-separator-recycle 1 for both reduced and high purity demands. Under the idealized assumptions used in this part (reaction equilibrium and negligible volume of side reactors), the results confirm the trends observed in [1] based on TMB models. Notably, completely integrated schemes (3 and 5) outperform the analogous partially integrated systems (2 and 4), independent of the chosen product and in particular for high purity requirements. This is due to the more pronounced effect of the reaction-assisted regeneration. The fully integrated three-zone process 5 appears as a particularly attractive option, since it combines good performance with a simple setup.

3.2 Side Reactors vs. Chromatographic Reactors

A particular observation in the previous section was that fully integrated processes can outperform such with side reactors, notably for high purity and when the product is the weaker adsorbing component.

In the first step above, the focus was on a rather limited number of reactors with instantaneously established reaction equilibrium and negligible volume of side reactors. The observed trends were along the results obtained earlier for TMB systems in [1]. However, these conditions do not fully reflect practical conditions. In particular, there exists an interplay of the column switching in SMB processes with the number and size of side reactors, which cannot be observed based on TMB models. To further elucidate this fact, the influence of finite reactor volume and maximum number of reactors will be inves-

Table 4. Optimization results for the schemes depicted in Fig. 1 (raffinate setups). High purity requirements with high efficiency columns ($N_s = 100$).

Process	OF	Pu^R	m^I	m^{II}	m^{III}	m^{IV}	R^1	R^2	R^3	R^4	R^5
1	6.515	99.92	21.185	9.848	18.723	13.339	–	–	–	–	–
2	6.040	99.90	20.650	9.322	18.756	13.334	1	1	1	1	1
3	5.645	99.92	20.582	7.528	18.683	13.295	0	1	1	0	–
4	8.378	99.90	18.279	19.676	13.604	–	1	1	1	–	–
5	5.717	99.90	17.503	19.371	13.208	–	1	1	1	–	–

Table 5. Optimization results for the schemes depicted in Fig. 2 (extract setups). High purity requirements with high efficiency columns ($N_s = 100$).

Process	OF	Pu^E	m^I	m^{II}	m^{III}	m^{IV}	R^1	R^2	R^3	R^4	R^5
1	7.894	99.90	22.001	13.346	19.944	13.344	–	–	–	–	–
2	6.637	99.90	20.828	13.537	20.928	14.645	1	1	1	1	1
3	4.898	99.90	20.886	13.547	25.106	15.674	1	1	0	0	–
4	6.259	99.90	21.046	13.881	15.928	–	1	1	0	–	–
5	5.196	99.92	21.225	13.386	15.920	–	1	1	0	–	–

tigated. The calculations focus on the interesting case that the weaker adsorbing component is the desired product (i.e., raffinate setups).

Fig. 4 illustrates the optimization results of process 4 (symbols) in Fig. 1 as a function of the number and volume of side reactors for a purity requirement of 90 %. In the calculations, the number of columns and side reactors in the reactive zone was increased simultaneously, while the nonreactive zones remained unchanged. To allow for a fair comparison, the results are compared to the corresponding process 5 (solid lines) with the same number of columns in the corresponding reactive zone.
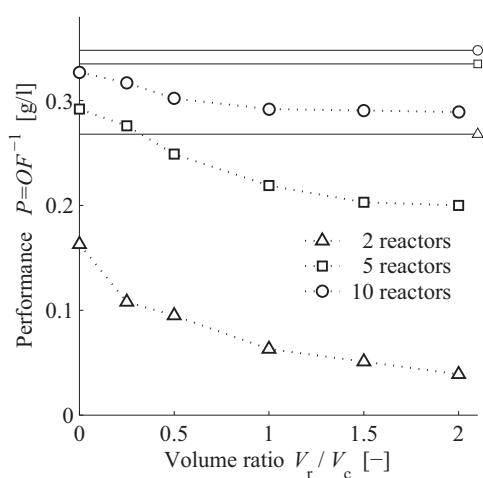

Figure 4. Performance of process 4 in Fig. 1 under moderate purity requirements (90 %) vs. the ratio between reactor and column volume, V_r/V_c. Low-efficiency columns ($N_s = 25$). Structures with two (triangles), five (squares), and ten (circles) side reactors and columns in zone I. Solid lines with small symbols: performance of process 5 with the same number of stages and columns.

In all cases shown in Fig. 4, the performance P of the fully integrated process 5 is better than that of the corresponding partially integrated process 4. Concerning the number of side reactors, first the idealized case of zero reactor volume (i.e., data points on the ordinate) is considered. One observes that an efficient partially integrated scheme will require a relatively large number of side reactors. Further, the difference between both options vanishes for a large number of side reactors with zero volume at infinitely fast reactions. This is in full agreement to the observations made using TMB models [1].

An interesting picture is obtained when taking into account also the volume of the side reactors. This was manipulated for Fig. 4 by keeping the column volume constant (cf. Tab. 1) and increasing only the reactor volume. It is observed that this volume plays a significant role for the performance. Furthermore, the gap between the partially and the fully integrated schemes is increasing with increasing reactor volume, which holds independently of the number of side reactors.

The mentioned deteriorating performance of the side reactor processes can be explained by the additional holdup of side

reactors in SMB systems. In order to illustrate this explanation, Fig. 5 demonstrates the internal concentration profiles of process 4 with three side reactors with zero volume (top) in comparison to those obtained with side reactors with a two-fold column volume (bottom). In both cases the same m-values were applied (cf. Tab. 4). While the ideal process (top) achieves a purity of 99.9 %, the setup with finite reactor volumes (bottom) reaches only 95.7 %. It is readily observed that this is due to an accumulation of the undesired component in the side reactors. Some of this component travels with the solid phase and contaminates the product. In order to achieve also in this case 99.9 % purity, the process in the bottom would require a higher m^I-value to regenerate zone I. This decreases process performance. Obviously this effect will increase with increasing reactor volume. Analogous observations are made when investigating the original Hashimoto concept 4 in Fig. 2.
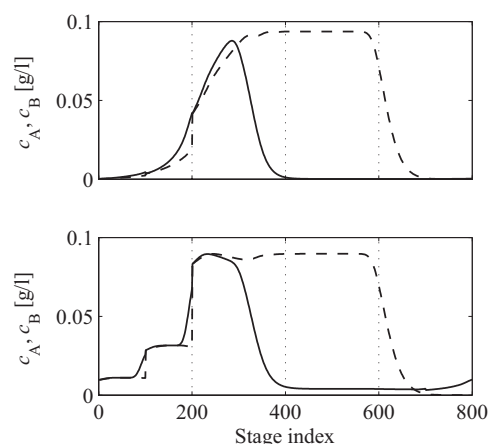
Figure 5. Internal concentration profiles of the three-zone process 4 in Fig. 1 with three side reactors under the same operating conditions (cf. m-values for process 4 in Tab. 4). Top: ideal case with zero volume of side reactors (purity 99.9 %); bottom: same process, but side reactors have the two-fold volume of a column (achieved purity 95.7 %).

An important consequence of the above is that, under realistic conditions where side reactors have a finite volume, such systems cannot reach the performance of fully integrated processes. This is a dynamic effect that cannot be observed based on steady-state TMB models.

Finally, it should be noted that, despite their lower performance, a relevant advantage of the side reactor concepts is their higher flexibility, since they allow adjusting different reaction conditions than required in the columns responsible for separation. Furthermore, different types of units can be implemented like enzyme reactors [7, 9] or electrochemical [29] reactors.

3.3 Integrated Three-Zone SMB Reactor

Due to its favorable performance and the simple setup that does not require solvent removal or recycle streams, process 5

(see Fig. 1) appears as a promising process variant. Below, a more detailed analysis of this new concept is given together with design considerations. In particular, practically relevant aspects like the purity requirement and distribution of the reaction are addressed.

For conventional four-zone SMB systems the triangle theory is used as a powerful design tool [22, 30]. Based on this theory, a region of complete separation can be plotted on the m^{II}-m^{III} plane. Usually, complete regeneration is assumed in zones I and IV. Analogously, such separation regions can be shown for the three-zone SMB reactor. In Fig. 6, the regions are plotted for different purity demands for the production of B and A (schemes 5 in Figs. 1 and 2). Complete regeneration is assumed to take place in zone III for the production of B. Similarly, complete regeneration is forced in zone I for the production of A. A large region of complete separation is obtained in both cases, which supports the possibility to produce pure enantiomers with 100 % yield and conversion.

As already mentioned, the switching of columns in SMB processes ideally requires turning on or off completely the chemical reaction in columns which enter or leave the reactive zone. Up to now, such ideal on and off switching was assumed for the fully integrated process, which exploits the full potential of this process. In practice this will be difficult to achieve.

Depending on the specific chemistry, the reaction in such integrated systems could be controlled by gradients of temperature, pH, or suitable additives and modifiers [1]. This implies that only a limited change in the kinetic rate constants of the reaction can be achieved between the reactive and nonreactive zones. As will be demonstrated, the efficiency of the process is determined by a quantity we denote as reaction rate gradient k'/k. The latter represents the achievable ratio of the kinetic constant in the zones where the reaction should be maximized to that in the zones where it should be suppressed, respectively.

In Fig. 7, the performance of process 5 in Fig. 1 is optimized for different purity requirements and plotted as function of the reaction rate gradient k'/k. For all cases studied, a critical value for the reaction rate gradient exists, below which the performance decreases rapidly. However, the critical ratio varies depending on the product purity required. Production of pure enantiomers will require an efficient tuning of the reaction kinetics. Nevertheless, under moderate purity requirements, a good performance can be achieved already for relatively low ratios of the kinetic constants.

An evaluation of this fact is depicted in Fig. 8, which shows the separation regions for a purity $Pu^{out} = 99.0$ % as a function
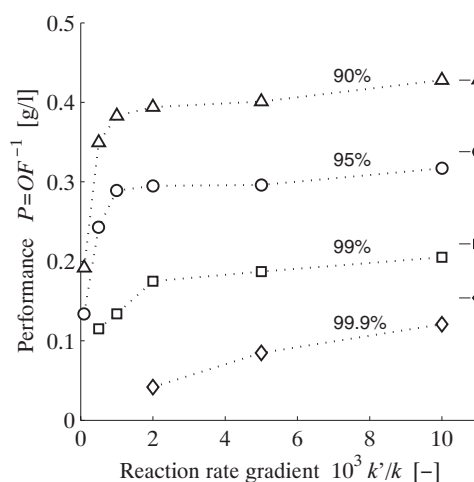
Figure 7. Performance of process 5 in Fig. 1 as function of the applied reaction rate gradient k'/k for different purity requirements. Filled symbols on the right: corresponding performance achievable if the ratio of k'/k approaches infinity ($k' = 10^5$, $k = 0$). Lines are guide for the eye.
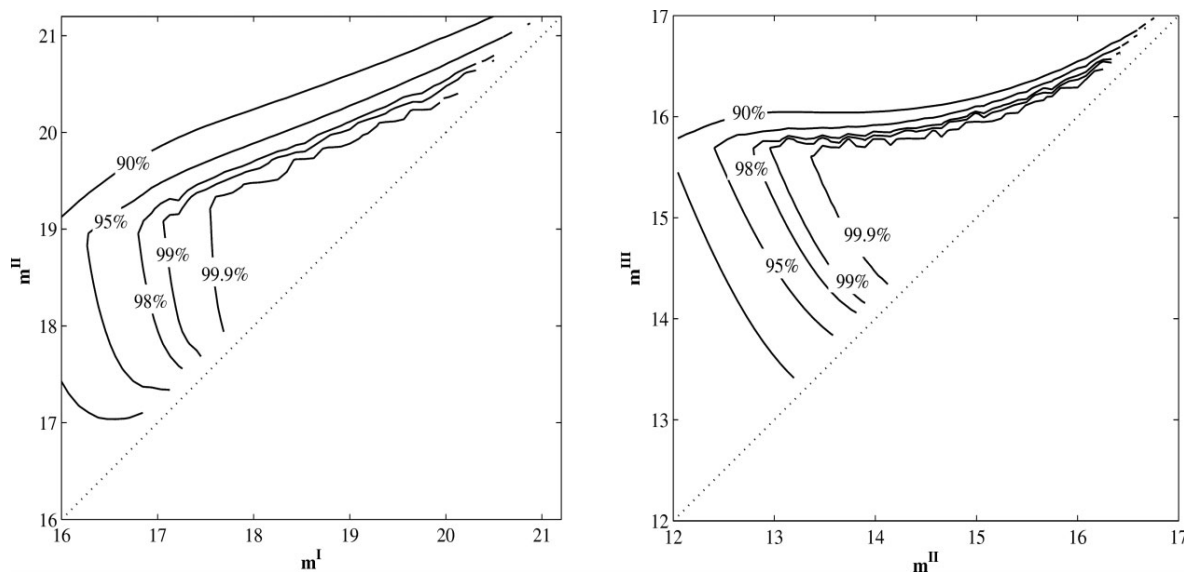
Figure 6. Simulation results for process 5 at different product purities (90, 95, 98, 99, 99.9 %). The surfaces are depicted on the m^I-m^{II} plane for the raffinate setup (left, cf. Fig. 1) and on the m^{II}-m^{III} plane for the extract configuration (right, cf. Fig. 2).
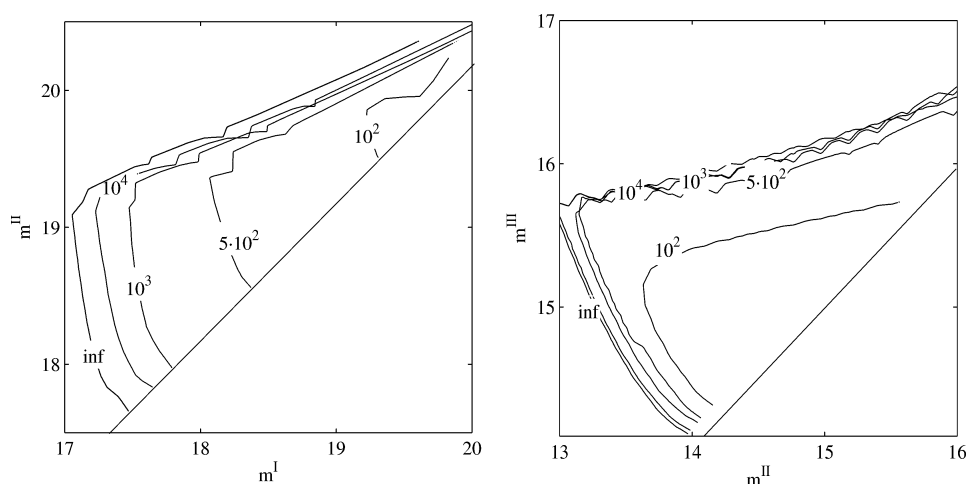
Figure 8. Simulation results for process 5 under different reaction rate gradients ($k'/k = 10^2$, $5 \cdot 10^2$, 10^3, 10^4, 10^5) for $Pu_{min} = 99\%$. The surfaces are depicted on the m^{I}-m^{II} plane for the raffinate setup (left, cf. Fig. 1) and on the m^{II}-m^{III} plane for the extract configuration (right, cf. Fig. 2).

of the ratio of the kinetic constants for raffinate and extract setups. In both cases, the size of the region decreases for lower kinetic ratios. However, this effect is more significant for the production of the less retained component B. As observed already in Fig. 7, for high purity requirements the performance can be strongly compromised by inefficient tuning of the reaction kinetics.

It is worth mentioning that the practical feasibility of the process discussed above was demonstrated recently for the production of the pure weaker adsorbing enantiomer of chlorthalidone. In this case, a 5000-fold difference between the kinetic constants in adjacent zones could be adjusted by means of a pH gradient [19].

4 Conclusions

Different options to combine continuous SMB chromatography and racemization reactions for the production of enantiomers were investigated. Each of the existing general concepts – flow sheet, partial, and full process integration, respectively – was represented by formulation of corresponding superstructures based on dynamic SMB models. These were subsequently subjected to an MINLP-based optimization to identify the optimal process setup and operating conditions for each category.

In a first step, the role of the purity requirements was investigated under idealized conditions with infinite reaction rate and negligible reactor volume. It was found that the spatial distribution of the reaction allows improving process performance. This is realized by partially integrated systems with side reactors or by fully integrated processes based on reactive chromatographic columns. The latter achieve the better performance, since they completely exploit the beneficial effect of reaction-assisted regeneration. This observation holds independent of the required product and the purity, but is particularly

significant under high purity requirements and for the production of the weaker adsorbing enantiomer.

Subsequently, fully integrated processes were compared to such with side reactors under more realistic conditions. The main finding is that an increasing volume of the side reactors causes decreasing performance, which cannot be fully compensated by increasing their number. This dynamic effect is not observed in studies based on TMB models.

A simple fully integrated three-zone process was identified as a particularly interesting new process option. In this process, for which an experimental proof of feasibility was given elsewhere, in particular the necessary tuning of the reaction rate within the unit has to be considered. A sufficiently high ratio of the reaction rate constants in the zones that perform the chemical conversion to that in the separation zones was identified as an important design criterion for this concept.

Acknowledgment

The authors have declared no conflict of interest.

Symbols used

b	[L g^{-1}]	isotherm parameter
c	[g L^{-1}]	liquid phase concentration
d_c	[dm]	column diameter
F	[–]	phase ratio

K_{eq}	[–]	equilibrium constant
k	[min^{-1}]	kinetic constant forward reaction
k_b	[min^{-1}]	kinetic constant backward reaction
k'/k	[–]	reaction rate gradient
m	[–]	dimensionless flow rate
OF	[L g^{-1}]	objective function
P	[g L^{-1}]	performance indicator
Pr	[g min^{-1}]	throughput
Pu	[%]	purity
Q	[L min^{-1}]	volumetric flow rate
q	[g L^{-1}]	solid phase concentration
q_s	[g L^{-1}]	saturation capacity
r	[g L^{-1}min^{-1}]	reaction rate
R^j	[–]	decision variable (reaction) at position j
t	[min]	time
t^*	[min]	switching time
V	[L]	stage volume
V_c	[L]	column volume
V_r	[L]	reactor volume
ε	[–]	porosity
υ	[–]	stoichiometric coefficient

Indices

A	strong-adsorbing component
B	weak-adsorbing component
E	extract
F	feed
R	raffinate
S	solvent
i	component
k	stage
n	column
out	outlet stream, out =(E, R)
z	zone

References

[1] J. G. Palacios, M. Kaspereit, A. Kienle, *Chem. Eng. Technol.* **2009**, *32 (9)*, 1392.

[2] M. Bechtold, S. Makart, M. Heinemann, S. Panke, *J. Biotechnol.* **2006**, *124 (1)*, 146.

[3] M. Bechtold, M. Füreder, N. Wagner, S. Panke, *Chem. Ing. Tech.* **2010**, *82 (1–2)*, 65.

[4] Y. Zhang, K. Hidajat, A. K. Ray, *Biochem. Eng. J.* **2007**, *35 (3)*, 341.

[5] G. Bergeot, D. Leinekugel-Le-Cocq, L. Wolff, L. Muhr, M. Bailly, *Oil Gas Sci. Technol.* **2010**, *65 (5)*, 721.

[6] M. Kaspereit, J. G. Palacios, T. Meixús Fernández, A. Kienle, *Comput.-Aided Chem. Eng.* **2008**, *25*, 97.

[7] K. Hashimoto, S. Adachi, H. Noujima, Y. Ueda, *Biotechnol. Bioeng.* **1983**, *25 (10)*, 2371.

[8] T. Borren, H. Schmidt-Traub, *Chem. Ing. Tech.* **2004**, *76 (6)*, 805.

[9] T. Borren, *Ph.D. Thesis*, Universität Dortmund **2006**.

[10] M. Minceva, P. Sá Gomes, V. Meshko, A. E. Rodrigues, *Chem. Eng. J.* **2008**, *140 (1–3)*, 305.

[11] E. A. Borges da Silva, D. P. Souza, A. A. Ulson de Souza, S. M. A. Guelli, U. Souza, A. E. Rodrigues, *Chem. Eng. J.* **2006**, *118 (3)*, 167.

[12] A. Küpper, S. Engell, *at* **2009**, *57 (7)*, 360.

[13] B. Cho, R. Aris, R. Carr, *Proc. R. Soc. London, Ser. A* **1982**, *383 (9)*, 147.

[14] H.-K. Rhee, R. Aris, N. Amundson, *First-Order Partial Differential Equations. Vol. II. Theory and Application of Hyperbolic Systems of Equations*, Prentice-Hall, Englewood Cliffs, NJ **1989**.

[15] A. Toumi, S. Engell, *Chem. Eng. Sci.* **2004**, *59 (18)*, 3777.

[16] A. K. Ray, R. W. Carr, R. Aris, *Chem. Eng. Sci.* **1994**, *49 (4)*, 469.

[17] A. K. Ray, R. W. Carr, *Chem. Eng. Sci.* **1995**, *50 (19)*, 3033.

[18] T. Borren, J. Fricke, *Preparative Chromatography of Fine Chemicals and Pharmaceutical Agents*, Wiley-VCH, Weinheim **2005**.

[19] J. G. Palacios, B. Kramer, A. Kienle, M. Kaspereit, unpublished.

[20] G. Guiochon, S. Shirazi, A. Katti, *Fundamentals of Preparative and Nonlinear Chromatography*, Academic Press, London **1994**.

[21] T. Fornstedt, G. Zhong, Z. Bensetiti, G. Guiochon, *Anal. Chem.* **1996**, *68 (14)*, 2370.

[22] M. Mazzotti, G. Storti, M. Morbidelli, *J. Chromatogr. A* **1997**, *769 (1)*, 3.

[23] M. Mangold, A. Kienle, K. D. Mohl, E. D. Gilles, *Chem. Eng. Sci.* **2000**, *55 (2)*, 441.

[24] R. Köhler, K. D. Mohl, H. Schramm, M. Zeitz, A. Kienle, M. Mangold, E. Stein, E. D. Gilles, in *Adaptative Method of Lines* (Eds: A. V. Wouwer, P. Saucez, W. E. Schiesser), Chapman & Hall, New York **2001**.

[25] R. Leven, B. Koch, B. Pompe, *Chaos in dissipativen Systemen*, Akademie Verlag, Berlin **1994**.

[26] H. P. Schwefel, *Evolution and Optimum Seeking*, Wiley, New York **1995**.

[27] M. Kaspereit, K. Gedicke, V. Zahn, A. W. Mahoney, A. Seidel-Morgenstern, *J. Chromatogr. A* **2005**, *1092 (1)*, 43.

[28] J. Fricke, *Ph.D. Thesis*, Universität Dortmund **2005**.

[29] M. Michel, H. Schmidt-Traub, R. Ditz, M. Schulte, J. Kinkel, W. Stark, M. Küpper, M. Vorbrodt, *J. Appl. Electrochem.* **2003**, *33 (10)*, 939.

[30] G. Storti, M. Mazzotti, M. Morbidelli, S. Carrà, *AIChE J.* **1993**, *39 (3)*, 471.

Contents lists available at ScienceDirect

Journal of Chromatography A

Experimental validation of a new integrated simulated moving bed process for the production of single enantiomers

Javier García Palacios[a], Bernhard Kramer[a], Achim Kienle[a,b], Malte Kaspereit[a,*]

[a] Max-Planck-Institut für Dynamik komplexer technischer Systeme, D-39106 Magdeburg, Germany
[b] Otto-von-Guericke Universität Magdeburg, Institut für Automatisierungstechnik, D-39106 Magdeburg, Germany

ARTICLE INFO

ABSTRACT

A new integrated 3-zone simulated moving bed (SMB) concept with internal racemization reaction was suggested recently for the production of single enantiomers from racemic mixtures [1,2]. The process utilizes an internal gradient to trigger the racemization within a single zone. It can deliver the pure enantiomer and outperforms conventional technologies. In this contribution, the concept is validated experimentally for the separation of a model system compound. The results demonstrate that the new concept is capable of producing a single enantiomer with purity, yield and conversion of 100%.

© 2011 Elsevier B.V. All rights reserved.

1. Introduction

Enantiomers constitute pairs of stereoisomers that are mirror images of each other. As regards their physiological impact, often only one enantiomer exhibits the desired effect while the other is ineffective or even harmful. Producing directly the desired enantiomer by chemical methods [3] as enantioselective catalysis, biocatalysis, or from enantiopure building blocks is, although desirable, frequently expensive due to long-lasting development efforts or expensive raw materials. Often developed syntheses are not fully enantioselective, and sometimes they are infeasible. Hence the alternative of obtaining single enantiomers from racemic mixtures plays a major role for companies that produce pharmaceuticals, fine chemicals, nutrition additives, or fragrances. The drawback of producing the racemate, which is the 50/50 mixture of both enantiomers, is that it necessitates a subsequent separation. Several techniques are available for this, for example, crystallization of diastereomeric salts, dynamic kinetic resolution, or chromatography. In particular continuous simulated moving bed (SMB) chromatography has been established in recent years for many enantioseparations on the industrial scale [4]. However, without a simultaneous interconversion of the counter-enanantiomer, the recovery yield of separation-based approaches is inherently limited to 50% only.

Recently, investigations of several new integrated process concepts combining racemization reaction and continuous chromatography were reported [1,2]. Theoretically, these processes can produce single enantiomers with yield and conversion of 100%. They can outperform the conventional engineering concept of flowsheet integrated processes (reactor-separator-recycle) and processes with side reactors due to an effect denoted as reaction-assisted regeneration. An integrated closed-loop 3-zone SMB unit was identified as a particularly attractive process idea. This scheme combines good performance with a relatively simple setup. It contains no external solvent removal devices or recycle streams. The racemization reaction is optimally performed within the regeneration zone. Fig. 1 shows schematically the suggested 3-zone processes for the production of the more (A) and less adsorbed component (B), respectively.

In order to fully exploit the potential of the scheme the racemization reaction needs to be performed only in a single specific zone of the SMB. This corresponds to zone *III* for the production of the stronger retained component *A*, and zone *I* for the production of the weakly adsorbing enantiomer *B* (see Fig. 1). In practice, the reaction could be controlled by gradients of, for example, temperature, pH, modifiers or additives, depending on the specific chemical system under consideration [1].

In this work, the new integrated process is validated experimentally for the production of the pure less retained enantiomer *B*

---

* Corresponding author. Tel.: +49 391 6110 282; fax: +49 391 6110 551.
  E-mail address: kaspereit@mpi-magdeburg.mpg.de (M. Kaspereit).
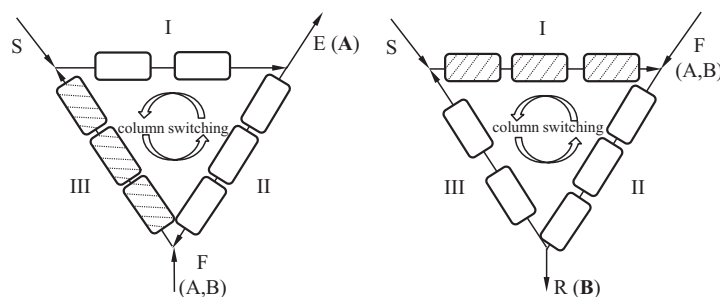
Fig. 1. Integrated 3-zone SMB processes combining chromatographic separation and racemization reaction, as reported in [1]. Hatched columns denote chromatographic reactors. Left – setup for the production of the strongly retained component *A*. Reaction takes place within zone *III*; right – setup for the production of the weakly retained component *B*. Reaction takes place within zone *I*. F – feed, S – solvent, E – extract, R – raffinate.

(Fig. 1, right). It should be noted that this is a particularly interesting case. The only concept that is comparable to this setup is the partially integrated Hashimoto process [5], which utilizes side reactors. To the authors' best knowledge, Hashimoto processes or similar concepts have never been applied to interconvert an isomeric mixture into the weaker adsorbing component only. As demonstrated in [2] this would in principle be possible, but requires a large number of columns and reactors. The schemes in Fig. 1 provided a better performance than the Hashimoto concept regardless of the target component, in particular for high product purity.

The enantiomers of chlorthalidone (CTD) will serve as experimental model system. In this particular example, an internal gradient of the pH value is used to control the reaction. Therefore, at first, the effect of the pH on the racemization kinetics and on the adsorption behavior is investigated. The obtained parameters are applied in a detailed mathematical process model used for designing the process. A semi-preparative SMB unit is used under pH-gradient operation to produce the less retained enantiomer in the validation experiments.

The paper is organized as follows. First, the mathematical model is explained. Afterwards, the chemicals, instrumentation and experimental strategy are described. In Section 4 the results of the parameter measurements and SMB experients are presented and discussed.

2. Theory

A conventional equilibrium stage model is applied to simulate the integrated SMB process. The mass balances for the two components in the fluid and solid phases within each stage read as:

$$\frac{dc_i^{k,n}}{dt} + F\frac{dq_i^{k,n}}{dt} = \frac{Q^z}{V\varepsilon}\left(c_i^{k-1,n} - c_i^{k,n}\right) + \nu_i\, r^{k,n}, \tag{1}$$

where the indices $i = A, B$ denote the component, $k = 1, \ldots, N_s$ the stage, $n = I, \ldots, N_c$ denote the column, and $z = I, \ldots, N_z$ the corresponding zone of the SMB unit. c_i and q_i are the liquid and solid phase concentrations, V is the volume of a stage, ε the porosity and $F = (1 - \varepsilon)/\varepsilon$ is the phase ratio. Q is the volumetric flow rate of the fluid phase. The axial dispersion is accounted for by the number of stages, N_s [6].

The last term in Eq. (1) describes the chemical reaction. r is the reaction rate and ν_i is the stoichiometric coefficient. The chemical reaction is taking place in the liquid phase. For the reaction rate in Eq. (1) holds:

$$r^{k,n} = k(\text{pH})\left[c_A^{k,n} - c_B^{k,n}\right], \tag{2}$$

with $k(\text{pH})$ the rate constant of the reaction as a function of pH.

The relation between the solid and the liquid phase concentrations in Eq. (1) is given by the adsorption equilibrium. The adsorption behavior of CTD was reported in a previous publication [7] for the same stationary phase using a bi-Langmuir adsorption isotherm model:

$$q_i = \frac{q_1^s(\text{pH})b_1 c_i}{1 + b_1(c_A + c_B)} + \frac{q_{i,2}^s b_{i,2} c_i}{1 + b_{A,2}c_A + b_{B,2}c_B}, \quad i = (A, B). \tag{3}$$

According to the Pasteur principle, Eq. (3) describes competitive adsorption of the two solutes (A, B) on two different types of adsorption sites of the solid: type 1 (achiral) and type 2 (chiral); q_1^s and $q_{i,2}^s$ are the saturation capacities for the corresponding sites, respectively. Here, the integrated SMB unit is operated using pH gradients. For the model system CTD it was found useful to describe the dependency of the adsorption behavior on the pH value in the term $q_1^s(\text{pH})$. This corresponds to cases where the capacity of the achiral sites depends most strongly on the pH [8].

The SMB configuration used for the validation experiments is a four column 2-zone open-loop system for the production of the weakly retained enantiomer (see Fig. 2). Zone *I* performs the solid phase regeneration and the racemization reaction, while zone *II* is responsible for the separation. The regeneration of the liquid phase is carried out in two external zones as shown in Fig. 2. In contrast to a 3-zone system with closed loop, in this setup the third zone and the recycle stream are omitted for the sake of simplicity. Furthermore, analyzing the effluents of the external zones allows us to identify possible issues such as incomplete regeneration or side product formation.

For this system, the corresponding boundary conditions are:

$$\begin{aligned}
&\text{if } n = 1: && Q^S c_i^S = Q^I c_i^{0,1}, \\
&\text{if } n = 3: && Q^I c_i^{N_s,n-1} + Q^F c_i^F = Q^{II} c_i^{0,n}, \\
&\text{if } n = 2, 4: && c_i^{N_s,n-1} = c_i^{0,n},
\end{aligned}$$

where $c_i^{0,n}$ corresponds to the concentration of component i entering column n.

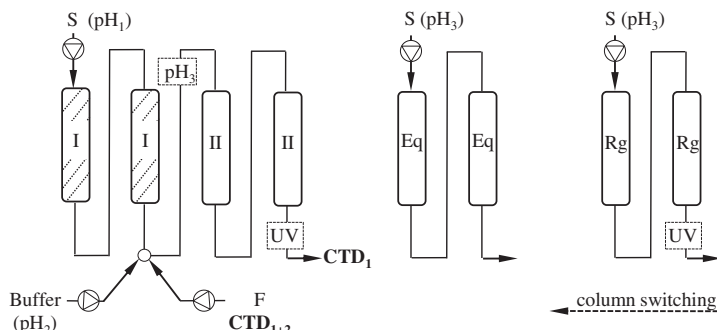The dimensionless zone flow rate ratios m^z are used as design variables for each zone z of the SMB:

$$m^z = \frac{Q^z t* - \varepsilon V_c}{(1 - \varepsilon)V_c}, \tag{4}$$

where V_c is the volume of a chromatographic column, and t^* is the switching time.

Fig. 2. Open-loop experimetal setup of the 2-zone integrated SMB for producing the less retained enantiomer CTD$_1$. Zone *I*, at pH$_1$ performs simultaneous reaction and separation benefiting from the effect of reaction-assisted regeneration [1]. Zone *II*, is responsible for the chiral separation at pH$_3$. Additional zones are implemented to equilibrate (Eq) and regenerate (Rg) the columns before re-entering zone *II*.

The performance parameters product purity, Pu^R, conversion, X, and recovery yield, Y, are defined as follows:

$$Pu^R = \frac{c_B^R}{c_A^R + c_B^R} \times 100, \tag{5}$$

$$X_A = \frac{c_A^F Q^F - c_A^R Q^R}{c_A^F Q^F} \times 100, \tag{6}$$

$$Y = \frac{(c_B^F + c_A^F) Q^F}{(c_B^R + c_A^R) Q^R} \times 100. \tag{7}$$

The dynamic simulations of the batch and SMB systems were performed using the simulation enviroment DIVA [9,10]. For the SMB unit, the periodic switching of the ports in the direction of the liquid flow was implemented with a Petri net routine. The dynamic simulation reaches a cyclic steady state (CSS) after a certain number of cycles. A stopping criterion based on a Poincaré map [11] was used to identify the CSS in each dynamic simulation.

3. Experimental

3.1. Chemicals

The enantiomers of chlorthalidone (CTD), (*RS*)-2-chloro-5-(1-hydroxy-3-oxo-2,3-dihydro-1*H*-isoindol-1-yl)benzene-1-sulfonamide, were used as model system for the experimental validation of the integrated SMB process. They were purchased from Sigma–Aldrich (Steinheim, Germany) and from Molekula (Gillingham, Dorset, UK). Two buffer systems were used for the different ranges of the pH value applied: Bis-Tris propane (BTP) (Sigma–Aldrich, Munich, Germany) and triethylammonium acetate (TEAA), 1 mol/L (Merck, Darmstadt, Germany). Further, acetic acid (AA), 100%, triethylamine (TEA), and HCl, 32%(v/v) (all from Merck, Germany) were required to prepare solutions at different pH values. Methanol (MeOH) at gradient grade LiChrosolv Reag. Ph Eur (Merck, Darmstadt, Germany) was used as a non-retained tracer compound. All aqueous solutions were prepared with ultrapure water prepared in-house using a Millipore Milli-Q gradient system (Molsheim, France).

3.2. Sample analysis by HPLC

The analysis of samples was carried out by HPLC using a Ultimate 3000 series chromatograph from Dionex (Idstein, Germany) controlled by the software Chromeleon. UV detection was set to 260 nm. A 200 mm × 4 mm Nucelodex-β-OH (Macherey-Nagel, Düren, Germany) column with an average particle size of 5 μm was used for the analysis, which was performed at 10 °C, a flow rate of 0.75 mL/min and an injection volume of 100 μL using TEAA at pH 5.0. MeOH/TEAA (aq.) (40/60, v/v) was used as solvent.

3.3. Racemization kinetics

The kinetic constant k of the racemization reaction in Eq. (2) had to be determined as a function of the pH. As already found by Lamparter et al. [13], the rate of the racemization reaction of CTD depends significantly on the pH value between pH = 2 and 6. They observed a minimum for the rate constant k at pH $\approx$ 3 and suggested a change in the reaction mechanism for acidic and basic enviroments as origin of this behavior. Here, we extend this range further by performing measurements between pH = 3.0 and 9.0 in order to increase the potential of a pH gradient to be applied in the investigated process.

Samples of pure CTD enantiomer were required for the batch experiments performed. For this purpose, a chromatographic column, Nucleodex-β-OH with 10 mm diameter and 125 mm length, was connected to the HPLC. Relatively large injections (2000 μL) of racemic CTD 0.4 g/L were injected and the fractions of highly purified S-enantiomeric form of CTD (*Pu* > 98 %) were recovered. The obtained S-enantiomer ic solutions were diluted in two different buffer systems (50 mM) to cover the whole pH-range of interest. TEAA was used for solutions at pH = 3.00, 4.05, 5.00, and 5.80, while BTP was used for mixtures at pH = 5.30, 5.95, 6.90, 8.10, and 9.00. Afterwards, these solutions were prepared to racemize at ambient temperature.

The experiments were performed in batch mode, using vials of approximately 15 mL volume. Samples were taken at different times and immediately frozen and stored at −18 °C. Each sample was analyzed later by HPLC to determine the extent of the racemization reaction. The time during which the samples were handled in liquid form was minimized in order to minimize possible errors due to spontaneous racemization. This attempt was successful, as indicated by negligible deviations between the purities of the fractionated original solutions and the samples taken at the beginning of the racemization experiments.

3.4. Adsorption behavior

Semi-preparative columns (16 mm × 65 mm) were used for the isotherm parameter determination as well as for the SMB experiments. The columns provided from Macherey-Nagel are packed with the same chiral stationary phase as the analytical column (same batch).

Classical methods to determine isotherm parameters experimentally are not suitable under reactive conditions. Therefore, an

200   [PII-11]

J.G. Palacios et al. / J. Chromatogr. A 1218 (2011) 2232–2239   2235

Table 1
System parameters of the reactive 2-zone SMB process.

L (mm)	d_c (mm)	ε (−)	c^F (g/L)	t_s (min)	T (°C)
65	16	0.681	0.5	7.0	25

inverse method ('peak fitting') was applied accounting also for the injection profile [12].

Column porosity was determined by a 20 µL injection of MeOH as a non-retained tracer compound. The flow rate was 2 mL/min. The column void volume was determined equal to 8.9 mL and the porosity $\varepsilon = 0.681$. The number of theoretical stages N_s in Eq. (1) was determined at a flow rate of 6 mL/min. From 20 µL injections of racemic CTD with a concentration of 0.05 g/L (rac.) an average value of $N_s = 750$ was obtained calculating the first and the second moments of the peaks. No significant influence of pH on N_s was observed.

For the isotherm determination MeOH/BTP (aq.) 50 mmol/L (40/60, v/v) was used as solvent. 2000 µL samples of racemic CTD in the aqueous BTP solution were injected at five different pH values (5.3, 6.0, 7.0, 8.0 and 9.0) adjusted using HCl. The flow rate was adjusted to 6 mL/min and the temperature was set to 25 °C. The concentration of racemic CTD was equal to 0.5 g/L corresponding to the maximum solubility in the used mobile phase composition.

3.5. SMB experiments

For the experimental validation of the new concept, the setup in Fig. 2 was equipped with eight columns. The SMB unit used is a CSEP C916 64 port SMB unit (Knauer, Berlin, Germany). This valve is designed for up to 16 column slots. Thus, the number of columns needs to be a divisor of 16 to perform symmetric switching conditions. It should be noted that, in principle, only three columns would be sufficient for the implementation of this process: one for the separation, one for the reaction and one for the equilibration/regeneration.

Five HPLC pumps (Knauer, Berlin) equipped with two 10 mL and three 50 mL pump heads, were used. Further, two UV detectors, model K-2600 (Knauer) were used at 1 Hz and 260 nm. The data from the UV detectors were monitored using the software EuroChrom2000 (Knauer). An Amersham Biosciences (now GE Healthcare, Freiburg, Germany) UPC-900 pH detector was used for inline pH measurement. Other parameters relevant for the experiments are summarized in Table 1.

The experiments were carried out at ambient temperature (25 °C). The product samples collected were cooled down rapidly by collecting them in an ice bath to stop racemization and analyzed inmediately by HPLC.

4. Results and discussion

4.1. Model parameters

In this section, the racemization kinetics and the adsorption isotherms are investigated as functions of the pH value. Appropiate simple models are suggested to describe the corresponding parameter dependencies.

4.1.1. Racemization kinetics

The reaction rate of the racemization of CTD enantiomers is influenced strongly by the temperature [7]. Thus, in principle, the integrated SMB process could be realized by temperature gradient since the kinetic constant changes by approximately a factor of 500 between 10 °C and 60 °C. However, for CTD, pH gradients are more attractive since they can provide an even stronger modulation of the racemization rate constant. To be able of fully exploiting
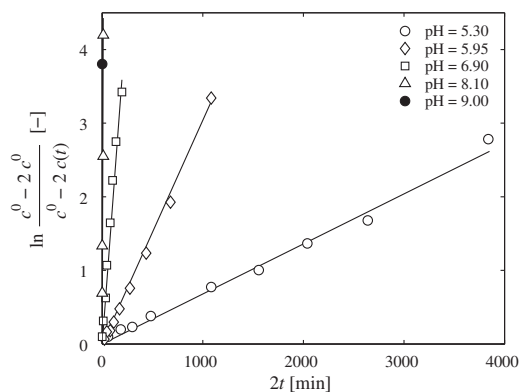

Fig. 3. Experimental results for the racemization kinetics of CTD$_1$ at different pH values. Lines are obtained by fitting the reaction racte constant k to Eq. (10).

the potential of such pH gradient, a large range of the pH value, between pH = 3.0 and pH = 9.0, was investigated.

The values of the kinetic constant k(pH) were obtained based on the material balance for the batch experiments:

$$\frac{dc_{CTD_1}}{dt} = k(pH)[c_{CTD_1} - c_{CTD_2}] = 2k(pH)c_{CTD_1} - k(pH)c^0, \quad (8)$$

where the indices 1 and 2 mark the S- and the R-enantiomer, and c^0 is the initial concentration of CTD (rac.) in the mixture. After integration and linearization: re-arranging we obtain the relation

$$k(pH) = \frac{1}{2t} Ln \frac{c^0 - 2c_{CTD_1}^0}{c^0 - 2c_{CTD_1}(t)}. \quad (9)$$

Fig. 3 shows the concentration profiles obtained by racemizing S-CTD solutions at five different pH values (5.30, 5.95, 6.90, 8.10, and 9.00) plotted according to the terms in Eq. (10).

Fig. 4 contains all experimental results obtained for the kinetic constant k as function of the pH value for the two different buffer systems. In analogy to [13], the logarithm of k (which has unit s^{-1}) is plotted in order to cope with the scale of the values. Also, the results at different temperatures as reported in [7] are plotted for comparison. The influence of the pH on the reaction kinetics is greater than that of the temperature. Changes in the kinetic constant of factor
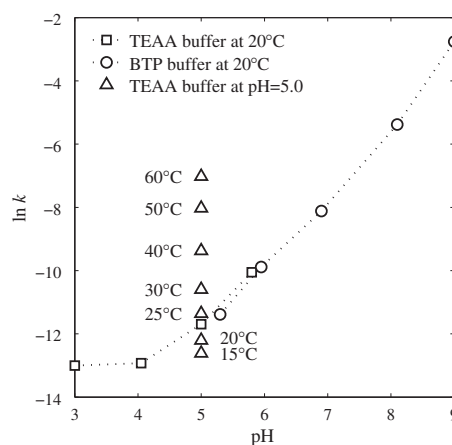

Fig. 4. Racemization kinetics for the model system chlorthalidone (CTD). Results for the thermal and pH-dependent racemization are depicted for two different buffer systems: triethylammonium acetate (□) and bis-tris propane (○). Lines are guide to the eye.

Table 2
Adsorption isotherm parameters for the enantiomers of CTD as a function of pH (as described in Eqs. (3) and (11)).

q_1^s(pH = 5.3) (g/L)	C_2 (−)	C_3 (−)	b_1 (L/g)	$q_{A,2}^s$ (g/L)	$q_{B,2}^s$ (g/L)	$b_{A,2}$ (L/g)	$b_{B,2}$ (L/g)
82.2888	10.2999	0.8034	0.0753	0.4337	3.2088	0.3554	0.6198

5600 are possible in the pH range between 5.3 and 9.0. Therefore, a pH gradient between 5.3 and 9.0 can provide an 'on and off' switching behavior of the reaction within the SMB unit. For this range, only BTP as buffer compound is required.

An exponential function can be used to describe k(pH) in Eq. (2) within this pH range:

$$k(\text{pH}) = k_0 \cdot e^{C_1 \cdot \text{pH}}, \tag{10}$$

where $k_0 = 5.67 \times 10^{-11}$ s^{-1} and $C_1 = 2.28$. The coefficient of correlation was $R_c = 0.997$.

It should be emphasized that the strong influence of the pH on the racemization rate of CTD enantiomers is not an isolated scenario. More examples can be found where the pH influences significantly the kinetics of racemization [14], epimerization [15] or isomerization [16].

4.1.2. Adsorption behavior

The adsorption isotherm model in Eq. (3) contains six parameters that need to be determined experimentally. Further, the saturation capacity of the achiral sites q_1^s(pH) is considered a function of the pH value. Since classical methods for isotherm determination are not applicable under reactive conditions, the isotherm parameters were estimated numerically by applying the inverse method (for details see, e.g., [17]).

First, the injection profile of the HPLC pump needs to be characterized. Fig. 5 shows a corresponding example. The profile deviates strongly from an ideal rectangular pulse. As shown in Fig. 5, it can be modelled with sufficient accuracy by fitting it piecewise to three sigmoidal functions.

Afterwards, five samples of racemic CTD were injected at pH values equal to 5.3, 6.0, 7.0, 8.0 and 9.0. The column model was solved using the previously obtained function for the kinetic constant in Eq. (10) and the injection profile as boundary condition. An evolutionary algorithm in DIVA [10] was used to estimate the isotherm parameters minimizing the differences between calculated and experimental chromatograms. The following sigmoidal function was assumed for q_1^s(pH):

$$q_1^s(\text{pH}) = \frac{q_1^s(\text{pH} = 5.3)}{1 + e^{(\text{pH} - C_2)/C_3}}, \tag{11}$$

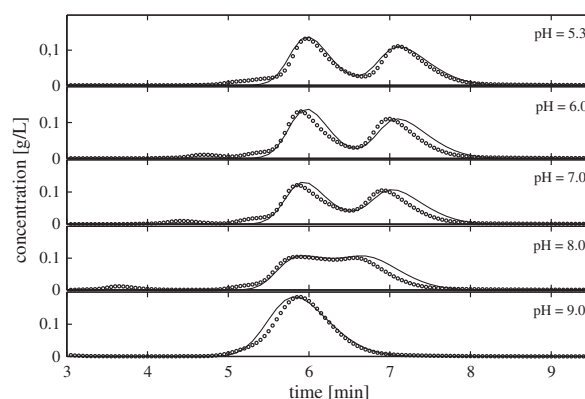with the two additional free parameters C_2 and C_3.
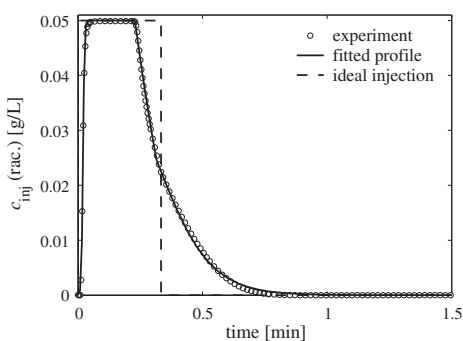
A total of seven free parameters in Eqs. (3) and (11) are used to describe the adsorption behavior. The experimentally determined isotherm parameters reported in [7] were used here as initial guess. The results of the parameter estimation are summarized in Table 2.

Fig. 6 shows the experimental chromatograms together with the numerical results. A good agreement is observed between them. Note that a simpler isotherm model might be applied requiring less parameters to be fitted. However, the bi-Langmuir model is most frequently suggested for enantiomers.

In the chromatograms, almost baseline separation can be observed at pH = 5.3. At pH = 8.0, an intermediate plateau is formed. Further, at pH = 9.0 a single peak is obtained due to the fast racemization kinetics. These are typical effects observed in 'on column' racemization [18–20]. The retention time decreases with increasing pH value. This is not only an effect of the reaction-assisted regeneration, but also due to a change of the adsorption strength. The effect of the pH on the retention time increases if the pH is in the proximity of the pK_a value of CTD, pK_a = 11.1 [21]. This effect has been observed also for other compounds [22–24].

4.2. Validation of the integrated SMB concept

For conventional non-reactive SMB processes so-called triangle theory is used as a powerful design tool [25,26]. Based on this method, a region of complete separation can be plotted on the m^{II}–m^{III} plane. Analogously, such complete separation region can be shown for the new integrated SMB system. In these considered here, where the weaker adsorbed enantiomer is produced, the corresponding reagion is defined in the parameter space m^I–m^{II}. In order to demonstrate this, the mathematical model was solved using the determined kinetic constant of the racemization and the adsorption isotherm parameters. A step gradient of the pH was assumed that gives maximum performance in the frame of the investigated parameter range. In the reactive zone I pH was set to 9.0, while in the non-reactive zone II a pH of 5.3 was used. Fig. 7 shows the simulation results where triangular regions are plotted for different purity requirements. Note that for processes producing the stronger adsorbed enantiomer, the corresponding separation regions are found in the m^{II}–m^{III} plane.

Fig. 5. Injection profile obtained experimentally (symbols) and fitting results (solid line) for a 2 mL injection of of 0.5 g/L racemic CTD at a flow rate of 6 mL/min. The three sigmoidal functions are connected at t = 0.23 and t = 0.32 min, respectively. Ideal rectangular profile (- - - dashed line) plotted for comparison.

Fig. 6. Experimental chromatograms (symbols) and fitting results (lines) of CTD enantiomers at different pH values.
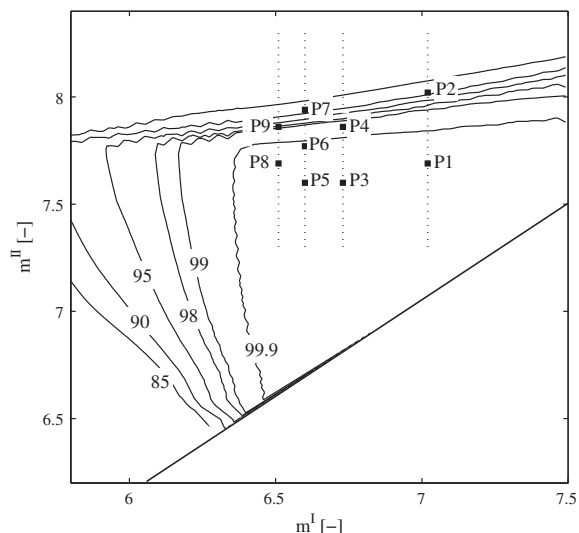
Fig. 7. Simulation results corresponding to the scanning of the m^I vs. m^{II} region for the model substance CTD. Surfaces denote the achievable product purity. Points $P1$ to $P9$ represent the operating conditions for the 9 experimental runs.

Fig. 8. Start-up behavior of the 2-zone SMB unit obtained for $P8$ (see Fig. 7). Signals of the UV online measurements for the product and the regeneration ports (see Fig. 2).

To validate the process experimentally, nine operating points are selected inside and outside of the region of complete separation ($P1$ to $P9$). No points are chosen left from the boundary of the 99.9% purity region since we are interested in achieving complete regeneration. These nine points were applied in nine different experimental runs using the setup in Fig. 2. The eluent used was methanol/50 mM BTP (40/60, v/v). The same pH gradient was used as in the simulations above. For this purpose, the pH of the desorbent S (pure eluent) was adjusted to $pH_1 = 9.0$, for the regeneration streams (pure eluent) to $pH_3 = 5.3$, and that of the additional buffer to $pH_2 \approx 1.0$ (cf. Fig. 2). The latter was in each case prepared such that, after mixing it with the effluent of zone I and the actual feed (0.5 g/L racemic CTD in pure methanol), the fluid entering zone II had the desired composition (methanol/50 mM BTP, 40/60, v/v) and pH value of 5.3. The switching time of $t_s = 7$ min was chosen as a compromise between throughput and pressure drop. All individual flow rates can be calculated from the parameters given in Table 1 and the m-values in Table 3.

For the sake of brevity, only the results for one operating point, $P8$, will be discussed in detail. $P8$ corresponds to the highest throughput among the operating points contained in the complete separation region. As indicated in Fig. 2, online measurement was carried out with two UV detectors: one at the product outlet of the 2-zone SMB, and the other at the outlet stream of the regen-
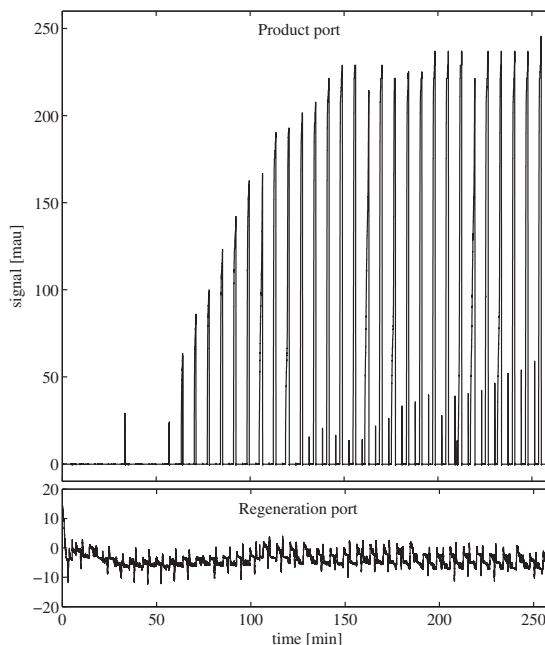
eration zone. In Fig. 8 the UV-signal is shown for the start-up of the experimental run of $P8$. The CSS is reached approximately after 150 min. That corresponds to 21 column switches, i.e., 5 cycles of the 2-zone SMB. After the CSS is reached, deviations from peak to peak can be observed for the product port. This is due to the different packing quality observed among the columns. However, this is a minor problem since SMB units can be operated successfully with columns giving significantly different retention times for the two compounds involved [27]. Further, perturbations are observed in the product port after every switching event. These perturbations can be observed in Fig. 8 after approximately 125 min. The peaks reach a considerable height in the cyclic steady state. However, their peak area is negligible and they are categorized as system peaks, since a detrimental effect on product quality was not observed.

Online pH-measurent was carried out after the feed port (as indicated in Fig. 2). The results indicated that during the operation in CSS regime lower pH values than adjusted in the buffer solutions occured temporarily in zone II. These lower pH values were observed inmediately after the switching of the columns. At this point in time, the pH of the liquid contained in the void volume of the column placed left to the feed port (coming from zone II) is equal to 5.3. Mixing this liquid with the feed stock and the acidic buffer leads to momentary low pH values (between 1.5 and 3.0). In the present case, this transient effect causes the formation of small amounts of side products (always <5% of the total feed). To avoid this, advanced feeding strategies could be implemented modulating the pH of the buffer periodically.

Once the unit reached the CSS, the product, regeneration and equilibration streams were collected and analyzed by HPLC. In Fig. 9, the analysis results are plotted for the three outlet streams. The analysis of the product stream shows a single peak eluting at the retention time of the less retained enantiomer CTD_1. The purity of CTD_1 is close to 100%. The detection limit of HPLC analysis with respect to enantiomeric purity was estimated to be 98% because a baseline separation could not be achieved. It could not be clarified

Table 3
Simulated and experimental results for the integrated 2-zone SMB process. $P1$ to $P9$ correspond to nine different operating points on the m^I–m^{II} plane.

Operating point	m^I (−)	m^{II} (−)	Simulation		Experiment		
			Pu^R (%)	X_{CTD_2} (%)	Pu^R (%)	X_{CTD_2} (%)	Y (%)
$P1$	7.02	7.69	99.9	99.9	>98	95.1	95.3
$P2$	7.02	8.02	87.6	75.3	71.2	42.1	94.3
$P3$	6.73	7.60	99.9	99.9	>98	95.1	98.7
$P4$	6.73	7.86	99.7	99.4	97.1	93.3	98.0
$P5$	6.60	7.60	99.9	99.9	>98	95.6	95.4
$P6$	6.60	7.77	99.9	99.9	>98	96.8	98.1
$P7$	6.60	7.94	86.9	73.8	91.1	79.5	97.0
$P8$	6.51	7.69	99.9	99.9	>98	96.1	98.0
$P9$	6.51	7.86	99.1	98.0	92.9	85.1	97.1
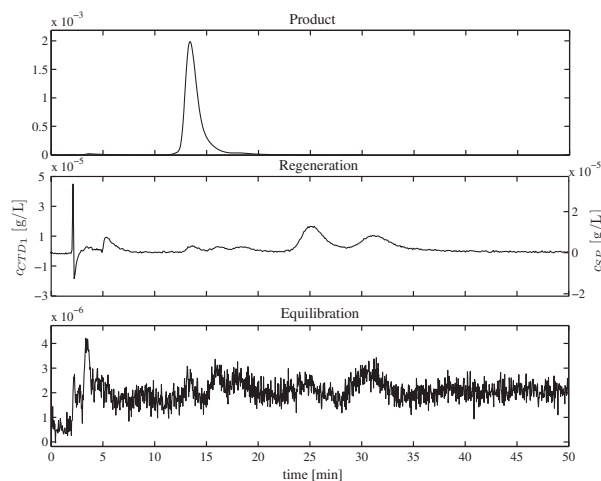
Fig. 9. Experimental results obtained for $P8$ (see Fig. 7). HPLC analysis of the product stream, regeneration and equilibration streams after reaching the cyclic steady state. c_{sp} denotes the concentration of the side products.

whether this is due to on-column racemization or other separation difficulty.

The analysis of the regeneration stream indicates that four different components are present in the mixture. CTD_1 and CTD_2, as well as the two side products SP_1 and SP_2. These were expected based on the reaction mechanism at low pH values suggested in [13]. Note that the scale of this plot is two orders of magnitude lower than the one for the product stream. This makes the amounts of CTD in the regeneration a 0.8% of the total throughput, while the side product formation makes up only a 1.2%. In the analysis of the equilibration stream only noise can be observed.

Note that in this work the 2-zone open loop concept was implemented for the sake of easier process monitoring and guaranteeing the proper functioning of the regeneration zone. Apart from that, in cases where the side product formation is significant and an accumulation of side products is expected due to their adsorption behavior, the open-loop concept might be preferred over a 3-zone closed-loop. An important aspect of 3-zone closed loop processes is related to the pH gradient. In order to maintain the magnitude of this gradient, the pH of the desorbent and feed streams will have to be adjusted to more "extreme" values.

The numerical and experimental results for the nine operating points are summarized in Table 3. Five operating points were chosen inside the complete separation region: $P1$, $P3$, $P5$, $P6$ and $P8$, where 100% purity, conversion and yield were expected. The other four operating points were chosen outside this triangle to determine the limits of the complete separation region. A good agreement is obtained between experiments and theoretical predictions. For the five operating points inside the complete separation region the detection limit for the product purity of 98% is reached. Conversions and yields above 95% are obtained in these cases from the overall material balances.

High product purity and negligible amounts of CTD enantiomers in the regeneration stream were observed in the experiments designed to produce pure product. This demonstrates that the new integrated SMB concept is capable of producing single enantiomers with purity, conversion and yield close to 100%.

5. Conclusions

A new integrated 3-zone SMB process was identified in previous publications [1,2] as a promising concept to produce single enan-

tiomers. In this work, the process was experimentally validated for the model system chlorthalidone (CTD).

First, the racemization kinetics of CTD were determined as a function of the pH value. Afterwards, the adsorption isotherms were determined applying the inverse method in the pH range of interest. To design the process, a mathematical model was implemented accounting for the experimentally investigated reaction rate and adsorption isotherms.

For the sake of easier controllability, the experimental validation was performed using a 2-zone open-loop configuration. A 3-zone implementation is straightforward if side product formation is negligible. Such side prduct formation can be reduced by a modified feed strategy.

In a semi-preparative open-loop SMB setup several experimental runs were carried out corresponding to different operating points. The results confirm that pure single enantiomers can be produced with the new integrated process achieving conversion and yield values of 100%.

The new integrated process can be applied to enantiomeric systems where the racemization kinetics can be tuned significantly by means of the pH value. The dependency of the racemization kinetics on the pH is reported for other species (e.g., in [14]), as well as for epimerization [15] and isomerization kinetics [16]. Alternatively, other gradients of, for example, temperature, modifiers, additives, homogeneous catalysts or inhibitors could also modulate sufficiently the reaction kinetics, enabling more applications of this concept.

Nomenclature

Symbols

b	adsorption isotherm coefficient (L/g)
c	liquid phase concentration (g/L)
C_1, C_2, C_3	constants
ε	total porosity (−)
F	phase ratio, $F = (1-\varepsilon)/\varepsilon$ (−)
k	reaction rate constant (s^{-1})
m	flow rate ratio (−)
N_c, N_s, N_z	number of columns/stages/zones
ν	stoichiometric coefficient (−)
Pu	purity (%)
q	solid phase loading (g/L)
q^s	saturation capacity (g/L)
Q	volumetric flow rate (mL/min)
r	reaction rate (g/L/s)
t	time (min)
t^*	switching time of SMB process (min)
V	volume of a single stage (mL)
V_c	volume of a single column (mL)
X	conversion (%)
Y	yield (%)

Sub- and superscripts

A	stronger adsorbing component
B	weaker adsorbing component
0	initial or boundary condition
F	feed stream
i	component, $i = (A, B)$
I, II, III	zone of SMB system
k	index of stage, $k = 1, \ldots, N_s$
n	Index of column, $n = I, \ldots, N_c$
S	desorbent stream
z	index of zone, $z = 1, \ldots, N_z$

Acknowledgements

References

[1] J.G. Palacios, M. Kaspereit, A. Kienle, Chem. Eng. Technol. 32 (2009) 1392.
[2] J.G. Palacios, M. Kaspereit, A. Kienle, Chem. Eng. Technol., in press.
[3] R.A. Sheldon, Chirotechnology, Marcel Dekker, New York, 1993.
[4] G. Subramanian (Ed.), Chiral Separation Techniques – A Practical Approach, 2nd ed., Wiley-VCH, Weinheim, 2000.
[5] K. Hashimoto, S. Adachi, N. Ueda, Biotechnol. Bioeng. 25 (1983) 2371.
[6] G. Guiochon, S. Shirazi, A. Katti (Eds.), Fundamentals of Preparative and Non-linear Chromatography, Academic Press, London, 1994.
[7] M. Kaspereit, J.G. Palacios, T.M. Fernández, A. Kienle, in: 18th European Sympo-sium on Computer Aided Process Engineering, Volume 25 of Computer-Aided Chemical Engineering, 2008, p. 97.
[8] T. Fornstedt, G. Götmar, M. Andersson, G. Guiochon, J. Am. Chem. Soc. 121 (1999) 1164.
[9] M. Mangold, A. Kienle, K.D. Mohl, E.D. Gilles, Chem. Eng. Sci. 55 (2000) 441.
[10] R. Köhler, K. Mohl, H. Schramm, M. Zeitz, A. Kienle, M. Mangold, E. Stein, E. Gilles, Adaptative Method of Lines, Chapman & Hall/CRC, 2001, p. 371.
[11] R. Leven, B. Koch, B. Pompe, Chaos in Dissipativen Systemen, Akademie Verlag, Berlin, 1994.
[12] A. Felinger, D. Zhou, G. Guiochon, J. Chromatogr. A 1005 (2003) 35.
[13] E. Lamparter, G. Blaschke, J. Schlüter, Chirality 5 (1993) 370.
[14] H. Diab, P. Hendry, A. Ludi, K.B. Reddy, R. van Eldik, Inorg. Chim. Acta 175 (1990) 83.
[15] L. Li, R. Thompson, J.J.R. Sowa, A. Clausen, T. Dowling, J. Chromatogr. A 1043 (2004) 171.
[16] J. Jacobson, W. Melander, G. Vaisnys, C. Horvath, J. Phys. Chem. 88 (1984) 4536.
[17] A. Seidel-Morgenstern, J. Chromatogr. A 1037 (2004) 255.
[18] O. Trapp, V. Schurig, J. Chromatogr. A 911 (2001) 167.
[19] O. Trapp, G. Schoetz, V. Schurig, Chirality 13 (2001) 403.
[20] K. Cabrera, M. Jung, M. Fluck, V. Schurig, J. Chromatogr. A 731 (1996) 315.
[21] O. Stålberg, M. Kruusmägi, M.A. Svensson, U. Norinder, C. Pettersson, J. Pharm. Sci. 96 (2007) 2057.
[22] R.M.L. Marques, P.J. Schoenmakers, J. Chromatogr. 592 (1992) 157.
[23] M. Rosés, E. Bosch, J. Chromatogr. A 982 (2002) 1.
[24] R. Bergés, V. Sanz-Nebot, J. Barbosa, J. Chromatogr. A 869 (2000) 27.
[25] G. Storti, M. Mazzotti, M. Morbidelli, S. Carrà, AIChE J. 39 (1993) 471.
[26] M. Mazzotti, G. Storti, M. Morbidelli, J. Chromatogr. A 769 (1997) 3.
[27] K. Mihlbachler, J. Fricke, T. Yun, A. Seidel-Morgenstern, H. Schmidt-Traub, G. Guiochon, J. Chromatogr. A 908 (2001) 49.